


Assessing Seismic Performance of Buildings with Configuration Irregularities

Calibrating Current Standards and Practices

FEMA P-2012 / September 2018

FEMA

nehrp

Assessing Seismic Performance of Buildings with Configuration Irregularities: Calibrating Current Standards and Practices

Prepared by

APPLIED TECHNOLOGY COUNCIL
201 Redwood Shores Parkway, Suite 240
Redwood City, California 94065
www.ATCouncil.org

Prepared for

FEDERAL EMERGENCY MANAGEMENT AGENCY
Mai (Michael) Tong, Project Officer
Farzad Naeim, Subject Matter Expert
Washington, D.C.

ATC MANAGEMENT AND OVERSIGHT
Jon A. Heintz, Program Executive, Program Manager
Veronica Cedillos, Project Manager
Ayse Hortacsu, Project Manager

PROJECT TECHNICAL COMMITTEE
Michael Valley (Project Technical Director)
Curt Haselton
Charlie Kircher
Laura Lowes
Rafael Sabelli
Thomas Sabol

PROJECT REVIEW PANEL
Greg Deierlein
Larry Fahnestock
James Harris
Conrad Hohener
John Hooper
Ryan Kersting
Roberto Leon*

*ATC Board Contact

WORKING GROUP MEMBERS
Kamal Ahmed
Dustin Cook
Jared DeBock
Sara Essila
Katie Fitzgerald
Heavenz Kaur
Kristijan Kolozvari
Dawn Lehman
Nasser Marafi
Diana Nishi
Josh Pugh
Ricardo Roldan
Negin A. Tauberg
Tsenguun Tsoqbadrakh

September 2018

FEMA

nehrp

Notice

Any opinions, findings, conclusions, or recommendations expressed in this publication do not necessarily reflect the views of the Applied Technology Council (ATC), the Department of Homeland Security (DHS), or the Federal Emergency Management Agency (FEMA). Additionally, neither ATC, DHS, FEMA, nor any of their employees, makes any warranty, expressed or implied, nor assumes any legal liability or responsibility for the accuracy, completeness, or usefulness of any information, product, or process included in this publication. Users of information from this publication assume all liability arising from such use.

Cover images: Partial collapse of a commercial building with a vertical irregularity in the 1995 Kobe earthquake, courtesy of Charlie Kircher (top left); severe damage to first story of Olive View Hospital in the 1971 San Fernando earthquake (NISEE, 1971a; bottom left); hillside home with tall cripple walls that have failed, courtesy of Los Angeles Department of Building and Safety (bottom right); example of soft-story multi-family wood residential building collapse in the 1989 Loma Prieta earthquake (FEMA; top right).

Foreword

The National Earthquake Hazards Reduction Program (NEHRP) at Federal Emergency Management Agency (FEMA) has a responsibility to help translate and implement new knowledge and research results to increase seismic hazard resilience nationwide. One of the effective ways to fulfill this responsibility is through FEMA NEHRP sponsored problem-focused studies to use new research results and tools for developing practical solutions and needed information suitable for implementation in national standards and codes. This FEMA document summaries a problem-focused study on seismic performance of buildings with configuration irregularities. It is one of many FEMA technical resource documents to help improve seismic design practices, it is also to support public education and awareness for critical issues related to seismic safety of buildings.

Most buildings in the United States have some irregularities, which are known to influence building seismic performances. Under ASCE/SEI 7-16, *Minimum Design Loads and Associated Criteria for Buildings and Other Structures*, restrictions are imposed on configuration irregularities in high seismic regions. In order to update and simplify the relevant design requirements and restrictions, it is necessary to conduct a comprehensive assessment of seismic performance of buildings with configuration irregularities. This study provides the needed assessment of ASCE/SEI 7-16 requirements and triggers for restrictions on irregularities. Consequently, the findings and recommendations will lead to improvements to specific code requirements for irregularities and better knowledge on the subject matter.

FEMA is greatly appreciative of the Applied Technology Council (ATC), the Project Technical Committee, and the Project Review Panel for the development of this invaluable technical resource document and dissemination of the key findings. FEMA is also thankful to the project workshop participants for their scrutiny and valuable comments to the reported findings. The national standards and codes provide the basic protection for buildings against natural hazard impacts. As we call for all at-risk communities to adopt and enforce current national standards and codes, it is important to ensure that the standards and codes are based on best engineering knowledge, and validated new technology and information. We are pleased to see that this report is already receiving broad attention among

earthquake engineering professionals, and some of the recommended code changes are under consideration by consensus committees such as the NEHRP Provisions Update Committee and ASCE 7 Seismic Subcommittee.

National Earthquake Hazards Reduction Program (NEHRP)

Federal Emergency Management Agency

Preface

In 2014, the Applied Technology Council (ATC), with funding from the Federal Emergency Management Agency (FEMA) under Task Order Contract HSFE60-12-D-0242, commenced a series of projects (ATC-123, ATC-123-1, ATC-123-2, and ATC-123-3) to quantitatively evaluate current code triggers for structural irregularities, the impact on performance from structural irregularities, and the effectiveness of relevant code provisions.

Irregularities are a common occurrence in buildings in the United States. Some of these irregularities are defined in existing standards, such as ASCE/SEI 7-16, *Minimum Design Loads and Associated Criteria for Buildings and Other Structures* (ASCE, 2017a), ASCE/SEI 41-17, *Seismic Evaluation and Retrofit of Existing Buildings* (ASCE, 2017b), ACI 318-14, *Building Code Requirements for Structural Concrete* (ACI, 2014), and ANSI/AISC 341-16, *Seismic Provisions for Structural Steel Buildings* (AISC, 2016).

Although irregularities are known to influence seismic performance, the triggers in the current design codes for vertical and horizontal irregularities had not been quantitatively evaluated to determine their effectiveness in providing the collapse performance target. NIST GCR 13-917-23, *Development of NIST Measurement Science R&D Roadmap: Earthquake Risk Reduction in Buildings* (NIST, 2013), identified the need to systematically evaluate irregularity triggers and requirements in all Seismic Design Categories as an important priority research topic.

This multi-year project (collectively referred to as the ATC-123 Project) calibrated quantitative triggers and related design requirements in relevant codes and standards, primarily ASCE/SEI 7-16. The ATC-123 Project conducted analysis work on four of the structural irregularities codified in ASCE/SEI 7-16—torsional stiffness irregularity (H1), soft story irregularity (V1), mass irregularity (V2), and weak story irregularity (V5)—and investigated other configuration issues, including torsional strength irregularity (H6), limitations of current strong-column/weak-beam requirements (V6), increased collapse potential due to gravity-induced lateral demand (V7), and wall discontinuity (V8).

ATC is indebted to the leadership of Michael Valley, Project Technical Director, and to the members of the ATC-123, ATC-123-1, ATC-123-2, and ATC-123-3 Project Teams for their efforts in developing this report. The Project Technical Committee (PTC) consisting of Curt Haselton, Charlie Kircher, Laura Lowes, Rafael Sabelli, and Thomas Sabol, managed and performed the technical development efforts. Kamal Ahmed, Dustin Cook, Jared DeBock, Sara Essila, Katie Fitzgerald, Heavenz Kaur, Kristijan Kolozvari, Dawn Lehman, Nasser Marafi, Diana Nishi, Josh Pugh, Ricardo Roldan, Negin Tauberg, and Tsenguun Tsoqbadrakh, as Working Group members, conducted the design, analysis, and quality assurance work under the leadership and supervision of the PTC. The Project Review Panel, consisting of Greg Deierlein, Larry Fahnestock, James (Jim) Harris, Conrad (Sandy) Hohener, John Hooper, Ryan Kersting, and Robert Leon (ATC Board Contact), provided technical review, advice, and consultation at key stages of the work. A workshop of invited experts, in addition to the Project Review Panel, was convened to obtain feedback on the draft report and the Project Technical Committee considered input from this group to finalize the report. The names and affiliations of all who contributed to this report are provided in the list of Project Participants.

ATC also gratefully acknowledges Mai (Mike) Tong (FEMA Project Officer) and Farzad Naiem (FEMA Subject Matter Expert) for their input and guidance in the preparation of this document. Veronica Cedillos and Ayse Hortacsu managed the project and Carrie Perna provided report production services.

Veronica Cedillos
ATC Director of Projects

Jon A. Heintz
ATC Executive Director

Table of Contents

List of Figures

List of Tables

Chapter 1
Introduction

This report documents the work and findings of the ATC-123 Project, Improving Seismic Design of Buildings with Configuration Irregularities, a multi-year study funded by the Federal Emergency Management Agency (FEMA) under the National Earthquake Hazards Reduction Program (NEHRP). The primary purpose of the project was to facilitate improvement of irregularity-related design requirements of: FEMA P-1050-1, *NEHRP Recommended Seismic Provisions for New Buildings and Other Structures* (FEMA, 2015); ASCE/SEI 7-16, *Minimum Design Loads and Associated Criteria for Buildings and Other Structures* (ASCE, 2017a); and ASCE/SEI 41-17, *Seismic Evaluation and Retrofit of Existing Buildings* (ASCE, 2017b).

1.1 Background

It is commonly accepted that structural configuration irregularities can affect seismic performance. For the purposes of this report, a structural irregularity is defined as an aspect of configuration that detrimentally affects a structure's performance during an earthquake leading to an unacceptable reduction in collapse safety or increase in damage. Generally, there are three remedies for such irregularities, as follows:

- Remove the irregularity from the design;
- Address the irregularity using an analytical approach; or
- Resolve the irregularity through a design approach (e.g., by changing the proportioning).

U.S. codes and standards, such as ASCE/SEI 7, ASCE/SEI 41, ACI 318, *Building Code Requirements for Structural Concrete*, and AISC 341, *Seismic Provisions for Structural Steel Buildings* contain requirements related to structural configuration, which tie prohibitions, analysis requirements, and design requirements to various triggers. The irregularity-related requirements found in codes and standards generally reflect the best judgment of practitioners and academics based primarily on anecdotal observations and fairly simple linear static and linear dynamic analyses, without explicit consideration of collapse probability.

In the last decade, a methodology to validate building system performance and response parameters for use in seismic design was developed. That methodology, reported in FEMA P695, *Quantification of Building Seismic Performance Factors* (FEMA, 2009) has been accepted as the rational basis for establishing global seismic performance factors, including the response modification coefficient (R factor), the system overstrength factor (Ω_0), and the deflection amplification factor (C_d) used for design of new seismic-force-resisting systems in accordance with U.S. model building codes and related standards. To date, most investigations of system performance using the FEMA P695 methodology have focused on classes of buildings without significant configuration irregularities.

1.2 Overview of Irregularities Considered

This report summarizes work conducted under the ATC-123 Project to quantitatively evaluate current building code triggers, the influence of structural irregularities on seismic building performance (in terms of collapse probability), and the effectiveness of relevant code provisions. The objective of the studies conducted under this project was to inform and improve U.S. codes and standards so that structures with configuration irregularities have a level of safety against collapse in an earthquake that is comparable to that for regular structures. The project focuses primarily on design requirements for new buildings, with limited consideration of the treatment of irregularities for existing buildings.

With a focus on irregularities that have detrimentally affected structural performance in past earthquakes or that are common in current construction trends, the project considered 12 classes of structural configuration irregularities identified in current U.S. codes and standards and two new classes as follows:

- Torsional stiffness
- Reentrant corner
- Diaphragm discontinuity
- Out-of-plane offset
- Nonparallel system
- Torsional strength
- Soft story
- Weight [mass]
- Vertical geometric

- In-plane discontinuity
- Weak story
- Weak-column/strong-beam
- Two new classes of irregularity: gravity-induced lateral demand and wall discontinuities

Treatment of these irregularities by the project ranges from explicit quantitative collapse evaluation (using the FEMA P695 methodology) to a general discussion of the most critical issues.

The structural systems addressed in this report include moment frames (both steel and reinforced concrete), reinforced concrete shear walls, combinations thereof, and simplified treatment of wood frame shear wall buildings.

1.3 Target Audience

This report is written and organized to facilitate the transfer of project findings to: (1) the FEMA-sponsored Building Seismic Safety Council (BSSC) NEHRP Provisions Update Committee; (2) the ASCE/SEI 7 Seismic Subcommittee; and (3) the ASCE/SEI 41 Committee. The work and findings of the ATC-123 Project are also of value to other engineering practitioners and researchers interested in building design and code development.

1.4 Content and Organization

Chapter 2 provides an overview of structural configuration irregularities, including observations of performance in past earthquakes, treatment of irregularities in the building codes of various countries, and a summary of key findings from earlier research. Each type of irregularity is illustrated, and key performance concerns are discussed briefly.

Chapter 3 describes the approach used to design, model, and analyze the building archetypes used to evaluate the impact of configuration irregularity on collapse resistance.

Chapter 4 summarizes analytical studies of torsional stiffness and torsional strength irregularities. Those studies are used to assess the effectiveness of current code requirements related to torsional irregularities and to identify corresponding recommended improvements.

Chapter 5 addresses concrete shear wall buildings with vertical irregularities. The impact of openings in the lowest one or two stories of mid-rise buildings on their collapse resistance is investigated using a variety of software platforms and model types.

Chapter 6 summarizes analytical studies of five aspects of vertical configuration—soft story irregularity, weight (mass) irregularity, weak story irregularity, strong-column/weak-beam provisions, and gravity-induced lateral demand—using reinforced concrete and structural steel moment frame buildings. Some of the studies also compare the performance of buildings designed using the equivalent lateral force procedure with those designed using the modal response spectrum analysis method.

Chapter 7 discusses the triggers and design consequences for several irregularities that were not the subject of extensive analysis in the course of the ATC-123 Project, including reentrant corners, diaphragm discontinuity, out-of-plane offset, nonparallel systems, vertical geometric, in-plane discontinuity, and wall discontinuity. Recommendations are made so the treatment of these irregularities can be more consistent with observed performance and the evolution of the related design requirements.

Chapter 8 summarizes recommended improvements for the seismic design of buildings with configuration irregularities and identifies areas for future study.

Appendices A through D provide more detailed information and results of the work reported in Chapters 4 through 6. Appendix E describes quality control review work conducted for each of the analytical studies. Appendix F documents a series of supplemental analyses performed to test the generality of observations made regarding the use of the equivalent lateral force procedure for buildings with mass irregularity. Appendix G provides recommendations for the calculation of story stiffness and story strength, which are used to assess soft story and weak story irregularities and to determine the redundancy factor. Appendix H provides a discussion and some general conclusions regarding steel systems not specifically detailed for seismic resistance.

A glossary of definitions and list of symbols used throughout this report, along with a list of references, are provided at the end of this report.

Chapter 2
Overview of Irregularities

Structural irregularities are a common occurrence due to the configuration of buildings to meet architectural and functional needs. Some of these irregularities are defined in existing standards, such as ASCE/SEI 7-16, *Minimum Design Loads and Associated Criteria for Buildings and Other Structures* (ASCE, 2017a); ASCE/SEI 41-17, *Seismic Evaluation and Retrofit of Existing Buildings* (ASCE, 2017b); ACI 318-14, *Building Code Requirements for Structural Concrete* (ACI, 2014); and ANSI/AISC 341-16, *Seismic Provisions for Structural Steel Buildings* (AISC, 2016). Table 2-1 lists these irregularities and their treatment in current U.S. standards. (This report uses the item numbers that appear in Table 12.3-1 and Table 12.3-2 of ASCE/SEI 7-16 with H or V prepended to indicate class of irregularity—horizontal or vertical.) Table 2-1 also indicates how each irregularity is treated in this project, where "Analysis" indicates an explicit assessment of collapse probability using the FEMA P695 method.

Table 2-1 Structural Irregularities in U.S. Codes and their Treatment in this Report

Structural Irregularities	Codified in	Treatment in this Report
H1. Torsional (stiffness) irregularity	ASCE/SEI 7-16	Analysis
H2. Reentrant corner irregularity	ASCE/SEI 7-16	Discussion
H3. Diaphragm discontinuity irregularity	ASCE/SEI 7-16	Discussion
H4. Out-of-plane offset irregularity	ASCE/SEI 7-16	Discussion
H5. Nonparallel system irregularity	ASCE/SEI 7-16	Discussion
H6.[(1)] Torsional strength irregularity	ASCE/SEI 41-17	Analysis
V1. Soft story irregularity	ASCE/SEI 7-16	Analysis
V2. Weight (mass) irregularity	ASCE/SEI 7-16	Analysis
V3. Vertical geometric irregularity	ASCE/SEI 7-16	Discussion
V4. In-plane discontinuity … irregularity	ASCE/SEI 7-16	Discussion
V5. Weak story irregularity	ASCE/SEI 7-16	Analysis
V6.[(1)] Story mechanism: weak-column/strong-beam	ACI 318-14, ANSI/AISC 341-16	Analysis
V7.[(1)] Gravity-induced lateral demand		Analysis
V8.[(1)] Wall discontinuity		Limited analysis

[(1)] The designations "H6" and "V6"–"V8" are used in order to extend the ASCE/SEI 7-16 code designations to additional irregularities addressed in this report.

Although irregularities are known to influence seismic performance, the triggers in the current design codes for vertical and horizontal irregularities are based on the judgment of code writers, not clearly demonstrated differences in structural performance, and have not yet been quantitatively evaluated. An exception is a Building Seismic Safety Council (BSSC) project on Simplified Seismic Design Procedures that found torsional irregularity triggers to have little effect on the collapse risk for Seismic Design Category (SDC) B buildings, resulting in a code change proposal to eliminate the requirement in areas of low seismic hazard (DeBock et al., 2014). The need to systematically evaluate other irregularity triggers and requirements in all Seismic Design Categories has been identified as a highly important priority for conducting further research activities in the NIST GCR 13-917-23 report, *Development of NIST Measurement Science R&D Roadmap: Earthquake Risk Reduction in Buildings* (NIST, 2013).

The tools for quantitative evaluation of the influence of structural irregularities and associated irregularity triggers on collapse performance are available (e.g., the FEMA P695 report, *Quantification of Building Seismic Performance Factors* (FEMA, 2009)). During development of FEMA P695 and numerous follow-on projects, the methodology set forth in the FEMA P695 report was used to investigate the collapse performance of a number of different seismic-force-resisting systems (SFRSs) against the quantitative collapse and overall risk performance criteria of ASCE/SEI 7-10 for life safety. In these studies, seismic-force-resisting systems were assumed to be regular in configuration. Similar work has not yet been conducted for systems with horizontal and vertical irregularities.

2.1 Literature Search

Phase I of the ATC-123 Project included a review of reported performance of irregular buildings in past earthquakes—with particular focus on the 1971 San Fernando, 1989 Loma Prieta, 1994 Northridge, 1995 Kobe, 2010 Maule, and 2011 Christchurch events. Also reviewed was the treatment of configuration irregularities in codes and standards throughout the world, including the codes used in Canada, Europe, New Zealand, Japan, China, Mexico, Venezuela, Panama, Costa Rica, and Chile. The literature search also included review of scores of prior studies of structural irregularities and related metrics and triggers, and analytical methods to quantify or assess such irregularities.

2.1.1 Observed Performance of Irregular Buildings

The ATC-123 Project included a review of reported performance of irregular buildings in past earthquakes. Findings concerning earthquake-related fatalities and causes of structural collapse are summarized below.

2.1.1.1 Earthquake-Related Fatalities

In general, earthquake-related fatalities are attributed to the performance of structures subjected to ground motion or ground failure, including medical-related deaths such as heart failure brought on by the earthquake, fire following, or tsunami. Deaths due to ground motion or ground failure are due primarily to injuries sustained because of building (or bridge) collapse.

Of the estimated 1,687 fatalities in U.S. earthquakes between 1900 and 2000, 573 are related to ground motion or failure, 640 to fire following, and 474 to tsunami. (This estimate does not reflect recent studies that suggest that the "official" 800 deaths in the 1906 San Francisco earthquake should be 3,000 deaths.) The relatively few number of earthquake fatalities in recent U.S. earthquakes (less than 200 deaths since 1970) reflects both good fortune (i.e., only moderate magnitude earthquakes have occurred off hours or away from the center of the areas of densest population), as well as the generally good earthquake resistance of U.S. (California) buildings. Larger magnitude events closer to the center of dense urban areas would be expected to cause a much greater loss of life due to collapse of vulnerable buildings such as those which have a significant structural irregularity.

For instance, the 6,434 fatalities in the 1995 Kobe earthquake, which is one of the most significant events to affect an urban region of modern construction, were primarily due to building collapse. More than 82,000 buildings collapsed in the 1995 Kobe earthquake, with building collapse rates of approximately 21% for sites within 5 km of the fault rupture and 1.2% for sites greater than 5 km from fault rupture (AIJ, 1995).

2.1.1.2 Causes of Structural Collapse

Recent U.S. Earthquakes

Since 1970, roughly one-half of the approximate 200 deaths in United States earthquakes are due to building collapse, and virtually all of these deaths occurred due to collapse of buildings of either unreinforced masonry (URM) or non-ductile concrete material (i.e., materials no longer permitted for construction in seismic regions) and/or of irregular structural configuration (e.g., soft-story light-frame wood buildings).

Figure 2-1, Figure 2-2, and Figure 2-3 are photos showing examples of collapse of the most vulnerable types of U.S. construction in past earthquakes. Vulnerable construction includes URM buildings (Figure 2-1), non-ductile reinforced concrete buildings (Figure 2-2), and soft/weak story wood frame buildings (Figure 2-3). Collapse of these three types of buildings caused over 70 of the approximate 100 deaths due to building collapse in U.S. earthquakes since 1970. These building types are either no longer permitted in regions of moderate or high seismicity (i.e., URM buildings) or, presumably, current seismic code provisions (ASCE/SEI 7-16) have adequately addressed issues of element ductility (e.g., for reinforced concrete buildings) or irregular configuration (e.g., soft/weak story wood buildings).

(a) (b)

(c) (d)

Figure 2-1 Examples of URM building collapse in the (a) 1983 Coalinga earthquake (NISEE, 1983); (b) the 1987 Whittier earthquake (NISEE, 1987), and (c, d) the 1989 Loma Prieta earthquake (photos courtesy of the U.S. Geological Survey and Bill Lovejoy of the Santa Cruz Sentinel, respectively). 5 deaths (San Francisco, photo c) and 3 deaths (Santa Cruz, photo d) out of 15 building collapse-related deaths occurred due to out-of-plane failure of URM walls in the 1989 Loma Prieta earthquake.

Figure 2-2 Example of non-ductile concrete frame building collapse at the Veterans Administration (VA) complex in the 1971 San Fernando earthquake; including total collapse of 4 of 26 buildings. 47 of the 58 deaths in the 1971 San Fernando earthquake occurred at the VA complex. Photo courtesy of the U.S. Geological Survey.

(a) (b)

(c) (d)

Figure 2-3 Examples of soft-story multi-family wood residential building collapse in the 1989 Loma Prieta earthquake (a, b) and in the 1994 Northridge earthquake (c, d). 16 of the 20 building collapse-related deaths in the 1994 Northridge earthquake occurred in the Northridge Meadows apartment complex (c). Photos (a) and (d) are from NISEE (1989; 1994); photos (b) and (c) are courtesy of EERI.

With respect to the cause of collapse and hence occupant fatality, failure of URM buildings (Figure 2-1) is typically associated with out-of-plane failure of bearing walls, especially at wall-to-diaphragm connections, and not related to structural irregularity. It might be noted that URM buildings could have a structural irregularity, but the building would still be more vulnerable due to out-of-plane wall failure. With respect to non-ductile concrete buildings, structural irregularity likely contributed to at least some of the collapse damage at the VA complex (Figure 2-2); however, like URM buildings, other factors are the primary cause of failure. With respect to soft/weak story wood buildings, by definition, collapse of these buildings is directly related to their soft/weak story irregularity.

In the case of the Olive View Hospital, vertical stiffness (strength) irregularity caused first floor collapse of the Community Mental Health Building and nearly caused collapse of the main building of the Olive View hospital. The hospital was staffed with 98 employees and had 606 patients at the time of the earthquake, but there were only three earthquake fatalities (i.e., 2 medical-related deaths and 1 death due to collapse of a stairwell). There were no deaths in the Community Mental Health Center, which was unoccupied (off hours) at the time of the earthquake. Arguably, the number fatalities in the Olive View Hospital complex could have been comparable to (or greater) than the 47 fatalities at the VA complex given the near collapse of the main building and first floor collapse of the unoccupied Community Mental Health Building.

Figure 2-4 shows photos of damage to buildings at the Olive Hospital caused by the 1971 San Fernando earthquake. Damage includes extreme distortion and near collapse of the "soft-story" moment-frame columns of the lower floors of the five-story main building of Olive View Hospital (Figure 2-4a, 2-4c). Columns at the lower levels had large ductile capacity due to spiral reinforcement (as shown in Figure 2-4c) and collapse would likely have occurred without such reinforcement. There was complete collapse of the 1st floor of the two-story Community Mental Health Building (Figure 2-4d). In this case, lateral deflection was concentrated at the 1st-floor level due in part to masonry walls at the 2nd floor limiting 2nd-floor lateral deflection and effectively creating a soft/weak 1st story.

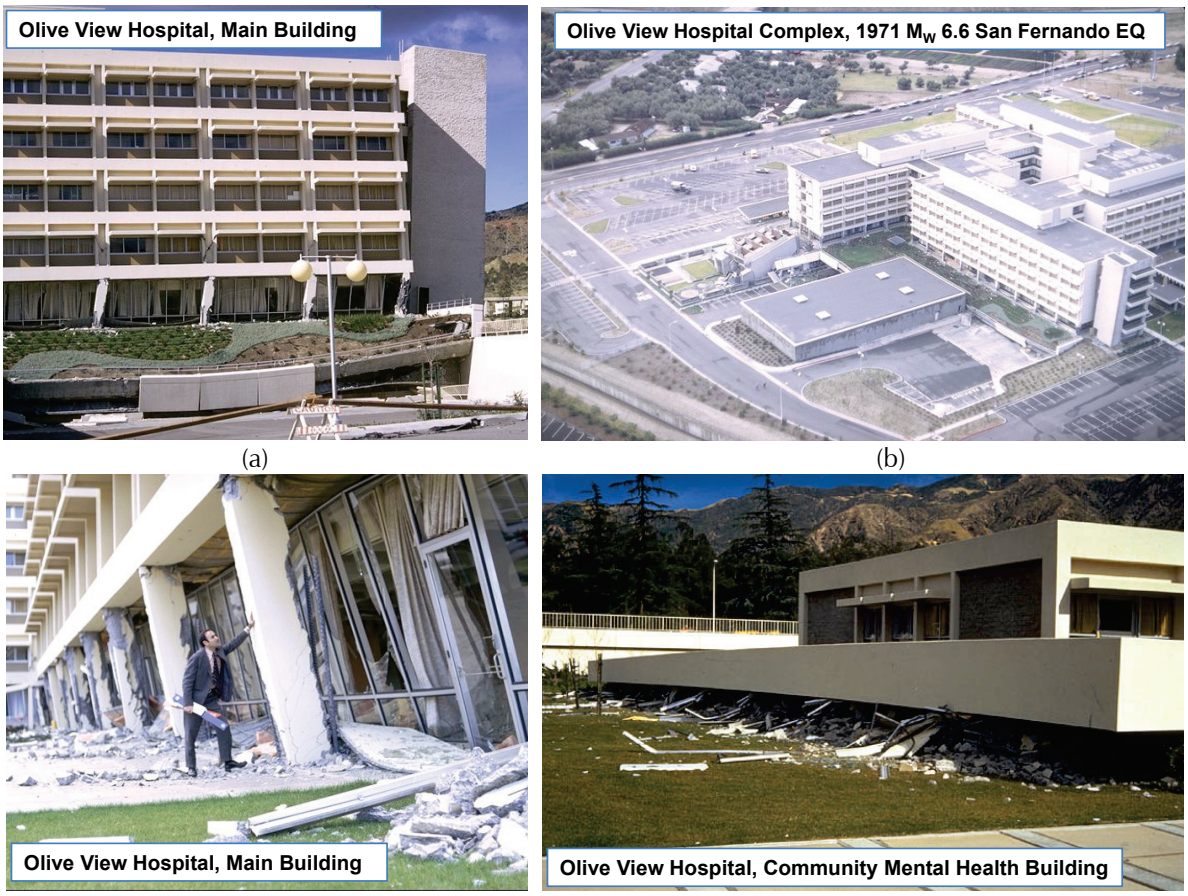

Figure 2-4 Photographs of severe damage and collapse of buildings of the Olive View Hospital due to the 1971 San Fernando earthquake. Photos from NISEE (1971a; 1971b; 1971c; 1971d, respectively).

1995 Kobe Earthquake

Most of the buildings that collapsed in the 1995 Kobe earthquake were of older construction that had the following three attributes: (1) weak lateral system; (2) non-ductile material; and (3) irregular structural configuration—conditions no longer permitted, or subject to greater penalties, by the Japanese building code (since 1981).

Smaller commercial and mixed-use Japanese buildings are typically 2-story and 3-story structures common to denser urban areas. The first floor is often used for the family business with the family living upstairs. Typically, several businesses (families) occupy different units of the same building. These buildings are typically made of wood, similar to low-rise residential construction, or light-gage steel. It is common for these buildings to have a soft/weak first story and significant torsional response since the first floor will typically have large openings (and no wall) on the street-side of the building. Figure 2-5 shows severe leaning and incipient collapse of a mixed-use building in Kobe City typical of damage to these types of buildings.

Figure 2-5 Photograph showing severe leaning and incipient collapse of a 2-story mixed-use building in Kobe City. Photo courtesy of Charlie Kircher.

Mid-rise Japanese buildings are 3-stories to 60 meters in height and are used for both residential (apartments) and commercial occupancies. They are constructed of steel framing or reinforced concrete (RC), or a combination of a steel frame encased in reinforced concrete (SRC). In older SRC buildings, the steel frame may not continue up the full building height of the building creating a hidden strength discontinuity at an upper floor. Japanese mid-rise buildings are the building type most similar to U.S. buildings. And, like the seismic provisions of the U.S. building codes, the seismic provisions of the Japanese building code have changed substantially over time (often for the same reasons).

In 1981, the Japanese building code was completely revised to incorporate a sophisticated two-phase design approach that retained traditional methods as the first phase of design for safety and serviceability during medium earthquake motions, and added a new, second phase of design for safety against severe ground shaking. As part of the new approach, vertical stiffness irregularity is checked using a "rigidity factor" and torsional irregularity is checked using an "eccentricity factor." Structures deemed to be irregular have more stringent design requirements; the underlying concept is to encourage use of regular configurations.

Differences in the performance of buildings of different design vintages is apparent in the tagging data compiled by engineers from Obayashi Corporation who inspected 332 buildings that their company had designed and constructed in Kobe since about 1950 (Obayashi, 1995). Over 50 percent of buildings designed before 1982 were assigned a yellow or red tag, whereas less than 10 percent of the buildings designed after 1982 were assigned a yellow or red tag. No post-1982 buildings collapsed, and it is likely that some the post-1982 buildings that were assigned a red tag (8 buildings) reflect damage due to nonstructural systems, rather than structural damage.

Figure 2-6 and Figure 2-7 are photographs of collapse damage to older mid-rise buildings with vertical and/or horizontal irregularities, including information about building type, configuration, and collapse failure mechanism when known. These buildings are representative of more common types of collapse damage observed in older mid-rise buildings.

Figure 2-6 Partial collapse of a 6-story commercial building (Chou Ward) with a torsional irregularity. The building was a reinforced concrete structure with perimeter shear walls on two orthogonal sides of the building and gravity framing on the other two orthogonal sides of the building. The torsional irregularity caused the building to rotate during the earthquake. As the building rotated, large displacement of the gravity frames at the corner away from the stiffer walls exceeded frame capacity causing failure of columns and collapse or sagging of floors above. Photo courtesy of Charlie Kircher.

Figure 2-7 Partial collapse of a 12-story commercial building (Sannomiya District) with plan and (presumed) vertical irregularities. The building was a 12-story reinforced concrete shear wall structure with perimeter shear walls on three sides. Shear walls were lightly reinforced. The torsional irregularity caused the building to rotate as well as displace laterally during the earthquake. As the building displaced and rotated, the capacity of gravity framing was exceeded and the building partially collapsed at the 4th floor on the side of the building facing the street (i.e., side without walls), most likely due to a vertical irregularity at this level although the source of the irregularity could not be confirmed. Photo courtesy of Charlie Kircher.

2010 Maule Earthquake

Evaluation of buildings damaged during the 2010 M8.8 Maule earthquake identified a number of building system design and configuration issues that could be expected to result in poor earthquake performance. These issues include discontinuities in walls; coupling of walls via slabs, beams, and spandrels; wall demands induced by nonstructural elements; and wall axial demands. These issues are described in detail in Appendix D of NIST GCR 14-917-25, *Recommendations for Seismic Design of Reinforced Concrete Wall Buildings Based on Studies of the 2010 Maule, Chile Earthquake* (NIST, 2014), and addressed in Birely (2012). The following provides a brief description of the building configuration issues considered to be most highly correlated with earthquake damage.

Many of the RC wall buildings damaged during the 2010 Maule earthquake were observed to have significant vertical discontinuities in walls that were primary elements of the lateral load resisting system. Figure 2-8 and Figure 2-9 show vertical discontinuities in which a significant length of wall is lost from an upper to a lower story. Appendix D of NIST GCR 14-917-25 discusses vertical discontinuities in detail and provides vertical discontinuity data for the Chilean buildings that were studied.

Section B.1.1 provides more detailed information on observed damage particular to concrete walls with irregularities in past earthquakes, including the 2010 Maule earthquake.

Figure 2-8 Coupled walls in upper stories do not continue to lower story (Plaza del Rio Building, Concepción, Chile). Photo courtesy of Ken Elwood.

Figure 2-9 A change in the wall section from the upper to lower story results in a loss of wall area and localization of flexural yielding (Plaza del Rio Building, Concepción, Chile). Photo courtesy of Ken Elwood.

2.1.2 Treatment of Configuration Irregularities in Codes and Standards

2.1.2.1 U.S. Codes and Standards

The 1976 *Uniform Building Code* (International Conference of Building Officials, 1976) contains the first explicit treatment of structural "irregularities" in a U.S. building code. Section 2312(e)3, reads as follows:

> **"Structures having irregular shapes or framing systems.** The distribution of the lateral forces in structures which have highly irregular shapes, large differences in lateral resistance or stiffness between adjacent stories or other unusual structural features shall be determined considering the dynamic characteristics of the structure."

This requirement was added at the recommendation of the Seismology Committee of the Structural Engineers Association of California (SEAOC) based on "observation of earthquake damage" (SEAOC, 1975). The commentary suggests that "due to the infinite variations of irregularities that can exist, the impracticality of establishing definite parameters and rational rules for the application of this Section are readily apparent." It goes on to identify four "categories of buildings or conditions that are deserving of special design consideration," as follows:

- Buildings with irregular configuration in plan or in the vertical dimension.
- Buildings with abrupt changes in lateral resistance within any level or between adjacent levels.
- Buildings with abrupt changes in lateral stiffness within any level or between adjacent levels.
- Unusual or novel structural features.

The SEAOC commentary also provides guidance for each of the four categories.

The ATC-3 project sought "to present, in one comprehensive document, current state-of-knowledge in the fields of engineering seismology and engineering practice as it pertains to seismic design and construction of buildings" (ATC, 1978). Project participants included design professionals, researchers, federal agency representatives, staffs from model code organizations, and representatives from state and local governments throughout the United States. The resulting report includes a provision that "buildings which have an approximately symmetrical geometric configuration and which have the building mass and seismic resisting system nearly coincident shall be classified as regular." Buildings would be classified as irregular where they have plan or vertical configuration as follows:

- Plan irregularity
    - The building does not have an approximately symmetrical geometric configuration or has re-entrant corners with significant dimensions.
    - There is the potential for large torsional moments because there is significant eccentricity between the seismic resisting system and the mass tributary to any level.
    - The diaphragm at any single level has significant changes in strength or stiffness.
- Vertical irregularity
    - The building does not have an approximately symmetrical geometric configuration about the vertical axes or has horizontal offsets with significant dimensions.
    - The mass-stiffness ratios between adjacent stories varies significantly.

In subsequent years, revisions were made to the *Uniform Building Code*, the *NEHRP Recommended Provisions*, ASCE/SEI 7, ASCE/SEI 31/41, ACI 318, and ANSI/AISC 341 to expand the list of irregularities, provide specific triggering thresholds, and prescribe related analysis, design, and detailing requirements—based on observed performance, ongoing research, and the consensus process.

In addition to the 10 irregularities addressed in ASCE/SEI 7-16 (identified as H1-H5 and V1-V5 in this report), ASCE/SEI 41-17 identifies a torsional strength irregularity, which is identified as H6 in this report.

U.S. design standards for concrete (ACI 318-14) and steel (ANSI/AISC 341-16) regulate moment frame proportioning to avoid weak-column/strong-beam systems to reduce the likelihood of the premature formation of a story mechanism; that type of configuration is identified as V6 in this report.

2.1.2.2 International Codes

This project reviewed the treatment of configuration irregularities in building codes applicable in Canada, Europe, Japan, China, Mexico, Venezuela, Panama, Costa Rica, and Chile. The following is a summary:

- The building code in Canada is similar to that of the U.S. Specifically, 8 of the 10 ASCE/SEI 7-16 irregularities are defined, excluding re-entrant corners and diaphragm discontinuity [H2 and H3]. In response to recent architectural trends to include sloping columns in large-scale construction, the *National Building Code of Canada* (National Research Council of Canada, 2015) triggers that configuration as a gravity-induced lateral demand irregularity based on recent analytical studies (Dupuis et al., 2014); this report uses the designation V7 for this condition.
- Section 4 of Eurocode 8 provides commentary-like guidance on good design, which states that it is good practice to have a regular structure. Table 4.1 in Eurocode 8 provides a method for choosing an analysis approach (European Committee for Standardization, 2004). It uses analysis methods and strength requirements to address irregularities.
- The New Zealand building code is similar to ASCE/SEI 7. MacRae and Deam (2009) compiled a series of papers summarizing the thinking of the New Zealand engineering community on irregularities before the 2010 Christchurch earthquake.
- The Japanese building code was summarized in a paper by Aoyama (1981). According to this paper, the guidance provided is that the building design should be simple, short, and regular—to avoid an elaborate design process. Rigidity and eccentricity factors determine if

the building is sufficiently regular to avoid more elaborate design. The detailed calculations prescribed in the Japanese building code differ from those in ASCE/SEI 7, but the conditions addressed roughly correspond to V1b (extreme soft story irregularity) and H1 (torsional stiffness irregularity).

- The building code in China is similar to that in the U.S. Specifically, 7 of the 10 ASCE/SEI 7-16 irregularities are defined, excluding out-of-plane offset, nonparallel system, and weight (mass) irregularities [H4, H5, and V2] (Ministry of Construction of the People's Republic of China and the State Quality Supervision and Quarantine Bureau, 2001).
- The building code in Mexico defines structural regularity and severe irregularity, but not irregularity per se (ISCDF, 2004). The consequence of an irregularity is a decrease in the *R*-factor (i.e., an increase in design base shear).
- The Venezuelan building code defines vertical and plan irregularities similar to those in the U.S., but adds items for excessive slenderness, short column effects, flexible diaphragms, and columns disconnected from diaphragms (FUNVISIS, 2001). The consequence is on values of design factors, not the use of a different analysis approach.
- The building code in Panama includes the 10 categories of irregularities defined in ASCE/SEI 7-16 (Junta Técnica de Ingeniería y Arquitectura, 2004).
- The building code in Costa Rica includes the 10 categories of irregularities defined in ASCE/SEI 7-16, but adds a torsional irregularity where the first torsional mode has a longer period than one (or both) of the fundamental translational modes in the two orthogonal horizontal directions (CFIA, 1986).
- The Chilean building code does not explicitly address irregularities.

2.1.3 Published Research on Irregularities

The project reviewed recent research on irregularities. In addition to papers for individual studies, the paper by De Stefano and Pintucchi (2008) is "a review of research on seismic behavior of irregular building structures since 2002," which summarizes findings from scores of studies between 2002 and 2008. None of the research reviewed addresses reentrant corner (H2), diaphragm discontinuity (H3), out-of-plane offset (H4), nonparallel system (H5), torsional strength (H6), or in-plane discontinuity (V4) irregularity. Key observations from the reviewed research for the addressed irregularities follow.

Torsional (stiffness) irregularity [H1]. A horizontal torsional irregularity is a function of the distribution of a structure's stiffness and mass at a given floor level. Specific ASCE/SEI 7-16 regulations pertaining to torsional (stiffness) irregularities are triggered if the deflection on one side of the story is greater than 1.2 times the average deflection of that story along the same axis where a load with 5% eccentricity from the story's center of mass is applied (the 5% eccentricity measured with respect to a building's dimension perpendicular to the direction of applied load). Out of all the irregularities to be studied in this project, torsional irregularity is the most previously studied irregularity. There has been much research using single-story analytical models to quantify the effects of torsional irregularities, and, in recent years, there has been a push to study the effects of nonlinearity on the torsional behavior of structures. Studies using simplified single-story models seem to show little difference between elastic and plastic effects of torsional irregularities, but several studies (e.g., Stathopoulos and Anagnostopoulus, as summarized by De Stefano and Pintucchi, 2008) using 3D multi-story models seem to contradict previous studies and find that torsional irregularities have greater effect the more nonlinear the model becomes. In all of these studies, there is a general expression of need to perform more research on the effects of torsional irregularities on nonlinear behavior using more advanced 3D multi-story models. There have also been several studies looking into the effects of accidental torsion requirements with torsional irregularities. In DeBock et al. (2014) it was concluded that the accidental torsion requirements in ASCE/SEI 7-16 for the equivalent lateral force (ELF) design procedure significantly impact collapse resistance only for structures with moderate to high torsional irregularity. It was also concluded in that study that the torsional amplification factor (A_x) as well as drift limits on building edges (rather than at the center of mass) are significant in preventing building collapse for torsionally irregular buildings in high seismic zones.

Soft story irregularity [V1]. According to ASCE/SEI 7-16, soft story irregularities occur where a given story has a stiffness less than 70% of the story above or less than 80% of the average stiffness of the 3 stories above. In Michalis et al. (2006), it was shown through analytical models of 9-story steel moment frames that soft story irregularities have the largest effect on collapse capacity where the soft story occurs at one of the first three stories. Where the soft story is more towards the middle or top of the structure, the study showed that it has little effect on collapse capacity. Even though this study found that soft story irregularities have an effect, both this study and other studies have shown that the weak story aspects of a vertical irregularity are more important than the soft story aspect of such an irregularity.

Weight (mass) irregularity [V2]. As defined in ASCE/SEI 7-16, weight irregularity occurs where the effective mass of one story is greater than 150% of that of an adjacent story. The effects of mass irregularities on 9-story steel moment frame buildings were studied by Michalis et al. (2006). It was found that mass irregularity had a similar but inverse effect to that of a soft story irregularity. The degree to which mass affects collapse capacity was shown to be similar to that of a soft story, but placement effects were inverse. Where the mass irregularity occurred on the top floor, it had the greatest effect; where it occurred on the middle or lower floors, it had little effect on collapse capacity. Both mass and soft story irregularities had less effect on collapse than a weak story irregularity in the Michalis et al. (2006) study. Other studies (Magliulo et al., 2002; Tremblay and Poncet, 2005) have also noted that vertical mass eccentric buildings perform well in seismic events.

Vertical geometric irregularity [V3]. As defined in ASCE/SEI 7-16 vertical geometry irregularities occur where the horizontal dimension of the seismic-force-resisting system on any story is greater than 130% of that on the adjacent story. A common example of vertical geometry irregularity is story setback. A 2004 study by Tena-Colunga (as summarized by De Stefano and Pintucchi, 2008) found that buildings with vertical setback performed well as long as there was adequate redundancy in the lateral system, but systems without redundancy and with vertical setback performed poorly. Several other studies mention the variability observed in studies on setback, and that more research is needed to better understand this irregularity.

Weak story irregularity [V5]. As defined in ASCE/SEI 7-16 weak story irregularities occur where the story lateral strength is less than 80% of that of the story above. As mentioned before, it was shown in the study by Michalis et al. (2006) that weak story irregularities have much larger effect on collapse capacity than mass or soft story irregularities. The effect seems to be the greatest where the weak story is near the bottom of the structure, causing the largest decrease in collapse capacity. However, there is a benefit to structural performance at levels of ground motion farther away from collapse. A fuse effect is created and the damage is concentrated in the weakened story, protecting the upper stories from damage. In general Michalis et al. (2006) conclude that the effects of vertical irregularities are not well understood and modern building codes are overly conservative where it comes to mass and soft story irregularities. FEMA P-807, *Seismic Evaluation and Retrofit of Multi-Unit Wood-Frame Buildings With Weak First Stories* (FEMA, 2012a), provides useful information for the seismic

evaluation and retrofit of multi-unit wood-frame buildings with weak first stories.

Story mechanism: weak-column/strong-beam [V6]. Weak-column/strong-beam occurs where the moment capacity of the column in the lateral force resisting system is weaker than that of the beam. Previous work studying the effects of a weak-column/strong-beam on building performance has shown that the ratio of column to beam strength has a large impact on the collapse safety of the building, and that the impact differs for various height buildings (Haselton et al., 2011). This study by Haselton et al. only included 4-story and 12-story reinforced concrete frame buildings, so further study on this topic is warranted.

Gravity-induced lateral demand [V7]. Gravity-induced lateral demand irregularity occurs where the vertical members of the gravity system are sloped and subject the lateral system to a continuous lateral load. Dupuis et al. (2014) describes the issue and reports the results of analyses to quantify this effect for concrete shear walls buildings. As a result of that study, the 2015 edition of the *National Building Code of Canada* introduces a new irregularity class to address gravity-induced lateral demands.

Wall discontinuity [V8]. Wall discontinuity occurs where there is an abrupt discontinuity or large variance of stiffness along the height of a shear wall. This may occur above or below a multi-story stack of openings or at building setbacks and major changes in the overall layout of walls. Naeim et al. (1990) and Moehle (2015) describe the mechanics of such discontinuities. NIST (2014) describes poor performance in the 2010 Maule, Chile earthquake as a result of such irregularities.

MacRae and Deam (2009) summarizes an effort in New Zealand to quantify the effect of different amounts and types of irregularity on structures designed using their implementation of the equivalent lateral force method in their loading standard. As such, it addresses relatively simple structures. The research addresses relationships between the amount of irregularity versus changes in behavior to assess when structural irregularities could be ignored as well as the magnitude of demand change due to these irregularities. It was concluded that diaphragm flexibility is unlikely to increase seismic force demand in most structures due to the increase in the building's period and the resulting decrease in spectral acceleration. The report presents a simplified method to assess the resulting increase in displacement using an amplifier based on a diaphragm flexibility ratio.

For more information on past laboratory test results related to concrete walls with vertical irregularities, see Section B.1.3.

2.2 Performance Concerns for Irregularities and Corresponding Code Requirements

Figure 2-10 and Figure 2-11 illustrate all 14 irregularities identified in this report. The notation in the figures is consistent with that in ASCE/SEI 7-16 and common U.S. practice, as follows:

- DCR = demand/capacity ratio
- K = stiffness
- M = mass
- M_c = column moment capacity
- M_b = beam moment capacity
- Q = demand or capacity action
- Δ = story drift

Performance concerns for these irregularities include additional proportioning considerations (such as amplified global or local loads or drifts), specific detailing issues (such as at collectors, connectors, or joints), and the possible need for additional analysis considerations (such as dynamic, 3-dimensional, bi-directional, or nonlinear). As noted in Section C12.3.2 of ASCE/SEI 7-16:

> "most seismic design provisions were derived for buildings that have regular configurations, but earthquakes have shown repeatedly that buildings that have irregular configurations suffer greater damage. This situation prevails even with good design and construction.
>
> There are several reasons for the poor behavior of irregular structures. In a regular structure, the inelastic response, including energy dissipation and damage, produced by strong ground shaking tends to be well distributed throughout the structure. However, in irregular structures, inelastic behavior can be concentrated by irregularities and can result in rapid failure of structural elements in these areas. In addition, some irregularities introduce unanticipated demands into the structure, which designers frequently overlook when detailing the structural system. Finally, the elastic analysis methods typically used in the design of structures often cannot predict the distribution of earthquake demands in an irregular structure very well, leading to inadequate design in the areas associated with the irregularity."

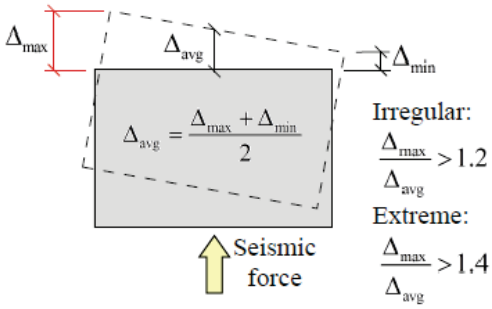

H1. Torsional stiffness

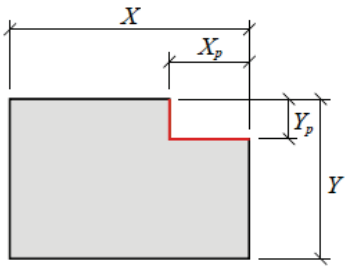

Irregular:

$\frac{X_p}{X} > 0.15$

and

$\frac{Y_p}{Y} > 0.15$

H2. Reentrant corner

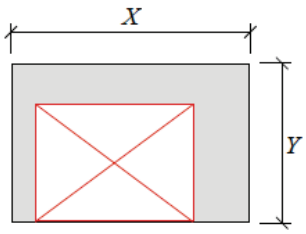

Irregular:

$A_{open} > \frac{1}{2} XY$

H3. Diaphragm discontinuity

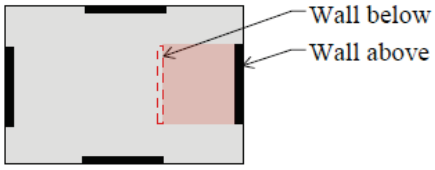

H4. Out-of-plane offset

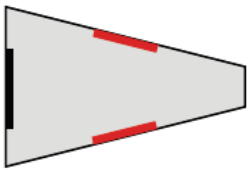

H5. Nonparallel system

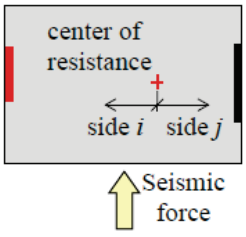

Irregular:

$\frac{\max DCR_i}{\max DCR_j} < 0.67 \text{ or } > 1.5$

H6. Torsional strength

Figure 2-10 Horizontal irregularities.

V1. Soft Story (Stiffness)

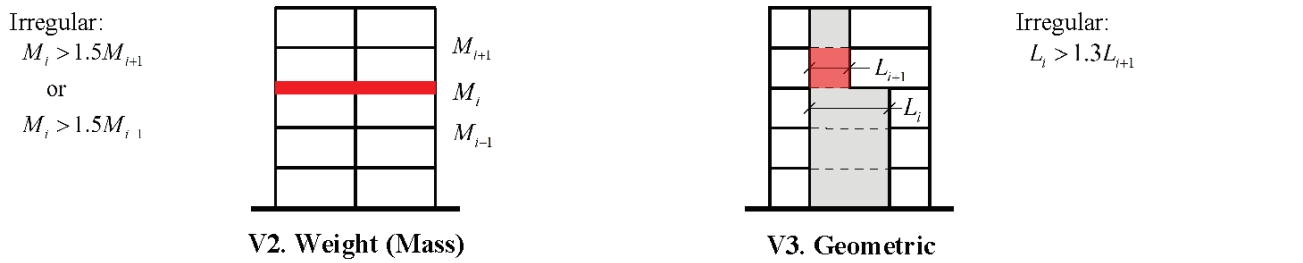

V2. Weight (Mass) **V3. Geometric**

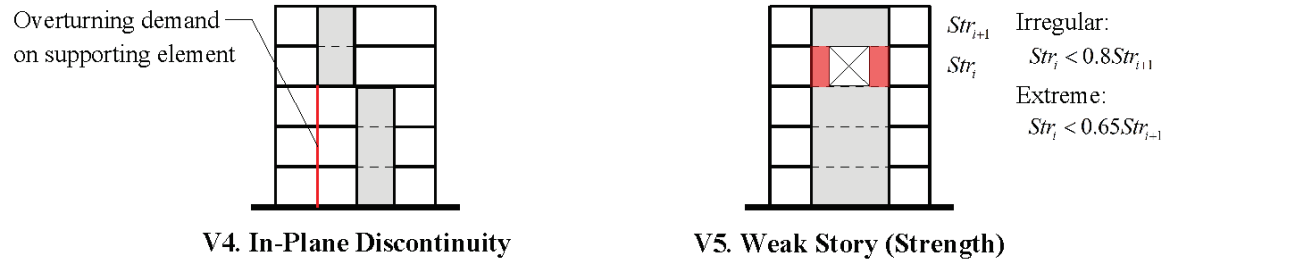

V4. In-Plane Discontinuity **V5. Weak Story (Strength)**

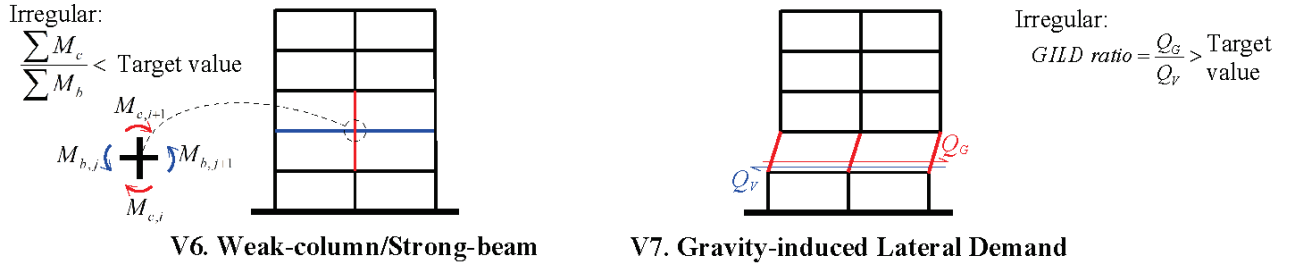

V6. Weak-column/Strong-beam **V7. Gravity-induced Lateral Demand**

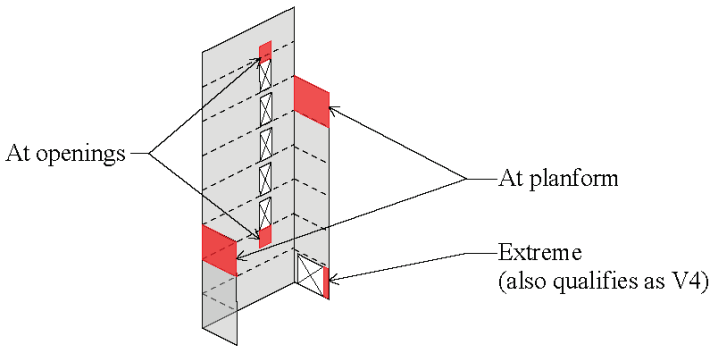

V8. Wall Discontinuity

Figure 2-11 Vertical irregularities.

A summary of key performance concerns for each irregularity is as follows:

Torsional (stiffness) irregularity [H1]. Twisting response of a building with this irregularity cannot be captured directly using 2-dimensional analysis in orthogonal plan directions. That twisting produces increased deformation demands at the perimeter, which could cause failure of gravity load resisting elements precipitating collapse. Force demands at the interface of horizontal and vertical elements of the seismic-force-resisting system may also be greater than those in a building without significant twisting response.

Reentrant corner irregularity [H2]. The projecting wings of the floor may respond somewhat independently, with an opening/closing or flapping motion, during an earthquake. This independent response can generate additional demands on the horizontal and vertical elements in the seismic-force-resisting system, particularly near the reentrant corner.

Diaphragm discontinuity irregularity [H3]. Significant differences in stiffness between portions of a diaphragm at a level may cause a change in the distribution of seismic forces to the vertical components and may create torsional forces not accounted for in the distribution normally considered for a regular building. Concentration of forces at the boundaries of the openings must be resolved in the design. Where the triggering condition is a change in diaphragm stiffness from one story to the next, the apparent concern is redistribution of forces, which would not be captured in typical seismic analyses idealizing the diaphragm as fully rigid or fully flexible.

Out-of-plane offset irregularity [H4]. The response parameters used in seismic design are based on the characteristics of the vertical elements of the seismic-force-resisting system. Where there is an out-of-plane offset, the horizontal elements that transfer story shears may be subjected to much greater demands than predicted by typical seismic analyses.

Nonparallel system irregularity [H5]. Where the vertical elements of the seismic-force-resisting system are not orthogonal to each other, response cannot be captured directly using 2-dimensional analysis in orthogonal plan directions.

Torsional strength irregularity [H6]. Where inelastic response can concentrate on one side of a building, linear elastic analysis may not reflect the resulting increases in deformation on the weak side. The increased twist could cause lateral- or gravity-load resisting elements to fail precipitating collapse.

Soft story irregularity [V1]. The simple static analysis that is the basis of the equivalent lateral force (ELF) procedure assumes a linear displaced shape

leading to reasonably uniform distribution of inelastic behavior. Where one story is much softer than adjacent stories dynamic amplification in the response should be considered.

Weight (mass) irregularity [V2]. Since the ELF procedure assumes a linear displaced shape, the concern is that significant variations in mass could cause an unanticipated increase of displacement at the affected story leading to a concentration of inelastic response and possible collapse.

Vertical geometric irregularity [V3]. This irregularity represents a qualitative indicator of systems that could have a non-uniform distribution of stiffness or strength, for which the load pattern assumed in the ELF procedure could be inaccurate.

In-plane discontinuity irregularity [V4]. The response parameters used in seismic design are based on continuous vertical elements of the seismic-force-resisting system with well distributed inelastic response. Where there is an in-plane discontinuity, overturning demands on the supporting elements may be much greater than those predicted by a linear elastic analysis using forces reduced by the response modification coefficient, R.

Weak story irregularity [V5]. Buildings with a weak story tend to develop all of their inelastic behavior and related damage at the weak story, increasing the likelihood of collapse.

Story mechanism: weak-column/strong-beam [V6]. Since the response parameters used in seismic design assume inelastic response that extends across multiple stories, moment frames should be proportioned to avoid premature yielding of all the columns at a particular story. Where inelastic response can concentrate at a single story, a column failure mechanism can lead to collapse.

Gravity-induced lateral demand [V7]. Where the inclination of gravity-load-resisting elements induces significant sustained lateral demands on the seismic-force-resisting system, there is concern that ground shaking could cause biased inelastic displacement, ratcheting in successive cycles of response, leading to collapse. As shown in Figure 2-11, the metric used to assess gravity-induced lateral demand is the ratio of gravity-induced story shear (Q_G) to story shear capacity (Q_V).

Wall discontinuity [V8]. Story-by-story analysis, as is commonly used in design of reinforced concrete walls, may not identify discontinuities that can concentrate damage during inelastic response. For instance, the panel zones within solid wall segments above and below a vertical stack of openings are subject to much higher stresses than simple analyses would indicate. Where

openings are close to the end of a wall (V4 irregularity), amplified overturning demands may cause poor performance in the small supporting pier. The response parameters used in seismic design are based on continuous vertical elements of the seismic-force-resisting system with well distributed inelastic response. Where the plan form of the wall changes dramatically, shear lag effects for flanged sections should be included in the design.

Sections 12.3.2 and 12.3.3 of ASCE/SEI 7-16 require classification of structures as regular or irregular, based on quantitative triggers, and set forth a series of requirements for irregular structures, including the analysis used to proportion the structure, design considerations for strength and stiffness, forces used in detailing, and system prohibitions.

The irregularity-related code requirements in ASCE/SEI 7-16 depend on the Seismic Design Category (SDC) to which a structure is assigned, ranging from few requirements in SDC B to system prohibitions in SDC E and F. Table 2-2 and Table 2-3 summarize quantitative triggers and code requirements, by SDC, for all 14 irregularities considered in this report.

Table 2-2 Code Requirements for Horizontal Structural Irregularities, by Seismic Design Category

Requirements	H1 Torsional (Stiffness)	H2 Reentrant Corner	H3 Diaphragm Discontinuity	H4 Out-of-Plane Offset	H5 Nonparallel System	H6 Torsional Strength
Quantitative trigger	Drift ratio > 1.2 (1.4, extreme)	Projection > 15% plan dimension	Opening area > 50%			maxDCR_i/ maxDCR_j > 1.5
Analysis						
3-D analysis required	B, C, D, E, F			B, C, D, E, F	B, C, D, E, F	
ELF prohibited	D, E, F					
Consider orthogonal effects					C, D, E, F	
Nonlinear analysis required				ASCE/SEI 41-17[(1)]		ASCE/SEI 41-17[(1)]
Design						
Amplify accidental torsion	C, D, E, F					
Assess drift at perimeter	C, D, E, F					
Overstrength forces at discontinuous elements				B, C, D, E, F		
Detailing						
Increase collector and diaphragm connector forces	D, E, F	D, E, F	D, E, F	D, E, F		
Other						
Extreme prohibited	E, F					

[(1)] Seismic Design Categories are not used in ASCE/SEI 41-17.

Table 2-3 Code Requirements for Vertical Structural Irregularities, by Seismic Design Category

Requirements	V1 Soft story	V2 Weight (mass)	V3 Vertical geometric	V4 In-plane	V5 Weak story	V6 Weak-column/ strong-beam	V7 Gravity-induced lateral demand	V8 Wall discontinuity
Quantitative trigger	Stiffness < 70% story above (60%, extreme); or < 80% 3-stories above (70%, extreme)	Mass > 150% adjacent	SFRS width > 130% adjacent		Strength < 80% story above (65%, extreme)	$\Sigma M_c / \Sigma M_b$ < target value	Q_G/Q_V > target value	
Analysis								
ELF prohibited	D, E, F	D, E, F	D, E, F					
Nonlinear analysis required				ASCE/SEI 41-17	ASCE/SEI 41-17			
Design								
Overstrength forces at discontinuous elements				B, C, D, E, F				
Detailing								
Increase collector and diaphragm connector forces				D, E, F				
Other								
Prohibited					E, F			
Extreme prohibited	E, F				D, E, F			

2.3 Treatment of Irregularities in this Report

From among the identified conditions, structural irregularities and configuration issues that are most likely to lead to increased collapse potential were identified. Most building collapses in past earthquakes have been associated with excessive torsional response (H1 and/or H2), soft or weak stories (V1 or V5), or story mechanisms for moment frame systems (V6). Analytical studies to assess collapse safety explicitly for buildings with these irregularities were performed and are presented in this report.

Published research suggests that mass irregularity (V2) does not necessarily result in increased inelastic demands, and the collapse mode is still similar to that for the base case (with identical mass at all stories). Analytical studies to

assess collapse safety and global behavior of systems with this condition are included in this report.

U.S. codes have not yet addressed gravity-induced lateral demands. The work reported in Dupuis et al. (2014), which led to provisions in the *National Building Code of Canada*, is limited to shear wall buildings and does not include assessment of relative collapse probability. This report includes analytical studies of steel and reinforced concrete moment frame systems with gravity-induced lateral demands (V7) to test whether it is advisable to add a corresponding structural irregularity to U.S. codes.

Some irregularities (H2, H3, H4, V4, V8) and configuration requirements (such as those for chords and collectors) reflect load path issues that are particularly sensitive to the specific structure, are usually associated with earthquake damage but not collapse, and are not well suited to quantification across a broad design space of archetypes. This report only includes discussion for these irregularities (see Chapter 7).

As currently written, application of ASCE/SEI 7-16 Section 12.3.3.4 triggers global design remedies (amplification of collector and connection forces for the entire structure) in response to local configuration irregularities (such as items H2 and H3); this report recommends improvements to this code requirement.

Items H5 and V3 are not irregularities as defined in this report as they are not generally associated with poor structural performance. Instead, they are codified as "irregularities" since two-dimensional application of the equivalent lateral force procedure may not adequately characterize their response. The code remedy of requiring three-dimensional dynamic analysis is considered sufficient, so further study is not warranted.

Other configuration-related design issues, such as distributing load in steel braced frame systems between tension and compression members, are best addressed (as currently) in the material standards. Such issues are outside the scope of this report.

The analytical studies focus primarily on issues related to design requirements for new buildings. Although some real buildings include multiple irregularities that could interact, the analyses of this project treat irregularities separately, just as they are defined independently in codes. Other variations in configuration, such as vertical or horizontal combinations of framings systems, which are treated in Sections 12.2.2 and 12.2.3 of ASCE/SEI 7-16, could also affect collapse probability. Except for the mixed system results reported in Chapter 4, such combinations are beyond the scope of this report.

Chapter 3
Archetype Design, Modeling, and Analysis Approach

This chapter provides an overview of the approach used to design, model, and analyze the building archetypes. This process was used for both the baseline archetypes and the variant archetypes that were used to gauge the effects of the various irregularities and related design provisions on building performance. The design, modeling, and analysis approach for the "simplified" three-dimensional archetypes that were used to study torsional irregularities is uniquely different and is described separately in Chapter 4 and Appendix A.

3.1 Scope of Analytical Studies

For the eight classes of irregularities that were addressed analytically (H1, H6, V1, V2, V5, V6, V7, V8), it is necessary to make appropriate selections of seismic-force-resisting systems (SFRSs), including quality (ordinary or special), building height, ground motion intensity (e.g., Seismic Design Category B or D), analysis method used in design, gravity load level, and degree of irregularity. Table 3-1 shows the SFRSs and building heights used to study each irregularity. Table 3-2 outlines the parameters varied in the designs and detailed analytical studies.

The detailed studies start with development of designs for regular "baseline" buildings and continue with the introduction of irregularities to the baseline buildings separately (as opposed to designing real buildings with multiple irregularities). This allows the development of a broad design space across a wide range of the parameters of interest, rather than a smaller set of anecdotal observations.

Baseline archetypes were designed using Special SFRSs for Seismic Design Category (SDC) D and Ordinary systems for SDC B. Initial designs (without configuration irregularities) were prepared in accordance with all current U.S. code requirements for new buildings. Modified systems were designed according to code requirements including requirements triggered by the configuration irregularity, but often ignoring prohibitions that may result due to the configuration irregularity (e.g., the prohibition of the equivalent lateral force procedure for buildings with weight (mass) irregularity). In some

cases, additional designs that do not comply with irregularity-related code requirements were also studied. This permits assessment of both the significance of the irregularity to building performance and the effectiveness of code remedies in producing desirable changes in performance.

Table 3-1 Systems Used to Study Structural Irregularities

Structural Irregularities	Systems for Study, # stories			
	RC Moment Frame	RC Shear Wall	Steel Moment Frame	Wood Shear Wall
H1. Torsional (stiffness) irregularity	8, 12	8		2
H2. Reentrant corner irregularity				
H3. Diaphragm discontinuity irregularity				
H4. Out-of-plane offset irregularity				
H5. Nonparallel system irregularity				
H6. Torsional strength irregularity	12			2
V1. Soft story irregularity	4,8,12, 20	8,12		
V2. Weight (mass) irregularity	20		3,20	
V3. Vertical geometric irregularity				
V4. In-plane discontinuity irregularity				
V5. Weak story irregularity	4,8,12, 20			
V6. Story mechanism: weak-column/strong-beam	4,8,12		3,9,20	
V7. Gravity-induced lateral demand	12		20	
V8. Wall discontinuity		8,12		

Designs were completed for Seismic Design Categories D_{max} and B_{max}, using general code-defined spectra for Site Class C and Risk Category II. Site Class C was selected, rather than the default Site Class D, to avoid the stopgap requirements in Section 11.4.8 of ASCE/SEI 7-16, *Minimum Design Loads and Associated Criteria for Buildings and Other Structures* (ASCE, 2017a), which would either complicate this general study by requiring site-specific ground motions or bias the findings by applying the scaling adjustments permitted in Exception 2 of that section. Additionally, the FEMA P695 analysis method used in this study (FEMA, 2009) is tied to this target spectrum. In the collapse capacity evaluations of the building designs, the FEMA P695 method is used, along with the FEMA P695 far-field ground

motion set being used for most analyses. For torsional irregularity studies, an additional set of FEMA P695 analyses was performed using pulse motions from the near-field record set.

Table 3-2 Parameters Varied in Designs and Detailed Analytical Studies

Parameter	Range
Seismic Design Category (SDC)	B_{max}: S_{DS} = 0.32, S_{D1} = 0.132 D_{max}: S_{DS} = 1.50, S_{D1} = 0.60
Seismic-Force-Resisting System (SFRS)	Reinforced Concrete Special/Ordinary Moment Frames (RC SMF and RC OMF) Reinforced Concrete Shear Walls (RC SW) RC SMF + RC SW Steel Moment Frames (SMF and OMF) Wood Shear Walls (simplified)
Seismic-Force-Resisting System quality	Ordinary Special
Building height	Low- to mid-rise for horizontal irregularities Mid- to high-rise for vertical irregularities
Analysis method used in design	Equivalent Lateral Force (ELF) Modal Response Spectrum Analysis (MRSA)
Gravity load level	Low High
Degree of irregularity	Regular to highly irregular

Designs are based on the results of modal response spectrum analysis (MRSA) or the equivalent lateral force (ELF) procedure found in Chapter 12 of ASCE/SEI 7-16. These variations permit assessment of how analysis methods used in design may predict different performance and how designs informed by different analysis methods may actually perform differently. Where MRSA was used in design, the scaling requirements of ASCE/SEI 7-16 (to 100% of the ELF base shear) were followed. All designs use fixed base models, with no direct consideration of foundation flexibility, as permitted by Section 12.7.1 of ASCE/SEI 7-16. Generally, the designs have variations in proportioning and a degree of refinement or optimization that is representative of typical design practice. In a few cases additional designs with highly optimized proportioning are prepared to assess the sensitivity of such "barely code-conforming" conditions.

Consistent with the performance criteria outlined in Section 1.3.1.3 of ASCE/SEI 7-16, the MCE_R probability of collapse is the primary metric of the FEMA P695 methodology for evaluation of the collapse capacity of the archetype model of interest. However, the adjusted collapse margin ratio (*ACMR*) is better suited for comparing the relative collapse performance of a given SFRS with and without a particular irregularity. This study compares

the ratio of the values of the *ACMR* parameter for a given SFRS with and without a particular irregularity to 1.0.

Although collapse is the primary metric of interest, other data were retained for use in this and future projects. Table 3-3 shows the metrics that were monitored in the detailed analytical studies performed using the FEMA P695 method.

Table 3-3 Metrics Monitored in Detailed Analytical Studies

Metric	Detail
Collapse	Simulated (analytically) Non-simulated (inferred from other metrics)
Story drift Floor displacement Residual story drift	Maximum and average for Floor plate and framing lines at 1/3 MCE, 2/3 MCE, MCE
Story twist (in three-dimensional models)	Maximum and average at 1/3 MCE, 2/3 MCE, MCE
Floor acceleration Floor velocity	Maximum and average for Multiple points
Ductility demand	Maximum and average at 1/3 MCE, 2/3 MCE, MCE
Relevant force-demand parameters (such as column axial load and moment)	Maximum and average at 1/3 MCE, 2/3 MCE, MCE

3.2 Archetype Configurations and Designs

The majority of the archetype buildings are composed of three different SFRSs: (1) steel moment frames; (2) reinforced concrete moment frames; (3) reinforced concrete shear walls. The intent of the archetype designs was to create structural models that represent realistic modern structures. Therefore, design assumptions and structural properties that are considered to be a good representation of the common building stock and new building design practices were selected. Detailed information about the configurations of the baseline designs for each system type is given in Sections 3.2.1 through 3.2.3. Modifications to the baseline configurations to introduce configuration irregularities are outlined in this chapter, but described in detail in Chapters 4 through 6. The baseline designs served as a basis against which to compare the impact of the irregularities studied.

3.2.1 Steel Moment Frame Archetypes

The baseline steel moment frames reflect the three building geometries shown in Figure 3-1, Figure 3-2, and Figure 3-3, and match the model buildings from Boston and Los Angeles found in Appendix B of FEMA 355C, *State of the Art Report on Systems Performance of Steel Moment Frames Subject to Earthquake Ground Shaking* (FEMA, 2000b). Baseline designs for 3-, 9-, and 20-story buildings were developed for SDC D_{max} and SDC B_{max}; these are summarized in Table 3-4. Table 3-5 summarizes the design values used to develop the steel moment frame archetypes and Table 3-6 documents an example 3-story special moment frame (SMF) design for SDC D_{max}. A comprehensive discussion of the design process and resulting frame designs is provided in Appendix C.

Gravity and wind loading criteria match those used in the earlier post-Northridge earthquake analyses documented in FEMA 355C. The baseline designs reflect ASCE/SEI 7-16 and AISC 341-10, *Seismic Provisions for Structural Steel Buildings* (AISC, 2010b), requirements. Ordinary moment frames (OMFs) are used for SDC B_{max} and special moment frames with reduced-beam sections are used for SDC D_{max}.

The baseline buildings for SDC D_{max} are governed by seismic forces and have been designed to satisfy a story drift limit of 0.02; note that Table 12.12-1 of ASCE/SEI 7-16 allows a drift limit up to 0.025 for moment frame buildings four stories or less, where nonstructural components are designed to accommodate the extra drift, but this option was not used in the present study. The baseline design base shears for SDC B_{max} are governed by wind forces from ASCE/SEI 7-16 for the 9- and 20-story buildings, while the base shear for the 3-story building is governed by seismic demands. Under service loads, the designs were checked to confirm that they satisfy a roof drift limit of $H/400$ using wind forces equivalent to a 50-year mean return period obtained from Appendix C of ASCE/SEI 7-16. Ultimately, wind demands controlled the final design of all SDC B_{max} buildings.

To study the relative collapse performance of buildings with vertical irregularities, 108 irregular designs were created by modifying the baseline steel moment frame archetypes. The separate modifications were made by:

- Increasing the mass of specific floors to introduce weight (mass) irregularity [V2].
- Modifying the minimum strong-column/weak-beam ratio used for design [V6].
- Introducing slanting columns at a given story to cause gravity-induced lateral demand [V7].

Chapter 6 describes in detail how each of these modifications are applied to the baseline archetypes and how their collapse resistance is affected as a result.

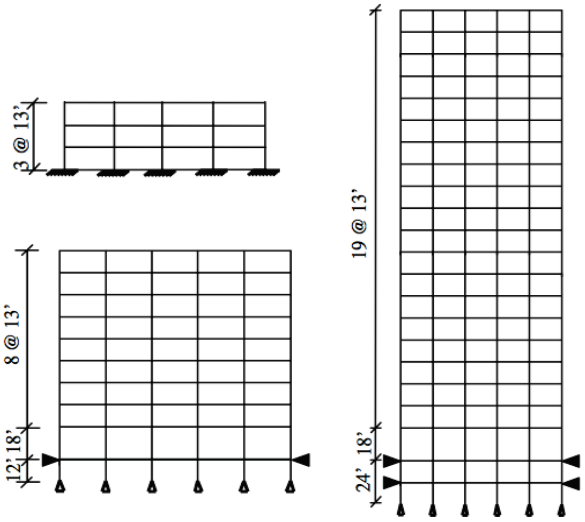

Figure 3-1 Building elevations for steel moment frames.

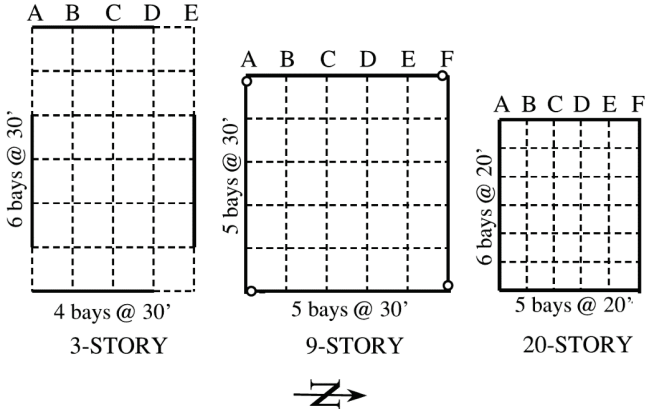

Figure 3-2 Seismic Design Category D steel building floor plans.

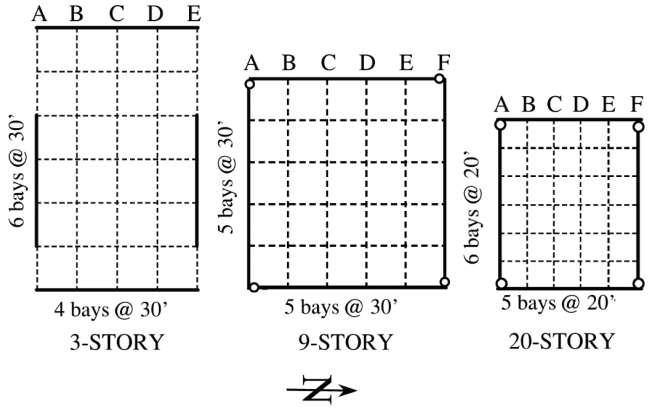

Figure 3-3 Seismic Design Category B steel building floor plans.

Table 3-4 Overview of Baseline Steel Moment Frame Building Designs

No. Stories	Frame Detail	SDC	Design Method	Period for Computing Design Forces ($C_u T_a$) [s]	Analytical Period [s][(1)]
3	OMF	B_{max}	ELF, MRSA	0.86	1.75, 1.93
3	SMF	D_{max}	ELF, MRSA	0.74	0.97, 1.46
9	OMF	B_{max}	ELF, MRSA	2.14	3.19, 3.19
9	SMF	D_{max}	MRSA	1.83	3.13
20	OMF	B_{max}	ELF, MRSA	3.98	4.23, 4.23
20	SMF	D_{max}	MRSA	3.40	4.54

(1) The reported analytical periods are from the linear structural design models, in the north-south direction. Where ELF and MRSA are used, the first listed value is for ELF. For designs governed by wind, ELF vs MRSA does not affect the fundamental period.

Table 3-5 Common Design Values Used for Steel Moment Frame Designs

Design Property	SDC B_{max}	SDC D_{max}
Short period design spectral acceleration, S_{DS}	0.32g	1.5g
One-second design spectral acceleration, S_{D1}	0.13g	0.6g
Response modification coefficient, R	3.5	8
Deflection amplification factor, C_d	3	5.5
Story drift limit (seismic)	2%	2%
Basic wind speed (strength, Exposure *B*)	130 mph	110 mph
Basic wind speed (service, Exposure *B*)	100 mph	85 mph
Roof drift limit (wind)	*H*/400	*H*/400
Risk Category	II	II
Floor dead load	96 psf	96 psf
Partition load (reduce by 50% for seismic mass)	20 psf	20 psf
Roof dead load	83 psf	83 psf
Roof dead load at penthouse	116 psf	116 psf
Live load	50 psf	50 psf
Roof live load	20 psf	20 psf

Table 3-6 Example Baseline Design Summary (3-Story Steel SMF)

3-Story Steel SMF, MRSA Design, SDC D_{max}								
Story/ Floor	Columns		Doubler Plates	Girder	Drift (%)		Moment Ratio	
	Exterior	Interior			Δ_X	Δ_Y	Exterior	Interior
Roof	W14×159	W14×176	No	W24×55	1.75	1.77	2.00	1.15
3rd	W14×159	W14×176	Yes	W27×94	1.86	1.88	1.89	1.09
2nd	W14×159	W14×176	Yes	W27×94	1.36	1.37	1.75	1.05

Note: Steel tonnage 2.81 psf (columns: 1.53 psf, beams: 1.28 psf)

3.2.2 Reinforced Concrete Moment Frame Archetypes

Concrete moment frame archetypes were designed to represent a modern commercial office structure using current design and construction practices for SDC B_{max} and SDC D_{max}, ranging from 4 to 20 stories. The baseline archetype design space is summarized in Table 3-7. Table 3-8 gives an overview of design parameters for designing the RC moment frames and Table 3-9 documents an example 4-story RC SMF design for SDC D_{max}. Summary design information for all RC moment frame archetypes is provided in Appendix D.

Table 3-7 Overview of Baseline RC Moment Frame Building Designs

No. Stories	Frame Detail	SDC	Design Method	Period for Computing Design Forces ($C_u T_a$) [s]	Analytical Period [s][(1)]
4	OMF	B_{max}	ELF	0.93	1.93
4	SMF	D_{max}	ELF	0.81	1.12
8	SMF	D_{max}	ELF	1.49	2.11
12	OMF	B_{max}	ELF	2.44	4.51
12	SMF	D_{max}	ELF	2.13	2.58
20	SMF	D_{max}	ELF, MRSA	3.36	3.66, 3.87

(1) The reported analytical periods are from the linear structural design models. Where ELF and MRSA are used, the first listed value is for ELF.

Table 3-8 Common Design Values Used for RC Moment Frame Designs

Design Property	SDC B_{max}	SDC D_{max}
Short period design spectral acceleration, S_{DS}	0.33g	1.5g
One-second design spectral acceleration, S_{D1}	0.13g	0.6g
Response modification coefficient, R	3	8
Deflection amplification factor, C_d	2.5	5.5
Story drift limit (seismic)	2%	2%
Basic wind speed (strength, Exposure *B*)	130 mph	-
Basic wind speed (service, Exposure *B*)	100 mph	-
Roof drift limit (wind)	*H*/400	-
Floor dead load	175 psf	175 psf
Roof dead load	140 psf	140 psf
Partition load	15 psf	15 psf
Live load	50 psf	50 psf
Roof live load	20 psf	20 psf
f'_c beams	4,000 psi	5,000 psi
f'_c columns	4,000 psi	7,000 psi
Reinforcing steel yield strength, f_y	60 ksi	60 ksi
Beam design stiffness	$0.35EI_g$	$0.35EI_g$
Column design stiffness	$0.7EI_g$	$0.7EI_g$

Table 3-9 Example Baseline Design Summary (4-Story RC SMF)

Level	Columns depth × width [tie spacing] (ρ_{total} , ρ_{sh})		Beams depth × width [hoop spacing] (ρ_{top} , ρ_{bot} , ρ_{sh})		Drift (%)	Moment ratio, $\sum M_c/\sum M_b$ Exterior (Interior)
	Exterior	Interior	Exterior	Interior		
4	26×22 [2.5] (0.0110, 0.0107)	26×22 [2.5] (0.0110, 0.0107)	24×18 [5] (0.0081, 0.0046, 0.0044)	24×18 [5] (0.0081, 0.0046, 0.0044)	1.2	1.16 (0.74)
3	26×22 [2.5] (0.0110, 0.0107)	26×22 [2.5] (0.0165, 0.0107)	24×18 [5] (0.0097, 0.0046, 0.0044)	24×18 [5] (0.0097, 0.0046, 0.0044)	1.5	1.96 (1.65)
2	30×22 [3.5] (0.0119, 0.0102)	30×22 [3.5] (0.0167, 0.0102)	34×20 [5] (0.0069, 0.0048, 0.0039)	34×20 [5] (0.0069, 0.0048, 0.0039)	1.2	1.37 (1.22)
1	30×22 [3.5] (0.0167, 0.0102)	30×22 [3.5] (0.0167, 0.0102)	34×20 [5] (0.0069, 0.0048, 0.0039)	34×20 [5] (0.0069, 0.0048, 0.0039)	1.0	1.89 (1.44)

Notes: ρ_{sh} is the area ratio of transverse reinforcement in the column or beam hinge region.
All dimensional units are in inches (e.g., column and beam sizes).

Story heights of the baseline RC moment frames are 15 feet at the first story and 13 feet at all other stories. Each has a 120 ft. by 120 ft. footprint with six bays in each direction and moment frames along the perimeter (see Figure 3-4). For simplicity, only three "typical" bays of the six-bay frame from one side of the building were designed and modeled. This is accomplished by designing a three-bay frame for half of the tributary weight and mass of the six-bay moment frame, except that overturning forces in the end columns are reduced to reflect the overturning forces in a six-bay frame. Since the nonlinear analysis models are two-dimensional, end columns were designed for uniaxial bending only—allowing for consistency between the design and analysis approaches. The concept of making a three-bay representation of a six-bay moment frame is consistent with the approach taken for analyzing RC moment frames in the original FEMA P695 studies (FEMA, 2009).

To study the relative collapse performance of buildings with vertical irregularities, 106 irregular designs were created by modifying the baseline RC moment frame archetypes. The separate modifications were made by:

- Increasing the mass of specific floors to introduce weight (mass) irregularity [V2].
- Adjusting story heights and strengths to introduce soft/weak story irregularities [V1/V5].
- Modifying the minimum strong-column/weak-beam ratio used for design [V6].

- Introducing slanting columns at a given story to cause gravity-induced lateral demand [V7].

Chapter 6 describes in detail how each of these modifications are applied to the baseline archetypes and how their collapse resistance is affected as a result.

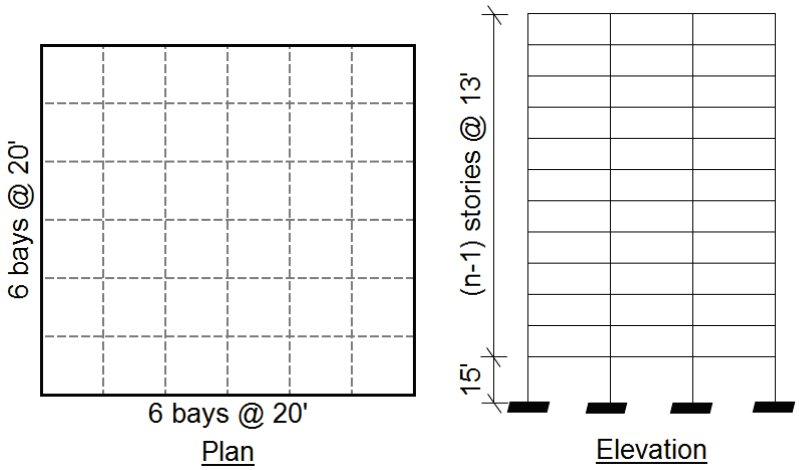

Figure 3-4 Plan and elevation of the RC moment frame archetypes.

3.2.3 Reinforced Concrete Shear Wall Archetypes

A set of five baseline RC wall designs were created, representing both special RC walls designed for SDC D_{max}, as well as ordinary RC walls designed for SDC B_{max} (Table 3-10). The designs cover two heights: 8 and 12 stories and are intended to represent a modern commercial office structure using current design and construction practices. Story heights are identical to the RC moment frame baselines—15 ft. at the first story and 13 ft. at all other stories. The archetypes employ a 120 ft. by 120 ft. footprint, (example shown in Figure 3-5). For 8-story buildings, lateral loads are resisted by two independent planar walls in each of two orthogonal directions; for 12-story designs, lateral loads are resisted by four (shorter) independent planar walls in each of two orthogonal directions. For D_{max} designs, earthquake demands control strength design, and wall length was determined by earthquake strength requirements; for B_{max} designs, wind demands control strength design, and wall length is controlled by earthquake drift limits. For all designs, walls are located such that the centers of stiffness and mass coincide.

Table 3-10 Overview of Baseline RC Wall Building Designs

Model ID	Number of Stories	Wall Detailing	SDC	Analysis Procedure
8-D-0-0-ELF	8	Special	D_{max}	ELF
8-D-0-0-MRSA	8	Special	D_{max}	MRSA
8-B-0-0-ELF	8	Ordinary	B_{max}	ELF
12-D-0-0-ELF	12	Special	D_{max}	ELF
12-B-0-0-ELF	12	Ordinary	B_{max}	ELF

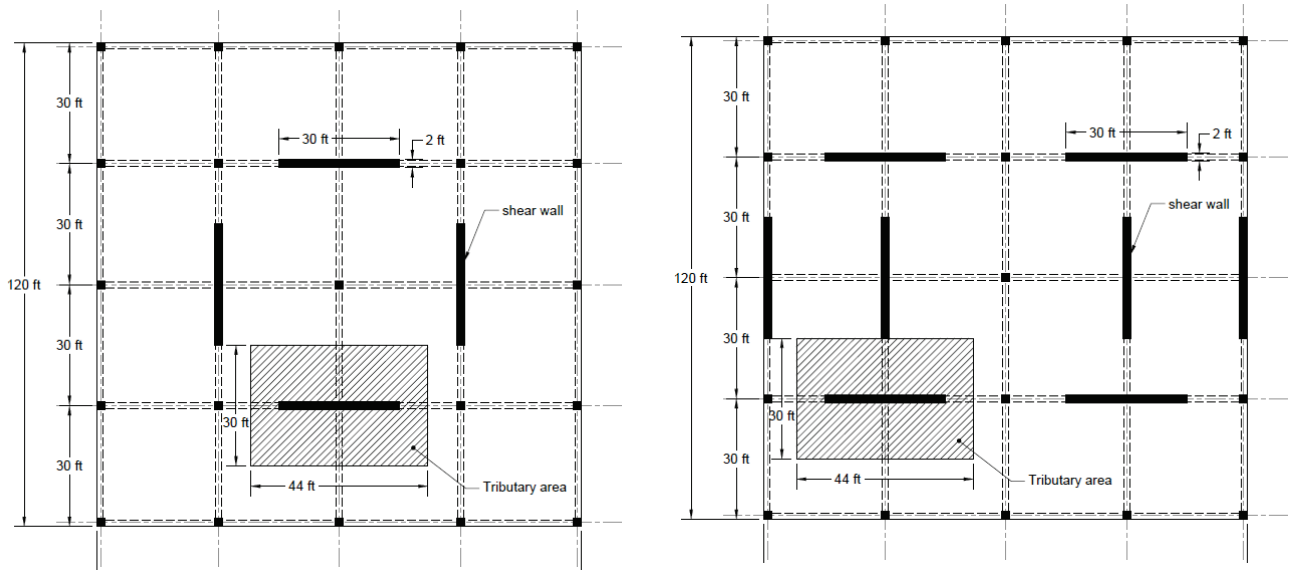

(a) 8-story building (b) 12-story building

Figure 3-5 Building prototype plans designed for D_{max} and B_{max} spectra for (a) 8-story buildings and (b) 12-story buildings. Wall length shown is for D_{max} designs; wall length is 20 ft. for B_{max} designs.

All RC wall building archetypes are designed according to ASCE/SEI 7-16 for concrete shear walls that are part of the building frame system; (i.e., $R = 6$ for special walls and $R = 5$ for ordinary walls). Four baseline archetypes were designed using the ELF procedure and an additional baseline design was created using the MRSA from Chapter 12 of ASCE/SEI 7-16. Walls with vertical irregularities were designed using both the ELF and MRSA procedures. Table 3-11 gives an overview of the common design properties that were used for the RC wall building designs. Summary design information for each archetype is in Appendix B.

To study the relative collapse performance of buildings with vertical irregularities, 19 irregular designs were created by modifying the archetype baselines discussed above. The baseline archetypes were modified to include stiffness irregularities resulting from openings located in the 1st, 1st and 2nd, and 5th (8-story buildings) or 8th (12-story buildings) stories. Openings were

sized to reduce story stiffness to 75% or 50% of the stiffness of the baseline building. Specifics for the designs analyzed for each irregularity appear Chapter 5.

Table 3-11 Common Design Values Used for RC Wall Designs

Design Property	SDC B_{max}	SDC D_{max}
Short period design spectral acceleration, S_{DS}	0.33g	1.5g
One-second design spectral acceleration, S_{D1}	0.13g	0.6g
Response modification coefficient, R	5	6
Deflection amplification factor, C_d	4.5	5
Story drift limit (seismic)	2%	2%
Basic wind speed (strength, Exposure *B*)	110 mph	-
Basic wind speed (service, Exposure *B*)	85 mph	-
Roof drift limit (wind)	H/400	-
Floor dead load	175 psf	175 psf
Roof dead load	140 psf	140 psf
Partition load	15 psf	15 psf
Live load	50 psf	50 psf
Roof live load	20 psf	20 psf
Concrete compressive strength, f'_c	5000 psi	5000 psi
Reinforcing steel yield strength, f_y	60 ksi	60 ksi
Wall stiffness used for MRSA	$0.5EI_g$	$0.5EI_g$

3.3 Structural Modeling of Archetype Buildings

Nonlinear structural models of the archetype buildings were developed to perform dynamic analysis and assess collapse resistance. The following sections describe the methods used to model the steel moment frame (Section 3.3.1), RC moment frame (Section 3.3.2), and RC wall (Section 3.3.3) building systems. Each of these systems were modeled with two-dimensional planar models for conducting nonlinear dynamic analyses in OpenSees.

Building mass tributary to moment frames and walls are lumped at the joint nodes and wall nodes, respectively. For analysis, an expected mass of 1.05 times the dead weight was considered. Raleigh damping, anchored to the first and third modes of vibration, was implemented; however, the stiffness proportional damping was applied only to linear elements, in order to avoid unintended damping forces that may develop in nonlinear elements (Charney, 2008). The steel and concrete models had damping ratios of 2% and 5% of critical, respectively.

For all models, the gravity system was represented by a linear elastic *P*-Delta leaning column, in order to model the destabilizing second-order geometric effects, but without adding any strength or stiffness from the gravity system. The *P*-Delta leaning column provided no lateral resistance and was connected to SFRS elements via stiff axial-only elements. Inclusion of the *P*-Delta leaning column enabled simulation of base moment demand and story shear associated with gravity load acting through large lateral displacements. Geometric nonlinearity was simulated using the "Linear with P-Delta" transformation rules in OpenSees.

Gravity loads were applied to the SFRS elements and to the *P*-Delta column, based on the tributary areas of each. Per FEMA P695, the load combination representing expected gravity loads, $1.05D + 0.25L$, was used to compute the vertical load effects. Gravity loads directly carried by the frames were distributed on the beams. Gravity loads carried by the wall were determined by the tributary area assigned to the wall. The remaining gravity load, which is carried by the building's gravity system, was applied to the *P*-Delta leaning column.

3.3.1 Steel Moment Frame Archetypes

3.3.1.1 System Modeling

Steel moment frames were modeled as recommended in NIST GCR 17-917-46v2, *Guidelines for Nonlinear Structural Analysis for Design of Buildings, Part IIa – Steel Moment Frames* (NIST, 2017). Nonlinear models of the moment frame archetype buildings were constructed in OpenSees using the lumped plasticity method. The lumped plasticity models consist of linear elastic beam and column elements, joined by nonlinear elements where plastic deformations are expected to concentrate, as depicted in Figure 3-6. Nonlinear behavior was simulated with plastic hinges at the ends of beams and columns and in the joint panel zones as well. In the 3-story steel moment frames, the rotational stiffness of the foundation was modeled with a rotational spring that approximates a grade-beam; however, it had significantly higher stiffness than the first-story columns, so column behavior was similar to what would be observed for a fixed base condition. The 9- and 20-story steel frames have basement levels below the first story, and the column connection at the bottom of the basement was modeled as pinned (it is also designed as pinned).

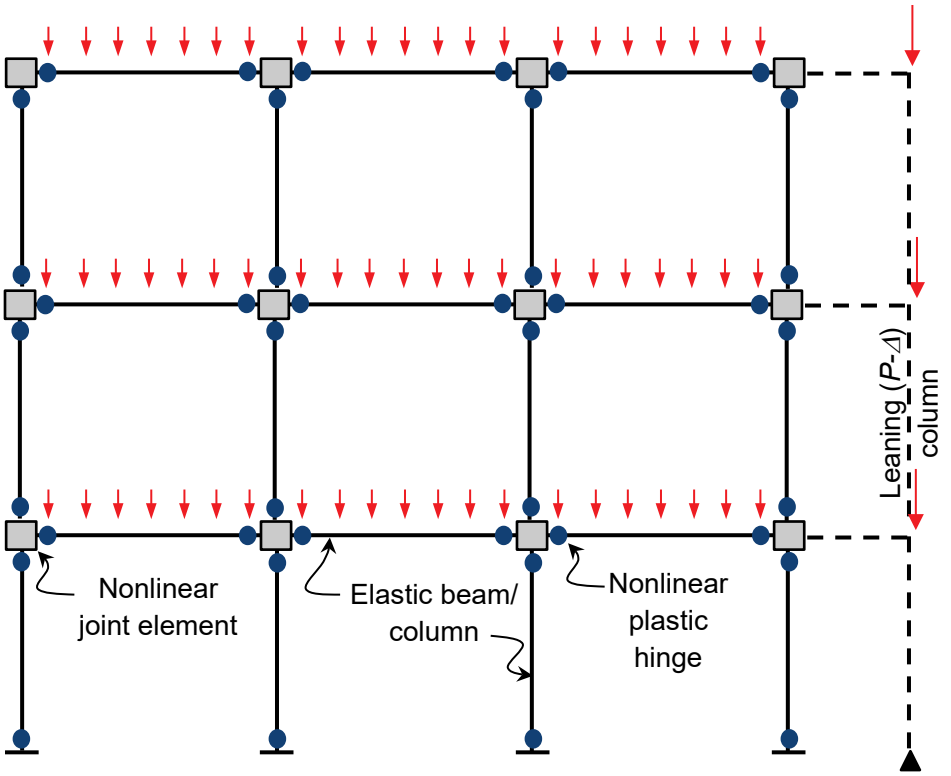

Figure 3-6 Schematic of a lumped plasticity nonlinear frame model (without basement levels).

3.3.1.2 Modeling of Beam and Column Components

Nonlinear beam and column hinges were modeled with the Modified Ibarra Krawinkler Deterioration Model in OpenSees (Ibarra et al., 2005; Lignos and Krawinkler, 2009), illustrated in Figure 3-7. Initial backbone properties were calculated with the equations recommended by Chapter 4 of NIST GCR 17-917-46v2 and cyclic deterioration parameters were computed from Lignos and Krawinkler (2011). For calculating the nonlinear properties of the beams and columns, the actual yield strength of the steel was assumed to be 10% higher than the nominal yield strength (per NIST GCR 17-917-46v2 recommendations). Properties of the beams that were used to determine the monotonic backbone are as follows: (1) the expected material yield strength; (2) plastic section modulus (Z); (3) web and flange depth-to-thickness ratios; (4) the ratio of beam depth to effective length; (5) composite action; and (6) potential for lateral torsional buckling. Additionally, backbone properties of the reduced beam sections (RBSs) were modified to account for plastic hinge offsets. That is, strength was increased and rotation capacity decreased to account for the actual hinges occurring at the location of the reduced beam section rather than the face of the joint (where they are modeled).

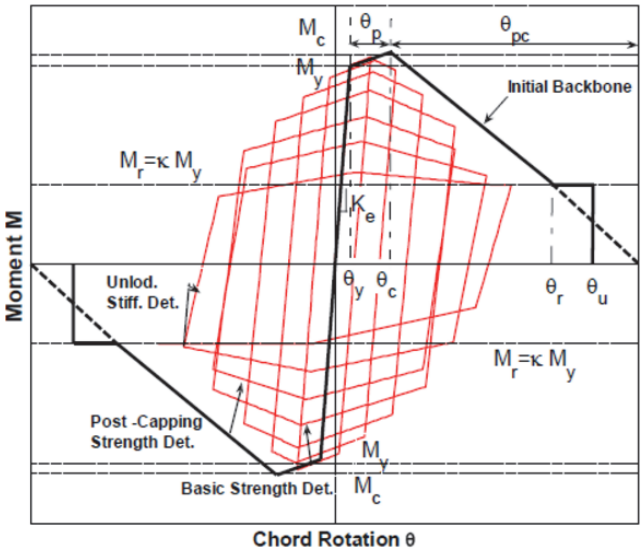

Figure 3-7 Modified Ibarra Krawinkler Deterioration Model (Image from Lignos et al., 2011).

Composite action was not considered for the design of the beams, but it was considered in the nonlinear analysis, because steel moment frames are commonly connected to a diaphragm. The controlling mechanism for composite action of the slabs is yielding of the shear studs, which are assumed to be ¾-inch diameter, 65 ksi steel, placed at 12 inches on center. Composite action was also considered for computing the effective moment of inertia of the linear beam elements. Plastic hinge behavior of an example beam is illustrated in Figure 3-8.

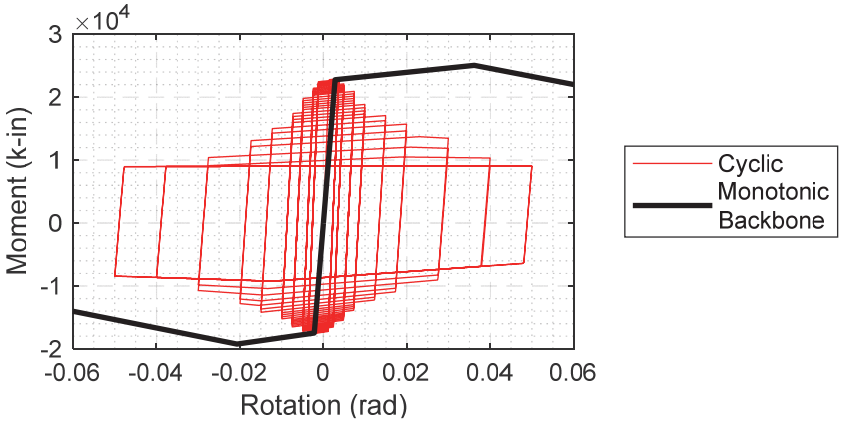

Figure 3-8 Example cyclic behavior of a W30×108 RBS beam with composite slab action. Moment increase (and rotation decrease) to account for plastic hinge offsets in the actual building are approximately 12%.

Plastic hinge behavior of an example column is illustrated in Figure 3-9. The monotonic backbone properties of the column hinges were computed according to Chapter 4 of NIST GCR 17-917-46v2. Column backbones tend

to be more ductile and deteriorate less quickly because they are more compact than the beams. An additional factor that was used for determining column hinge strengths is the ratio of the expected axial load to the yield axial load (P_g/P_y), which affects both strength and rotation capacity. However, axial load ratios of the perimeter frame columns tend to be low ($P_g/P_y < 0.1$), so axial load effects are generally small.

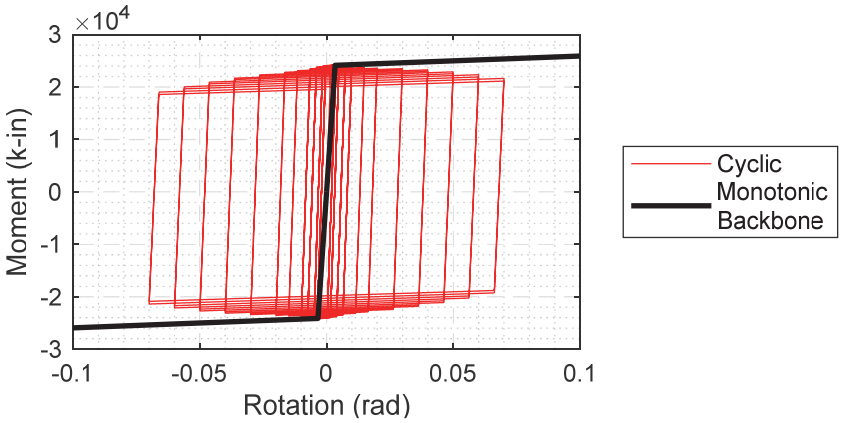

Figure 3-9 Example cyclic behavior of a W14×193 column. Ultimate rotation (not shown on figure) is 0.15 radians.

3.3.1.3 Modeling of Joint Panel Zones

Plastic deformation of the joint panel zones is expected to occur in the steel moment frames, particularly the ordinary moment frames. Panel zones were modeled with the Joint2D element (Altoontash, 2004) in OpenSees with nonlinear behavior idealized as trilinear without cyclic deterioration or isotropic hardening, based on Gupta and Krawinkler (1999). Figure 3-10 illustrates the idealized relationship between panel zone shear force and distortion. Panel zone moment (M) and shear (V) are related as follows:

$$M = Vd_b$$

in which d_b is the depth of the beam. The yield shear force (V_y) is given as follows:

$$V_y = 0.60F_y d_c t_p$$

in which F_y is the expected steel yield strength, d_c is the depth of the column, and t_p is the thickness of panel zone. The yield distortion of the panel (γ_y) was computed as follows:

$$\gamma_y = \frac{F_y}{\sqrt{3}} G$$

in which G is the modulus of rigidity of steel. The fully plastic shear strength occurs at a distortion four times γ_y and was determined as follows:

$$V_p = V_y\left(1+\frac{3b_c t_{cf}^2}{d_b d_c t_p}\right)$$

in which b_c and t_{cf} are the width and thickness of the column flange. The strain hardening parameter (α) was taken as 1.5%.

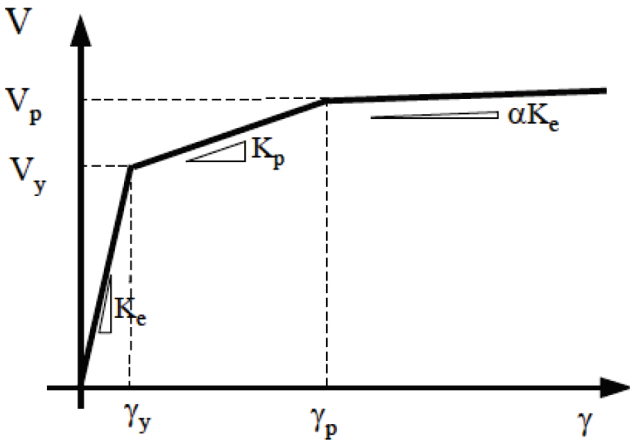

Figure 3-10 Idealized panel zone shear force deformation relationship (Gupta and Krawinkler, 1999).

3.3.2 Reinforced Concrete Moment Frame Archetypes

3.3.2.1 System Modeling

Reinforced concrete moment frames were modeled with the lumped plasticity method. They use the same elements as the steel moment frames (i.e., linear beam-columns, nonlinear plastic hinges, nonlinear joint elements, as shown in Figure 3-6), but with material models calibrated to simulate RC moment frame behavior. Like the 3-story steel frames, the rotational stiffness of the foundation was modeled with a rotational spring that approximates a grade-beam and footing; however, it had significantly higher stiffness than the first-story columns, so column behavior was closer to what would be observed for a fixed base condition.

3.3.2.2 Modeling of Beam and Column Components

Nonlinear beam and column hinges were idealized with trilinear backbones having peak-oriented hysteretic response and cyclic deterioration, using the model developed by Ibarra et al. (2005), shown in Figure 3-11. The backbone and hysteretic properties of the nonlinear beam-column hinges were computed from empirical relationships developed by Haselton et al. (2008) based on the design properties of the beams and columns (i.e., concrete strength, element dimensions, axial load ratio, and reinforcement detailing). The expected axial load ratio was used to calibrate column hinge backbones, but it was not updated throughout the analysis, therefore dynamic

axial-flexure interaction effects were ignored. This simplification should minimally affect the performance for two reasons: (1) the columns tend to have axial load ratios less than 0.2; and (2) increases in axial force at one end of the frame coincides with decreases in axial force at the other end, so axial load effects at the two ends of a frame counteract one another. An example hysteresis of a concrete column is shown in Figure 3-12.

Flexural stiffness of the linear beam-column elements was computed using an effective moment of inertia based on empirical equations recommended by Haselton et al. (2008). The effective moment of inertia can range from 35% to 80% of the gross moment of inertia and depends upon member dimensions and axial load ratio.

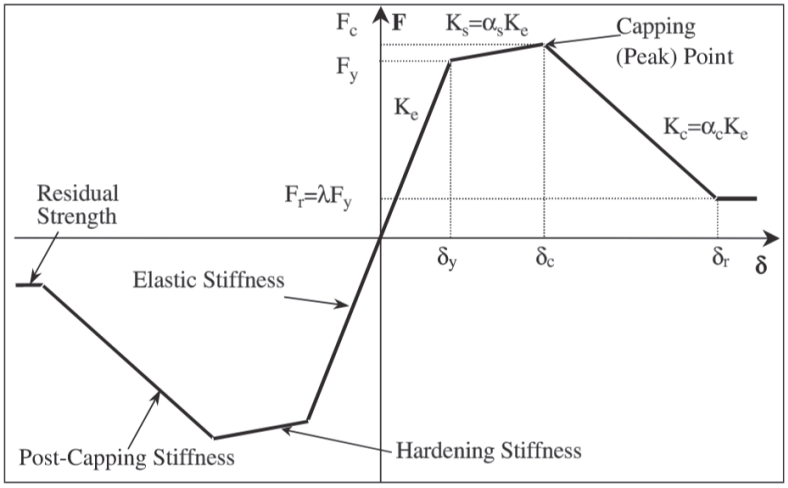

Figure 3-11 Backbone properties of the Ibarra et al. (2005) material model (Image from Ibarra et al., 2005).

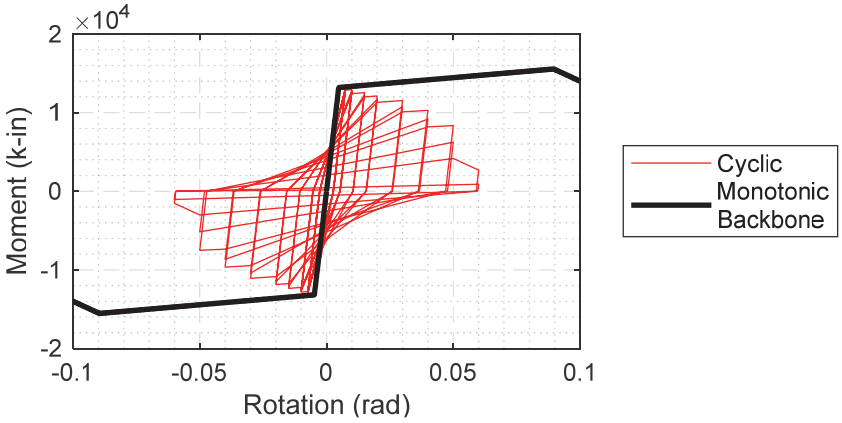

Figure 3-12 Example hysteretic properties of a 30 in. by 26 in. RC column with low axial load ratio. Total longitudinal reinforcement ratio and shear reinforcement ratio are 0.014 and 0.01, respectively.

3.3.2.3 Modeling of Joint Panel Zones

Joint panel zones were modeled with the Joint2D element (Altoontash, 2004) in OpenSees. The panel zones were modeled as linear for the RC SMFs, because special detailing requirements relating to the size, confinement, and reinforcement of joints are expected to prevent joint failure. Ordinary moment frame joints were modeled with the pinched Ibarra material model (Ibarra et al., 2005). Nonlinear properties of the joints were determined using a procedure developed by Lowes and Altoontash (Lowes et al., 2004; Altoontash, 2004), which is the same procedure used for OMF joints in FEMA P695. A detailed summary and background for the procedure for determining OMF joint properties is documented by Liel (2008).

Strength of the OMF joints were computed according to ACI 318-14, *Building Code Requirements for Structural Concrete* (ACI, 2014), using the joint area and concrete strength. Initial stiffness was based on the secant stiffness to 40% yield (effective stiffness). The hardening stiffness was set at 4% of the effective stiffness, and the pinch point at 25% of the maximum historic stress and rotation. The cyclic deterioration parameter was set to the same value that is computed for the beam-columns. The rotation capacity to peak strength was set as 0.010 radians and 0.015 radians for exterior and interior joints, respectively, based on recommendations by Moehle et al. (2006). Figure 3-13 shows the cyclic properties of an example RC OMF joint.

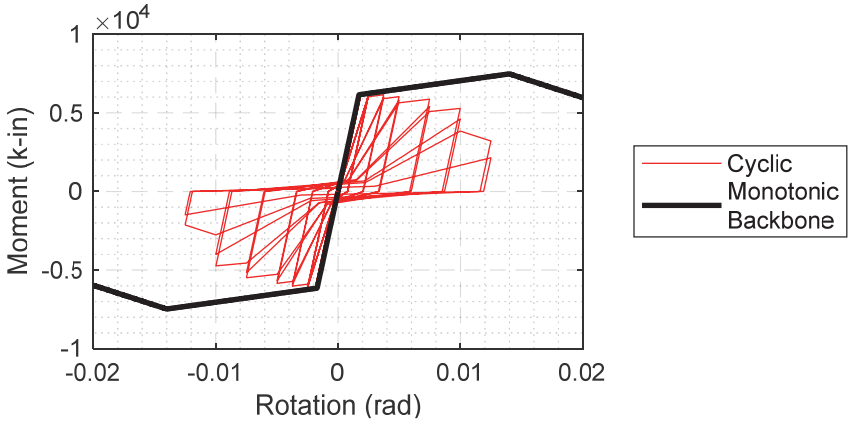

Figure 3-13 Example hysteretic properties of a RC OMF joint with axial load ratio of 0.11, 4000 psi concrete, joint area of 378 in.^{2}, and effective beam depth of approximately 13 inches.

3.3.3 Reinforced Concrete Shear Wall Archetypes

3.3.3.1 System Modeling

Nonlinear models of the RC wall buildings were constructed using three different methods in OpenSees. They were also modeled by finite elements with ATENA, but for validation purposes only. Brief descriptions of the modeling methods are provided here, and detailed descriptions are provided in Appendix B.

Collapse simulations of RC wall buildings were performed with the OpenSees models, because of their computational efficiency. The three methods by which RC walls were modeled in OpenSees are: (1) force-based beam-column elements (FBE) with fiber-type section models and the distributed plasticity modeling approach developed by Pugh et al. (2015); (2) displacement-based beam-column elements (DBE) with fiber-type section models and the distributed plasticity modeling approach developed by Pugh et al. (2015) and updated by Marafi et al. (2018); and (3) the shear-flexure-interaction multi-vertical line-element model (SFI-MVLEM) developed by Kolozvari et al. (2015a,b, 2018). The final collapse assessment results reported in Chapter 5 are obtained using method two in the preceding list—displacement-based beam-column elements with the Pugh et al. (2015) approach.

The modeling approaches developed by Pugh et al. (2015) and Marafi et al. (2018) employ regularization of material softening to achieve mesh-objective simulation of strength loss; by doing this, the effective size of the plastic hinge region (which essentially maps the material strain capacities to the element plastic deformation capacities) is controlled and is not arbitrarily affected by the details of the mesh size, even after the onset of negative stiffness. These have been verified using a large database of planar and non-planar wall tests, to provide accurate, mesh-objective, simulation of onset of strength loss, which is required for accurate assessment of collapse risk.

The SFI-MVLEM employs the fixed-strut angle approach (Orakcal et al., 2012) to characterize the biaxial constitutive response of the two-dimensional RC panel fibers that compose the SFI-MVLEM (Orakcal et al., 2004). Axial-shear coupling is achieved within each two-dimensional fiber through the two-dimensional RC panel constitutive model.

Figure 3-14 shows an idealization of the OpenSees model of a baseline 8-story RC wall building, which includes a single vertical line of nonlinear force-based beam-column elements to represent a wall, in addition to the line of elastic elements defining the *P*-Delta leaning column. The wall is fixed at its base.

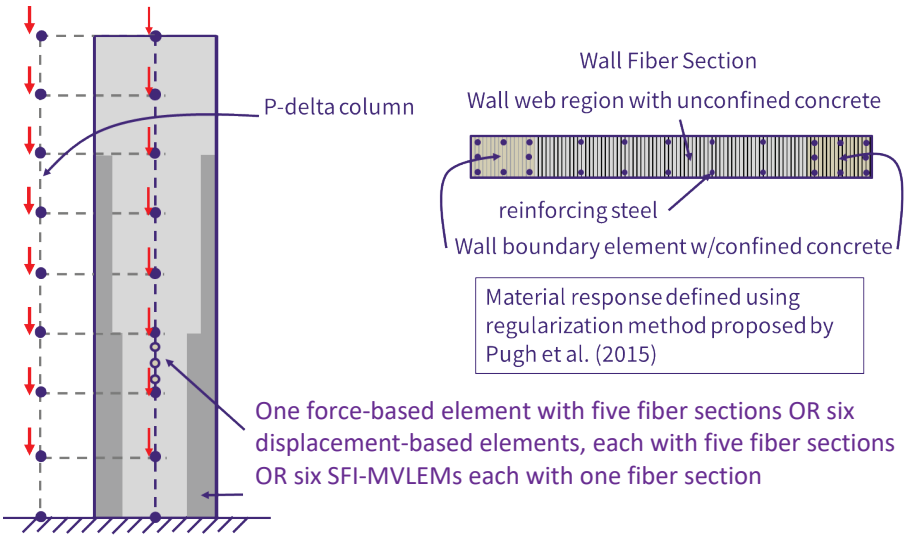

Figure 3-14 Schematic of OpenSees RC wall building model.

3.3.3.2 Modeling of Walls using Fiber Elements

The force-based and displacement-based beam-column elements represent nonlinear flexural response of the wall via fiber-type section models that comprise nonlinear confined and unconfined concrete and reinforcing steel fibers. Concrete and steel material model response was defined using standard material models and were modified using the regularization method proposed by Pugh et al. (2015). A linear moment distribution and constant axial load distribution along the length of the element was assumed, where flexure and shear response was decoupled in element formulation. Fiber-type section models employed approximately 150 fibers along the in-plan length of the wall. Figure 3-15 shows the element layout for walls with and without openings.

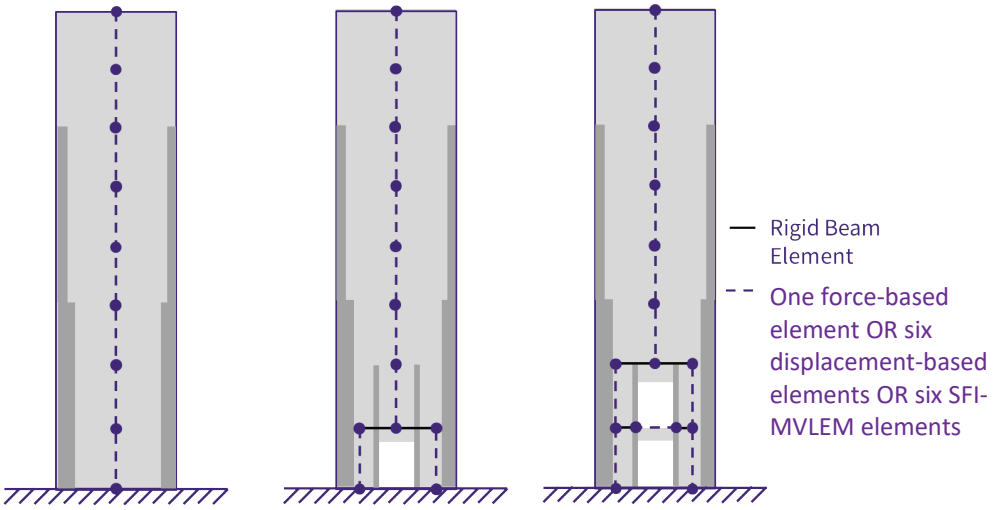

Figure 3-15 OpenSees model configurations for walls with and without openings.

Concrete and steel material response models used in the SFI-MVLEM were calibrated such that the SFI-MVLEM predicted drift capacities for the wall designs that were equal to those predicted using models comprising distributed-plasticity beam-column elements.

3.3.3.3 Material Constitutive Models for Concrete and Rebar

Concrete response was simulated using the OpenSees Concrete02 material model. In compression, this model represents a quadratic response to peak strength with linear deterioration to a residual compressive strength. In tension, the model represents a linear response history to tensile strength with linear strength loss to zero tensile capacity. Tensile strength for unconfined and confined concrete was defined as $4\sqrt{f_c'}$ psi; regularization of post-peak response in tension was not required as concrete cracking did not result in section or element softening. Unconfined concrete was assumed to reach peak strength at a strain of -0.002 in./in.; confined concrete strength and strain at maximum strength were defined using the model by Saatcioglu and Razvi (1992). Per the recommendations of per the recommendations of Pugh et al. (2015) and Marafi et al. (2018), concrete post-peak response was defined by the unconfined or confined concrete crushing energy and a mesh-dependent length; this was required to ensure that simulation of onset of strength loss was accurate and did not depend on mesh size. Concrete residual strength was defined as 20% of peak strength for confined concrete and 10% of peak strength for unconfined concrete.

For reinforcing steel, the OpenSees Steel02 model was used. Reinforcing steel was assumed to lose compressive and tensile strength, due to buckling, at the regularized strain at which concrete strength deteriorates to the residual compressive strength.

Figure 3-16 shows concrete and steel material model response under cyclic loading. Figure 3-17 shows regularization of concrete and steel response using unconfined, G_{fc}, and confined concrete, G_{fcc}, crushing energies and L_{IP}, which is the element length associated with the fiber section in which the material model is used. Note that the red 'X' in Figure 3-17 shows the strain at which reinforcing steel loses strength due to buckling.

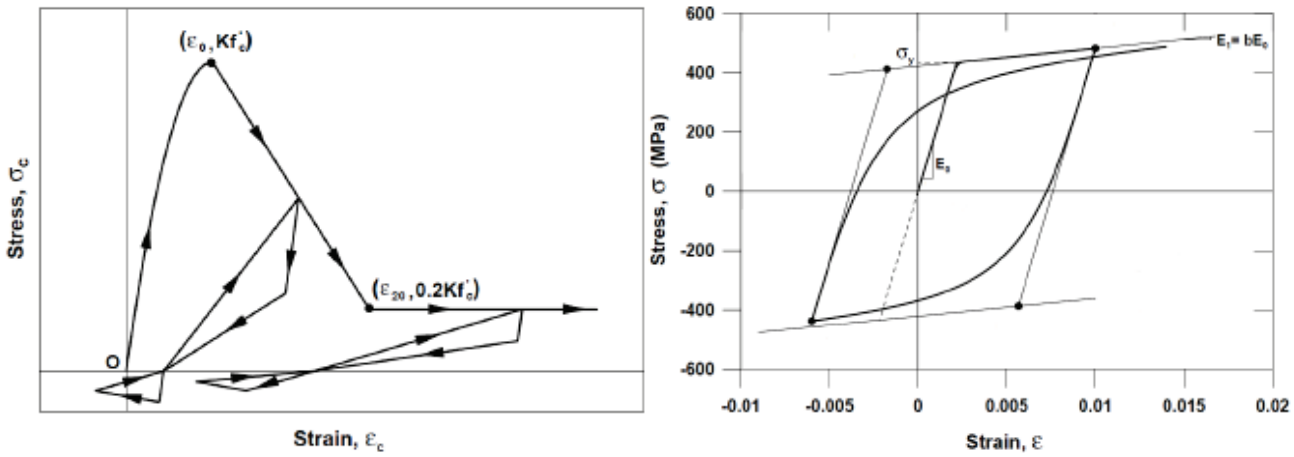

(a) (b)

Figure 3-16 Nonlinear 1D cyclic material models. (a) Yassin cyclic concrete model, which employs the monotonic Modified Kent-Park model (Yassin, 1994; Scott et al., 1982) as presented by Orakcal and Wallace (2006). Note that compressive stress-strain is positive. (b) Menegotto-Pinto-Filippou reinforcing steel model (Filippou et al., 1983) as presented by Orakcal and Wallace (2006).

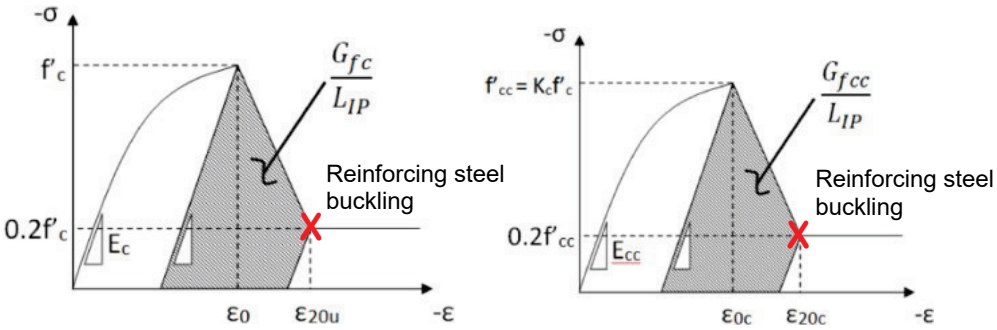

(a) unconfined concrete compression envelope

(b) confined concrete compression envelope

Figure 3-17 Regularization of concrete material response using mesh dependent length. Note that steel buckling occurs at ε_{20u} and ε_{20c}. (Figure adapted from Pugh et al., 2015)

3.4 Archetype Analysis Methods

The nonlinear analysis methods of FEMA P695 were used to investigate archetype response and collapse performance. The FEMA P695 methodology was developed to provide a rational basis for determining global seismic performance factors, including the response modification coefficient (R factor), the system overstrength factor (Ω_0), and the deflection amplification factor (C_d) that, when properly implemented in the seismic design process, will result in "*equivalent safety against collapse in an earthquake, comparable to the inherent safety against collapse intended by current seismic codes, for buildings with different seismic-force-resisting systems*" (FEMA, 2009). The primary acceptance criterion of FEMA P695 is that the SFRS be shown to have not more than a ten percent probability of

collapse conditioned on MCE_R ground motions (i.e., conditional collapse criterion subsequently adopted by ASCE/SEI 7-10).

The FEMA P695 methodology is intended for use with United States model building codes and resource documents to set minimum acceptable criteria for new SFRSs seeking adoption by seismic codes. The methodology also provides a basis for evaluation of current code-approved SFRSs for their ability to achieve intended seismic performance objectives, and to improve design requirements for current SFRSs to better achieve these objectives, the subject application of the methodology for the work summarized in this report.

The FEMA P695 report provides a complete methodology for establishing and documenting seismic performance factors of new SFRSs, including collecting requisite system information (e.g., test data), developing performance groups of representative archetypes, developing designs of archetypes, developing analytical models of archetype designs, analyzing the nonlinear response of archetype models to failure, evaluating the MCE_R collapse performance of archetype models from the results of the nonlinear response analyses, documenting results, and peer reviewing the entire process. The studies described in this report selectively used the analysis and collapse evaluation methods of FEMA P695 to calculate nonlinear response behavior and collapse performance of specific building archetypes modeled with and without irregularities.

3.4.1 Overview of FEMA P695 Analysis Methods

The FEMA P695 methodology relies on collapse simulation through nonlinear dynamic response history analysis. Analysis methods are rigorously and unambiguously defined by the FEMA P695 methodology, including the specification (selection and scaling) of ground motion records to be used in dynamic response history analysis of nonlinear models. FEMA P695 intentionally excludes nonstructural components and structural elements not part of the SFRS from archetype models of a new SFRS seeking adoption by seismic codes, although the analysis methods are generally applicable to all building elements subject only to availability of test data required to establish model properties. Similarly, FEMA P695 does not require modeling of potential building irregularities, although the analysis methods are generally applicable to archetype models with irregular configurations.

FEMA P695 analysis methods include: (1) nonlinear static (pushover) analysis to determine post-yield displacement capacity expressed in terms of

the period-based system ductility parameter (μ_T); and (2) incremental dynamic analysis (IDA) to calculate median collapse capacity expressed in terms of a corresponding value of response spectral acceleration ($\hat{S}_{CT}$) at the elastic, fundamental-mode, period, *T*, of the archetype model of the system of interest. The collapse margin ratio (*CMR*) is defined as the value of median collapse response spectral acceleration divided by the value of MCE_R response spectral acceleration at the elastic period (S_{MT}) used as the basis for design of the archetype model (i.e., $CMR = \hat{S}_{CT}/S_{MT}$). The larger the value of the *CMR*, the lower the probability of collapse. The adjusted collapse margin ratio (*ACMR*) is the value of the *CMR* adjusted by the spectrum shape factor (*SSF*) to account for the inherent "rareness" of MCE_R ground motions (i.e., $ACMR = SSF \times CMR$). The *SSF* accounts for the post-yield elongation of the elastic period based on the value of the system ductility parameter. The larger the value of the system ductility parameter, the larger the adjustment (increase) in the value of the *CMR* and the lower the probability of collapse. It should be noted that, for the comparisons between collapse performance of irregular archetypes and baseline archetypes presented in Chapters 4-6, irregular archetypes are assigned the same *SSF* as their corresponding baseline archetypes.

3.4.2 Selection of Ground Motions

The FEMA P695 methodology provides two sets of ground motion records for collapse assessment using nonlinear dynamic analysis—the far-field record set and the near-field record set. The far-field record set includes 22 component pairs of horizontal ground motions from sites located greater than or equal to 10 km from fault rupture. The near-field record set includes 28 component pairs of horizontal ground motions recorded at sites less than 10 km from fault rupture. The record sets do not include the vertical component of ground motion since this direction of earthquake shaking is generally not considered of primary importance for collapse evaluation and is not required for nonlinear dynamic analysis. The far-field record set is used by this study for nonlinear response calculations and collapse evaluations.

The far-field ground motion record set is composed of strong-motion records (i.e., records with PGA > 0.2g and PGV > 15 cm/s) from all large magnitude (M > 6.5) events in the PEER NGA West1 Database (PEER, 2006). Large magnitude events dominate collapse risk and generally have longer durations of shaking, which is important for collapse evaluation of nonlinear degrading models. The ground motion sets include records from soft rock and stiff soil sites (predominantly Site Class C and D conditions) and from shallow crustal sources (predominantly strike-slip and thrust mechanisms). To avoid event bias, no more than two of the strongest records are taken from each

earthquake. Figure 3-18 shows the 44 individual response spectra (i.e., 22 records, 2 components each), the median response spectrum, and spectra representing response at +1- and +2-standard deviations of the far-field record set.

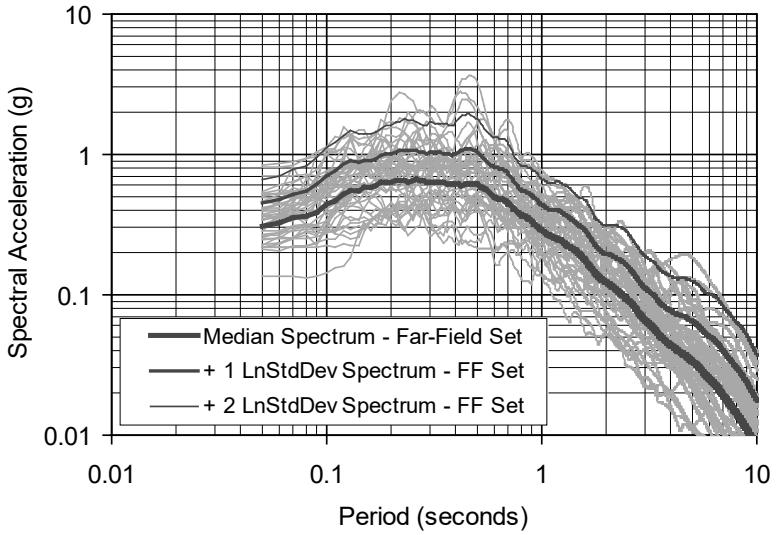

Figure 3-18 Far-field record set response spectra normalized by peak ground velocity (Figure 6-3 of FEMA P695; FEMA, 2009).

The far-field record set provides a fully-defined set of records for use in a consistent manner to evaluate collapse of all possible types of SDC B, C, and D systems located in any seismic region. The FEMA P695 methodology uses actual earthquake records (in contrast to artificial or synthetic records) recognizing that regional variation of ground motions would not be addressed. Large magnitude events are rare and few existing earthquake ground motion records are strong enough to collapse large fractions of modern, code-compliant buildings. In the United States, strong-motion records date back to the 1933 Long Beach earthquake, with only a few records obtained from each event until the 1971 San Fernando earthquake.

3.4.3 Incremental Dynamic Analysis

FEMA P695 methods utilize IDA to determine median collapse capacity of the archetype model of interest. Median collapse capacity is the value of response spectral acceleration, $\hat{S}_{CT}$, at the fundamental-mode period, T, at which the archetype model has a 50 percent probability of collapse. For defining $\hat{S}_{CT}$, the fundamental period is limited by the ASCE/SEI 7-16 upper bound equation $T \leq C_u T_a$.

Median collapse capacity is determined by applying the far-field set of 22 records (2 components each) to the model incrementally scaled from

relatively low to relatively high values of response spectral acceleration. For a given ground motion, an archetype is assumed to have collapsed when either the analysis will not converge (often due to loss of stability) or an engineering demand parameter (EDP) such as interstory drift ratio (*IDR*) exceeds a predetermined threshold for which the building is expected to lose its capability to carry vertical loads. In some cases, the analytical model may still be stable, but the building is considered collapsed because of a non-simulated mode of failure (e.g., a failure mode that is not explicitly modeled, such as failure of the gravity system). Conceptually, median collapse capacity is the value of response spectral acceleration at which 22 of the 44 analyses effect collapse of the archetype model. To avoid potential problems with interpolation of discrete data, fitted median values of responses were estimated by fitting a lognormal curve to the 44 collapse data.

Figure 3-19 is an example plot from FEMA P695 that is used to illustrate the FEMA P695 methodology for determining collapse resistance from IDA. For collapse evaluation of two-dimensional (planar) archetype models, each of the 44 far-field components (i.e., 22 records, 2 components each) are individually applied to the model generating 44 values of response and collapse data at each increment of ground motion intensity. For collapse evaluation of three-dimensional archetype models, the 22 far-field records (two components each) are applied to the archetype model in two orthogonal orientations (e.g., NS-EW and EW-NS orientations of components) also generating 44 values of response and collapse data at each increment of ground motion intensity. However, the *CMR* based on median collapse intensity, $\hat{S}_{CT}$, is multiplied by 1.2 when three-dimensional archetypes are used to evaluate collapse capacity (i.e., $CMR_{3D} = 1.2CMR_{2D}$). Adjustment of the *CMR* for three-dimensional analyses is required by Section 6.4.5 of FEMA P695 to achieve parity with two-dimensional analyses.

In this study, spectral acceleration of a ground motion was defined as the geometric mean spectral acceleration of its two horizontal components. This is a modification to the FEMA P695 approach, which first normalizes the entire ground motion set to have the same peak ground velocity (to obtain the "cloud" of response spectra in Figure 3-18), and then defines spectral acceleration as the geometric mean spectral acceleration of the cloud (scaled all together). Scaling on geometric mean of individual ground motions, rather than cloud-scaling, has relatively inconsequential effects on estimates of $\hat{S}_{CT}$; although, it does result in an underestimation of record-to-record variability, particularly for nonductile buildings. However, since FEMA P695 recommends a standard record-to-record variability of $\beta = 0.4$, there is no need to compute it from IDA.

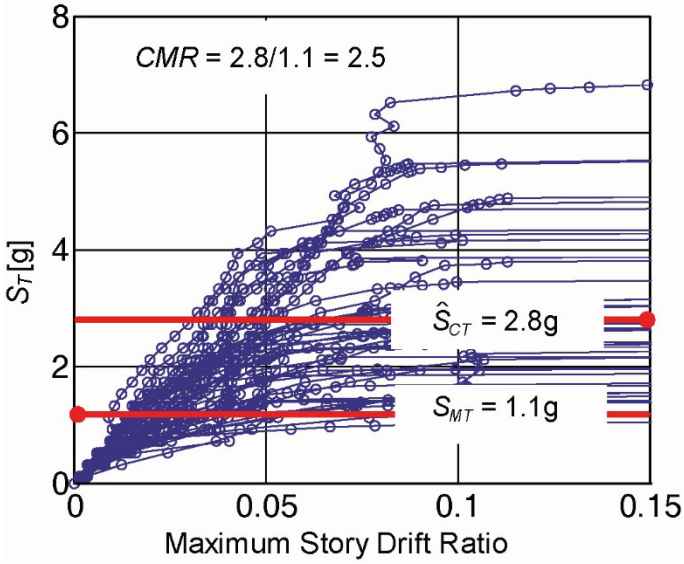

Figure 3-19 Incremental dynamic analysis response plot of spectral acceleration versus maximum story drift ratio (FEMA, 2009).

While evaluation of median collapse capacity requires only the identification of the ground motion intensity at which 22 of the 44 analyses effect collapse, the studies described in this report also tracked values of other key response parameters (e.g., peak story drift ratio and peak floor acceleration) over a broad range of ground motion intensities, as described in Section 3.4.6.

3.4.4 Evaluation of MCE_R Collapse Performance

The probability of collapse as a function of ground motion intensity (at the period, T, of archetype model) is assumed to be lognormally distributed with an adjusted median, $\hat{S}_{ACT}$ (i.e., $ACMR \times S_{MT}$), and a lognormal standard deviation, β_{TOT}, that accounts for total collapse uncertainty related to: (1) record-to-record variability; (2) design requirements (for the SFRS of interest); (3) test data (used to establish nonlinear properties); and (4) modeling methods, as described in Section 7.3 of FEMA P695. Reasonably well-defined archetype models have total collapse uncertainty values of β_{TOT} = 0.50 – 0.60; β_{TOT} = 0.50 was used as the default in this study. Note that the comparisons presented in Chapters 4-6 of this study are based on $ACMR$, not the probability of collapse for an MCE_R ground motion level, so they are insensitive to the total collapse uncertainty parameter, β_{TOT}; this is discussed further in Section 3.4.5.

3.4.5 Collapse Evaluation Using Absolute and Relative Measures of Collapse Risk

Both the collapse probability for MCE_R ground motions and the *ACMR* values are tracked for each archetype building in this study. This section discusses both of these performance metrics and explains why the relative comparisons of *ACMR* values between irregular archetypes and a corresponding regular baseline archetype was used as the primary measure of performance (used in Chapters 4-6).

The MCE_R probability of collapse is the primary metric of the FEMA P695 methodology for evaluation of the collapse capacity of the archetype model of interest as well as the parameter used by ASCE/SEI 7-10 to define anticipated reliability of the structure to resist total or partial collapse (e.g., see Table C.1.3.1b of ASCE/SEI 7-10). The MCE_R collapse probability represents an absolute measure of collapse risk that may not be the best metric for comparing the relative collapse performance of a given SFRS with and without a particular irregularity for the following reasons. The MCE_R collapse probability is very sensitive to the value β_{TOT} (i.e., total collapse uncertainty) when the MCE_R collapse probability is low (e.g., less than 10 percent) and relatively insensitive to the value β_{TOT} when the MCE_R collapse is near the median. For the purpose of comparing the collapse performance of a given SFRS with and without a particular irregularity, it is desirable to have a metric that is not sensitive to total collapse uncertainty. Arguably, the SFRS of interest has the same (or nearly the same) value of total collapse uncertainty with and without the irregularity, since individual uncertainties associated with design requirements, testing, and modeling are similar. The *ACMR* provides a more suitable metric that is independent of collapse uncertainties and is linearly related to the value of MCE_R ground motions used as the basis for design and collapse evaluation.

The *ACMR* parameter is an absolute measure of median collapse resistance, values of which necessarily vary for different SFRSs and corresponding configurations. That is, values of the *ACMR* parameter will be different for archetype models of different SFRSs and corresponding configurations even when those SFRSs are seismic code compliant and, in concept, should have the same, acceptably low, MCE_R collapse probability. For the purpose of comparing the relative collapse performance of a given SFRS with and without a particular irregularity, it is deemed useful to compare the ratio of the values of the *ACMR* parameter for a given SFRS with and without a particular irregularity to 1.0 (i.e., compare $ACMR_{irregular}$ / $ACMR_{baseline}$ to 1.0). Thus, the collapse performance of a given SFRS with and without a particular irregularity would be considered the same if the ratio of the *ACMR*

values is 1.0, even if the *ACMR* parameter is relatively small or large (e.g., $ACMR_{irregular}$ / $ACMR_{baseline}$ of 1.5/1.5 versus 2.0/2.0 versus 2.5/2.5). If the ratio of *ACMR* values is less than 1.0, that would indicate that the presence of the irregularity has caused a decrease in the building collapse resistance.

While the ratio $ACMR_{irregular}$ / $ACMR_{baseline}$ is the primary metric for evaluating the effects that configuration irregularities (and the accompanying design requirements, where applicable) have on collapse resistance, the MCE_R probability of collapse was still monitored in this study. In some cases, where the MCE_R probability of collapse was extremely low, a larger reduction of $ACMR_{irregular}$ / $ACMR_{baseline}$ was considered acceptable, due to the overall low collapse risk of the archetype design group. An additional use of computing the MCE_R probability of collapse was to provide a sanity check for the design and modeling approaches in this study; values of MCE_R for the baseline archetypes generally should (and did) fall within a range that is consistent with prior studies (e.g., 1%-15% for SDC D_{max} designs, as seen in FEMA P695).

3.4.6 Tracking of Non-Collapse Archetype Response Parameters

Nonlinear dynamic analyses were conducted on all models across the design space by applying the FEMA P695 far-field ground motions at increasing intensities until collapse (i.e., incremental dynamic analysis). The majority of the results presented in this report focus on collapse and IDR (e.g., Figure 3-20 and Figure 3-21). A number of other engineering demand parameters (EDPs) were tracked as well, including residual story drift ratios, roof drift ratio, residual roof drift ratio, peak floor accelerations and velocities, and peak column axial forces.

Each of the aforementioned EDPs are recorded for a broad range of intensities, up to the point of collapse. The set of EDPs for a given ground motion intensity is referred to as a "stripe." As an example, Table 3-12 reports stripes at three key levels of ground motion intensity for the 12-story baseline RC special moment frame (SMF) designed for SDC D_{max}: 1/3 MCE, 2/3 MCE, and MCE. Note that the maximum story drift for this example archetype building is 0.015 under design level motions (due to some conservatism in the design process), which is similar to the median drift at 2/3 MCE of 0.018.

The EDPs selected for tracking at each stripe level were selected by the project team that developed this report. In addition to providing detailed information to support the results of the study, these data are intended to also be made available for other future uses. It should be noted that these data are

non-collapse cases and they are not adjusted for spectral shape effects, so the reported values are likely to overestimate the response in cases where the ground motion demands have favorable spectral shapes (i.e., "high epsilon" cases) (as summarized in Appendix B of FEMA P695; FEMA, 2009).

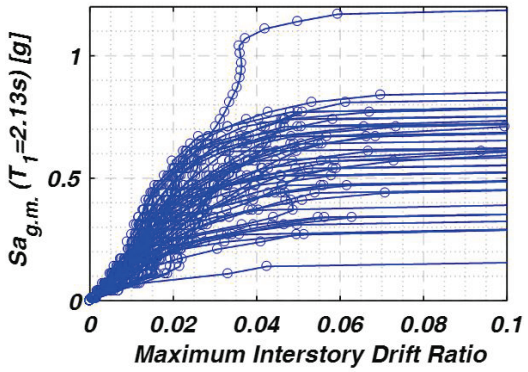

Figure 3-20 Collapse IDA, Baseline 12-story RC SMF.

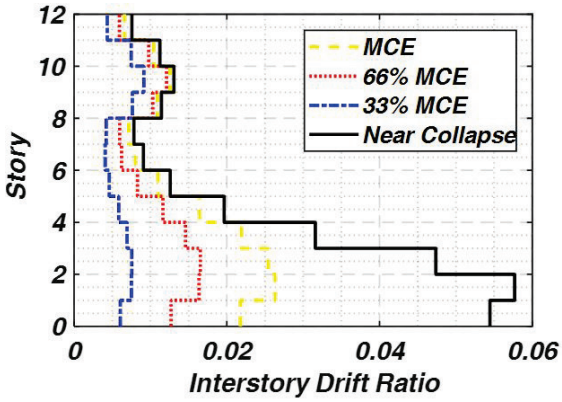

Figure 3-21 Interstory Drift Ratio (IDR), Baseline 12-story RC SMF.

Table 3-12 Mean Stripe Results at Selected Intensities, Baseline 12 Story RC SMF

Engineering Demand Parameter	1/3 MCE	2/3 MCE	MCE
Fraction collapsed	0.00	0.02	0.20
IDR max all stories	0.011	0.018	0.028
IDR residual max all stories	0.003	0.007	0.017
Roof drift ratio (RDR) max	0.005	0.008	0.012
RDR residual max	0.001	0.003	0.006
Peak floor acceleration (PFA) max all stories, g	0.306	0.592	0.807
Peak floor velocity (PFV) max all stories, in./s	141	302	412
Peak column axial force max all columns, kips	1,031	1,072	1,071
Column shear force abs max all columns, kips	205	236	248
Column moment abs max all columns, kip-in.	16,410	21,438	22,837

Chapter 4

Buildings with Torsional Irregularities (H1, H6)

4.1 Overview

This chapter summarizes the analytical studies for torsionally irregular buildings that were designed per ASCE/SEI 7-16, *Minimum Design Loads and Associated Criteria for Buildings and Other Structures* (ASCE, 2017a). The effects on building performance of the following torsional irregularities were studied:

- **H1, Torsional (stiffness) irregularity.** This condition is a Type 1a or Type 1b horizontal irregularity, as defined in Table 12.3-1 of ASCE/SEI 7-16. The torsional studies were mostly focused on this torsional irregularity, because it affects the design requirements for new buildings.
- **H6, Torsional (strength) irregularity.** This condition is considered an irregularity per Section 7.3.1.1.4 in ASCE/SEI 41-17, *Seismic Evaluation and Retrofit of Existing Buildings* (ASCE, 2017b). This condition is not considered an irregularity in ASCE/SEI 7. It is included in this study to determine if this condition should be considered in ASCE/SEI 7.

The following are covered in this chapter: (1) objectives of the torsional irregularities studies and overview of findings (Section 4.2); (2) methodology to assess torsion design provisions (Section 4.3); (3) archetype design space (Section 4.4); (4) results (Section 4.5); and (5) conclusions and recommendations (Section 4.6).

4.2 Objectives of Studies and Summary of Findings

The analytical torsion studies described in this chapter addressed two primary objectives:

1. Determine the effectiveness of ASCE/SEI 7-16 torsion design requirements for preventing seismic-induced collapse of torsionally irregular buildings; and
2. Propose modifications to the ASCE/SEI 7-16 torsion design requirements to address deficiencies and/or unnecessary sources of conservatism.

4.2.1 Objective 1: Evaluate ASCE/SEI 7-16 Torsion Design Provisions

ASCE/SEI 7-16 seismic design provisions were evaluated systematically to address a number of questions relating to the effectiveness of the provisions for ensuring adequate collapse resistance of torsionally irregular buildings. This included studies to answer the following questions:

- When are the ASCE/SEI 7-16 seismic provisions unconservative for torsionally irregular buildings? When are they conservative?
- How important are the various torsion design requirements (e.g., accidental torsion) for ensuring adequate collapse resistance?
- Are certain prohibitions necessary (e.g., prohibition of buildings in Seismic Design Category (SDC) E and F with extreme torsional irregularity)?

4.2.2 Objective 2: Propose Modifications to the ASCE/SEI 7-16 Seismic Torsion Provisions

In addition to evaluating existing provisions for seismic design of torsionally irregular buildings, the analytical torsion studies evaluated a number of potential revisions to the ASCE/SEI 7-16 requirements. The purpose of the proposed revisions is to improve the design process for torsionally irregular buildings without adding complexity to the existing ASCE/SEI 7-16 seismic provisions. The following were the specific focuses when considering potential modifications to ASCE/SEI 7-16:

- Improve the design of buildings with configurations having inherently poor torsion performance, but without over-penalizing other configurations that already perform satisfactorily.
- Eliminate sources of unnecessary conservatism for designing torsionally irregular buildings. Where possible, this includes eliminating or relaxing the code triggers for prohibitions related to torsional irregularities.

4.2.3 Summary of Findings

The study found that ASCE/SEI 7-16 torsion design provisions are generally conservative for most building configurations, with the exception of some buildings that rely heavily on the orthogonal lines of lateral resistance to resist building torsion (i.e., the lines of resistance orthogonal to the design earthquake force). It was also observed that the accidental torsion amplification (Section 12.8.4 of ASCE/SEI 7-16) and requiring drift and stability limits to be satisfied at the most critical building edge in torsionally irregular buildings (Section 12.8.6 of ASCE/SEI 7-16) are important design

requirements for ensuring adequate collapse resistance of torsionally sensitive buildings.

Based on the findings of this study, the following modifications to ASCE/SEI 7-16 would prevent reductions in collapse resistance and make collapse capacity more consistent over a large range of building configurations and degrees of torsional irregularity:

- Alter the triggers for requiring a redundancy factor of 1.3 in Section 12.3.4.2 of ASCE/SEI 7-16 so that fewer buildings are affected.
- Consider the effects of the orthogonal ground motion component for designing buildings that are classified as torsionally irregular.
- Classify buildings as torsionally irregular if more than 75% of their lateral strength is located on one side of the center of mass (CM).
- Allow only the static method of applying accidental torsion (i.e., Section 12.8.4 of ASCE/SEI 7-16) for buildings with extreme torsional irregularity. In other words, do not permit use of 5% mass offsets with modal response spectrum analysis or linear response history analysis for such buildings.

Based on the findings of this study, the following modifications to ASCE/SEI 7-16 would remove some current restrictions that were found to be conservative:

- Do not prohibit extremely torsionally irregular buildings in SDC E and F, as long as the lateral system is proportioned according to the recommendations in this report.
- Do not prohibit the equivalent lateral force (ELF) procedure on the basis of torsional irregularity.

4.3 Methodology to Assess Torsion Design Provisions

Torsion design provisions were assessed by comparing the collapse resistance of torsionally irregular archetype buildings to the collapse resistance of a baseline archetype that is regular in plan. Ideally, the collapse resistance should remain relatively constant for varying levels of torsional irregularity. Of primary importance is ensuring that the collapse resistance does not decrease as the torsional irregularity increases. Of secondary importance, but still kept as a priority in this study, is avoiding excessive conservatism caused by torsion design requirements (i.e., the code requirements should not result in conservatively large increases in collapse resistance for torsionally irregular buildings).

To measure torsional irregularity, this study utilized the Torsional Irregularity Ratio (*TIR*), which is the ratio of the maximum drift at a building's edge to the average drift, given a lateral force with 5% eccentricity as shown in Figure 4-1. This is identical to the ratio used for determining the presence of torsional irregularity in Table 12.3-1 of ASCE/SEI 7-16. Table 12.3-1 classifies buildings as having a Type 1a torsional irregularity if the *TIR* is greater than 1.2 and Type 1b (extreme) torsional irregularity if the *TIR* is greater than 1.4.

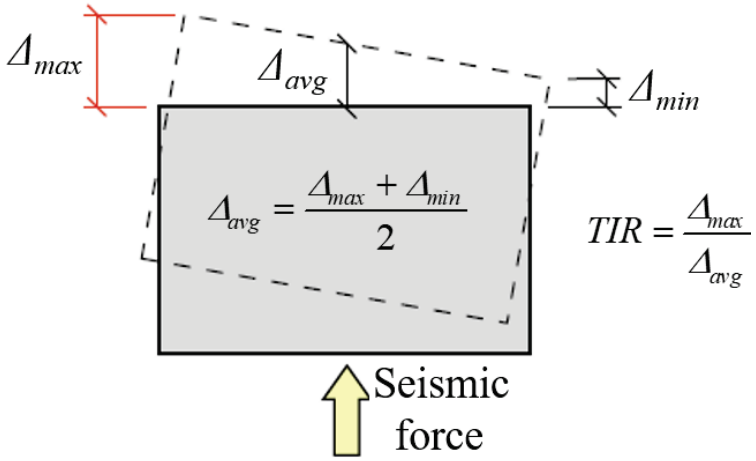

Figure 4-1 Torsional Irregularity Ratio (*TIR*).

Archetype buildings used in this study are represented by single-story, nonlinear three-dimensional models which were calibrated to represent the aggregate behavior of multi-story buildings. These models are described in detail in Appendix A. To use single-story representative models effectively, the following steps were taken:

1. The models were calibrated so that their design properties (e.g., drift and stability coefficient) are consistent with that of a multi-story design.
2. The nonlinear backbones of the single-story models were made to approximate the aggregate behavior of a multi-story building backbone.
3. Nonlinear response history results for a set of single-story archetypes were validated through comparison to nonlinear response history results of three-dimensional multi-story models.

Extensive information about modeling multi-story torsion responses with single-story models can be found in the literature (e.g., De Stefano and Pintucchi, 2008; Anagnostopoulos et al., 2010; Anagnostopoulos et al., 2015). A key finding of these studies is that emulating the response of more realistic multi-story models is an essential step to gleaning meaningful results from single-story models, especially for torsional responses. This finding

informed the above steps taken to ensure that the single-story models adequately emulated the behavior of the multi-story models.

4.4 Archetype Design Space

4.4.1 Plan Configurations

More than 2,000 archetype models were analyzed under this study. The baseline configuration (Figure 4-2a) has a 1:1 plan aspect ratio with lines of lateral resistance (representing either shear walls or moment frames) along the perimeter. Archetypes with varying degrees of torsional irregularity were created by adjusting the aspect ratio of the building plan and varying the locations of the lines of lateral resistance, as illustrated in Figure 4-2b where α, β, δ, and γ indicate the location of each line of lateral resistance.

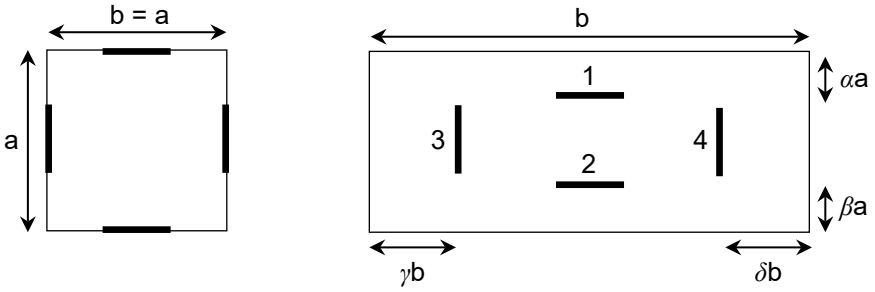

Figure 4-2 Plan view of: (a) the baseline archetype configuration; and (b) a generic configuration. Thickened lines represent lines of lateral resistance.

Plan configurations for the majority of the archetypes fall into three categories that make up the "core" archetype design space, illustrated in Figure 4-3:

- **Symmetric, "Sym."** Torsional irregularity was introduced by moving all of the seismic-force-resisting system (SFRS) lines toward the center of plan by increasing α, β, δ, and γ together, thereby decreasing the torsional stiffness of the system. Irregularity in the symmetric archetypes is due to torsional flexibility only, not inherent torsion.
- **Double asymmetric, "Double Asym."** These archetypes have inherent eccentricity in both orthogonal directions, due to shifting SFRS lines 1 and 3 away from the building perimeter by increasing α and γ. Lines 2 and 4 of the SFRS were kept at the perimeter.
- **Single asymmetric, "Single Asym."** These archetypes have inherent eccentricity in only one direction, due to shifting line 3 of the SFRS

away from the perimeter by increasing γ. Lines 1, 2, and 4 of the SFRS were kept at the perimeter.

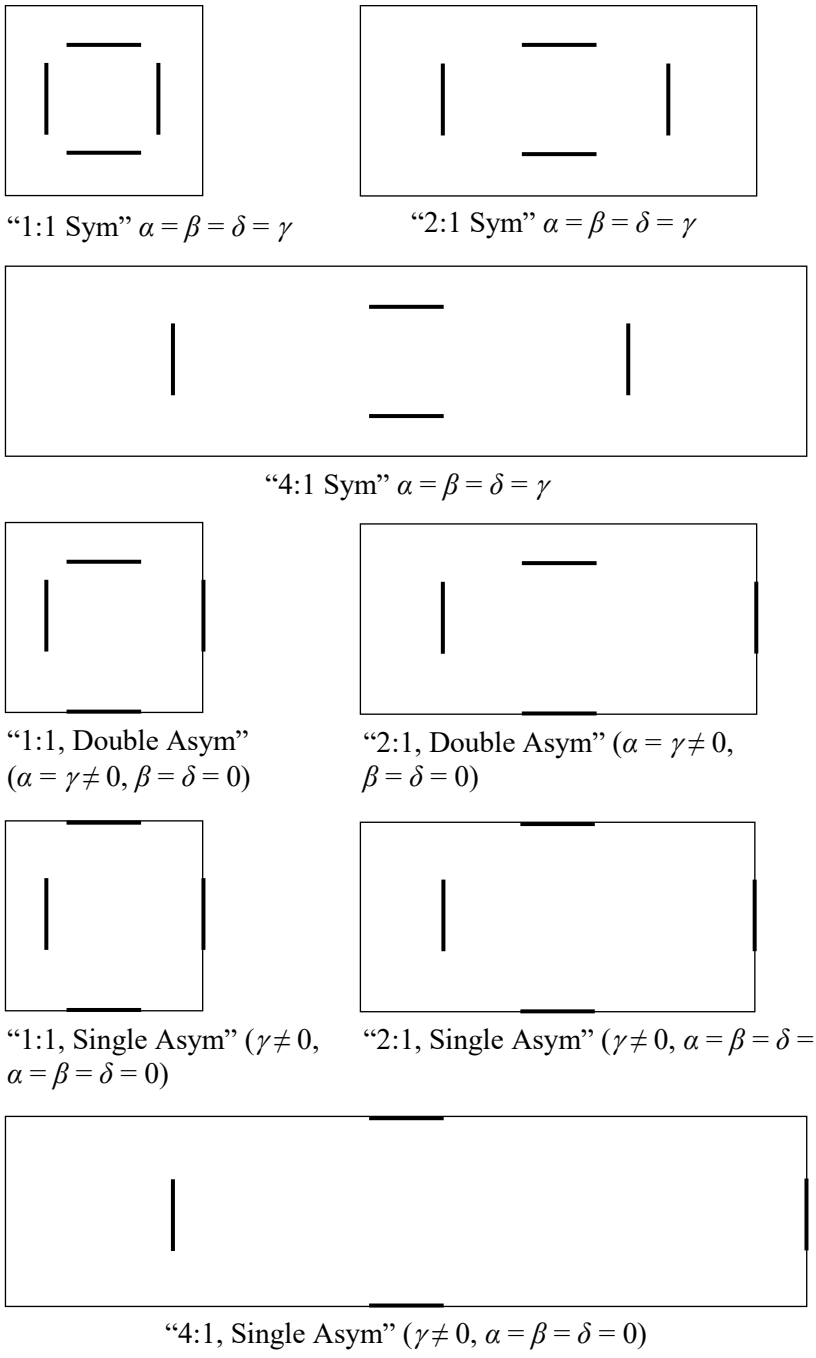

Figure 4-3 Illustration of archetype configurations. Thickened lines represent lines of lateral resistance.

In addition to the core archetype design space, an additional set of plan configurations were utilized to further expand the scope of building layouts (and associated irregularities) that were considered in the study. These additional configurations have 7:3 aspect ratio and are shown in Figure 4-4

and Figure 4-5. The "Mixed" archetype variants shown in Figure 4-4 were used to evaluate the effects of buildings that have a mixture of SFRSs consisting of reinforced concrete shear walls and reinforced concrete moment frames. In addition, Figure 4-5 shows building plans without a line of lateral resistance on one side, which are referred to as "three-sided" systems in this study.

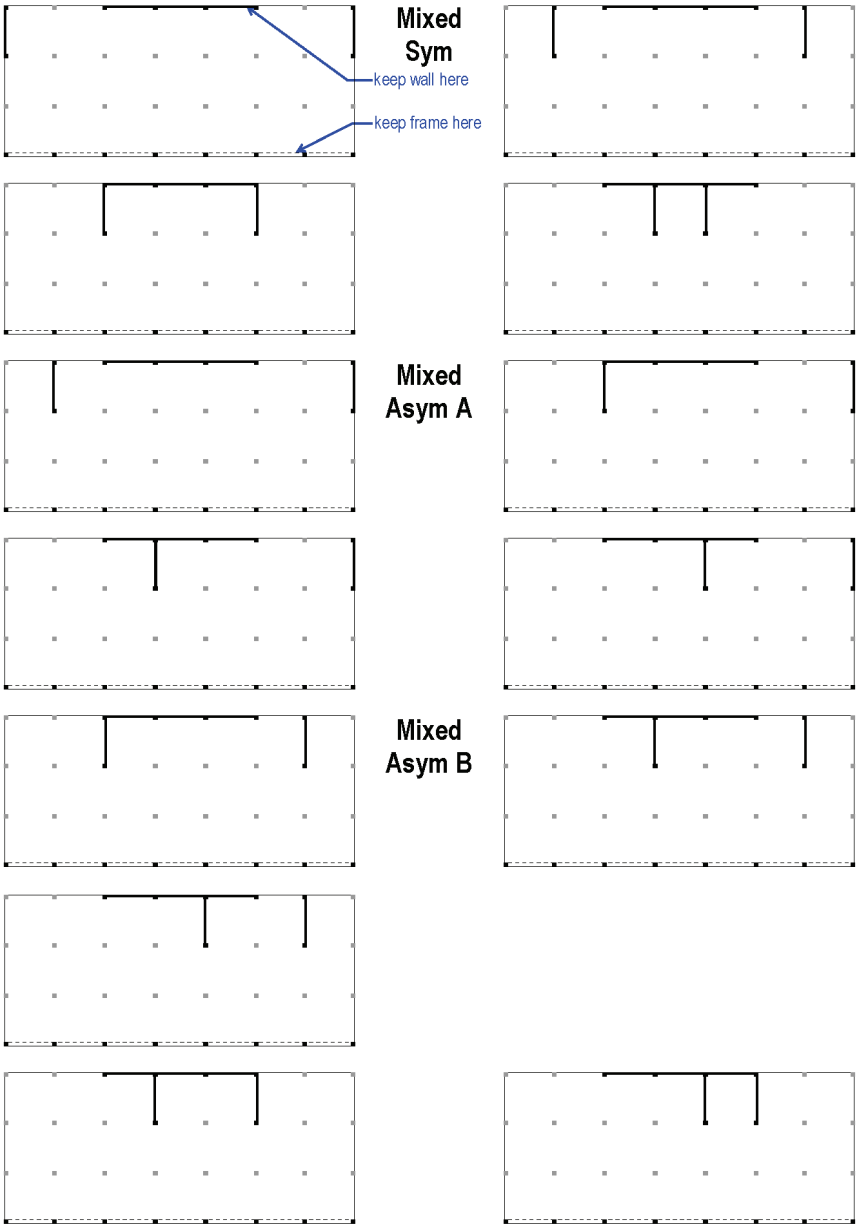

Figure 4-4 Illustration of "Mixed" archetype configurations.

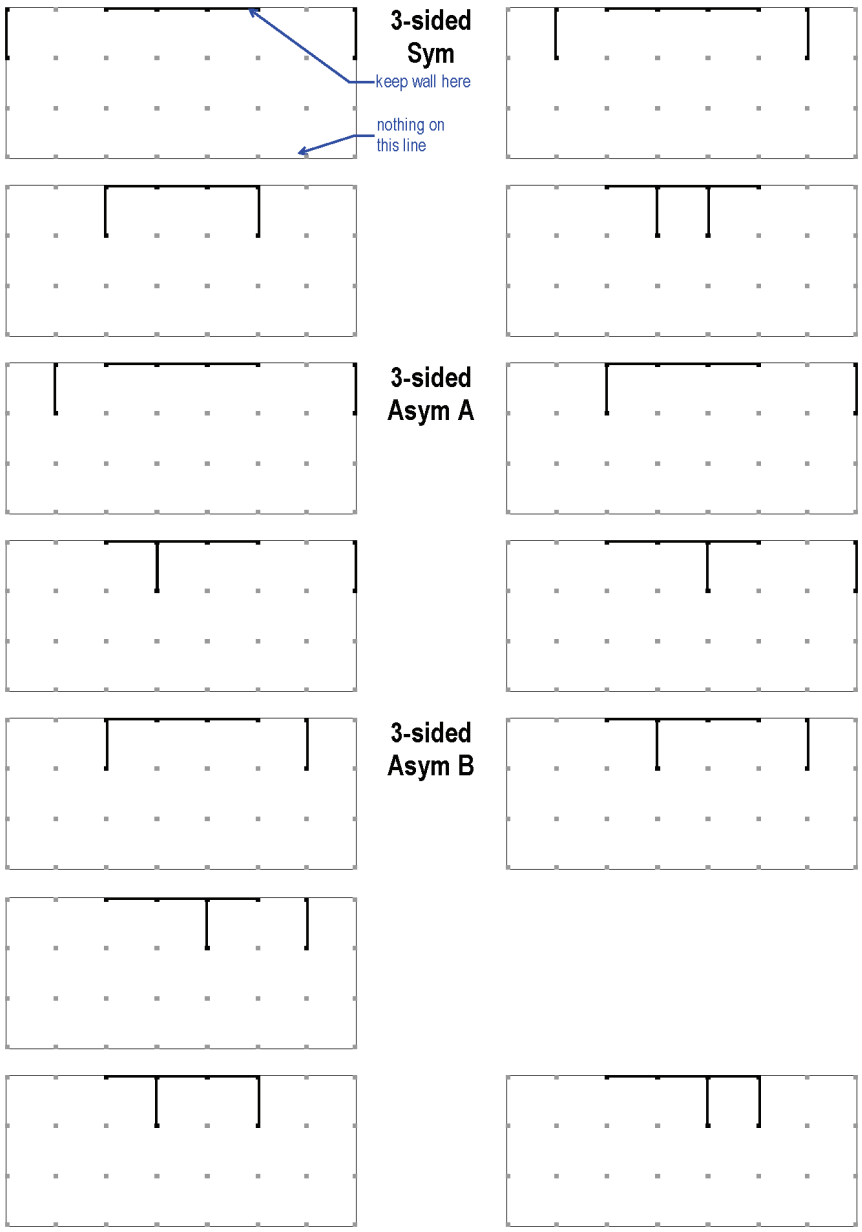

Figure 4-5 Illustration of "three-sided" archetype configurations.

4.4.2 Baseline Archetypes

The baseline archetypes define three categories of buildings from which all of the other archetypes were derived, outlined as follows:

- **Short.** The short baseline archetype defines a class of short-period buildings with an upper bound design period, $C_u T_a$ = 0.3 s, as defined in ASCE/SEI 7-16, Section 12.8.2. The properties of this archetype were calibrated to represent the behavior of a two-story wood shear wall building. The "short" archetype baseline design was force-controlled

(rather than drift-controlled), which is also the case for the majority of the torsionally irregular design variants.

- **Mid-rise.** The mid-rise baseline defines a class of buildings with longer periods ($C_u T_a$ = 2.0 s) whose designs were often controlled by drift limits and/or stability requirements as they became more torsionally irregular. The properties of this archetype were calibrated to represent a 10-12 story reinforced concrete (RC) special moment frame (SMF) building, and it was verified to behave similarly to the 12-story RC SMF baseline building developed in Chapter 6.
- **Mixed.** The mixed system archetypes were meant to represent a combination of special reinforced concrete shear walls (RC SW) and RC SMFs, either as a dual system or as a combination in accordance with Section 12.2.2 or 12.2.3 of ASCE/SEI 7. The baseline archetype for the mixed system represents a building whose SFRS is comprised solely of RC SWs. The properties of this baseline archetype were calibrated to represent the behavior of a mid-rise RC SW building ($C_u T_a$ = 0.93 s), and it was verified to behave similarly to the 8-story RC SW buildings developed in Chapter 5. The RC SW parallel to the moment frame in the irregular archetypes started out stronger than the walls in the wall-only direction because it is stiffer than the frame and attracts more force. The lines of resistance representing RC SMFs are similar to the 8-story baseline RC SMF developed for the vertical irregularity studies in Chapter 6, except that they are weaker, because the frame is softer than the wall and attracts less force.

Table 4-1 summarizes the key design properties of the baseline archetype models. For comparison, the design properties of the two-dimensional 12-story RC SMF and 8-story RC SW baselines (from Chapters 6 and 5, respectively) are also provided in the table. For all archetype designs, including the baseline designs and the irregular variants, the period (T) for determining seismic base shear is taken as the minimum of $T = C_u T_a$ and the fundamental period computed from the structural model in the direction of interest, but not less than the approximate period, T_a. Where the torsional mode contained significant modal mass in the translational direction, the fundamental period was taken as the longer of the lateral and torsional periods; this simplification is *not* recommended for design because it can result in smaller demands, but it is conservative regarding the conclusions that are drawn from this study. In the case of the mid-rise archetypes, the design base shear was often controlled by Equation 12.5 of ASCE/SEI 7-16 which requires that the base shear be no less than $0.044 S_{DS}$. Forces for computing drifts were determined using the fundamental period from the

structural model, and a drift limit of 2% was used for all archetypes. The stability design requirements were also enforced in the design process, in accordance with Section 12.8.7 of ASCE/SEI 7-16.

The nonlinear properties of the baseline models are discussed in detail in Appendix A. It should be noted that, although the nonlinear properties are calibrated to match the macro-behavior of wood shear walls, RC frames, and RC walls, the purpose is not to study any one of these building systems specifically. Rather, the purpose of the various archetypes is to capture a range of global system behaviors that could affect the impacts of torsion design requirements (e.g., buildings with periods in the constant acceleration part of the spectrum and with low *P*-Delta sensitivity versus buildings with periods beyond the constant acceleration part of the spectrum with significant *P*-Delta effects).

Table 4-1 Design Properties of Baseline Archetypes

Baseline Archetype	Period for Computing Design Forces [$C_u T_a$, s]	Analytical Period [s]	R	C_d	C_s	Drift	Stability Coefficient (θ)
Short	0.30	0.40	6.5	4	0.154	0.7%	0.01
Mid-rise	2.00	2.20[(1)]	8	5.5	0.044	1.2%	0.07
Comparison: 12-story RC SMF design	2.13	2.58	8	5.5	0.044	1.2%[(2)]	0.07
Mixed, Baseline has only RC walls	0.93	1.15	6[(3)]	5	0.108	0.7%	0.02
Comparison: 8-story RC SW	0.93	1.14	6	5	0.108	N/A	N/A

(1) The period of the mid-rise baseline archetype increases to 2.34 s if gravity loading and geometric effects are considered. For design, however, geometric effects are accounted for indirectly by dividing displacements by the quantity (1-θ), per Section 12.8.7 of ASCE/SEI 7-16.

(2) The maximum drift in the 12-story RC SMF is 1.5% and occurs in the upper third of the building. The maximum drift in the bottom half of the building, 1.2%, is used for calibrating the simplified model, because that is the portion of the structure that experiences damage leading to collapse.

(3) The RC SW baseline is designed with $R = 6$, but the mixed system variants are designed with $R = 7$ in the mixed direction and $R = 6$ in the RC SW direction.

4.4.3 Proportioning the Lateral System for Seismic Design

For each archetype, the properties of the four lines of lateral resistance were adjusted to meet strength, drift, and stability requirements, considering the effects of inherent torsion, accidental torsion, and any additional code requirements that apply (e.g., accidental torsion amplification).

Two methods were used to proportion the lateral system to meet code requirements. Method 1 assumes that the designer can vary strength and stiffness of the SFRS independently (i.e., decoupled strength and stiffness)—for example, an RC moment frame where altering the reinforcing ratio and/or section sizes allows strength and stiffness to be adjusted relatively

independently. Method 2 assumes that strength and stiffness remain proportional (i.e., coupled)—for example, adding an additional wall to a shear wall building or adding an additional bay to a moment frame. In reality, most building systems are somewhere between the two extremes, (i.e., partially coupled). To bound the possible behaviors, this study used both the decoupled and coupled methods of scaling strength and stiffness of the SFRS. Therefore, the characteristics of most real structural systems fall within the bounds of the studied archetypes.

Method 1: Decoupled strength and stiffness

1. Start with the "baseline" lateral resistance.
2. Adjust stiffness to meet drift requirements, if necessary.
3. Adjust strength to exactly meet strength requirements. Sometimes this results in a decrease in strength for certain lines of lateral resistance.
4. Adjust stiffness and/or strength to meet stability requirements, if necessary.

Method 2: Coupled strength and stiffness

1. Start with the "baseline" lateral resistance.
2. Scale strength and stiffness by exactly the same amount until strength, drift, and stability requirements are satisfied. Some lines of lateral resistance may have their strength and stiffness decreased.

4.5 Results

4.5.1 Collapse Performance under Current Code Requirements

Figure 4-6 and Figure 4-7 show the trends in collapse resistance with respect to the *TIR* for short and mid-rise archetypes designed according to ASCE/SEI 7-16. The relative collapse resistance on the vertical axis is computed by dividing the adjusted collapse margin ratio (*ACMR*) of the variant archetype by the *ACMR* of the baseline archetype. A relative collapse resistance greater than 1.0 means that an archetype has better collapse resistance than the baseline configuration, and a value less than 1.0 indicates a reduction in collapse resistance. The horizontal axis shows the maximum *TIR* value for each variant design (i.e., maximum *TIR* for the two orthogonal directions), as computed in Table 12.3 of ASCE/SEI 7-16. The computed *TIR* value tends to saturate, and even decrease in some cases, with increased inherent eccentricity; this causes the trends for some archetype groups to "double back" on themselves (e.g., the 2:1 single asymmetric archetypes). This "doubling back" behavior is explained in more detail in Appendix A.

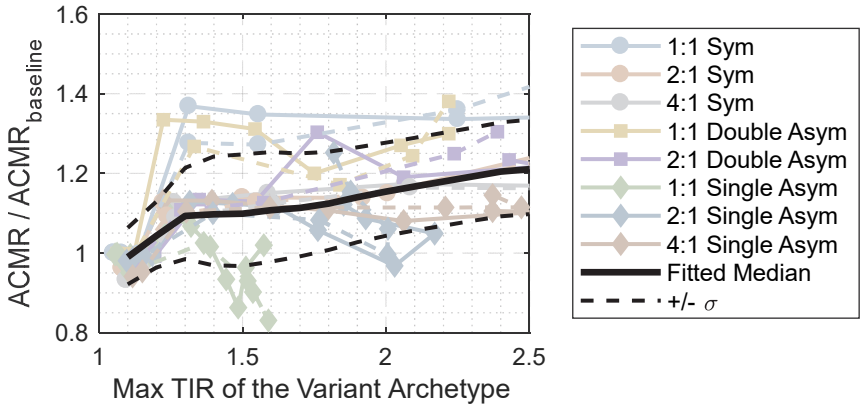

Figure 4-6 Collapse resistance relative to the baseline for short code-conforming archetypes. Archetypes with decoupled strength and stiffness are represented by solid lines with markers; dashed lines with markers represent archetypes with coupled strength and stiffness. The moving median of all results, +/- one logarithmic standard deviation, is overlaid to illustrate the general trend.

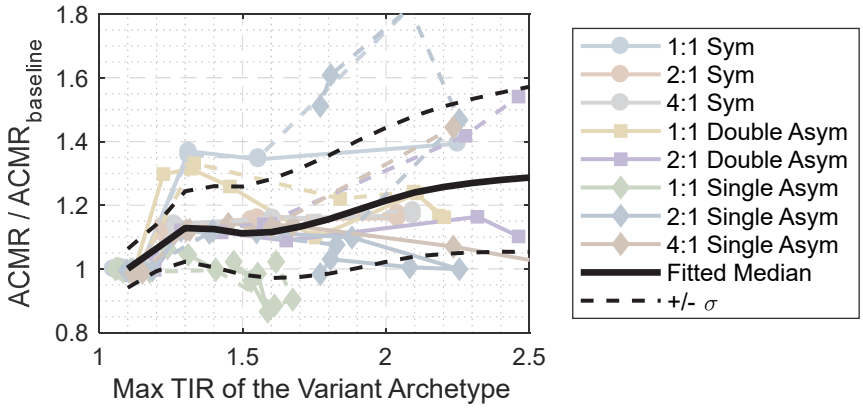

Figure 4-7 Collapse resistance relative to the baseline for mid-rise code-conforming archetypes. Archetypes with decoupled strength and stiffness are represented by solid lines with markers; dashed lines with markers represent archetypes with coupled strength and stiffness. The moving median of all results, +/- one logarithmic standard deviation, is overlaid to illustrate the general trend.

Generally, the collapse resistance of the irregular archetype buildings is higher than the collapse resistance of the baseline archetype; this is the result of torsion design requirements (e.g., accidental torsion amplification) somewhat overcompensating for the negative effects of the torsional irregularity. In some cases, however, the collapse resistance declines as torsional irregularity increases. An example case of declining collapse resistance is the 1:1 single asymmetric archetypes, where torsion moments are resisted primarily by lines of lateral resistance that are perpendicular to the lateral seismic force. Seismic demands in those lines of resistance result

from lateral forces in both orthogonal directions, even though, the two lateral force components are decoupled in the design step, which leads to poor performance under bi-directional ground shaking.

Looking closely at the results in Figure 4-6 and Figure 4-7, the immediate increase in collapse resistance for low values of *TIR* is due to triggering an increase in the redundancy factor (ρ) from 1.0 to 1.3, per Section 12.3.4.2 of ASCE/SEI 7-16. For simplicity in the design process of the archetypes, it is assumed that buildings with $TIR > 1.2$ do not comply with Table 12.3-3 of ASCE/SEI 7-16 and therefore get a redundancy factor of 1.3; systems that do comply with Table 12.3-3 would trigger $\rho = 1.3$ when $TIR > 1.4$.

Figure 4-6 and Figure 4-7 provide the results for decoupled strength and stiffness (solid lines) and coupled strength and stiffness (dashed lines). In most cases, this design difference only minimally affects the collapse resistance. Exceptions are buildings that are heavily drift controlled (e.g., the 2:1 Single asymmetric mid-rise archetypes shown in Figure 4-7). This comes from the fact that, for drift-controlled buildings, stiffening the SFRS enough to satisfy drift limits results in significant overstrength for the coupled strength and stiffness design approach, making the building more resistant to collapse.

It is critical to note that torsionally irregular archetypes often outperform the baseline only because ASCE/SEI 7-16 requires that torsional effects be accounted for in the design, and the additional requirements tend to be conservative for many of the configurations studied. Assessments of torsionally irregular archetypes for which torsion design requirements are not followed confirm that torsionally irregular buildings can perform poorly if ASCE/SEI 7-16 safeguards for torsional effects are not properly considered in the design step. As an example, Figure 4-8 shows the performance of the mid-rise archetypes when the seismic torsion safeguards of ASCE/SEI 7-16 are ignored in the design process; their collapse resistance declines steadily and substantially as the *TIR* increases.

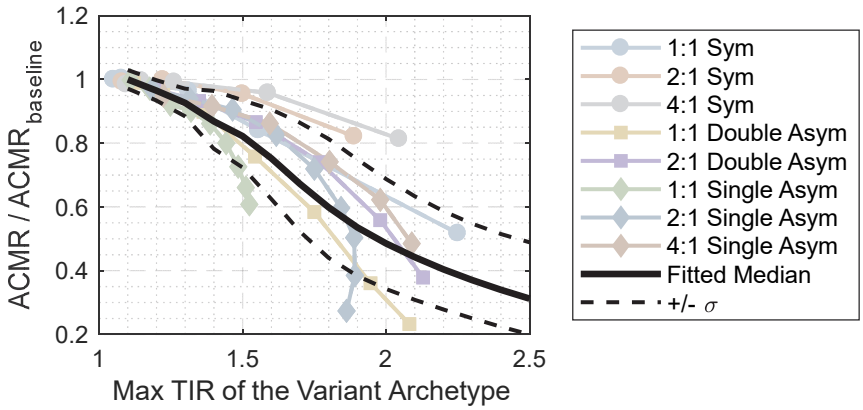

Figure 4-8 Trends in collapse resistance for mid-rise archetypes with torsional effects neglected in the design process.

4.5.2 Observations about Torsion Design Requirements

To quantify the effectiveness and necessity of the various torsion design requirements, a number of sensitivity studies were conducted to determine how the torsion design requirements affect the collapse resistance of the buildings. These studies and results are documented in Appendix A and some of the primary findings from these studies are as follows:

- Accidental torsion design requirements are relatively unimportant for torsionally regular buildings. This has been observed in past studies as well (e.g., DeBock et al., 2014).
- Simulating accidental torsion effects using modal response spectrum analysis with 5% mass offsets is ineffective for torsionally sensitive buildings whose fundamental mode is a torsional mode with limited modal mass participation in the translational directions (see Section A.5 in Appendix A for more detail).
- When checking the drift limits and stability requirements for torsionally irregular buildings, measuring the drifts at the building edge rather than the center of mass, as required in Section 12.8.6 of ASCE/SEI 7-16, is important for ensuring adequate collapse resistance (see Section A.4 in Appendix A for more detail).
- Buildings that rely heavily upon lines of lateral resistance perpendicular to the design earthquake force to resist torsion moments tend to be the poorest performers, because those lines of resistance also resist seismic demands in the perpendicular direction and therefore are "overworked" (e.g., see plot for 1:1 Single Asymmetric archetypes in Figure 4-6). For this type of building, the study shows that sufficient performance can be achieved by implementing the following:
    - Use a redundancy factor (ρ) of 1.3.

- Apply 30% of the design lateral force simultaneously in the orthogonal direction, for computing member forces.

- A torsional strength irregularity, defined by differing demand-to-capacity ratios on either side of the center of mass (per ASCE/SEI 41-17), does not negatively affect the performance of code-conforming buildings. This comes from the fact that a torsional strength irregularity in a code-conforming building only occurs when one side of the building is much stronger than required; if one side were too weak, it would no longer be code-conforming. A side-study, documented in Appendix A, shows that adding strength to one side of a building does not negatively affect collapse performance, but also does not provide much benefit in many cases. Similar conclusions may be true for some existing buildings, but these are outside of the scope of the present study.

4.5.3 Recommended Minimum Requirements

This section outlines the minimum set of torsion design recommendations that were found to be needed to ensure adequate collapse safety of code-compliant buildings. These requirements are based on the analytical studies documented in this report, with the objective that the requirements provide consistent collapse resistance over a broad range of building configurations (i.e., ensure that collapse resistance does not decrease for torsionally irregular buildings, but also avoid adding conservatism in the design process, where possible).

Table 4-2 lists suggested modifications to torsion requirements in ASCE/SEI 7-16. These suggested modifications include both new requirements and recommendations for removing existing requirements, with the overall recommendations making the design requirements arguably slightly less restrictive than the current ASCE/SEI 7-16 requirements. As for added requirements, an additional trigger for torsional irregularity is recommended for cases where more than 75% of the lateral strength is on one side of the center of mass.

Each of the proposed modifications to the ASCE/SEI 7-16 seismic torsion provisions, as outlined in Table 4-2, are summarized below with a brief explanation of how the changes to the requirements affect the collapse performance of torsionally irregular buildings.

- **Require 100%-30% orthogonal load combination for computing seismic design forces in torsionally irregular buildings.** Adding this requirement increases the design force on lines of lateral resistance that

Table 4-2 Recommended Modifications for ASCE/SEI 7-16 to Achieve Minimum Torsion Design Requirements Resulting in Adequate Collapse Resistance for a Broad Range of Building Configurations

Torsional Irregularity Classification	Triggering Criteria for the Irregularity	Add Requirements	Remove Requirements
Type 1a. Torsional irregularity	-*TIR* > 1.2 -Add additional trigger if **>75% of strength on one side of the CM.**	- Use 100%-30% orthogonal load combination rule	-N/A
Type 1b. Extreme torsional irregularity	-*TIR* > 1.4	- Use 100%-30% orthogonal load combination rule	- Automatic $\rho = 1.3$ - SDC E and F prohibition - ELF prohibition
Handle with code text (i.e., not a defined irregularity category)	If one or more of the following occurs: - *TIR* > 1.4 in both orthogonal directions - Lines of lateral resistance all on same side of CM	- Use 100%-30% orthogonal load combination rule - $\rho = 1.3$	- SDC E and F prohibition - ELF prohibition

resist a significant portion of the torsional moment from the lateral earthquake force in the orthogonal direction. The benefits of adding this requirement are most apparent in the 1:1 Single Asymmetric archetypes. To achieve the appropriate design safeguard, the 100%-30% orthogonal load combination rule need not be considered for story drift calculations.

- **Trigger Type 1a torsional irregularity if more than 75% of story strength is on the same side of the center of mass**. This recommendation results from observing that buildings with significant inherent eccentricity can still have *TIR* < 1.2 (i.e., not be classified as torsionally irregular according to Table 12.3-1 in ASCE/SEI 7-16) where there is significant torsional stiffness from lines of lateral resistance in the orthogonal direction. For such buildings, the lines of lateral resistance orthogonal to the direction with inherent eccentricity resist the majority of the torsional moment and triggering the 100%-30% orthogonal load combination rule is necessary for proportioning those elements. Without this requirement, some of the three-sided and mixed system variants with *TIR* < 1.2 would perform significantly worse than the baseline archetypes (with examples presented in Section A.4 of Appendix A).
- **Relax the triggers requiring $\rho = 1.3$.** ASCE/SEI 7-16 requires that all buildings classified as extremely torsionally irregular have a redundancy factor of 1.3, regardless of whether the system is redundant. While some torsionally irregular buildings need the benefit of the 30% increase in design force, not all do. Only building configurations with *TIR* > 1.4 in both directions or with a large inherent eccentricity (e.g., lines of lateral

resistance all on the same side of the CM), are found to need the 30% increase in design lateral force.

- **Remove prohibition of the ELF design procedure**. The archetype buildings in the torsion study where designed using the equivalent lateral force (ELF) design procedure (for design displacements and distribution of design forces), and their performance was shown to be satisfactory when the proposed design provisions are implemented (see Figures 4-9, 4-10, and 4-11). Additionally, the vertical irregular studies in this report show that the ELF procedure generally results in more conservative vertical distributions of seismic forces, leading to better collapse resistance as compared with design using modal response spectrum analysis (e.g., Appendix F and Chapter 6). Therefore, the ELF procedure should not be prohibited on the basis of a torsional irregularity.

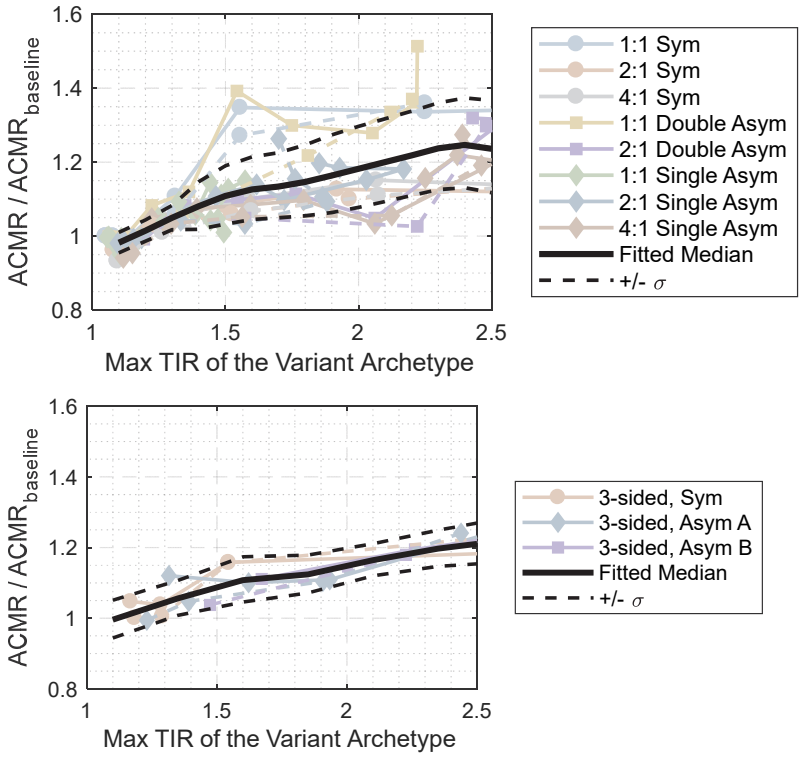

Figure 4-9 Collapse resistance relative to the baseline for short archetypes designed with the proposed minimum standards. Archetypes with decoupled strength and stiffness are represented by solid lines with markers; dashed lines with markers represent archetypes with coupled strength and stiffness. The moving median of all results, +/- one logarithmic standard deviation, is overlaid to illustrate the general trend.

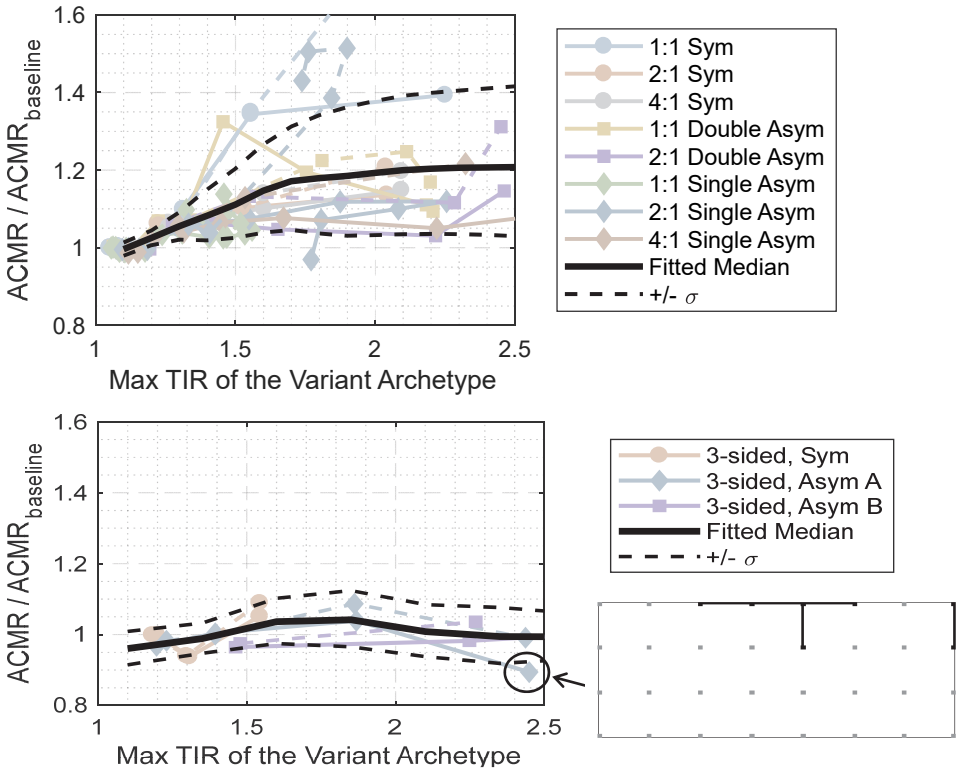

Figure 4-10 Collapse resistance relative to the baseline for mid-rise archetypes, designed with the proposed minimum standards. Archetypes with decoupled strength and stiffness are represented by solid lines with markers; dashed lines with markers represent archetypes with coupled strength and stiffness. The moving median of all results, +/- one logarithmic standard deviation, is overlaid to illustrate the general trend.

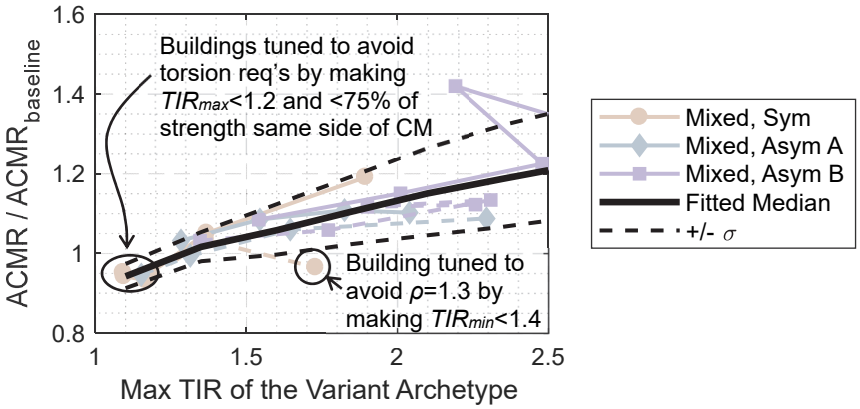

Figure 4-11 Collapse resistance relative to the baseline for mixed system archetypes, designed with the proposed minimum standards. Archetypes with decoupled strength and stiffness are represented by solid lines; dashed lines represent archetypes with coupled strength and stiffness. The moving median of all results, +/- one logarithmic standard deviation, is overlaid to illustrate the general trend.

- **Require that the accidental torsion loading be computed using a static accidental torsional moment when designing buildings with extreme torsional irregularity.** This recommendation is that, when a building with extreme torsional irregularity is designed using linear design methods, the accidental torsion loading must be accounted for by applying a static accidental torsional moment in accordance with Sections 12.8.4.2 and 12.8.4.3 of ASCE/SEI 7-16. It should not be permitted to use explicit 5% mass offsets in linear dynamic analysis for buildings with extreme torsional irregularity. This recommendation is based on the finding that modal response spectrum analysis with 5% mass offsets produces unsafe designs for extremely torsionally irregular buildings whose torsional modes contain little modal mass in the translational direction (e.g., the symmetric archetypes, as shown in Section A.5 of Appendix A). This finding is consistent with a previous study by De la Llera and Chopra (1994), which illustrated that modal response spectrum analysis with 5% mass offsets does not adequately amplify accidental torsion effects for buildings with long torsional periods.
- **Remove prohibition of extremely torsionally irregular building configurations in SDC E and F.** If the torsion design provisions recommended in this study are utilized, the study shows no reduction in collapse resistance for $TIR > 1.4$ (the cut-off for Type 1b extreme torsional irregularity in Table 12.3-1 of ASCE/SEI 7-16) for SDC D building designs; therefore, there is no need to prohibit such buildings in SDC D. To verify whether this conclusion could be extended to SDC E and F, the archetype models were also analyzed with 12 ground motion pairs from the FEMA P695 near-field ground motion set having pulse characteristics, since the seismic hazard for SDC E and F sites is dominated by near-field ground motions. The near-field motions with pulses caused all of the archetypes to collapse at lower spectral acceleration intensities as compared with the far-field motions; however, the trends in relative collapse resistance with *TIR* were nearly identical to those observed with the far-field ground motion set. This demonstrated that torsionally irregular buildings still perform equivalently with the baseline archetypes (and often somewhat better than), even when subjected to pulse-type ground motions. It should be noted that the FEMA P695 near-field record set has a broad range of spectral shapes, as does the far-field set, therefore the similarity in trends among the two ground motion record sets is expected. A significant benefit of removing the prohibition of extremely torsionally irregular buildings is that very strong and stiff buildings with large plan aspect ratios would no longer

be prohibited. Such buildings are expected to perform well under seismic demands but are often classified as extremely torsionally irregular according to Table 12.3-1 of ASCE/SEI 7-16 simply based on relative stiffness, regardless of how strong and stiff they are in an absolute sense. In a side-study, it was found that such buildings still need the proposed force requirements (e.g., the 100%-30% lateral seismic load application rule), but they should not be prohibited. With the proposed modifications, it is recommended that these buildings no longer be prohibited.

To assess the results of the proposed torsion requirements, Figure 4-9 through Figure 4-11 provide relative collapse safety results for archetype buildings designed with the Table 4-2 modifications. These figures show that the performance of the irregular buildings is generally better than that of the baseline, even when the *TIR* is significantly greater than the threshold for extreme torsional irregularity (*TIR* > 1.4). The lowest observed *ACMR* is approximately 90% of the baseline (i.e., a 10% decrease), which is for the worst case of a three-sided mid-rise variant with decoupled strength and stiffness; this result is annotated in Figure 4-10. However, the proposed torsion provisions are still considered satisfactory, even for that archetype, for two reasons:

1. The base shear for computing drifts is based on the fundamental period of 2.57 s, however, the fundamental mode of vibration is torsionally dominated. The mode with the most modal mass in the translational y-direction has a significantly shorter period of 0.8 s. In practice, the period with the most modal mass should be considered the fundamental period for calculating base shear. Allowing the use of the approximate period per Section 12.8.2 of ASCE/SEI 7-16, the design period in the y-direction could be taken as $T = T_a = 1.45$ s. In that case, the base shear for computing drifts increases by 80%, raising the design drift to 2.9% in the y-direction (well above the 2% limit). Redesigning the archetype accordingly results in an *ACMR* that is within 5% of the baseline *ACMR*.
2. The observed 10% reduction in collapse resistance is small, given that it only occurs for one archetype. For context, a 10% reduction in *ACMR* causes a building with 10% probability of collapse given MCE_R to change to 14% probability of collapse given MCE_R; this falls within the tolerance of the FEMA P695 guidelines, which allow up to a 20% probability of collapse given MCE_R for an individual archetype, even though 10% is the upper limit for the average of a group of archetype buildings.

4.6 Conclusions and Recommendations

Based on analyses of a broad set of archetype building designs, this chapter suggests modifications to the torsional-irregularity design requirements of ASCE/SEI 7-16. The modifications include both removing some existing requirements to reduce conservatisms and also adding some new requirements that were necessary to ensure adequate collapse safety.

The following lists ASCE/SEI 7-16 design requirements that were found to add unnecessary conservatism to the design process and are proposed to be removed:

- Prohibition of extremely torsionally irregular buildings in Seismic Design Categories E and F. Such buildings need not be prohibited, provided that the recommended modifications to the ASCE/SEI 7-16 seismic design procedures are implemented.
- Prohibition of the equivalent lateral force procedure. The equivalent lateral force procedure is shown to produce safe designs for torsionally irregular buildings and need not be prohibited on the basis of torsional irregularity.
- Triggers for making the redundancy factor, ρ, equal to 1.3. If the 100%-30% load combination rule is utilized as this study suggests, the additional amplification of seismic forces caused by the redundancy factor is not always necessary. Therefore, the triggers for making the redundancy factor, ρ, equal to 1.3 can be relaxed.

The following lists new proposed design requirements that are not currently in ASCE/SEI 7-16 but are necessary to ensure adequate collapse performance of buildings with torsional irregularities:

- Require a 100%-30% lateral load combination rule for computing design forces in torsionally irregular buildings. This elevates the performance of buildings that rely heavily on lines of lateral resistance orthogonal to the design earthquake force to resist torsion moments. Effects on buildings with little to no inherent eccentricity are minimal. Note that the 100%-30% lateral load combination is not necessary for evaluating story drifts.
- Classify buildings as Type 1a torsionally irregular if more than 75% of the story strength is on the same side of the center of mass. Some buildings with large inherent eccentricity can still fall below the ASCE/SEI 7-16 threshold for Type 1a torsional irregularity. For such buildings, the seismic response in the two orthogonal directions is highly

coupled, so triggering the 100%-30% orthogonal combination rule is important.

- Require application of a static accidental torsional moment, M_{ta}, (i.e., Sections 12.8.4.2 and 12.8.4.3 of ASCE/SEI 7-16) for buildings with extreme torsional irregularity. In other words, do not permit use of explicit 5% mass offsets in linear dynamic analysis of such buildings.

It is also found that special treatment of buildings with "torsional strength irregularity," as defined by demand/capacity ratios in ASCE/SEI 41, is not necessary for new building design.

Chapter 5
Concrete Wall Buildings with Vertical Irregularities (V1, V8)

5.1 Overview and Summary of Findings

This chapter summarizes the analytical studies for reinforced concrete (RC) wall buildings that were designed per ASCE/SEI 7-16, *Minimum Design Loads and Associated Criteria for Buildings and Other Structures* (ASCE, 2017a). The effects on building performance of the following vertical irregularities were studied:

- **V1, Soft story irregularity.** This condition is Type 1 vertical irregularity, as defined in Table 12.3-2 of ASCE/SEI 7-16. The RC wall building studies were mostly focused on this irregularity and it is the subject of most of this chapter.
- **V8, Wall discontinuity.** This condition is not defined as a vertical irregularity in current U.S. codes and standards. It is defined in this report as a condition where there is an abrupt discontinuity or large variance of stiffness along the height of a shear wall. Discussion of this vertical irregularity is covered in Section 7.6 and a description of a limited study conducted on this irregularity is provided in Section B.2.

The following are covered in this chapter: (1) summary of current design procedures for walls and commonly observed vertical irregularities (Section 5.2); (2) an overview of archetype designs to investigate the impact of vertical irregularities (Section 5.3); (3) information related to the modeling approach (Section 5.4); (4) an overview of the collapse risk assessment and corresponding results (Section 5.5); and (5) conclusions and recommendations (Section 5.6). Details supporting the information in this chapter, including the RC wall building design process, modeling details, and detailed analysis results, are provided in Appendix B.

The results of the studies described in this chapter show that: (1) the collapse risk posed by RC wall buildings, in which walls respond in flexure, is relatively low whether or not the system is irregular and whether or not failure of the gravity system is considered in the analysis; (2) collapse risk does not vary significantly (less than 20%) with the introduction of a vertical stiffness irregularity if the collapse risk posed by the baseline wall is not

excessively small (less than 0.11%); and (3) the use of different modeling approaches does not significantly affect collapse risk.

5.2 Design Procedures and Common Irregularities

Reinforced concrete walls are commonly used to resist lateral forces from earthquakes and wind. They provide high stiffness and strength under service-level loads, can be detailed to provide ductility under design-level earthquake loads, and can take on many configurations, including the introduction of isolated openings to accommodate architectural requirements. Figure 5-1 shows regular and irregular vertical configurations for wall systems and Figure 5-2 shows common cross-sectional configurations for walls.

Wall cross section is largely a function of architectural layout. Mid- to high-rise buildings typically have walls located around a central service or elevator core as illustrated in Figure 5-3. Typically, the core walls are arranged to form a closed box, with C, L, or rectangular piers that are connected by coupling beams extending over wall openings (Figure 5-2d). In low-rise buildings or buildings without a central elevator core, it is common to have walls distributed throughout the floor plate as the location and shape of the walls is typically constrained by the architectural layout. Planar walls (Figure 5-2b) and asymmetric wall configurations are typically used, with the L-shape wall layout being the most common asymmetric wall configuration. Irregular patterns of openings may be introduced into the wall configurations shown in Figure 5-1c to accommodate architectural requirements.

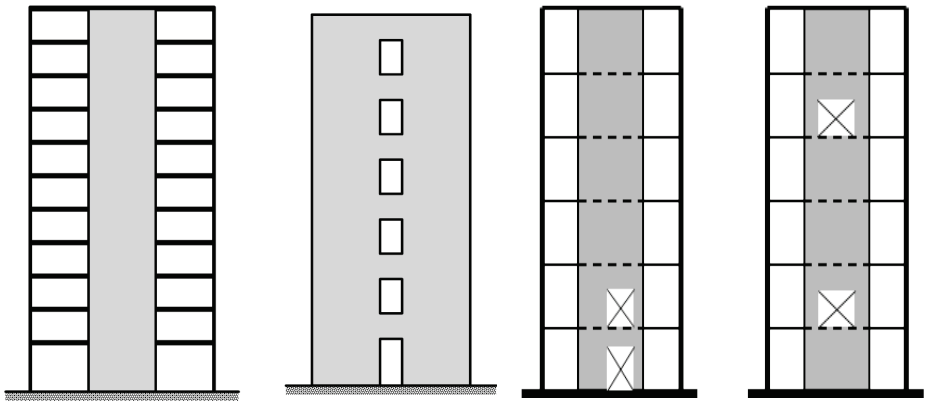

(a) Cantilever wall (b) Coupled wall (c) Walls with vertical irregularities

Figure 5-1 Vertical wall-system configurations (a,b from NIST, 2011).

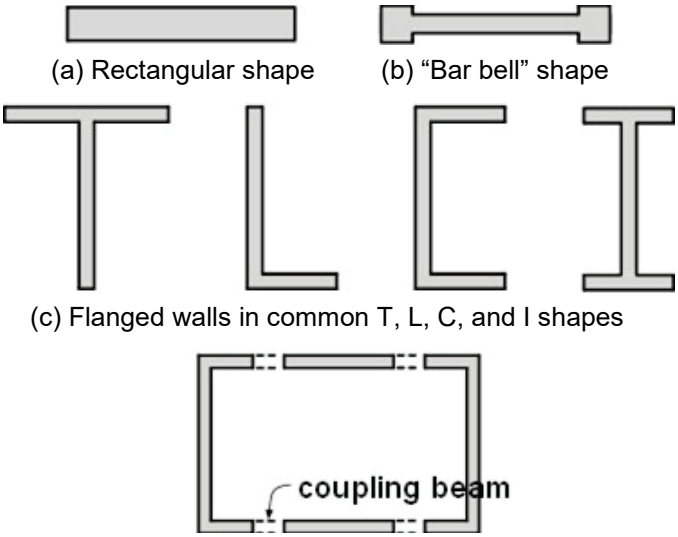

Figure 5-2 Common wall cross-sectional configurations (NIST, 2011).

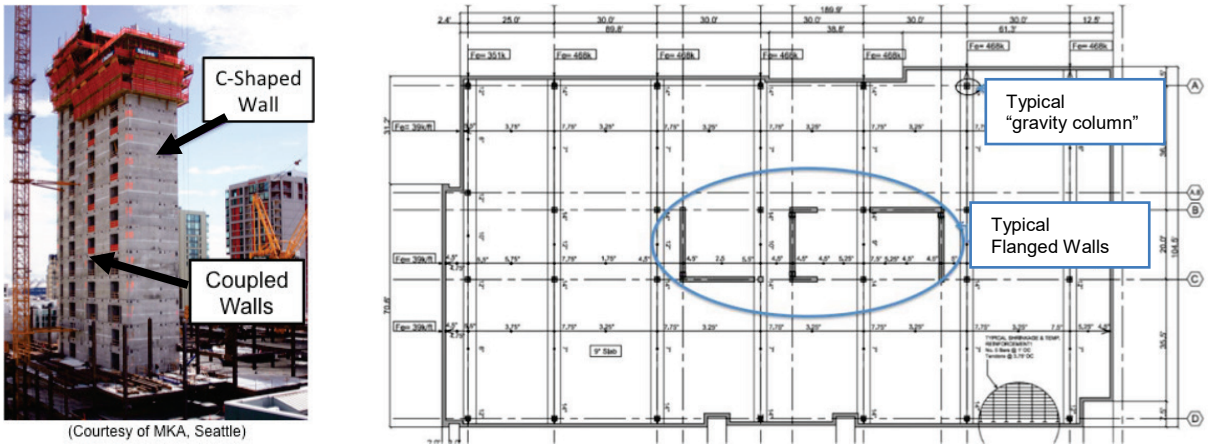

(a) Core wall (b) Distributed planar and flanged walls

Figure 5-3 Core wall versus distributed planar and flanged walls.

Design of continuous flexural concrete walls used as the primary lateral-load-resisting system includes:

- Determination of longitudinal reinforcement required for flexural demand. Often much of this reinforcement is concentrated at the ends of the walls as it is the optimal location for flexural resistance. These regions are referred to as boundary elements in ACI 318-14, *Building Code Requirements for Structural Concrete* (ACI, 2014).
- Sizing and detailing of confining reinforcement.
- Design of horizontal reinforcement to meet the shear demand. ACI 318-14 allows use of a larger strength-reduction factor to calculate shear strength if the shear demand corresponds to plastic hinging (ACI, 2014).

For walls with discontinuities, the design process also requires an adequate load path around the discontinuity (ACI, 2014) and placement of reinforcing steel to resist loads and ensure capacity through multiple load cycles. This is further discussed in NIST GCR 11-917-11REV-1, *Seismic Design of Cast-in-Place Concrete Special Structural Walls and Coupling Beams* (NIST, 2011).

5.3 Overview of Archetype Designs

To investigate the impact of vertical irregularities on the earthquake performance of mid-rise RC wall buildings, a series of RC wall buildings were designed in which lateral loads are resisted by planar reinforced concrete walls. An overview of the baseline design (i.e., no vertical irregularities) is presented in Chapter 3; details of the design process and all wall designs are provided in Appendix B.

Walls were designed without openings and then with openings located at the 1st, 1st and 2nd, and an upper story. Opening length was determined to achieve a stiffness for the stories with the opening that was either 50% of the baseline building or 75% of the baseline building; Section B.3 presents the process used to compute story stiffness. Wall demands were determined using the ASCE/SEI 7-16 ELF procedure and, for the case of the D_{max} design spectrum, using the results of a MRSA procedure (ASCE, 2017a). Table 5-1 presents the design space.

Table 5-1 Design Space for RC Wall Buildings

Number of Designs	Stories	Method Used to Determine Demands	Design Spectrum Used for Design	Stories with Openings	Stiffness of Floor with Opening Normalized by Stiffness of Floor Above
6	8	ELF	D_{max}	None, 1st, 1st & 2nd, 5th	50% and 75%(1)
5	8	MRSA	D_{max}	None, 1st, 1st & 2nd	50% and 75%
6	8	ELF	B_{max}	None, 1st, 1st & 2nd, 5th	50% and 75%(1)
6	12	ELF	D_{max}	None, 1st, 1st & 2nd, 8th	50% and 75%(1)
6	12	ELF	B_{max}	None, 1st, 1st & 2nd, 5th	50% and 75%(1)

(1) For buildings with openings on the 5th or 8th story, only the case of a wall with an opening producing a section stiffness equal to 50% of the section stiffness on adjacent walls was considered.

Figure 5-4 shows elevation views for the 8-story RC wall buildings; 12-story elevations are similar. For D_{max} designs, an opening of 2.5 ft. was used to create a story stiffness equal to 75% of the stiffness of the baseline building and an opening of 7.5 ft. was used to create a story with a stiffness equal to 50% of the story stiffness of the baseline building. For B_{max} designs,

openings of 1.5 ft. and 5 ft. were used, respectively, to create story stiffnesses equal to 75% and 50% of the story stiffnesses of the baseline building.

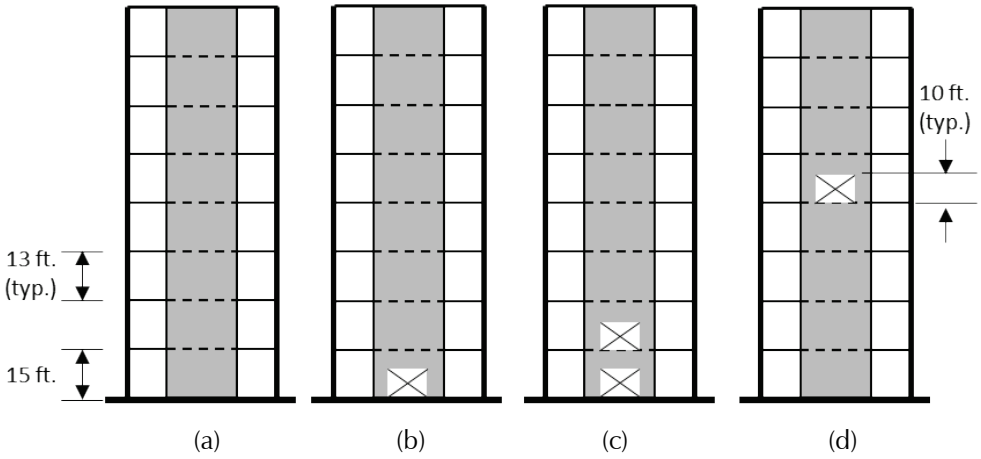

Figure 5-4 Idealized building elevations (a) without openings; (b) with openings in 1st story; (c) with openings in 1st and 2nd stories; and (d) with openings in upper stories (5th for 8-story building, shown here, and 8th for 12-story building).

Each RC wall building design has a unique identification tag that includes information about all relevant design characteristics. The 8-story RC wall building designed using the MRSA method to determine demands for the D_{max} spectrum with no wall openings is identified as 8-D-0-0-MRSA while the 12-story RC wall building designed using the ELF procedure to determine demands for the D_{max} spectrum with openings in the 1st and 2nd stories to produce a story stiffness equal to 50% of the 3rd story is identified as 12-D-2S-50-ELF. Table 5-2 provides seismic design parameters for the RC wall buildings.

Table 5-2 RC Wall Building Periods and Base Shear Demands

Design ID	Period(s) from MRSA	$C_u T_a$ [s]	Base Shear Demand: Earthquake	Base Shear Demand: Wind
8-D-0-0-*	1.14	0.93	0.11W	
8-D-*-*-*	1.14 – 1.18	0.93	0.11W	
8-B-0-0-*	2.03	1.12	0.01W	0.02W
8-B-*-*-*	~2.03	1.12	0.01W	0.02W
12-D-0-0-*	2.41	1.25	0.08W	
12-D-*-*-*	2.41 – 2.42	1.25	0.08W	
12-B-0-0-*	3.07	1.15	0.01W	0.02W
12-B-*-*-*	~3.07	1.15	0.01W	0.02W

Individual walls were designed to achieve required strength and stiffness and were detailed to achieve deformation capacity per ACI 318-14 (ACI, 2014).

Specified material strengths used for design were f_c' = 5000 ksi and f_y = 60 ksi. Walls were sized to achieve required strength and stiffness and to keep longitudinal reinforcing ratios in heavily reinforced boundary element regions below 3%. Appendix B provides detailed design information for the 8-story baseline shear wall building designed using the ASCE/SEI 7-16 ELF procedure (8-D-0-0-ELF) and provides all 8- and 12-story wall designs.

Design of the baseline 8-story RC wall building (8-D-0-0-ELF) resulted in walls 30 ft. long by 2 ft. thick. At the base, the wall included 6 ft. long boundary elements with 2.5% longitudinal reinforcement ratios, web region longitudinal and horizontal reinforcement was approximately equal to the ACI 318-14 minimum of 0.25%, and maximum shear stress demand was $1.9\sqrt{f_c}$ psi. To facilitate comparison of the different wall designs, the 30 ft. by 2 ft. gross wall dimensions were maintained for all 8-story wall designs. Table 5-3 provides relevant design details for all 8-story wall designs, with:

- ρ_{BE} equal to the boundary element longitudinal reinforcement ratio at the base of the wall (two values are provided by walls with openings as different reinforcement ratios are provided for boundary elements on the interior and exterior of the wall pier);
- ρ_{web} and ρ_h equal to the web region longitudinal and horizontal reinforcement ratios at the base of the wall;
- $\rho_{h\_opening}$ equal to the horizontal reinforcement ratio in the wall above the openings; and
- ρ_{CB} equal to the coupling beam diagonal reinforcement ratio (total diagonal or horizontal bar area divided by coupling beam cross-sectional area).

Table 5-3 Design Properties for RC Walls

Wall ID	Opening Length [ft.]	Boundary Element Length [ft.]	ρ_{BE} [%]	ρ_{web} [%]	ρ_h [%]	$\rho_{h\ opening}$ [%]	ρ_{CB} [%]
8-D-*-*-ELF walls are 30 ft. long by 2 ft. thick							
8-D-0-0-ELF	-	6	2.5	0.25	0.25	-	-
8-D-1S-75-ELF	2.5	5	3.5	0.25	0.25	0.65	-
8-D-1S-50-ELF	7.5	5	3.7	0.25	0.25	0.42	-
8-D-2S-75-ELF	2.5	5	3.7	0.25	0.25	0.65	0.71 (diag)
8-D-2S-50-ELF	7.5	5	3.9	0.25	0.25	0.65	0.87 (diag)
8-D-5S-75-ELF	2.5	6	2.5	0.25	0.25	0.25	-
8-D-5S-50-ELF	7.5	6	2.5	0.25	0.25	0.25	-

Table 5-3 Design Properties for RC Walls (continued)

Wall ID	Opening Length [ft.]	Boundary Element Length [ft.]	ρ_{BE} [%]	ρ_{web} [%]	ρ_{h} [%]	$\rho_{h\_opening}$ [%]	ρ_{CB} [%]
8-B-*-*-ELF walls are 20 ft. long by 2 ft. thick							
8-B-0-0-ELF	-	-	0.25	0.25	0.25	-	-
8-B-1S-75-ELF	1.5	-	0.25	0.25	0.25	0.25	-
8-B-1S-50-ELF	5.0	-	0.25	0.25	0.25	0.25	-
8-B-2S-75-ELF	1.5	-	0.25	0.25	0.25	0.25	-
8-B-2S-50-ELF	5.0	-	0.25	0.25	0.25	0.25	-
8-B-5S-75-ELF	1.5	-	0.25	0.25	0.25	0.25	-
8-B-5S-50-ELF	5.0	-	0.25	0.25	0.25	0.25	-

5.4 Modeling RC Wall Response

An overview of the modeling approach for studies covered in this report is provided in Section 3.3. The following sections provide more details on specific aspects particular to the RC wall building studies.

5.4.1 Methodology Validation and Comparison Studies

Both ATENA and OpenSees were used in modeling RC wall buildings for this study. Nonlinear models of the RC wall buildings were constructed by using finite elements in ATENA (for validation purposes only) and by using three different methods in OpenSees, as follows: (1) force-based beam-column elements (FBE) with fiber-type section models and the distributed plasticity modeling approach developed by Pugh et al. (2015); (2) displacement-based beam-column elements (DBE) with fiber-type section models and the distributed plasticity modeling approach developed by Pugh et al. (2015) and updated by Marafi et al. (2018); and (3) the shear-flexure-interaction multi-vertical line-element model (SFI-MVLEM) developed by Kolozvari et al. (2015a,b; 2018).

Studies validating the modeling approaches for RC wall buildings (against experimental data for a large dataset) are described in detail in Section B.4. These studies show that the modeling approach provides accurate simulation of planar wall response to lateral loading, including onset of lateral strength loss for walls that respond in flexure. Similar comparisons for the SFI-MVLEM shows accurate simulation of stiffness and strength; this model was calibrated to provide simulation of drift capacities that were similar to those predicted using the beam-column elements.

Preliminary analyses were conducted using all modeling methods for the purposes of validating and comparing the different analysis methods. These included: (1) pushover analyses to compare OpenSees to ATENA models; (2) dynamic analyses to compare DBE and FBE models in OpenSees; and (3) dynamic analyses to compare DBE models and SFI-MVLEM in OpenSees. Details of these comparison and validation studies are provided in Section B.5. These comparison studies showed significant differences in drift capacity, and to a lesser extent stiffness and strength of an RC wall building, depending on the method used. These differences could be expected to affect the assessment of collapse risk for RC wall buildings and, in particular, the impact of vertical irregularities resulting from the introduction of openings on this risk. The OpenSees DBE modeling approach was selected for the use in the study because:

- The ATENA model, which likely provides the most accurate simulation of response, is not practical for dynamic analyses due to the computational time required to complete the continuum analyses.
- The OpenSees FBE modeling approach exhibits failures of the numerical solution algorithm that result in an inaccurate and reduced calculation of collapse risk.
- The OpenSees SFI-MVLEM has not be extensively validated for use in simulating response beyond onset of strength loss.
- The OpenSees DBE modeling approach has been extensively validated for simulation of onset of strength loss, provides plausible simulation of response following onset of strength loss (minimal experimental data exist for validation), and provides the greatest numerical robustness and efficiency.

5.4.2 Non-Simulated Failure Modes

The OpenSees and ATENA modeling approaches described in Appendix B have been shown to provide accurate simulation of onset of lateral strength loss due to compression-controlled flexural failure, which is the most common failure mode observed in the laboratory for concrete walls. However, building *collapse* is defined by loss of gravity load carrying capacity, not loss of lateral load carrying capacity. Loss of lateral load carrying capacity can produce loss of gravity load carrying capacity if large story drifts result in instability. However, instability due to *P*-Delta effects may require very large story drifts. Consideration of the gravity system in a RC wall building suggests that failure of the gravity system will likely cause collapse long before wall instability. Thus, it is necessary to consider the non-simulated failure mode of collapse of the gravity load system.

Most of the gravity load was assumed to be carried by a two-way reinforced concrete "slab-column" gravity system. Slab-column systems must transfer shear and moment at the column-slab connection. Typically, these systems utilize continuous longitudinal reinforcement of the slab through the column. The primary damage mode of flat-slab-to-column connections is punching shear. The reinforcement serves to sustain the moment demands resulting from vertical and lateral loading. For severely damaged slabs, catenary action is needed to prevent full collapse of the floor system (Figure 5-5b). Figure 5-5a shows a collapsed building for which catenary action did not occur in the exterior connections, demonstrating the need to limit damage to slab-column connections to prevent structural collapse. One of the most common solutions to increase the strength and deformability of slab-column connections is to strengthen the region prone to punching shear. Solutions include: (1) addition of shear reinforcement; (2) addition of internal shear studs; (3) addition of external shear studs; and (4) addition of column capital. Although column capitals have been shown to improve the performance (see, for example, Wey and Durrani, 1992), they are typically not desired for architectural reasons and have fallen out of favor. Instead, engineers have sought solutions to improve the response with internal reinforcement. Hueste et al. (2009) collected test data to compare the drift capacity of slab-column connections with and without shear reinforcement ("improved" specimens had either traditional shear reinforcement or internal shear studs, as shown in Figure 5-6). In general, the response improved only a modest amount for low shear ratios, but a more significant drift capacity is noted for connections with higher shear ratios; this can be demonstrated by comparing the markers in the two plots.

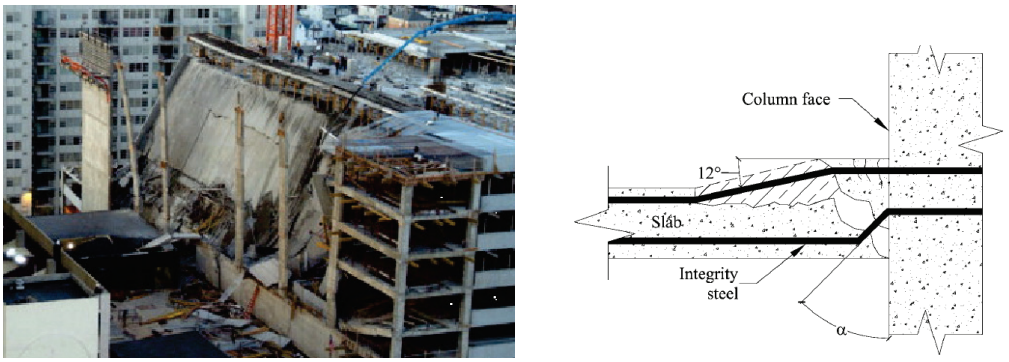

(a) (b)

Figure 5-5 Typical response of slab-column connections: (a) collapse of building with slab-column connections; (b) catenary action in exterior slab-column connection (Pan and Moehle, 1992).

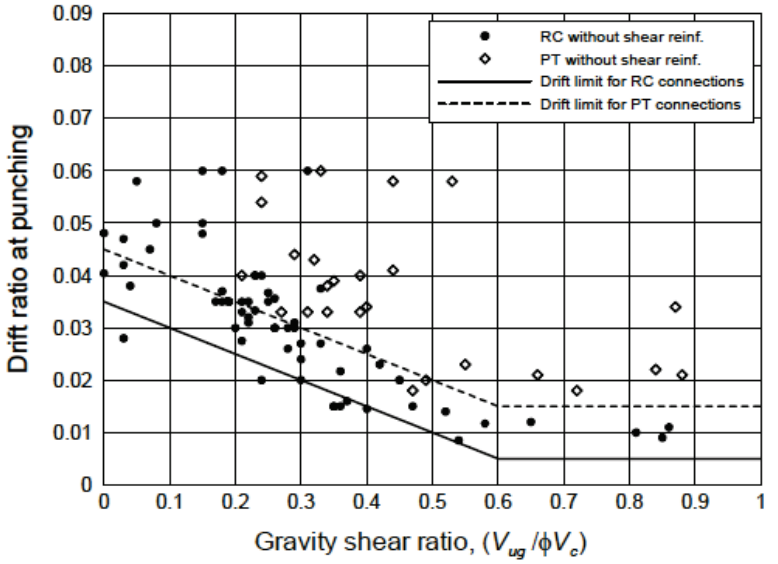

(a)

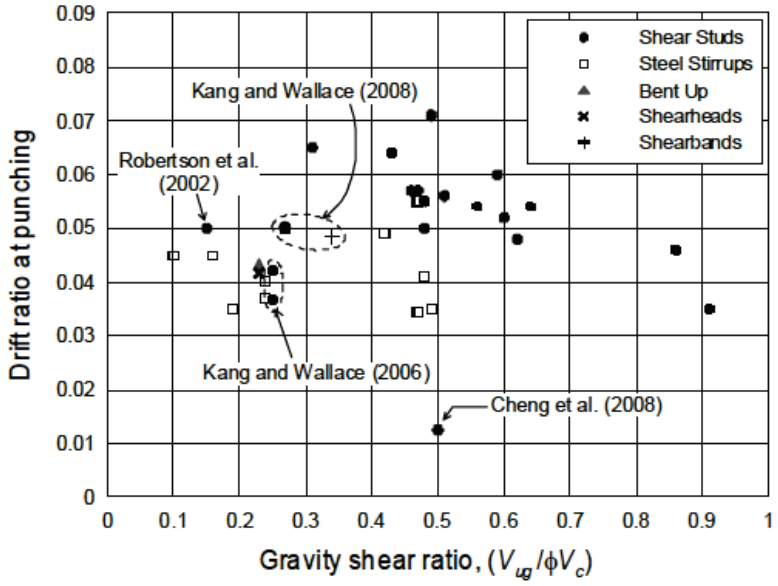

(b)

Figure 5-6 Drift of slab-column connections (a) without and (b) with shear reinforcement (Hueste et al., 2009).

As stated above, gravity loads were assumed to be carried primarily by a two-way reinforced concrete slab-column system. The assumption is extended to include a two-way reinforced concrete slab-column system in which shear reinforcement is provided at the column-slab connection. As such, the data in Figure 5-6 indicate that the system could be expected to lose gravity load carrying capacity at story drift ratio of approximately 5%.

5.5 Assessment of Collapse Risk

5.5.1 Overview

The FEMA P695 methodology was used to assess the collapse risk posed by the 8- and 12-story RC wall building designs, as described in Section 3.4. Nonlinear dynamic analyses were conducted using the OpenSees analysis platform and the DBE modeling procedure described above. For each building archetype, collapse risk was computed using the suite of nonlinear analysis results, for two different definitions of collapse: (1) collapse due to failure of the gravity system at a maximum story drift of 5%; and (2) collapse due to a sidesway mechanism characterized by a maximum story drift in excess of 10%. The following highlight the process (particular to RC wall buildings) for determining certain parameters in the FEMA P695 methodology:

- System overstrength, Ω, was computed using: (1) the results of nonlinear pushover analysis; (2) the OpenSees DBE modeling approach described in Chapter 3, Section B.4, Figure 3-14, and Figure 3-15; and (3) the ELF load distribution for ELF designs or a modal force distribution for MRSA designs.
- System ductility, μ, was defined as $\mu = \delta_u/\delta_{y,eff}$ where δ_u is the roof drift corresponding to 20% lateral strength loss from the pushover analysis and $\delta_{y,eff}$ is the effective drift at yield. The parameter $\delta_{y,eff}$ was defined using pushover analysis data rather than the recommended period-dependent method because the nonlinear response model used this study does not overestimate pre-yield stiffness, but instead simulates stiffness loss due to concrete cracking. Pushover analyses of RC wall buildings show that many RC wall buildings have significant residual lateral strength such that the definition of ductility based on 20% strength loss does not provide an accurate representation of earthquake load resistance (see Figure 5-7 and Figures B-26 through B-28). Thus, for this study, for all wall designs, the adjusted collapse margin ratios (*ACMR*s) and collapse probabilities were also computed for the case of $\mu = 8$, the maximum ductility considered in the methodology.
- Total system collapse uncertainty, β_{TOT}, was defined by the quality of the model, design requirements, and test data. The quality of the model, design requirements, and test data were taken as "good," resulting in $\beta_{TOT} = 0.525$.

Results show that collapse risks for RC wall structures, with and without introduction of openings in lower stories, is relatively low (less than 4%).

5.5.2 Results

Pushover and IDA were conducted for all 8- and 12-story concrete shear wall building designs (Table 5-1) using the OpenSees DBE modeling approach. Figure 5-7 and Figure 5-8 provide examples of the results from the pushover analyses and results from suites of dynamic analyses, respectively. These particular figures are for 8-story RC wall buildings designed for the D_{max} spectrum. Appendix B provides the full set of results for all cases described in this chapter. The results suggest that the introduction of vertical irregularities via openings that reduce story stiffness has relatively little impact on collapse risk.

Dynamic analysis results for the wall configurations listed in Table 5-1 were combined with pushover analysis results and assessment of design, modeling, and uncertainty to determine collapse probabilities for RC wall buildings with vertical irregularities resulting from openings that reduce stiffness. Table 5-4 lists collapse probabilities for RC wall buildings designed for the D_{max} spectrum and Table 5-5 lists these quantities for RC wall buildings designed for the B_{max} spectrum for collapse defined by a maximum story drift in excess of 5%. Table B-5 and Table B-6 list these quantities for collapse defined by a maximum story drift in excess of 10%.

Figure 5-9 shows normalized *ACMR*s versus building height for different levels of irregularity for buildings designed using the ELF procedure. Figure 5-10 shows similar data for buildings designed using the MRSA procedure.

The data in Figure 5-9 through Figure 5-11, and Tables 5-4, 5-5, B-5, and B-6 support the following conclusions for RC wall buildings for which collapse is defined by maximum interstory drift in excess of 5% or 10%:

- Collapse margin ratios are relatively high and collapse probabilities were relatively low for the buildings and failure/collapse modes considered in this study. The maximum computed collapse risk was 2.3% for collapse resulting from interstory drifts in excess of 5% and 10%.
- For 8- and 12-story RC wall buildings designed for the D_{max} spectrum and considering collapse associated with failure of the gravity system at a maximum interstory drift of 5%, the collapse probability of the solid wall system is low (0.5% to 1.2%). The introduction of a vertical stiffness irregularity increases collapse risk and reduces the collapse margin ratio moderately (maximum reduction is less than 25%).
- The ASCE/SEI 7-16 classification of irregular versus extremely irregular does not consistently correlate with collapse probability. For walls with the same height and designed using the same design procedure (i.e.,

8-story wall with an opening in the 1st story designed using the ELF procedure), irregular and extremely irregular walls are equally likely to have larger or smaller collapse probabilities.

- Severe irregularities located in upper stories of the wall, away from the base where flexural yielding occurs, have less impact on collapse probability than do irregularities introduced at the base of the wall.

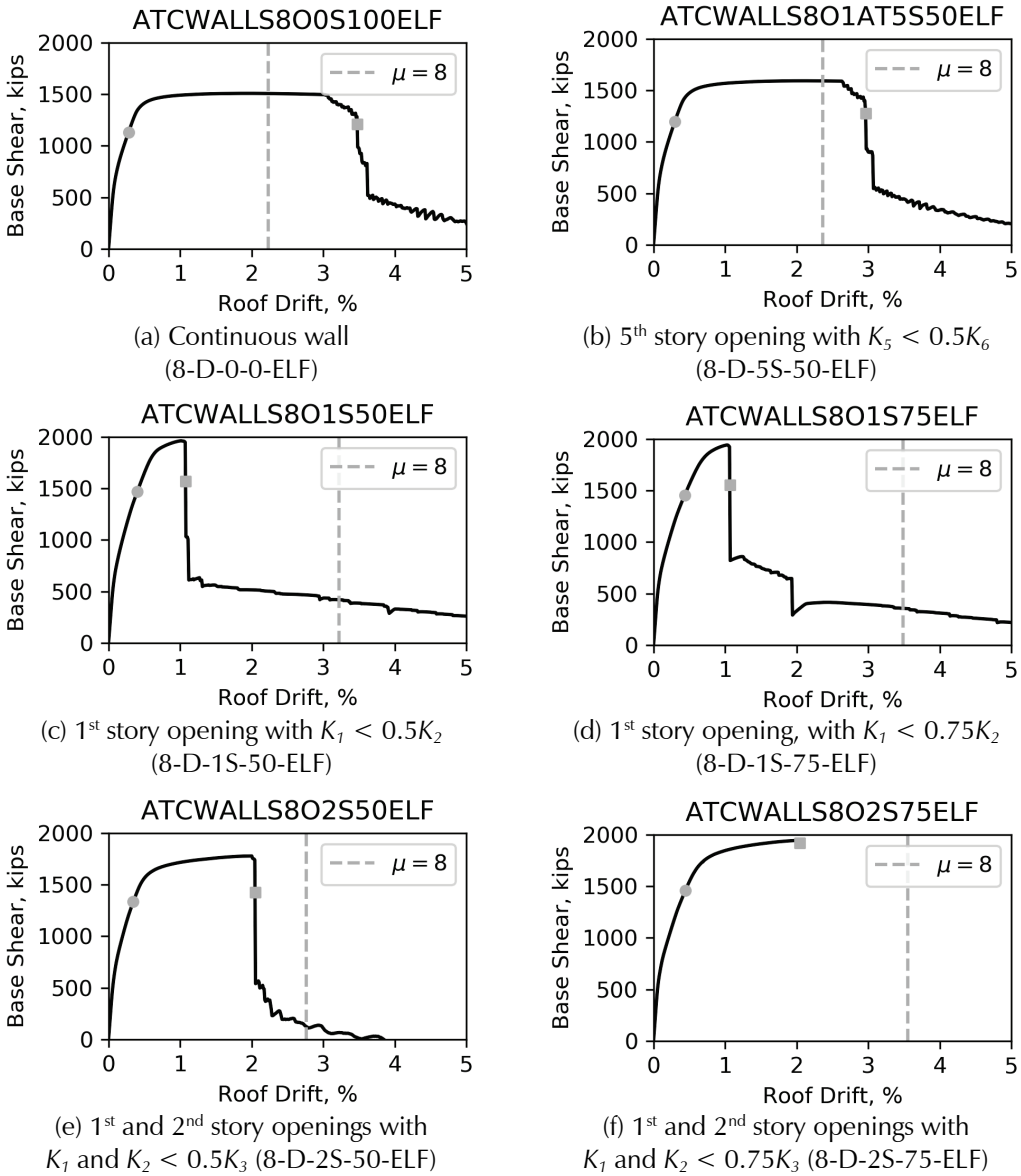

(a) Continuous wall (8-D-0-0-ELF)

(b) 5th story opening with $K_5 < 0.5K_6$ (8-D-5S-50-ELF)

(c) 1st story opening with $K_1 < 0.5K_2$ (8-D-1S-50-ELF)

(d) 1st story opening, with $K_1 < 0.75K_2$ (8-D-1S-75-ELF)

(e) 1st and 2nd story openings with K_1 and $K_2 < 0.5K_3$ (8-D-2S-50-ELF)

(f) 1st and 2nd story openings with K_1 and $K_2 < 0.75K_3$ (8-D-2S-75-ELF)

Figure 5-7 Base shear versus roof drift for 8-story walls designed for D_{max} spectrum using the ASCE/SEI 7-16 ELF procedure. Grey marker indicates yield drift (circle) and drift at 20% strength loss (square); dashed grey line indicates ductility of 8. K_i indicates stiffness of story i defined per Section B.3.

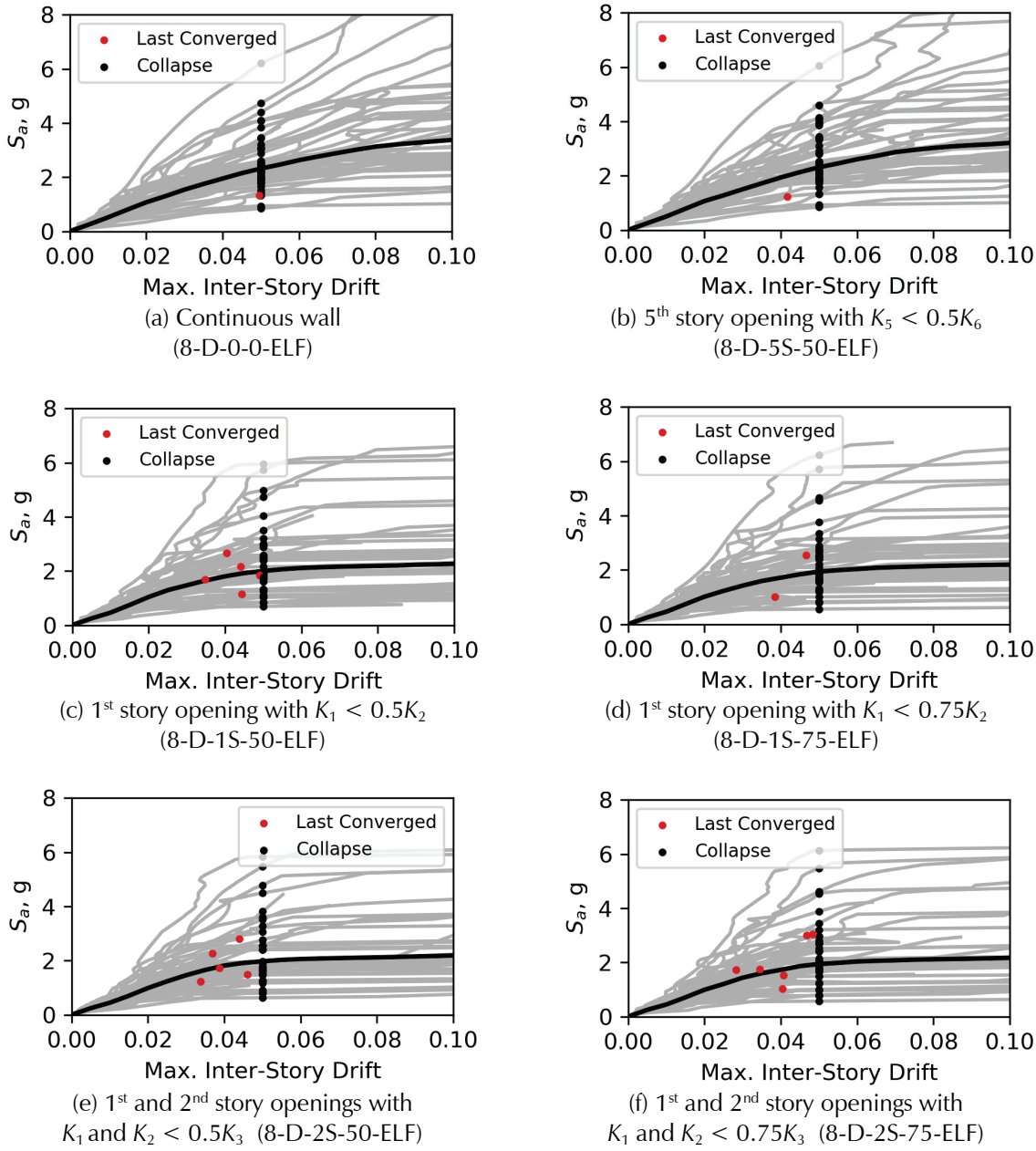

(a) Continuous wall (8-D-0-0-ELF)

(b) 5th story opening with $K_5 < 0.5K_6$ (8-D-5S-50-ELF)

(c) 1st story opening with $K_1 < 0.5K_2$ (8-D-1S-50-ELF)

(d) 1st story opening with $K_1 < 0.75K_2$ (8-D-1S-75-ELF)

(e) 1st and 2nd story openings with K_1 and $K_2 < 0.5K_3$ (8-D-2S-50-ELF)

(f) 1st and 2nd story openings with K_1 and $K_2 < 0.75K_3$ (8-D-2S-75-ELF)

Figure 5-8 Earthquake intensity at design period, S_a, versus maximum interstory drift for 8-story walls designed for D_{max} spectrum using the ASCE/SEI-16 ELF procedure. Black line indicates median acceleration. Non-simulated collapse defined to occur at maximum interstory drift of 5%. K_i indicates stiffness of story i.

Table 5-4 Collapse Probabilities for RC Wall Building Archetypes Designed for the D_{max} Spectra for the Case of Collapse at Maximum Story Drifts in Excess of 5%

Archetype	$\hat{S}_{CT}$	S_{MT}	*CMR*	μ_T	*SSF*	*ACMR*	*ACMR* / $ACMR_{baseline}$	*SSF* (μ=8)	*ACMR* (μ =8)	Collapse Prob. (μ =8)	*ACMR* / $ACMR_{baseline}$ (μ =8)
8-story RC wall buildings designed for D_{max} spectrum using ELF											
8-0-0-D-ELF	2.28	0.91	2.50	12.40	1.45	3.60	-	1.40	3.60	0.71	-
8-1S-50-D-ELF	2.00	0.91	2.20	2.70	1.22	2.70	0.75	1.40	3.20	1.37	0.89
8-1S-75-D-ELF	1.92	0.91	2.10	2.50	1.21	2.60	0.72	1.40	3.10	1.66	0.86
8-2S-50-D-ELF	1.93	0.91	2.10	5.90	1.37	2.90	0.81	1.40	3.10	1.62	0.86
8-2S-75-D-ELF	1.93	0.91	2.10	4.60	1.32	2.80	0.78	1.40	3.10	1.62	0.86
8-5S-50-D-ELF	2.25	0.91	2.50	10.00	1.45	3.60	1.00	1.40	3.60	0.75	1.00
8-story RC wall buildings designed for D_{max} spectrum using MRSA											
8-0-0-D-MRSA	2.07	0.91	2.30	15.80	1.45	3.30	-	1.40	3.30	1.15	-
8-1S-50-D-MRSA	1.95	0.91	2.10	5.60	1.36	2.90	0.88	1.40	3.10	1.56	0.94
8-1S-75-D-MRSA	1.91	0.91	2.10	5.40	1.35	2.80	0.85	1.40	3.00	1.72	0.91
8-2S-50-D-MRSA	1.89	0.91	2.10	7.10	1.41	2.90	0.88	1.40	3.00	1.79	0.91
8-2S-75-D-MRSA	1.91	0.91	2.10	6.60	1.39	2.90	0.88	1.40	3.00	1.71	0.91
8-5S-50-D-ELF	-	-	-	-	-	-	-	-	-	-	-
12-story RC wall buildings designed for D_{max} spectrum using ELF											
12-0-0-D-ELF	1.71	0.67	2.50	8.70	1.53	3.90	-	1.50	3.90	0.47	-
12-1S-50-D-ELF	1.64	0.67	2.40	3.30	1.30	3.20	0.82	1.50	3.70	0.61	0.95
12-1S-75-D-ELF	1.69	0.67	2.50	3.20	1.30	3.30	0.85	1.50	3.90	0.50	1.00
12-2S-50-D-ELF	1.68	0.67	2.50	2.40	1.25	3.10	0.79	1.50	3.80	0.53	0.97
12-2S-75-D-ELF	1.69	0.67	2.50	2.30	1.23	3.10	0.79	1.50	3.80	0.52	0.97
12-5S-50-D-ELF	-	-	-	-	-	-	-	-	-	-	-
12-story RC wall buildings designed for D_{max} spectrum using MRSA											
12-0-0-D-MRSA	1.61	0.67	2.40	20.40	1.53	3.70	-	1.50	3.70	0.66	-
12-1S-50-D-MRSA	1.45	0.67	2.10	7.30	1.50	3.20	0.86	1.50	3.30	1.15	0.89
12-1S-75-D-MRSA	1.52	0.67	2.20	7.20	1.50	3.40	0.92	1.50	3.50	0.91	0.95
12-2S-50-D-MRSA	1.25	0.67	1.90	3.60	1.33	2.50	0.68	1.50	2.80	2.32	0.76
12-2S-75-D-MRSA	1.42	0.67	2.10	3.60	1.33	2.80	0.76	1.50	3.20	1.27	0.86
12-5S-50-D-MRSA	-	-	-	-	-	-	-	-	-	-	-

Table 5-5 **Collapse Probabilities for RC Wall Building Archetypes Designed for the B_{max} Spectrum for the Case of Collapse at Maximum Story Drifts in Excess of 5%**

Archetype	$\hat{S}_{CT}$	S_{MT}	*CMR*	μ_T	*SSF*	*ACMR*	*ACMR* / $ACMR_{baseline}$	*SSF* (μ=8)	*ACMR* (μ =8)	Collapse Prob. (μ =8)	*ACMR* / $ACMR_{baseline}$ (μ =8)
8-story RC wall buildings designed for B_{max} spectrum using ELF											
8-0-0-B-ELF	0.96	0.22	4.50	16.40	1.45	6.40	-	1.40	6.40	0.02	-
8-1S-50-B-ELF	0.90	0.22	4.20	11.60	1.45	6.00	0.94	1.40	6.00	0.03	0.94
8-1S-75-B-ELF	0.91	0.22	4.20	12.40	1.45	6.10	0.95	1.40	6.10	0.03	0.95
8-2S-50-B-ELF	0.79	0.22	3.70	11.20	1.45	5.30	0.83	1.40	5.30	0.08	0.83
8-2S-75-B-ELF	0.86	0.22	4.00	8.80	1.45	5.80	0.91	1.40	5.80	0.04	0.91
8-5S-50-B-ELF	-	-	-	-	-	-	-	-	-	-	-
12-story RC wall buildings designed for B_{max} spectrum using ELF											
12-0-0-B-ELF	0.76	0.16	4.70	7.70	1.52	7.20	-	1.50	7.30	0.01	-
12-1S-50-B-ELF	0.77	0.16	4.80	6.70	1.48	7.10	0.99	1.50	7.40	0.01	1.01
12-1S-75-B-ELF	0.77	0.16	4.80	6.50	1.47	7.10	0.99	1.50	7.40	0.01	1.01
12-2S-50-B-ELF	0.52	0.16	3.30	5.60	1.43	4.70	0.65	1.50	5.00	0.11	0.68
12-2S-75-B-ELF	0.74	0.16	4.60	4.90	1.40	6.50	0.90	1.50	7.10	0.01	0.97
12-5S-50-B-ELF	-	-	-	-	-	-	-	-	-	-	-

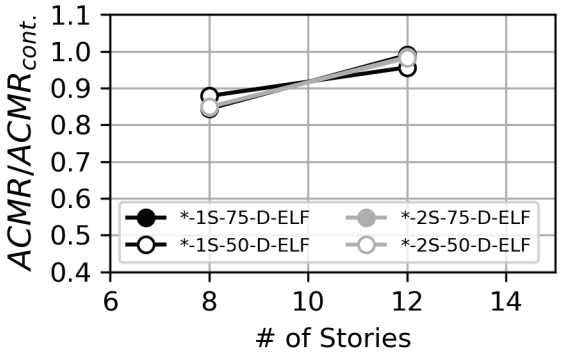

Figure 5-9 Impact of vertical irregularity and building height on *ACMR* for walls designed for D_{max} demands using ASCE/SEI 7-16 ELF procedure. Gravity system failure at 5% interstory drift.

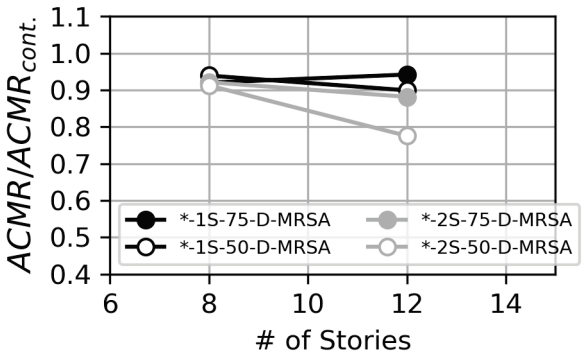

Figure 5-10 Impact of vertical irregularity and building height on *ACMR* for walls designed for D_{max} demands using ASCE/SEI 7-16 MRSA procedure. Gravity system failure at 5% interstory drift.

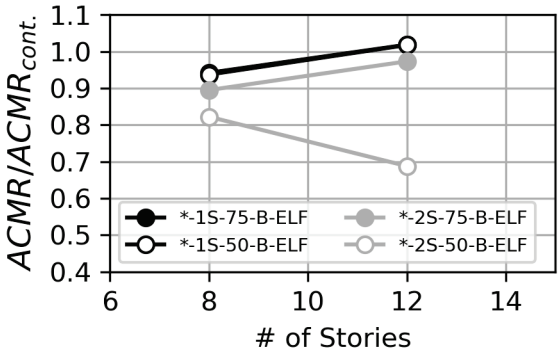

Figure 5-11 Impact of vertical irregularity and building height on *ACMR* for walls designed for B_{max} demands using ASCE/SEI 7-16 ELF procedure. Gravity system failure at 5% interstory drift.

5.6 Conclusions and Recommendations

No code changes are recommended as a result of the study presented in this chapter. Analysis results suggest that: (1) collapse probabilities are very low for walled buildings without and with openings (typically less than 2%); and (2) for most regular systems, vertical irregularities have limited impact on collapse risk.

However, the studies presented in this chapter and Appendix B were limited in that: (1) only two building heights were considered; (2) irregularities in the form an opening were placed at the center of a wall, which is not the most critical location; (3) collapse was solely defined by maximum interstory drift without consideration of shear demand-capacity; and (4) numerical modeling did not include simulation of interaction of flexural and shear response modes. It is recommended that future work address these limitations by considering a broader design space and employing more advanced modeling techniques.

Chapter 6
Moment Frame Buildings with Vertical Irregularities (V1, V2, V5, V6, V7)

6.1 Overview

This chapter summarizes the analytical studies for vertically irregular steel and concrete moment frame buildings that were designed per ASCE/SEI 7-16, *Minimum Design Loads and Associated Criteria for Buildings and Other Structures* (ASCE, 2017a). The effects on building performance of the following vertical irregularities were studied:

- **V2, Weight (mass) irregularity.** This condition is Type 2 vertical irregularity, as defined in Table 12.3-2 of ASCE/SEI 7-16.
- **V1/V5, Soft/weak story irregularities.** These conditions are Type 1 and Type 5 vertical irregularities, respectively, as defined in Table 12.3-2 of ASCE/SEI 7-16.
- **V6, Strong-column/weak-beam (SCWB) design provisions.** This design aspect is not classified as a vertical irregularity in ASCE/SEI 7-16, but rather is handled in material standards. SCWB design provisions were included in this study of vertical irregularities because of their impact on damage localization over building height.
- **V7, Gravity-induced lateral demand (GILD) irregularity.** This design aspect is not currently classified as a vertical irregularity in the United States per ASCE/SEI 7-16, although it is categorized as an irregularity in the *National Building Code of Canada* (National Research Council of Canada, 2015). It was included in this study to determine if this condition should be considered a vertical irregularity in ASCE/SEI 7.

The following are covered in this chapter: (1) objectives of the vertical irregularities studies with moment frame buildings and overview of findings (Section 6.2); (2) methodology to assess vertical irregularity design provisions (Section 6.3); (3) archetype design space by system (Section 6.4); (4) archetype descriptions, results, and conclusions and recommendations for

each of the vertical irregularities studied (Sections 6.5-6.8); and (5) overview of conclusions and recommendations (Section 6.9).

6.2 Objectives of Studies and Summary of Findings

The analytical studies of vertical irregularities in steel and moment frame buildings were structured to address two primary objectives:

1. Assess the adequacy of the existing ASCE/SEI 7-16 provisions in guarding against collapse of buildings with vertical configuration irregularities; and
2. Consider whether additional irregularity classifications should be recognized in ASCE/SEI 7-16.

6.2.1 Objective 1: Assess the Adequacy of ASCE/SEI 7-16 Vertical Irregularity Provisions

ASCE/SEI 7-16 places additional limits and restrictions on buildings with vertical irregularity. These include limits on Seismic Design Category (SDC), building height, and analysis methods (i.e., equivalent lateral load procedure or modal response spectrum analysis). The studies summarized in this chapter are structured to answer the following two questions:

- Are the existing limitations placed on vertically irregular buildings sufficient for providing adequate resistance to collapse?
- Are any of the existing limitations placed on vertically irregular buildings unnecessary or too conservative?

6.2.2 Objective 2: Assess the Necessity for Expanding the ASCE/SEI 7-16 Vertical Irregularity Provisions

GILD and SCWB design requirements are not addressed in ASCE/SEI 7-16 as possible irregularity conditions. However, both are considered in this study, because they are aspects of building configuration that impact the distribution of damage along the height of the building and, therefore, may affect seismic performance.

Although GILD is not directly addressed in ASCE/SEI 7-16 as a vertical irregularity, Dupuis et. al. (2014) led GILD irregularities to be addressed in the *National Building Code of Canada*. The present study addresses the following two questions regarding buildings with GILD:

- Does GILD significantly affect collapse performance in buildings which are designed considering the induced lateral loading? If so, should any limitations or additional requirements be placed on buildings with GILD?

- How does GILD affect the collapse performance in buildings which are *not* designed considering the induced lateral forces?

SCWB provisions are currently found in material-specific design provisions (e.g., AISC, 2016; ACI, 2014). The following two questions were considered in the analytical studies of buildings with varying SCWB design requirements:

- How do modifications of existing SCWB requirements affect collapse performance?
- Are there more efficient ways to proportion members for SCWB ratios along the height of the building, which could provide similar or enhanced collapse performance?

6.2.3 Summary of Findings

The study found that the presence of weight (mass) irregularities, soft/weak story irregularities, and gravity-induced lateral demand (GILD) generally do not significantly reduce the collapse resistance of moment frame buildings, provided that the lateral system is proportioned to satisfy the seismic demands (which often increase due to the presence of the irregularity).

Further, using the equivalent lateral force procedure (ELF) to design buildings with mass irregularity resulted in satisfactory, and even superior, collapse performance compared with buildings designed using modal response spectrum analysis (MRSA). This finding holds even when considering the new ASCE/SEI 7-16 provisions that require the MRSA design to be scaled to 100% of the base shear from the ELF method (as compared with the previous 85% base shear scaling requirement in ASCE/SEI 7-10). Based on these findings, this study concludes that the limitation on use of the ELF method for buildings with mass irregularity (V2) is unnecessary.

6.3 Methodology to Assess Vertical Irregularity Design Provisions

Moment frames with varying degrees of irregularity were utilized to examine the effects of the vertical irregularities on collapse performance. Three-dimensional frame designs were developed using linear elastic procedures according to ASCE/SEI 7-16 and appropriate material standards (i.e., AISC 2010a, 2010c, 2016; ACI, 2014). From the three-dimensional design, a two-dimensional nonlinear OpenSees model of each building was constructed using the methods described in Chapter 3. This study used both steel

moment frames and reinforced concrete moment frames to investigate the various types of vertical irregularities.

The adjusted collapse margin ratio (*ACMR*) of each archetype building was determined by incremental dynamic analysis (IDA) using the FEMA P695 approach. The performance of each archetype building is compared to a "baseline" version (i.e., one with no structural irregularity) to determine the relative impacts of the vertical irregularities on collapse resistance. To avoid ambiguity in the comparisons, *ACMR* of each archetype is computed using the same spectral shape factor (*SSF*) as the baseline model to which it is compared. Methods for design and analysis of the moment frame buildings are described in more detail in Chapter 3.

6.4 Archetype Design Space by System

Steel frames were used to examine the effects of mass irregularities, SCWB ratios, and GILD irregularities. These were examined in 3-, 9-, and 20-story models of both special moment frames (SMFs) and ordinary moment frames (OMFs). In total, 151 steel moment frames were designed and analyzed.

Reinforced concrete (RC) moment frames were used to study mass irregularities, soft/weak story irregularities, and SCWB ratios. These were examined in 4-, 8-, 12-, and 20-story RC SMF and OMF models. In total, 113 RC moment frames were designed and analyzed.

The following sections provide more detail on the designs for each specific type of irregularity. Detailed design documentation (including fundamental period and other key parameters) on the steel moment frame and concrete moment frame studies is provided in Appendix C and Appendix D, respectively.

6.5 Studies of Weight (Mass) Irregularity (V2)

According to ASCE/SEI 7-16 Table 12.3-2, "Weight (mass) irregularity is defined to exist where the effective mass of any story is more than 150% of the effective mass of an adjacent story. A roof that is lighter than the floor below need not be considered." Figure 6-1 illustrates a weight (mass) irregularity. ASCE/SEI 7-16 prohibits the use of the ELF design method for buildings with a weight (mass) irregularity. The following questions guided this study on the collapse performance of weight (mass) irregular buildings:

- Does weight (mass) irregularity decrease collapse performance?
- Does MRSA design result in better collapse resistance than ELF?

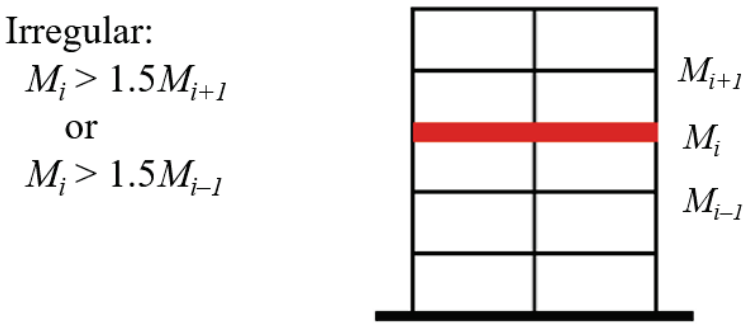

Figure 6-1 Mass irregularity per ASCE/SEI 7-16.

6.5.1 Archetype Descriptions

Mass irregularity is examined in both steel and RC SMF archetypes by increasing the mass of a given story to produce a mass ratio ranging from 1.5 to 3 relative to the adjacent lower story, as depicted in Figure 6-1, and then calculating the resulting change in building collapse resistance. Ordinary moment frames were not considered, because mass irregularity requirements only apply in SDC D, E, and F and the use of OMFs is significantly restricted in these SDCs. For each increase in mass ratio, the building was redesigned (if needed) considering checks on both strength and story drift requirements. Table 6-1 summarizes the archetype design space.

Table 6-1 Weight (Mass) Irregularity Archetype Space

System Types		Stories	SDC	Irregular Stories	Mass Ratios	Analysis Used for Design	
RC Moment Frame	Steel Moment Frame					ELF	MRSA
	Special	3	D_{max}	2, 3	1.5, 2.0, 3.0	×	×
	Special	20	D_{max}	3, 11, 19	1.5, 2.0, 3.0		×
Special		20	D_{max}	3, 11	2.0, 3.0	×	×

6.5.2 Results

Collapse performance sometimes improves and sometimes diminishes with increasing mass ratio, as seen in Figure 6-2a (RC frames) and Figure 6-2b (steel frames). At first look, it appears that steel buildings are more negatively affected by mass irregularity than concrete buildings, but this observation is an artifact of the archetype designs, and it is not expected to be true in general. The negative trend seen in Figure 6-2b is caused by the baseline steel variants having much higher design overstrength than some of the irregular variants; the static overstrength of mass irregular steel models decreases by as much as 30% relative to the baseline. For comparison, the mass-irregular concrete models maintain static overstrength values within

2% of the baseline. In all of the 3-story MRSA designed steel frame variants with mass irregularity at the second story, the member sizes in the steel buildings did not change when the mass irregularity was introduced, even though the design base shear increased substantially (as much as a 60% increase with a mass ratio = 3.0 for the 3-story building). These design details are fully documented in the Supporting Documentation of Appendix C. Therefore, the decline in collapse resistance in the steel buildings is attributed to a reduction in "overdesign"; when the overdesign of each member remains nearly the same, as in the RC SMF archetypes shown in Figure 6-2, no declines in collapse resistance are observed. Although the relative collapse performance decreases with increasing mass ratio in the steel buildings, it is important to note that mean interstory drift at the MCE remains below the 4% limit set in ASCE/SEI 7-16 Section 16.4.1.2. Figure 6-3 shows that even for the worst performing mass-irregular building (3-story MRSA designed building with a mass ratio of 3.0 at the 3rd floor), the interstory drift at MCE is acceptable.

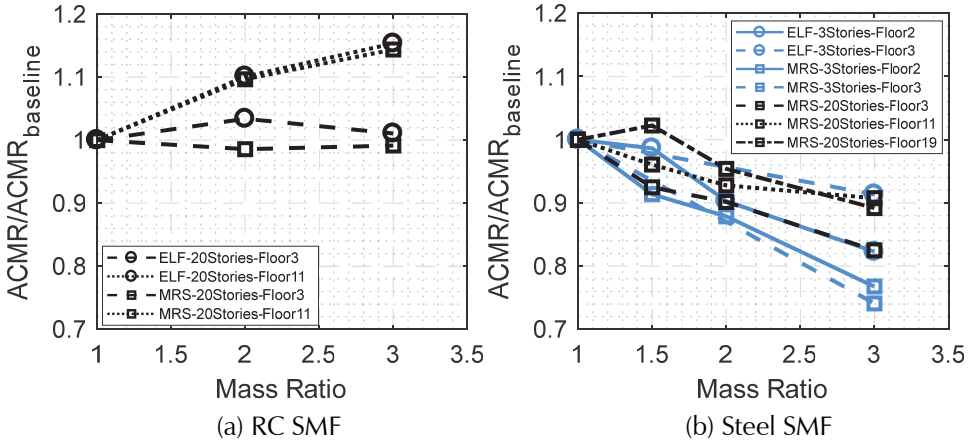

(a) RC SMF (b) Steel SMF

Figure 6-2 V2 mass irregularity. Legend indicates design method, number of stories, and location of the irregular story.

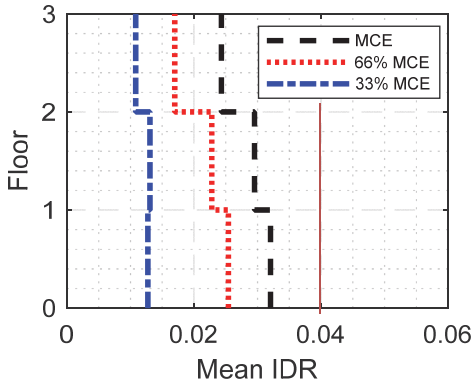

Figure 6-3 Interstory drift profile at increments of MCE for the 3-story MRSA designed steel building with a mass ratio= 3.0 at the 3rd floor.

Generally, the mass irregular variants designed with the ELF method perform better than those designed with MRSA analysis. This observation is important because the only design requirement that is triggered by mass irregularity in ASCE/SEI 7-16 is the prohibition of the ELF design procedure for SDC D, E, and F.

The performance of the buildings designed with ELF and MRSA can be further investigated by examining the design demands produced by each method. Figure 6-4 examines the design forces for an RC frame building with a mass irregularity at the third story. The MRSA design picks up the increased force demand at the mass-irregular third story; however, overall, the ELF designed building will be equally strong at the irregular story and stronger than the MRSA buildings at all floors above.

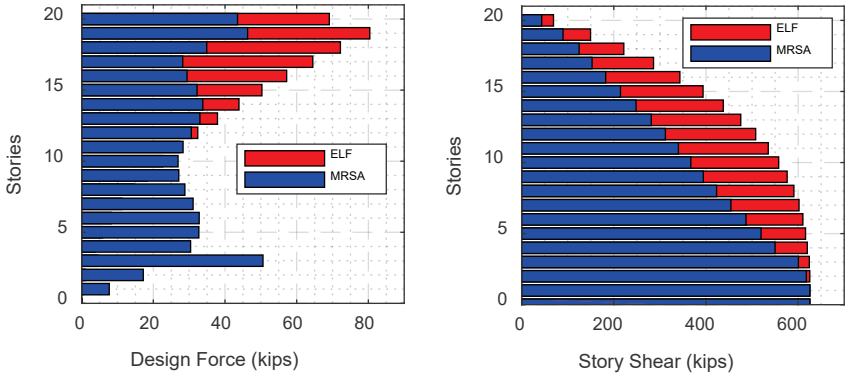

Figure 6-4 Comparison of ELF and MRSA design forces for a 20-story RC frame building with a mass irregularity at the third story.

The investigation also found that the location of the mass irregularity along the height of the building affects collapse performance; archetypes with the mass irregularity located where the collapse mechanism is already more likely to form (i.e., in lower stories) tend to have lower collapse resistance as compared with buildings with mass irregularities located where the collapse mechanism is less likely to form (i.e., upper stories).

6.5.3 Conclusion and Recommendations

Based upon the findings in this section, specifically the superior performance of ELF designed buildings relative to MRSA designed buildings, it is recommended that ELF procedure be allowed for mass-irregular buildings. This recommendation is further supported by a broader study of extreme mass irregularities documented in Appendix F, where it is shown that the ELF procedure generally produces higher story shears and overturning moments than MRSA, even for extreme mass ratios up to 10.

It is noted that mass irregularities were studied by adjusting the mass of single stories at different locations in the building. A future study investigating the effects of applying greater mass to multiple floors may be of value.

6.6 Studies of Soft- and Weak-Story Irregularities (V1/V5)

ASCE/SEI 7-16 limits the analysis procedure, height, and/or SDC for buildings with stiffness or strength irregularities. The following questions guided this study on the collapse performance of stiffness/strength irregular buildings:

- Are the existing limitations placed on soft/weak story buildings sufficient in terms of resistance to collapse?
- Are any of the existing limitations placed on soft/weak story buildings conservative?

6.6.1 Archetype Descriptions

Soft/weak story irregularities (illustrated in Figure 6-5 and 6-6) are investigated using RC SMFs and OMFs for target strength and stiffness ratios between 0.6 and 0.8 relative to the story above. According to ASCE/SEI 7-16 Table 12.3-2, a soft story irregularity occurs when the stiffness of a story is less than 70% of the stiffness of the story above or less than 80% of the average stiffness of the three stories above. If the story stiffness is less than 60% of the story above or less than 70% of the average of the three stories above, then it has an extreme soft story irregularity. Weak story and extreme weak story irregularities occur when the strength of a story is less than 80% or 65% of the strength of the story above, respectively.

Soft/weak story irregularities were introduced two different ways: (1) by increasing story height so that stiffness (and possibly strength) of the story are reduced; and (2) by increasing the strength of the story above. Table 6-2 summarizes the soft/weak story archetype design space. It should be noted that all of the soft/weak story archetypes comply with ASCE/SEI 7-16, except for height limits and prohibitions of the ELF procedure. Therefore, the soft/weak archetypes in this study differ from many of the soft/weak story buildings for which poor performance has been observed in past earthquakes because many of those buildings had a story that was too soft/weak to meet current code requirements.

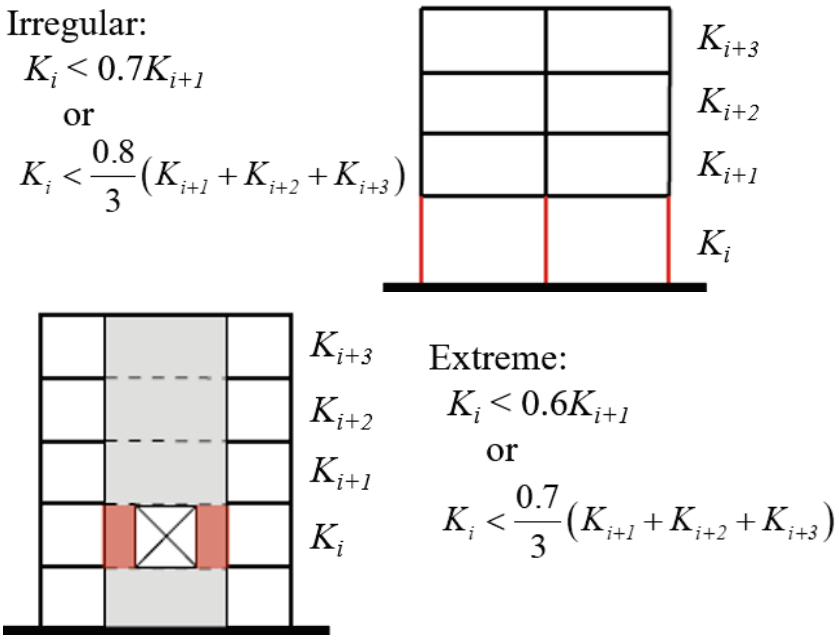

Figure 6-5 Soft story irregularity per ASCE/SEI 7-16.

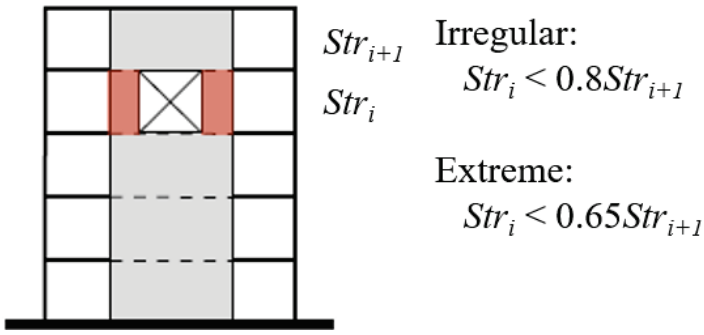

Figure 6-6 Weak story irregularity per ASCE/SEI 7-16.

Table 6-2 Soft/Weak Irregularity Archetype Space

System Types							
RC Moment Frame	Steel Moment Frame	Stories	SDC	Irregular Stories	Stiffness Ratios	Strength Ratios	Analysis Used for Design
Ordinary		4	B_{max}	1, 2	0.6, 0.7, 0.8	0.6, 0.8	ELF
Ordinary		12	B_{max}	1, 2, 5	0.6, 0.7, 0.8		ELF
Special		4	D_{max}	1, 2	0.6, 0.7, 0.8		ELF
Special		8	D_{max}	1, 2, 5	0.6, 0.7, 0.8	0.6, 0.8	ELF
Special		12	D_{max}	1, 2, 5, 9	0.6, 0.7, 0.8	0.6, 0.8	ELF
Special		20	D_{max}	1		0.6, 0.8	ELF

6.6.2 *Results*

Figure 6-7 shows that the first method (Method 1) for creating a soft/weak story (increased story height) does not result in any consistent positive or negative trends in collapse resistance for either SMF or OMF archetypes. For all design cases investigated, the collapse performance stays above at least 85-90% of the baseline model performance and reaches 130% in some cases. Similar observations are made when collapse resistance is plotted against relative stiffness, rather than relative strength.

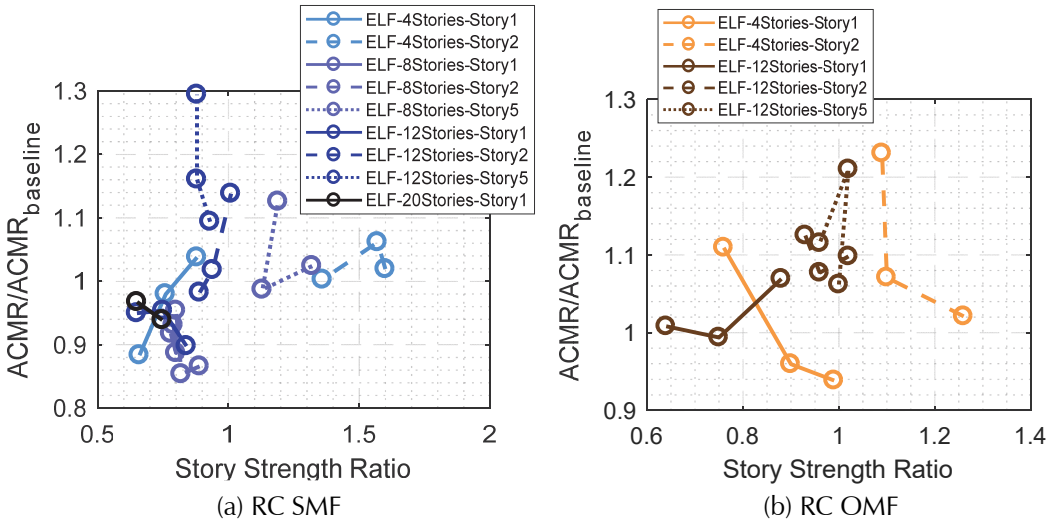

Figure 6-7 V1/V5 soft/weak story (increase story height to achieve soft/weak story). The legends indicate design method, number of stories, and location of the irregular story.

The lack of a clear trend from Method 1 is mostly because increasing the story height may cause the taller story to have lower stiffness, but it often does not cause a decrease in the strength of the story for code-conforming buildings since the code requires a minimum strength. For example, the results for the 12-story RC SMF with increasing story height at the fifth story (dark blue dotted line in Figure 6-7a) form a nearly vertical line because increasing the story height does not actually reduce story strength.

The reason that the story strength does not decrease is because the beam members at the location of the increased story height are re-proportioned to meet the higher demands caused by the taller story—the end result is a story with similar strength. Similar results are observed for the OMF variants (Figure 6-7b) except that strength is governed by column capacity, rather than beam capacity. When examining these results, it is important to keep in mind that the "weak" story still meets all of the code force and drift demands; this is in stark contrast to non-current-code-conforming weak-story buildings that have been severely damaged in past earthquakes.

Figure 6-8 shows that second method (Method 2) for achieving a weak story—increasing the strength of the story above (no strength adjustment is made to any stories beyond the story immediately above the irregular story)—tends to result in collapse resistance that is somewhat higher for extremely low weak-story strength ratios as compared to moderate weak-story ratios. For example, the 20-story model with a first story irregularity (the black line in Figure 6-8a) experiences a 7% increase in collapse capacity when the strength ratio decreases from 0.78 (weak story irregularity) to 0.62 (extreme weak story irregularity). This trend of improved collapse performance with decreasing story strength ratio is also reflected in the static overstrength for the SMF models (see Figure 6-9). The static overstrength is improved by strengthening one of the stories in the building. A consistent finding was found in a past study (Haselton et al., 2011), which showed that a weak-story irregularity caused by strengthening all the stories above similarly does not detrimentally affect the collapse performance of RC moment frame buildings.

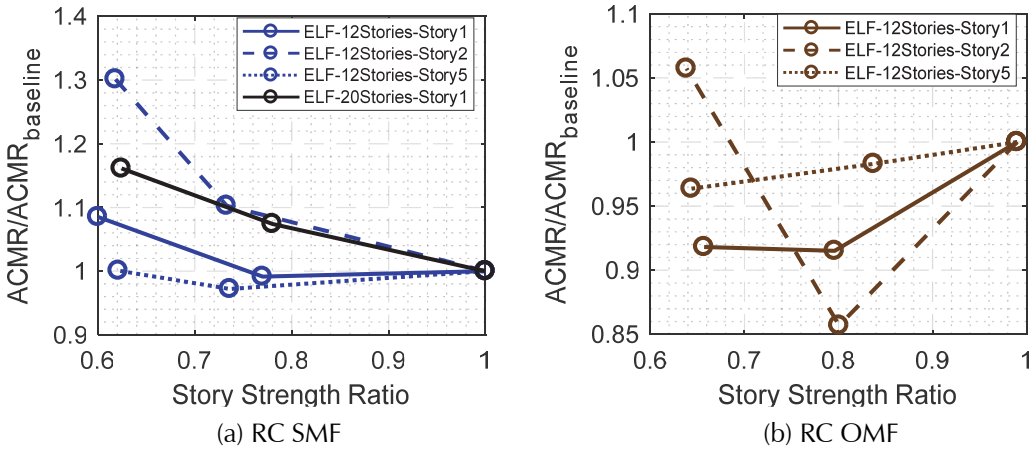

Figure 6-8 V1 weak story (increase strength in story above).

Soft/weak story irregularities do not appear to pose a problem in code-conforming moment frame buildings. This is partially because, as long as the building is code-conforming, "weak story" really means "strong adjacent stories"; the "weak" story still must be strong enough to resist the design lateral force demand per code requirements. Similarly, a "soft" story must still satisfy story drift requirements, which prevents it from becoming excessively soft. It is reasonable to think that the expected collapse performance may decline when the weak story causes the damage distribution over height to change from several stories to just one or two, as has been observed in the poor seismic performance of non-current-code-conforming soft/weak story buildings in past earthquakes. However, in this study of code-conforming irregular buildings, such a reduction in collapse

resistant is not observed; rather, the negative effects of having more concentrated damage are offset by the positive effects of having strengthened members in the adjacent stories.

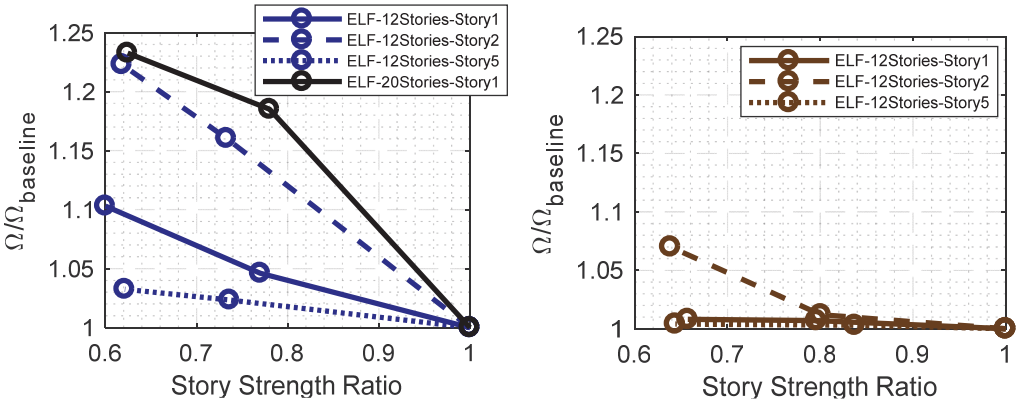

Figure 6-9 V1 weak story overstrenth. Legend indicates design method, number of stories, and location of the irregular story.

6.6.3 Conclusion and Recommendations

Based upon the findings from this section, specifically the enhanced performance of extreme weak story irregular buildings relative to the baseline building, the prohibition of extreme weak story irregularities in SDC D and the height limitation on in SDC B and C may be overly conservative. Further study is recommended to evaluate the prohibition of weak/soft story irregularities in SDC E and F.

It is noted in the previous section that buildings designed using the ELF procedure tend to outperform buildings designed using MRSA, in terms of collapse resistance. As soft-story irregular buildings are similarly limited to MRSA (i.e., ELF is prohibited), a future study may compare the performance of ELF and MRSA designed buildings with soft-story irregularity to determine if prohibiting the ELF procedure is needed.

6.7 Studies of Strong-Column/Weak-Beam Design Provisions (V6)

Even though SCWB is not defined as an irregularity, it is a configuration characteristic that has been clearly shown to impact system ductility and collapse resistance. SCWB requirements are provided by material specifications (ACI, 2014; AISC, 2016) and are not specifically addressed in ASCE/SEI 7-16. The material standards specify a minimum ratio of the total flexural strength of the columns framing into a joint to the total flexural strength of beams framing into the joint (i.e., the SCWB ratio), so that column failures are limited. Calculation of SCWB ratio is illustrated in

Figure 6-10; in the figure, M_c is column flexural strength, M_b is the beam flexural strength, and i and j are the story and beam numbers, respectively.

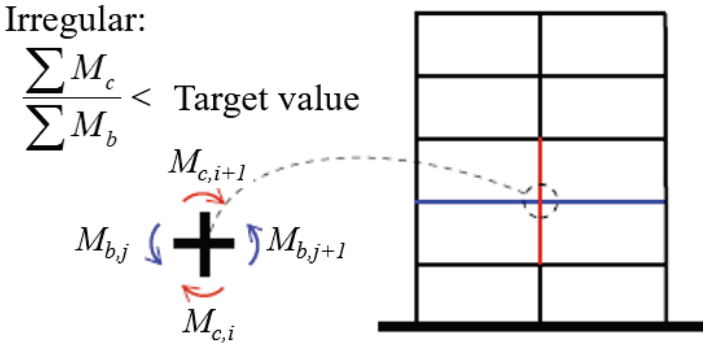

Figure 6-10 Weak-column/strong-beam.

The following questions are explored in this section:

- How sensitive is collapse performance to SCWB requirements?
- Could adjusting requirements for SCWB ratio along the height of the building (resulting in "stepped" SCWB ratio) provide similar or enhanced collapse performance?

6.7.1 Archetype Descriptions

The effects of SCWB are examined by analyzing suites of moment frame buildings designed for a range of SCWB ratios. In addition, archetypes with stepped SCWB ratios are examined; for these, the minimum SCWB ratio is higher at the lower stories and "steps" down in the upper stories of the building. For the stepped designs, minimum SCWB ratio at the first, second, and third quarters of the buildings are 1.5, 1.0, and 0.8 respectively or 2.0, 1.5, and 1.0, respectively, with no SCWB ratio requirement in the top quarter. Generally speaking, failing to satisfy SCWB requirements would be a violation of the material design standards. The archetype design space for studying SCWB is summarized in Table 6-3.

The SCWB variants are designed two ways: (1) "realistic" where the minimum SCWB ratio is adjusted in the design, but the design process allows the ratio to be greater than the minimum when other design factors control the building proportioning (e.g., joint size and minimum reinforcing requirements); and (2) "exact" where the design enforces an exact SCWB ratio, even if it makes the design unrealistic (e.g., impossible reinforcing configurations).

Table 6-3 SCWB Archetype Space

System Types						Analysis Used for Design	
RC Moment Frame	Steel Moment Frame	Stories	SDC	Distribution of SCWB Requirements	SCWB Ratios	ELF	MRSA
Ordinary		4	B_{max}	constant	0.4, 0.7, 1.0	×	
Ordinary		12	B_{max}	constant	0.4, 0.7, 1.0	×	
Special		4	D_{max}	constant	0.5, 1.0, 1.5, 2.0	×	
Special		8	D_{max}	constant	0.5, 1.0, 1.5, 2.0	×	
Special		12	D_{max}	constant	0.5, 1.0, 1.5, 2.0	×	
Special		12	D_{max}	stepped	0.8, 1.0, 1.2, 1.5, 2.0	×	
	Ordinary	3	B_{max}	constant	0.4, 0.7, 1.0	×	×
	Ordinary	9	B_{max}	constant	0.4, 0.7, 1.0	×	×
	Ordinary	20	B_{max}	constant	0.4, 0.7, 1.0	×	×
	Special	3	D_{max}	constant	0.5, 1.0, 1.5, 2.0		×
	Special	9	D_{max}	constant	0.5, 1.0, 1.5, 2.0		×
	Special	20	D_{max}	constant	0.5, 1.0, 1.5, 2.0		×

6.7.2 Results

The concrete frames (both SMF and OMF) show a distinct trend of increasing collapse performance with increasing SCWB ratio (Figure 6-11) as a result of stronger plastic hinges at the base of the first story columns and damage spreading more over the height of the building as the SCWB ratio increases. Similar observations have been made in a number of prior studies, e.g., Haselton et al. (2011) and Elkady (2016). The minimal decline in collapse resistance (no more than 10% lowered collapse capacity relative to the baseline) for realistic designs with low SCWB ratio is a result of increasing the beam strength in order to reduce the SCWB ratio where column strength was controlled by lateral force demands rather than capacity design requirements (i.e., reducing SCWB ratio actually resulted in a stronger building because column strength could not be reduced any further). In contrast, the 12-story RC SMF designed to exactly meet a SCWB ratio of 0.5 (the dark blue dashed line in Figure 6-11a) experiences collapse capacity 20% lower than the baseline, because other code requirements such as joint shear requirements (which often increase column sizes) were not considered in the design (note, that joint failure is only modeled in the RC OMF archetypes, so RC SMF archetypes with non-conforming joints may have even lower collapse resistance if they are susceptible to joint failure).

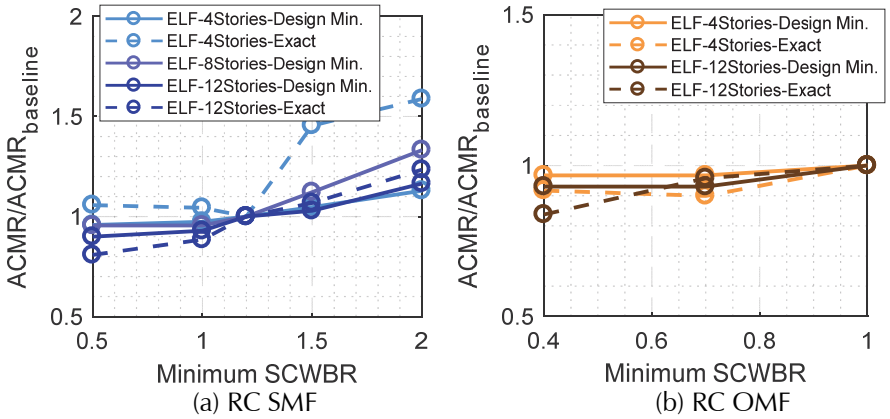

Figure 6-11 V6 strong-column/weak-beam. Baseline in these plots refers to the SCWB ratio (SCWBR) of: (a) 1.2 variant for each story height and design type; (b) 1.0 variant for each story height and design type.

Figure 6-12 shows the performance of RC SMF buildings with stepped SCWB requirements, showing results for buildings designed by both the realistic and exact design methods. Targeting higher SCWB ratio in the lower portions of buildings and relaxing SCWB requirements in the upper stories may be an efficient way to proportion a building without sacrificing collapse resistance because it improves collapse resistance by placing additional column strength where it is most effective—the lower portion of the building. However, lower collapse resistance of the exact designs with low SCWB ratios in the upper stories shows that allowing SCWB ratio to go below current code limits, even in the upper portion of the building, can have negative implications; the reduced collapse resistance in those buildings is caused by column failures in the upper portions of the buildings. Allowing lower SCWB ratios in the upper portion of the realistic designs did not cause upper story failures or lower the collapse resistance because joint size and minimum reinforcing requirements prevented SCWB ratios in the upper stories from getting below 0.9 and 1.0 for the interior and exterior joints, respectively. It is important to note in both cases (uniform and stepped SCWB ratio requirements) that the archetypes with exact SCWB ratios often violated one or more ACI design requirements (e.g., reinforcing steel detailing, joint strength requirements); therefore, they are valuable for determining the effect of a single design constraint (SCWB ratio), but they do not necessarily reflect trends in real buildings.

An additional exact SCWB variant for which the SCWB ratio is set to 1.5 in the bottom third of the building and 1.2 elsewhere (rightmost bar of Figure 6-12) has the best performance of all the exact SCWB designs by a significant margin. This result indicates that increasing SCWB ratio in only the lower portion of a building boosts collapse resistance, as long as the upper stories still meet minimum code requirements for SCWB ratio.

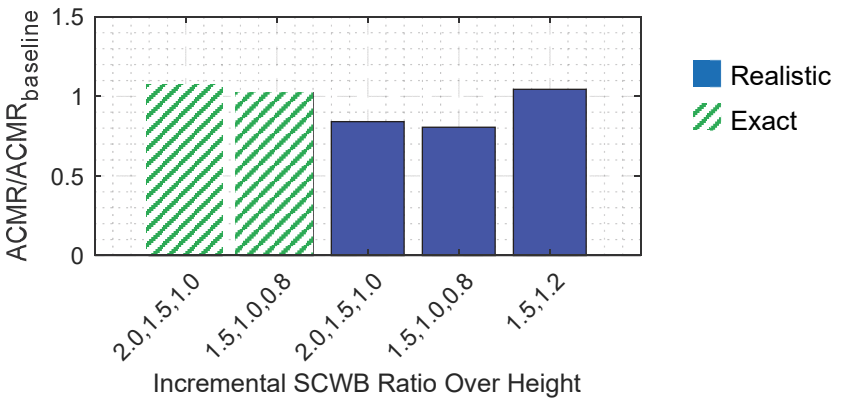

Figure 6-12 V6 stepped SCWB ratio, 12-story RC SMF.

The steel frames, both SMF and OMF, show less consistent trends with increasing SCWB ratio, as seen Figure 6-13. This inconsistent performance is partly due to increasing girder sizes to achieve lower SCWB ratio (rather than only decreasing column sizes) and partly due to a mechanism shift from joint shear yielding at low SCWB ratios to beam failure at higher SCWB ratios. A side-study revealed that adding oversized doubler plates to completely eliminate panel zone yielding reduced the collapse resistance of the archetypes with low SCWB ratio by shifting the failure mechanism from the joint panel zones (which are modeled to have no cyclic deterioration and continue to harden out to 6% distortion) to the columns and beams (which have more rapid strength deterioration). When the panel zones are reinforced to prevent yielding, a trend of increasing performance with increasing SCWB ratio is produced, similar to what is observed for the RC SMF archetypes. The benefit of moderate yielding in the joint panel zone has been noted in prior studies as well, e.g., FEMA 355D, *State of the Art Report on Connection Performance* (FEMA, 2000a), and the influence of joint panel zone yielding on overall building performance warrants additional study in the future.

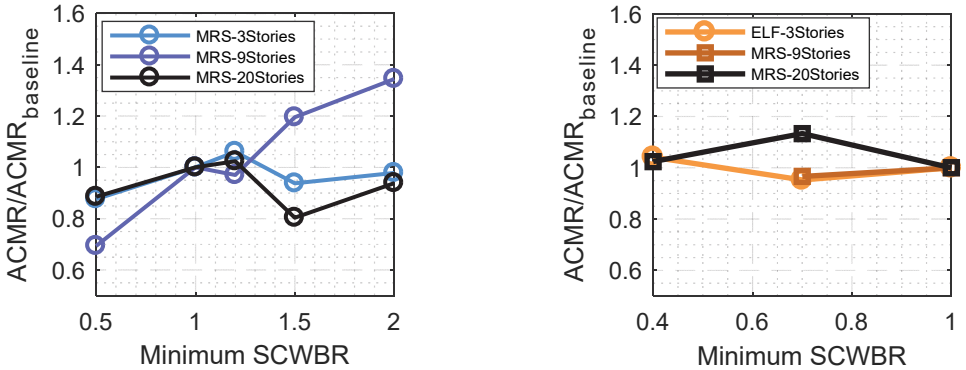

Figure 6-13 V6 strong-column/weak-beam. Baseline in these plots refers to the SCWB ratio (SCWBR) 1.0 variant for each story height and design type.

6.7.3 Conclusion and Recommendations

Increasing the required minimum SCWB ratio (even beyond current material code requirements) tends to improve collapse performance. The advantage of increased SCWB ratio could potentially also be achieved more economically by stepping down SCWB ratio requirements along the height of a building (with the highest SCWB ratio being in the lower portion of the building). To get to a point of specific recommendations for updated SCWB requirements, further study is needed to determine the optimal approach for stepping down the SCWB requirements over the building height and to examine the costs of this approach versus other design approaches.

6.8 Studies of Gravity-Induced Lateral Demands (V7)

Recent studies (Dupuis et al., 2014; Shoraka et al., 2014) on shear wall buildings with gravity-induced lateral demand (GILD) have recommended that code limits be placed on buildings with GILD irregularities. Those studies are based predominately on displacement demands and conclude that increasing GILD can cause "ratcheting of displacement demands and potentially collapse." This study seeks to determine whether collapse capacity is significantly decreased by GILD irregularities.

6.8.1 Previous Studies

Dupuis et al. (2014) examined displacement demands on shear wall buildings ranging from 5 to 50 stories with GILD irregularity. The GILD demand was supplied by sloping gravity columns along the entire height of the building. The study found that the GILD irregularity amplified the displacement demands significantly relative to an equivalent building without GILD. Therefore, limitations on GILD displacement and the method in which the building is analyzed were recommended.

A later study by Shoraka et al. (2014) examined displacement and collapse capacity together. For crustal ground motions and GILD ratio up to 0.4 (note that the GILD ratio was calculated as the GILD base shear normalized by the base yield strength), it was found that collapse capacity is acceptable for GILD irregular buildings (similar to the findings of this report). However, it is observed that subduction ground motions and GILD achieved through eccentric floor spans may have a more significant effect on collapse capacity. It is also noted that inclined columns at an intermediate level cause a less extreme displacement demand in GILD irregular buildings than when columns are inclined along the entire building height.

6.8.2 Archetype Descriptions

The effects of GILD irregularities were examined with 20-story steel frame and 12-story concrete frame buildings; the full set of GILD archetypes is summarized in Table 6-4. The "irregularity" is achieved by sloping the columns at one of the stories, as shown in Figure 6-14. The severity of the irregularity is quantified by a GILD ratio, which is gravity-induced story shear (Q_G) divided by story shear capacity (Q_V) according to the *IBC SEAOC Structural/Seismic Design Manual* (SEAOC, 2015), illustrated in Figure 6-14.

Table 6-4 GILD Archetype Space

System Types						Analysis Used for Design	
RC Moment Frame	Steel Moment Frame	Stories	SDC	Irregular Stories	GILD Ratios	ELF	MRSA
Ordinary		12	B_{max}	1, 2	0.5	×	
Special		12	D_{max}	1, 2	0.5	×	
	Ordinary	20	B_{max}	1, 7, 14	0.1, 0.3, 0.5		×
	Special	20	D_{max}	1, 7, 15	0.1, 0.3, 0.6		×

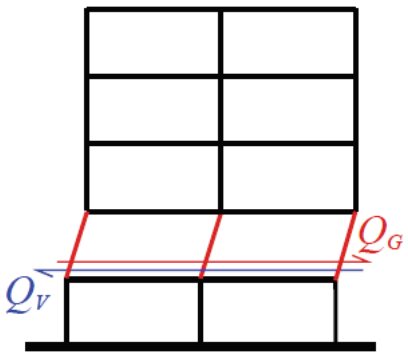

Irregular:

$$GILD\ ratio = \frac{Q_G}{Q_V} > \text{Target value}$$

Figure 6-14 Gravity-induced lateral demand (GILD).

6.8.3 Results

Figure 6-15 shows variations in collapse resistance for 20-story steel frames with GILD ratios up to 0.5. Collapse resistance rarely diminishes more than 10% and in some cases it improves. Negative effects of GILD are not observed for the steel frames because these buildings are designed to account for the effects of the GILD (i.e., lateral demands incorporate GILD). Shoraka et al. (2014) found that GILD applied along the entire height of the building can have a negative effect on collapse performance, but that GILD applied over only a portion of the building height results in smaller displacement demands relative to the former configuration. Although the analyses in this study did not examine a case where GILD is applied along

the full height of the building, maximum interstory drift and residual drift do increase due to GILD, demonstrating agreement with prior studies (Dupuis et al., 2014; Shoraka et al., 2014).

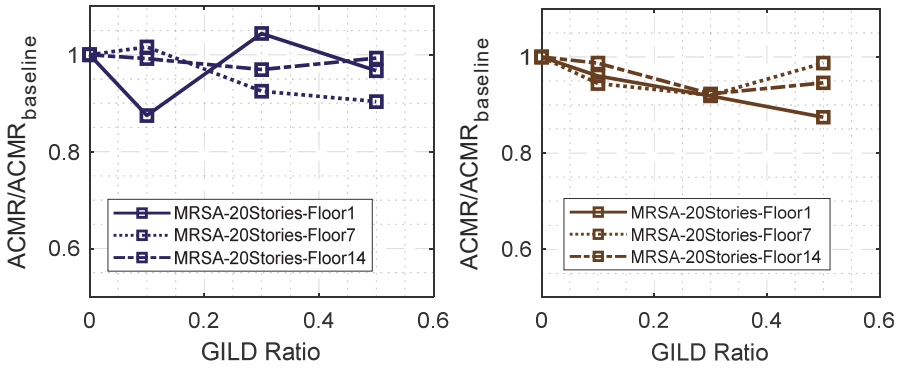

Figure 6-15 V7 gravity-induced lateral loading *with* design for GILD (i.e., code-compliant). Legend indicates design method, number of stories, and location of the irregular story.

The consequences of neglecting GILD in the design process are illustrated in Figure 6-16; shown in the figure are the performance of 20-story steel frames and 12-story concrete frames with GILD ratios up to 0.5 that are designed without considering GILD (e.g., sloping columns are introduced at a particular story of the baseline design, but members are not re-proportioned for the additional lateral demand). Declines in collapse resistance as great as 50% are observed; ordinary moment frames are affected most because lower SCWB ratios limit their ability to engage the stories adjacent to the story with the GILD irregularity. The negative effect of failing to design for GILD is also visible in Figure 6-17b, the poorest performing un-designed SMF building violates the MCE drift requirements of ASCE 7-16 Section 16.4.1.2; Figure 6-17a also shows how the drifts are adequately controlled, even at the GILD stories, when GILDs are accounted for in the building design process.

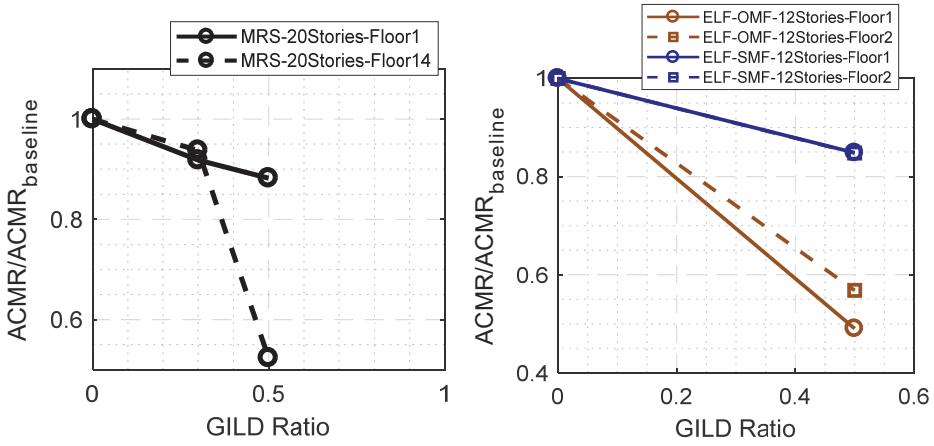

(a) Steel SMF, 20-story (b) RC SMF/OMF, 12-story

Figure 6-16 V7 gravity-induced lateral loading *without* design for GILD (i.e., not code-compliant, provided to show the effects of GILD when not considered in the design). Legend indicates design method, number of stories, and location of the irregular story.

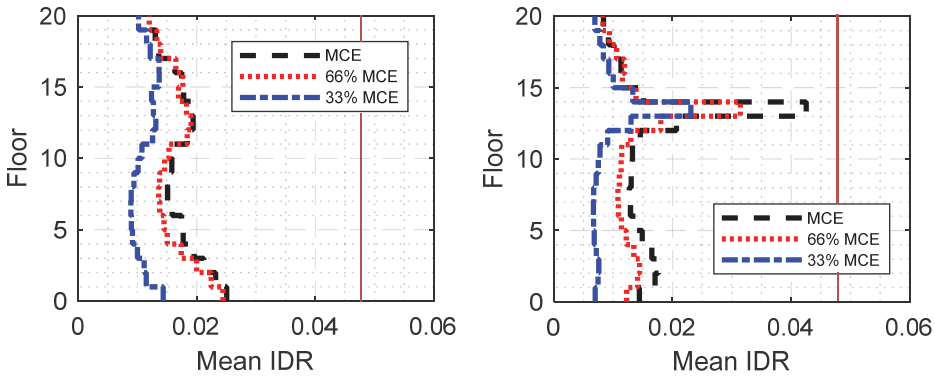

(a) Steel SMF GILD ratio 0.1 at Floor 1 (*with* design for GILD)

(b) Steel SMF GILD ratio 0.5 at Floor 14 (*without* design for GILD)

Figure 6-17 Mean interstory drift at MCE of the poorest performing GILD designed and un-designed irregular buildings.

6.8.4 Limitations of the GILD Studies

GILD irregularities were examined in this study for a limited set of archetype models, with GILD occurring at only one predetermined story within a given building. The models are subjected to only crustal horizontal ground accelerations, and, to reduce analysis time and convergence difficulties, *P*-Delta effects are simulated using the "Linear with P-Delta" transformation in OpenSees, which is a linear (i.e., not exact) transformation that approximates *P*-Delta effects.

The effect of GILD on buildings is expected to be more significant when the location of the irregular story and the portion of the building prone to damage coincide. In the case of the steel 20-story SMF building, it was found that

the second story was often the most damaged in the baseline model; therefore, it would be meaningful to assess the GILD irregularity for the second story, where the buildings is most susceptible to damage. Additionally, prior studies (Shoraka, 2014; Dupuis, 2014) have shown that GILD caused by sloping columns at multiple stories increases displacements more than when columns are sloped at only one story. Therefore, the archetype design space should be expanded to include buildings with GILD at multiple stories rather than just one.

To test the impact of the vertical ground motion component on collapse resistance of buildings with large GILD, the 12-story concrete moment frames with GILD of 0.5 were re-analyzed with the vertical ground motion component included and their resulting *ACMR* lowered an additional 6%, which does not appear significant. However, lighter buildings may be more affected by the vertical component of the ground motion, due to the larger columns slopes they can achieve; for context, the column slopes introduced in the RC SMF and RC OMF frames to achieve GILD of 0.5 at the second story were 3% and 1%, respectively. Nonetheless, it may be reasonable to expect that the increasing significance of vertical ground motions one would expect to accompany larger column slopes is balanced by including the vertical seismic effect in design, as ASCE/SEI 7-16 requires. Further study is required to validate this hypothesis.

The effect of using the approximate linear transformation with *P*-Delta, as outlined in Chapter 3, rather than the "exact" corotational transformation in OpenSees, was tested by re-evaluating two of the GILD archetypes with the corotational transformation. For the 12-story RC SMF archetypes with GILD ratio of 0.5, *ACMR* was reduced by 2% and 3% for the variants with GILD at the first and second story, respectively, so the more approximate linear *P*-Delta transformation did not affect the collapse analysis results in any meaningful manner.

6.9 Overview of Conclusions and Recommendations

This study finds that the potentially negative effects of vertical irregularities are generally insignificant for moment frame buildings. Therefore, prohibitions or penalties placed on buildings with vertical irregularities, particularly those within the scope of this study, deserve careful re-examination. In making these conclusions, it is important to note that this study focused on new code-compliant buildings, where the effects of the irregularities (e.g., additional story shear from sloping columns) are considered in the design process. Therefore, the general conclusion is that the effects of vertical irregularities are insignificant for moment frame

buildings when they are designed to fully meet ASCE/SEI 7-16 design requirements (but ignoring certain prohibitions, such as on the equivalent lateral force (ELF) procedure). The conclusion is not applicable to older, non-code-compliant buildings where the effect of irregularities may not have been considered in the building design process, for which safety has been clearly shown to be deficient in past earthquakes.

Generally, moment frame buildings designed with the ELF procedure have collapse resistance that meets or exceeds their counterparts designed with modal response spectrum analysis (MRSA), even when MRSA demands are scaled to achieve 100% of the ELF base shear. This observation holds for regular and irregular archetypes alike. Therefore, prohibiting the ELF procedure on the basis of a vertical irregularity seems unnecessary. A future study may further investigate the scope of applicability of this finding by examining the relative performance of ELF and MRSA designed buildings with additional configurations and site locations.

Specific conclusions for each irregularity studied in this chapter are described in the following sections.

6.9.1 Weight (Mass) Irregularity (V2)

Weight (mass) irregularity tends to reduce collapse resistance, but not dramatically. The location of the mass irregularity along the height of the building moderately affects collapse performance; archetypes with the mass irregularity in lower stories (where the building is already more likely to have damage) tend to have lower collapse capacity than those with mass irregularities in their upper stories. The ELF procedure, which is currently prohibited for designing buildings with mass irregularities, tends to produce safer buildings than MRSA.

6.9.2 Soft/Weak Story Irregularity (V1/V5)

Soft/weak story irregularities do not appear to pose a problem in moment frame buildings, as long as they meet code demands (e.g., strength requirements and drift limits). This is due to the fact that "weak story" really means "strong adjacent stories" if the "weak" story is still strong enough to resist the required lateral force demand per current code. It is logical to expect the collapse performance to still reduce in situations where the distribution of damage over height changes from several stories to just one as the result of a weak story irregularity, but for the design cases evaluated in this study, the negative effects of having more concentrated damage are offset by the positive effects of having strengthened members in the adjacent stories. This finding is consistent with other past studies on this topic. Based

upon this study, the prohibition of extreme weak story irregularities in SDC D and the height limitation on in SDC B and C may be overly conservative. Further study is recommended to evaluate the prohibition of weak/soft story irregularities in SDC E and F.

6.9.3 Strong-Column/Weak-Beam (V6)

Strong-column/weak-beam (SCWB) is not categorized as an irregularity in ASCE/SEI 7-16, but it is an aspect of configuration that affects the distribution of damage over the height of the building, and which can have a corresponding impact on seismic performance. As shown in prior studies, increasing SCWB ratios generally improves collapse resistance. It is also found that implementing higher SCWB ratios in the lower stories of a building (where damage most commonly occurs) may improve collapse resistance, but this was based on a limited initial study. The studies show that this stepped approach may be an effective way to improve collapse safety at minimal material cost, although a broader study is needed to set limits for stepped designs. The future study could examine different building configurations, as well as a broader range of stepped SCWB ratio configurations; for steel frames specifically, the economy of increasing column sizes to remove the need for doubler plates is also something that could be further investigated.

6.9.4 Gravity-Induced Lateral Demand (V7)

Gravity-induced lateral demand (GILD) is not currently identified as an irregularity in ASCE/SEI 7-16. GILD does not significantly affect the collapse performance of a building, as long as the additional lateral force is taken into account in proportioning the lateral system. However, failing to account for GILD in the building design process can result in significant reductions in collapse resistance, particularly if the irregularity occurs at a location in the building where earthquake damage already tends to accumulate (i.e., the first few stories). Although the findings suggest that buildings with GILD do not need special treatment in ASCE/SEI 7, the GILD studies were limited to a relatively small number of archetypes, and further study is recommended.

Chapter 7
Discussion of Other Irregularities (H2, H3, H4, H5, V3, V4, V8)

This chapter discusses several irregularities found in ASCE/SEI 7-16 that were not the subject of the extensive analysis described in earlier chapters. This chapter describes the irregularity, discusses its trigger and consequences relative to ASCE/SEI 7-16, and where warranted, suggests revisions to current ASCE/SEI 7-16 requirements. The following irregularities are discussed:

- H2, Reentrant corner
- H3, Diaphragm discontinuity
- H4, Out-of-plane offset
- H5, Nonparallel system
- V3, Vertical geometric
- V4, In-plane discontinuity
- V8, Wall discontinuity

7.1 Reentrant Corner (H2) Irregularity

ASCE/SEI 7-16 Table 12.3-1 defines a reentrant corner irregularity where both plan projections of the structure beyond a reentrant corner are greater than 15% of the plan dimension of the structure in the given direction. A reentrant corner might be thought of as a "notch" taken out of the plan of a structure, such as that shown in Figure 7-1. The concern is that this condition can generate additional demands on the horizontal and vertical elements in the seismic-force-resisting system (SFRS), particularly near the reentrant corner, not otherwise captured using conventional analytical methods.

Discussion of reentrant corners in seismic design pre-standards and standards stretches back to at least ATC-3-06 Section 3.4.1 (ATC, 1978), which called for classifying a structure as "irregular" if a building had "reentrant corners with significant dimensions." The qualifier "significant" was not defined in the provisions, but the ATC-3-06 *Commentary* has figures suggesting that

notches amounting to at least 15% to 20% of the plan dimension for L, U, T, and X plan geometries would be considered irregular.

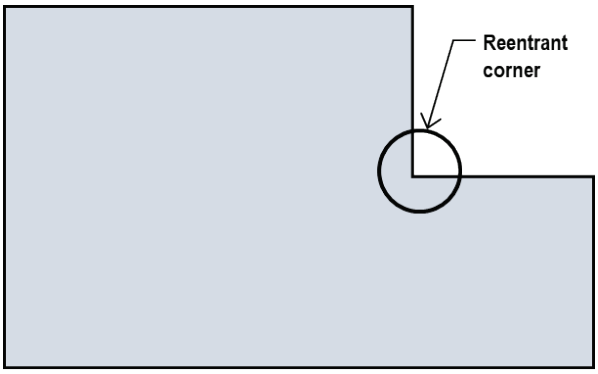

Figure 7-1 Example of reentrant corner.

Figure 7-2 compares ATC-3-06 *Commentary* Figure C3-4 showing three of these plan geometries, with how the geometries would appear if the 15% to 20% notches were drawn to scale. Only the X plan geometry is drawn reasonably to scale. Examination of the other plan geometries shows that the 15% to 20% notches are actually significantly smaller than suggested by appearance of the ATC-3-06 *Commentary* figure, making the eventually adopted 15% trigger appear quite conservative; nevertheless, the trigger stuck.

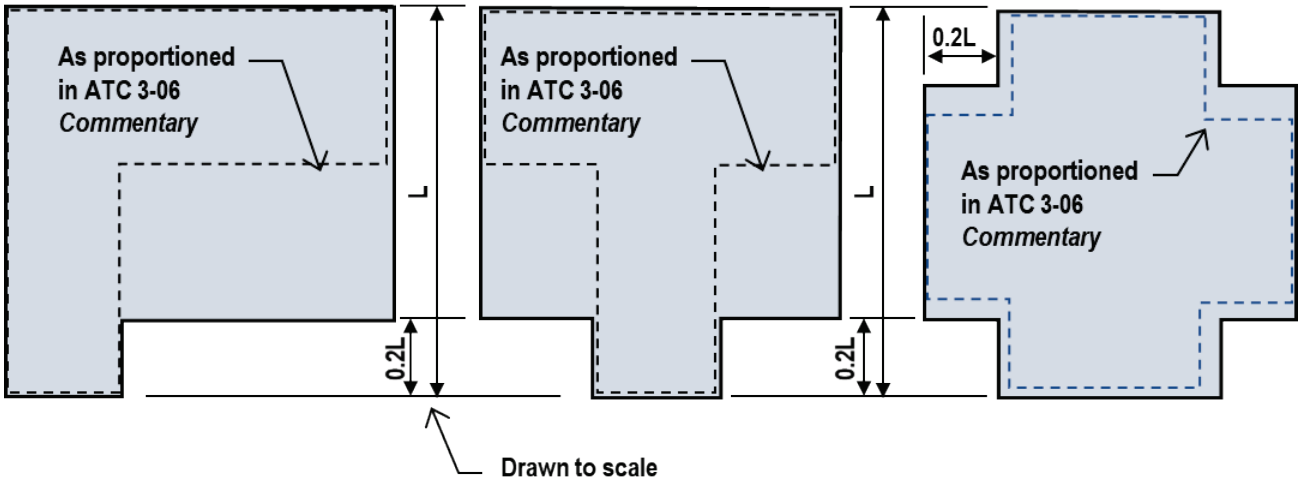

Figure 7-2 Comparison of reentrant corner examples as proportioned in ATC-3-06 *Commentary* and drawn to scale.

Starting with 1985 *Uniform Building Code* (UBC) Section 2312(h)3 and 1985 *NEHRP Provisions* Section 3.4.1, using the qualitative term "highly irregular shapes," building codes and pre-standards began to address buildings with reentrant corners (International Conference of Building

Officials, 1985; FEMA, 1986). The 1988 UBC Table 23-N defined as irregular a building where "both projections of the structure beyond a reentrant corner are greater than 15 percent of the plan dimensions of the structure in the given direction" (International Conference of Building Officials, 1988). Similar language can be found in the 1988 *NEHRP Provisions* in Section 3.41 and Table 3-3 and SEAOC Blue Books from 1988, 1990, and 1996 (FEMA, 1988; SEAOC, 1988, 1990, 1996). Subsequent editions of ASCE/SEI 7-16 also used the 15% plan dimension as a trigger for classifying a building as irregular.

According to ASCE/SEI 7-16 Section 12.3.3.4, when a structure is classified as having a reentrant corner irregularity, diaphragm forces increase by 25% for the design of:

1. Connections of diaphragms to vertical elements and to collectors;
2. Collectors and their connections, including connections to vertical elements, of the seismic-force-resisting system.

The increased diaphragm forces apply not just to stories of the building that have the reentrant corner but for all other stories, as well, because ASCE/SEI 7-16 uses the introductory phrase, "For structures assigned to Seismic Design Categories D, E, or F…" Forces calculated using the seismic load effects including the overstrength factor, Ω_0, need not be increased by 25%.

Although reentrant corners were not studied analytically in this project, a review of the data generated for irregularities that were studied, particularly torsional response, suggests that reconsidering the existing irregularity trigger is warranted.

The irregularity trigger should continue to consider the size of a reentrant corner as it relates to both dimensions of a building. For example, Figure 7-3 shows how the ratios of X_p/X and Y_p/Y together are likely better predictors of reentrant corner irregularities of significance than either X_p/X or Y_p/Y alone.

The irregularity trigger could consider the relative mass of the one diaphragm section relative to the other. If a reentrant corner impacts only a small portion of the structure, then it will have limited impact on the response of the entire structure, even if the building geometry meets the current definition of a reentrant corner. While maintaining a focus on demands resisted by collectors and their connections related to the reentrant corner appears reasonable, the significance of this irregularity on the behavior of the diaphragm as a whole should also be considered.

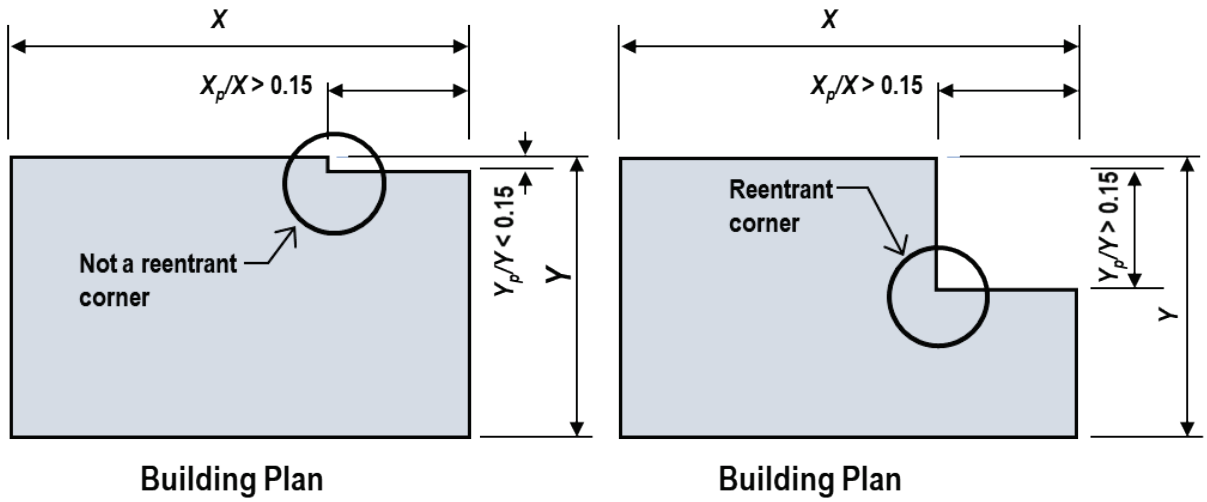

(a) Not a reentrant corner irregularity because significant plan offset does not occur about both axes.

(b) Reentrant corner irregularity because significant plan offsets occur about both axes.

Figure 7-3 Impact considering dimensions of plan offsets about both axes in identifying reentrant corner irregularity.

For example, if the dimensions of the cantilever portion of the diaphragm in a square building footprint are 0.15*L* about both X- and Y-axes, the plan offset would be 0.85*L*, which would trigger the reentrant corner irregularity. On the other hand, the mass of the smaller, cantilevered section of the diaphragm is only 3% of the total floor area. When X_p/X and Y_p/Y both equal either 0.25 or 0.3, the mass of the smaller section of the diaphragm is still only 10% and 15.5% of the total floor mass, respectively. If X_p/X and Y_p/Y are significantly different, the relative mass would change even more slowly. This suggests that some of the current penalties imposed when a reentrant corner irregularity is triggered, such as increases on the connection demands of diaphragms to vertical elements of the SRFS, may be difficult to justify.

While the number of different building geometries are infinite, the relatively small area of the mass of the cantilevered section of the geometries for plan offsets of less than 25% suggests that the 15% trigger may be unrealistically conservative.

Based on these observations, it appears that the 15% trigger could be relaxed along the following lines:

1. A reentrant corner irregularity should be triggered when both X_p/X and Y_p/Y are greater than 25% as shown in Figure 7-3.
2. Although the efficacy of the currently required force increase itself was not studied analytically, the increase in diaphragm forces should be limited to the stories with the reentrant corner irregularity, the elements at the corner should be classified as collectors and the required strength

of these elements should be increased by 25%. Recognizing the potential for load redistribution within the SFRS due to the reentrant corner, these recommendations could also be applied to the stories above and below the reentrant corner.

3. In lieu of the prescriptive 25% increase in required strength, a diaphragm response analysis considering diaphragm flexibility could be undertaken to better assess the response of the building due to the reentrant corner.

7.2 Diaphragm Discontinuity (H3) Irregularity

ASCE/SEI 7-16 Table 12.3-1 classifies a structure as irregular when it has a diaphragm discontinuity, which is defined as "a diaphragm with an abrupt discontinuity or variation in stiffness, including one that has a cutout or open area greater than 50% of the gross enclosed diaphragm area, or a change in effective diaphragm stiffness of more than 50% from one story to the next," as shown in Figure 7-4 (ASCE, 2017a).

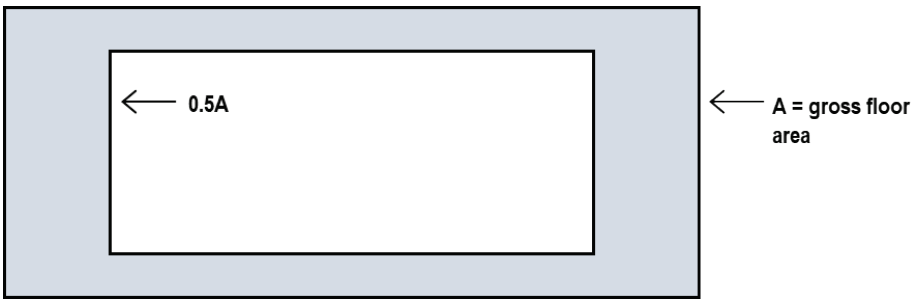

Figure 7-4 Diaphragm discontinuity comprising 50% of the gross floor area drawn to scale.

According to ASCE/SEI 7-16 Section 12.3.3.4, when a structure is classified as having a diaphragm discontinuity irregularity, diaphragm forces increase by 25% for the design of:

1. Connections of diaphragms to vertical elements and to collectors;
2. Collectors and their connections, including connections to vertical elements, of the seismic-force-resisting system.

As with the reentrant corner irregularity, the increased diaphragm forces in Seismic Design Categories C through F apply not just to stories of the building that have the diaphragm discontinuity, but for all other stories as well. Forces calculated using the seismic load effects including the overstrength factor, Ω_0, need not be increased.

There are two diaphragm discontinuity triggers: (1) one that relates to the size of openings (i.e., the 50% trigger) or other changes in diaphragm

strength or stiffness within a single floor; and (2) one that relates to a change in diaphragm stiffness from one floor to the next.

The 50% opening trigger appears to be overly permissive, as shown in Figure 7-4, as an opening of this size leaves little of the diaphragm around the opening to distribute loads to the seismic-force-resisting system. With openings of this size, diaphragm flexibility also begins to be a potential issue. Diaphragm force increases and a requirement to treat the elements around the opening as collector elements may be a reasonable requirement.

The trigger related to a change in stiffness from one level to another, which reflects a vertical issue triggered by a horizontal element, does not appear relevant to diaphragm irregularity classification. ATC-3-06 Section 3.4.1 classifies a structure as irregular if the diaphragm at any single level has significant changes in strength or stiffness. Although not quantified, this description is consistent with diaphragms that have openings or changes in thickness on a single floor that might impact the distribution of seismic forces and result in force concentrations in the diaphragm or create torsion not otherwise accounted for in a typical analysis, as noted in the ATC-3-06 *Commentary*. ATC-3-06 focuses on diaphragm changes on a single level rather than from one level to another.

The first appearance of the changes in diaphragm stiffness between adjacent floors triggering a horizontal irregularity is the 1988 *Uniform Building Code* (UBC) Table 23-N and the 1988 *NEHRP Provisions*, where the 50% stiffness change is listed (International Conference of Building Officials, 1988; FEMA, 1988). Prior editions of the UBC and NEHRP Provisions did not contain this trigger, nor did editions of the Blue Book prior to 1996. In the 1996 Blue Book, the 50% stiffness change appears for the first time in that publication (SEAOC, 1996).

Common examples where diaphragm strength or stiffness changes from one level to another are:

- Steel deck or plywood roof diaphragms (i.e., generally flexible diaphragms) above floors with concrete filled diaphragms;
- Floors with thickened slabs needed to resist high gravity loads or to assist in distribution of seismic loads at podium levels.

While these changes in stiffness from one floor to another may result in force redistributions that would not be captured in typical seismic analyses idealizing the diaphragm as fully rigid or fully flexible, the 25% force increase for all levels in the building does not appear warranted as the impact of the change in diaphragm strength or stiffness is expected to be focused on

the floor with the significantly different diaphragm strength or stiffness and perhaps, a level or two above and below that floor. The studies of mass irregularities studied in this project suggest that adequate protection against collapse can be expected if the irregularity is accounted for in the design. Therefore, it is recommended that these changes in diaphragm strength and stiffness be addressed through appropriate modifications to the analytical model.

Possible approaches to address the impact of a significant change in diaphragm strength or stiffness include:

1. Explicit modeling of the diaphragm stiffness for the level with the changed strength or stiffness.
2. In lieu of explicitly modeling the diaphragm, the force increase prescribed by ASCE/SEI 7-16 Section 12.3.3.4 could be required for the level with the strength of stiffness change as well as the level above and below.

7.3 Out-of-Plane Offset (H4) and In-Plane Discontinuity (V4) Irregularities

These two irregularities represent discontinuities in the load path between the vertical elements of the seismic-force-resisting system above and below an offset. In both discontinuities the vertical element above the discontinuity does not continue below insofar as its resistance to the horizontal (shear) forces, which must be transferred to other vertical elements below that level either through an in-plane or out-of-plane load path. The irregularity provisions address both this load path for horizontal forces and the load path for the overturning of the discontinuous element.

ASCE/SEI 7-16 Table 12.3-1 defines a structure to have an out-of-plane offset irregularity if the horizontal forces from the discontinued vertical element above the discontinuity must be transferred through a diaphragm or similar element in order to reach the vertical element or elements below. Similarly, ASCE/SEI 7-16 Table 12.3-2 defines a structure to have an "in-plane discontinuity in vertical lateral force-resisting element irregularity" if there is an in-plane offset of a vertical seismic-force-resisting element resulting in overturning demand on a supporting structural element (ASCE, 2017a). Figure 7-5 shows idealizations of buildings with out-of-plane and in-plane discontinuities in wall systems.

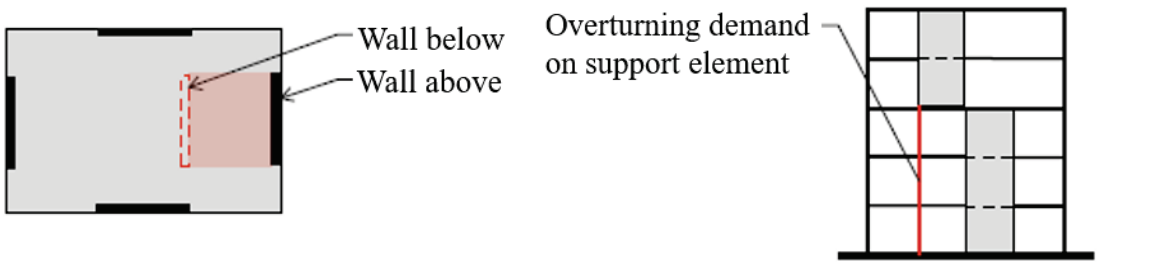

Figure 7-5 Walled buildings classified as irregular due to out-of-plane and in-plane offset of the wall system.

According to ASCE/SEI 7-16 Section 12.3.3.3, when a structure has an out-of-plane offset or in-plane discontinuity:

1. Members that support discontinuous walls or frames as well as the connections between those members and the discontinuous wall or frame must be designed to resist seismic load effects, including overstrength. For capacity-limited design, seismic load effects including overstrength are defined by the capacity-limited horizontal seismic load effect (Section 12.4.3.2). (Such capacity-limited design is permitted for all systems and is required for certain systems. For example, AISC 341 requires capacity design for special concentrically braced frame (SCBF), buckling restrained braced frame (BRBF), eccentrically braced frame (EBF), and special plate shear wall (SPSW) systems.) For all other cases, seismic load effects including overstrength are calculated using the overstrength factor, Ω_0, to amplify horizontal seismic forces.
2. Design forces for structures assigned to Seismic Design Category D, E, or F must be increased by 25% for the design of:
   a. connections of diaphragms to vertical elements and to collectors;
   b. collectors and their connections, including connections to vertical elements, of the seismic-force-resisting system

   with the exception that forces calculated using the seismic load effects including the overstrength factor, Ω_0, need not be increased.

7.3.1 Impact of Out-Of-Plane and In-Plane Discontinuities in RC Wall Buildings

No new research was conducted as part of the current study to investigate the impact of in-plane and out-of-plane discontinuities on building performance to earthquake loading. Instead, the results of previous work addressing this issue in RC wall buildings were reviewed. Specifically, NIST GCR 14-917-25, *Recommendations for Seismic Design of Reinforced Concrete*

Wall Buildings Based on Studies of the 2010 Maule, Chile Earthquake (NIST, 2014), which documents the results of an investigation of the impact on earthquake performance of in-plane and out-of-plane discontinuities in reinforced concrete walls was reviewed.

A general review of building drawings and earthquake damage patterns for multiple buildings damaged during the 2010 Maule, Chile earthquake resulted in the observation that damage was concentrated where:

- Severe horizontal or vertical discontinuities were introduced into a wall and supplemental reinforcement was not provided to assist in transfer of forces through the discontinuity; and
- Wall area was reduced substantially in a lower story, including cases where walls were supported on very small piers (i.e., columns).

As part of the NIST study, building drawings and damage patterns were reviewed for four mid-rise reinforced concrete wall buildings that were moderately to severely damaged during the earthquake. Each of the buildings employed multiple walls to resist both gravity and earthquake loads; each of the buildings included multiple walls with local in-plane and out-of-plane discontinuities. A total of 120 wall discontinuities were identified and classified as: (1) wall termination in which an upper wall is terminated such that no lower wall exists in the story below; (2) wall opening in which there is a new opening in a lower wall; (3) wall shift in which there is a change in the centroid of a wall cross-section, including a change in the dimension or location of a wall flange; and (4) flag wall in which a change in the dimension of the web of a wall in which the upper wall is larger than the lower wall. Each discontinuity was quantified using multiple measures: change in wall area, the change in wall dimension, the movement of the wall centerline, and the movement of the wall centroid. Measures of the severity of the wall discontinuity were compared with observed damage.

The NIST study concluded that damage is correlated with: (1) a change from one story to the story below in the location of the centroid of the wall that exceeds 30% of the in-plane length of the wall in the direction of the change; and (2) a reduction in the centerline length of the wall greater than 30% going from an upper to a lower story.

The findings of the NIST study suggest two possible revisions to the current ASCE/SEI 7-16 requirements with respect to consideration of in-plane and out-of-plane discontinuities:

1. The required increase in forces used for design of connections of diaphragms to vertical elements and collectors, and of collectors and

their connections, per Section 12.3.3.4 of ASCE/SEI 7-16, need only be applied in the vicinity of the discontinuity and not throughout the entire structure.

2. The NIST study of local wall geometric discontinuities, using ASCE/SEI 31-03 and ASCE/SEI 41-06 (which have since been combined in ASCE/SEI 41), found that Tier 2 "lack[s] correlation at the individual component level, [but] is consistent with the observed performance of the overall building in the earthquake," and Tier 3 "generally resulted in a conservative assessment of performance at the component level" and "provided an acceptably accurate measure of overall building performance." Since there is no corresponding Tier 1 checklist item, the NIST study recommends adding a Tier 1 Basic Structural Checklist item to flag walls with changes in cross-sectional geometry from one story to the story below that results in either a change in the location of the centroid of the wall that exceeds 30% of the length of the wall in the direction of the move or a reduction in the centerline length of wall that exceeds 30%. Since geometric changes of this magnitude would be identified by ASCE/SEI 7-16 as irregularity type V3 or V4, no corresponding change to ASCE/SEI 7-16 is needed.

7.4 Nonparallel System (H5) Irregularity

ASCE/SEI 7-16 Table 12.3-1 defines a building with a nonparallel system irregularity when any of the lateral force-resisting elements are not parallel to a major orthogonal axis of the seismic-force-resisting system. This is not an irregularity per se, but represents a condition where otherwise acceptable simplifications of analysis (e.g., using only independent orthogonal directions of load) are not appropriate.

ASCE/SEI 7-16 does not prohibit this condition, but instead adds modeling requirements in the design of the building. These additional requirements include:

- Required three-dimensional structural modeling (per Section 12.7.3 and Section 16.2.2 in ASCE/SEI 7-16);
- Consideration of direction of loading through the orthogonal combination procedure per Sections 12.5.3 and 12.5.4 (e.g., the "100%-30%" orthogonal combination rule) or orthogonal ground motions applied simultaneously (where response history analysis is used); and
- Prohibition on using the equivalent lateral force (ELF) procedure for a building taller than 160 feet in a high-seismic zone (SDC D, E, or F) (per Table 12.6-1 in ASCE/SEI 7-16).

While this condition was not analytically studied, it is assumed that the remedy of additional structural modeling requirements appropriately handles this configuration condition. Future studies may be able to validate the removal of the prohibition on the ELF procedure for the H5 condition since past studies have shown that designs based on the ELF procedure generally result in a lower probability of collapse than those based on the modal response spectrum analysis (MRSA) procedure (FEMA, 2009; NIST, 2010; NIST, 2012).

7.5 Vertical Geometric (V3) Irregularity

ASCE/SEI 7-16 Table 12.3-1 defines a building to have a vertical geometric irregularity where the horizontal width of the seismic-force-resisting system changes by more than 30% between two adjacent stories. Similar to the H5 irregularity, the code remedy is to add an additional modeling requirement. In this case, only one requirement is included:

- A prohibition on the equivalent lateral force (ELF) procedure for a building taller than 160 feet in a high-seismic zone (SDC D, E, or F) (per Table 12.6-1 in ASCE/SEI 7-16)

The vertical geometric irregularity definition was developed as a qualitative indicator of systems that could have a non-uniform distribution of stiffness, for which the load pattern assumed in the equivalent lateral force procedure could be inaccurate. However, as noted earlier, past studies have shown that the ELF procedure generally produces buildings that have a lower calculated probability of collapse than buildings designed by the MRSA procedure. Since the soft story irregularity (V1) captures the most concerning non-uniform stiffness distribution based on explicit stiffness calculations, it may be possible to eliminate the less direct V3 irregularity. However, this would require further study.

7.6 Wall Discontinuity (V8) Irregularity

A review of earthquake damage to RC wall buildings, as well as consideration of current design practice, suggests the potential need for code language addressing wall discontinuities such as shown in Figure 7-6.

These types of discontinuities were investigated as part of the development of NIST GCR 14-917-25, *Recommendations for Seismic Design of Reinforced Concrete Wall Buildings Based on Studies of the 2010 Maule, Chile Earthquake* (NIST, 2014). This study used data collected following the 2010 Maule, Chile earthquake. Design to accommodate load transfer above and below stacked openings in walls is addressed in detail in Moehle

(2015) and NIST (2011). Section B.1 provides more details on previous research and studies related to discontinuities in walls. Given the previous work addressing these types of discontinuities and the availability of guidance on design to accommodate these discontinuities, it was concluded that code changes would not be recommended. The following sections summarize previous research as well as design recommendations addressing wall discontinuities. Section B.2 provides more details on a limited study conducted on this type of irregularity.

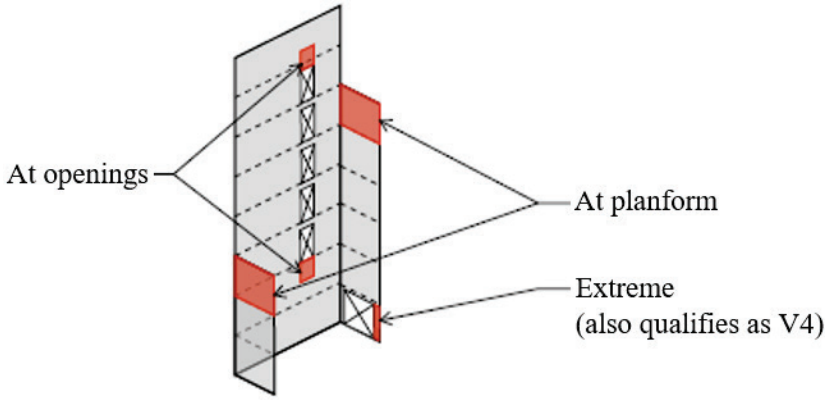

V8. Wall Discontinuity

Figure 7-6 Vertical wall discontinuities potentially constituting an irregularity.

7.6.1 Discontinuities Associated with Initiation or Termination of Stacked Openings in Walls

A vertical discontinuity arises when coupled walls terminate in a solid wall panel below or above the coupled region (Figure B-3a). The solid *panel zone* above or below the stacked openings can be subjected to large shear stresses when the wall system is loaded laterally, and significant damage has been observed in RC wall buildings in the vicinity of this type of discontinuity (Figure B-3b and Figure B-4). The vulnerability of this panel zone to high shear demand has also been investigated by Naeim et al. (1990) using linear finite element analysis.

NIST (2011) provides a discussion of the issues to be considered in design, and Moehle (2015) provides a detailed discussion of design of these *panel zone* discontinuity regions that exist above and below stacked openings. The discussion in Moehle (2015) includes calculations and figures demonstrating that shear in the panel zone results from anchorage of wall pier boundary element reinforcement. Moehle (2015) also includes the following design recommendations: (1) provide two layers of heavy horizontal "chord" reinforcement above and below the primary anchorage zone for wall pier longitudinal reinforcement; (2) provide reinforcement within the panel zone

to carry shear associated with anchorage of the wall pier longitudinal reinforcement; (3) continue 50% of wall pier reinforcement through to the base or top of the wall; and (4) use a *capacity* designed approach that accounts for overstrength of reinforcing steel.

The above suggests that the discontinuities associated with initiation or termination of stacked openings in a wall is best addressed not at the system level via classification as a vertical structural irregularity, but as a local design and detailing issue. As such, changes to ASCE/SEI 7-16 to address this irregularity are not recommended; instead, it is recommended that efforts be made to encourage appropriate design and detailing of the region in the vicinity of the irregularity.

7.6.2 Discontinuities Associated with Increased Wall Area to Capture Forces Introduced by New Structural Elements

Wall geometry may change significantly over the height of the building to reflect increased or reduced lateral demand; most often changes in demand are associated with changes in floor plan. Figure 7-6 includes two vertical discontinuities associated with the addition of wall flanges to resist forces introduced by an expanded floor plan. Damage to RC wall buildings suggest that changes in wall geometry can result in damage and inadequate performance under earthquake loading.

The impact on earthquake performance of changes in wall cross section was investigated as part of the NIST GCR 14-917-25 report, which documents RC wall building damage resulting from the 2010 Maule, Chile earthquake (NIST, 2014). This NIST study resulted in the conclusion that significant earthquake damage was correlated with a change in the centerline length or the location of the centroid of the wall of greater than 30%. However, this study specifically concluded that only changes resulting in a reduction in wall centerline length going from one story to the story below were detrimental to RC wall building performance. Damage data indicated that increasing wall centerline length from one story to the story below rarely resulted in damage. Thus, on the basis of this NIST study, changes to ASCE/SEI 7-16 are not recommended to address this type of discontinuity. However, as discussed in Section 4.3 of NIST (2011), shear lag effects for flanged sections should be included in the design, most commonly by means of effective flange widths as defined in ACI 318-14.

Based on recommendations in NIST (2014), a Tier 1 Basic Structural Checklist item should be added to ASCE/SEI 41-17 to flag walls with local discontinuities caused by changes in cross-sectional geometry from one story to the story below that exceed either: (1) a reduction in centerline length

greater than 30% (in either orthogonal direction); or (2) a change in centroid location greater than 30% of the wall length measured in the direction of the change. For more information on related damage data that supports this recommendation, see Section B.1.2.

Chapter 8
Recommended Improvements

The regularity-related requirements found in current codes and standards generally reflect the best judgment of practitioners and academics based primarily on anecdotal observations and fairly simple linear static and linear dynamic analyses, without explicit consideration of collapse probability. The studies described in this report are some of the few to apply modern analytical and probabilistically based techniques to systematically evaluate the performance of buildings with and without irregularities.

Chapters 4 through 7 provide a detailed assessment of the significance of structural irregularities (in most cases, in terms of collapse probability), current code triggers, and the effectiveness of related code provisions. In many cases irregular structures that satisfy current code requirements have safety against collapse in an earthquake comparable to that for regular structures. In a few cases detailed studies suggest that code triggers or design requirements should be strengthened or can be relaxed to achieve comparable collapse resistance. This chapter summarizes recommended improvements for the seismic design of buildings with configuration irregularities and identifies areas for future study.

8.1 Codes and Standards

This section summarizes recommended improvements to ASCE/SEI 7-16 for seismic design of new buildings and ASCE/SEI 41-17 for seismic evaluation and retrofit of existing buildings.

8.1.1 NEHRP Recommended Provisions and ASCE/SEI 7-16

Recommended improvements to ASCE/SEI 7-16 are summarized by four categories: (1) revised triggers and prohibitions; (2) revised modeling requirements; (3) revised design requirements; and (4) improved commentary and other clarifications.

Revised Triggers and Prohibitions

Torsionally Irregular Buildings [H1]: Based on explicit collapse assessments, as detailed in Chapter 4, the following revisions are recommended for torsionally irregular buildings:

- Classify buildings as torsionally irregular if more than 75% of their lateral strength is located at or on one side of the center of mass.
- Do not prohibit extremely torsionally irregular buildings in Seismic Design Categories E and F.
- Do not prohibit use of the equivalent lateral force procedure for torsionally irregular buildings.

Reentrant Corner and Diaphragm Discontinuity Irregularities [H2, H3]: Considering the historical development of reentrant corner and diaphragm discontinuity irregularities and reasonably anticipated consequences, as detailed in Chapter 7, the following revisions are recommended:

- A reentrant corner irregularity should be triggered where both X_p/X and Y_p/Y are greater than 25% (rather than the current 15%).
- A diaphragm discontinuity irregularity should be triggered where a cutout or open area is greater than 25% of the gross enclosed diaphragm area (rather than the current 50%).

Mass (Weight) Irregularity [V2]: Based on explicit collapse assessments, as detailed in Chapter 6, and global behavior comparisons of buildings with mass irregularity, as detailed in Appendix F, it is recommended that irregularity Type V2 be eliminated. The only consequence of that irregularity is a requirement to base the design on the results of modal response spectrum analysis (MRSA), but MRSA is found to provide no advantage over the equivalent lateral force (ELF) procedure.

Revised Modeling Requirements

***P*-Delta Effects:** *P*-Delta effects in three-dimensional models can be categorized as global translational (*P*-Delta), local deformational (*P*-delta), and rotational (P-θ); all should be considered where torsion response is important. The global translational *P*-Delta effect can be captured by ensuring that all vertical loads on the building are included in the model. Local deformational *P*-delta effects can be captured in the element formulation (for instance, using consistent geometric stiffness rather than linearized geometric stiffness) or by discretizing individual elements to capture second order effects in the analysis solution. If portions of the gravity system are not modeled explicitly, then the remaining vertical loads on unrepresented elements should be applied to "leaning columns," which are vertical elements that are pinned to the diaphragms.

To capture twisting response more accurately, including P-θ effects, vertical loads should be applied to the structure at the locations where they are

expected to occur. Location is important for simulating *P-θ*, because *P-θ* is a cross-product of *P*-Delta with the distance vector from the center of rigidity; in other words, the torque caused by *P*-Delta from a given column is equal to the lateral *P*-Delta component of that column times its perpendicular distance (lever arm) to the center of rigidity.

As an alternative to modeling vertical loads on every vertical component in a building, *P-θ* effects in rigid diaphragm models can be simulated by placing leaning columns strategically throughout the plan, such that the center of gravity and radius of gyration of the leaning column loads are the same as the center of gravity and radius of gyration of the actual vertical load carrying elements in the building. For the rectangular buildings in Chapter 4 of this study, this was accomplished by placing one leaning column in each quadrant of the building plan, each located one polar radius of gyration from the center of mass (i.e., assuming an equally distributed gravity system in the actual building).

Gravity-Induced Lateral Demands: Section 12.7.3 of ASCE/SEI 7-16 should be revised to address gravity-induced lateral demands. For instance, the requirement could read, "Where the configuration of structural elements is such that application of gravity loads induces lateral demands on the seismic-force-resisting system, those effects shall be considered explicitly in the mathematical model used to determine seismic design forces and drifts."

Story Stiffness and Strength [V1, V5]: To assess soft story and weak story vertical configuration irregularities and to determine the redundancy factor, ρ, in accordance with Table 12.3-3 of ASCE/SEI 7-16, story stiffness and strength should be computed as follows.

For each story in each orthogonal direction, the apparent story stiffness should be computed as:

$$K_x = V_x / (\delta_x - \delta_{x-1})$$

where:

V_x = the story shear at level x determined by an elastic analysis using the forces defined in Section 12.8.3 of ASCE/SEI 7-16; and

δ_x = the deflection at the center of mass of level x determined by an elastic analysis using the forces defined in Section 12.8.3 of ASCE/SEI 7-16.

For each story in each orthogonal direction, the story lateral strength should be computed as the sum the shear contributions of seismic-force-resisting elements as follows:

- **Brace members.** The shear contribution for each brace is the horizontal component of the lesser of the connection capacity or brace capacity. The brace capacity (in tension or compression) should be consistent with the direction of load application being considered. Where uplift of a shallow foundation, column capacity, or the capacity of an element supporting a discontinuous frame controls the response, the computed strength should reflect that limit state.
- **Moment frame columns.** The shear contribution is that corresponding to the least lateral capacity. For frame columns with weak column-strong beam conditions, the shear contribution is the lesser of that developed when the top and bottom of the column are at flexural capacity, or the column shear capacity. For frame columns with a strong column-weak beam condition, the shear contribution is the lesser of the shear corresponding to development of flexural yielding at each end of the column (from adjoining beam yield hinges or column base connection capacity), or the column shear capacity.
- **Shear wall piers.** The shear contribution is the lesser of either the shear at development of the flexural strength, or the shear strength. Where wall flexure controls the response, both the 1.2*D* and 0.9*D* axial load cases should be considered. Where the capacity of an element supporting a discontinuous wall controls the response, the computed strength should reflect that limit state.

Revised Design Requirements

Torsionally Irregular Buildings [H1]. Based on explicit collapse assessments, as detailed in Chapter 4, the following revisions are recommended for torsionally irregular buildings:

- Require consideration of orthogonal loading effects, such as by the 100%-30% orthogonal combination procedure of ASCE/SEI 7-16 Section 12.5.3.1, for all torsionally irregular buildings assigned to Seismic Design Category C, D, E, or F.
- Require use of redundancy factor, $\rho = 1.3$ (for Seismic Design Category D, E, or F), only where the structure has extreme torsional irregularity in both orthogonal directions or lines of lateral resistance in a given direction are all on one side of the center of mass.
- Require that effects of accidental torsion be accounted for by application of a static accidental torsional moment (rather than explicit 5% mass offsets in linear dynamic analysis) for buildings with extreme torsional irregularity assigned to Seismic Design Category B, C, D, E, or F.

Design Forces for Collectors and Connections [H1, H2, H3, H4, V4]. Section 12.3.3.4 of ASCE/SEI 7-16 requires that design forces determined in accordance with Section 12.10.1.1 be increased for connections of diaphragms to vertical elements and to collectors and for collectors and their connections, for systems with one of several horizontal or vertical irregularities. Considering the historical development of these irregularities and reasonably anticipated consequences, as detailed in Chapters 4 and 7, it is recommended to limit the extent of such increased forces as follows:

- For structures with torsional stiffness irregularity [H1] or reentrant corner irregularity [H2], increased forces need be considered only at levels with the irregularity.
- For structures with diaphragm discontinuity irregularity [H3], out-of-plane offset irregularity [H4], or in-plane discontinuity irregularity [V4] increased forces need be considered only at levels with the irregularity and at adjacent levels above and below, due to possible load redistribution within the seismic-force-resisting system.

Recognizing the approximate nature of diaphragm inertial forces computed in accordance with Section 12.10.1.1 of ASCE/SEI 7-16, exceptions to the related force increases for irregular structures could be made where transfer conditions and diaphragm flexibility are modeled explicitly.

Improved Commentary and Other Clarifications

In addition to the technically substantive recommendations made above, the following revisions would improve the clarity and application of regularity-related code requirements.

- For ease of reference, the item numbers that appear in Tables 12.3-1 and 12.3-2 of ASCE/SEI 7-16 could be prepended with H or V to indicate class of irregularity—horizontal or vertical. For instance, "irregularity type 4 of Table 12.3-1" becomes "irregularity H4."
- The commentary figures in ASCE/SEI 7-16 should be updated using those from this document. In particular, the figure for V4 in ASCE/SEI 7-16 is incorrect as it reflects the definition of that irregularity in ASCE/SEI 7-05.
- For the simple redundancy exception in ASCE/SEI 7-16 Section 12.3.4.2 item b, "regular in plan at all levels" means "without irregularity type 1b, 4, or 5 as defined in Table 12.3-1".
- Section 12.3.2.2 of ASCE/SEI 7-16 should be revised in indicate that "Structures *with more than one story* that have one or more of the

irregularity types…" are subject to the requirements, and "one-story buildings in any Seismic Design Category or for" should be struck from exception 2.

- The designation for irregularity type H5 could be changed from "nonparallel system" to "non-orthogonal systems" to better reflect the concern that two-dimensional analysis in each of two orthogonal directions cannot capture system behavior adequately.
- The triggering condition for vertical geometric irregularity [V3] could be inverted as "the horizontal dimension of the seismic-force-resisting system in any story is less than 75% of that in an adjacent story" so that the trigger focuses attention on the story with the reduced stance.

8.1.2 ASCE/SEI 41-17

Based on recommendations in NIST (2014), as detailed in Chapter 7, a Tier 1 Basic Structural Checklist item should be added to ASCE/SEI 41-17 to flag walls with local discontinuities caused by changes in cross-sectional geometry from one story to the story below that exceed either: (1) a reduction in centerline length greater than 30% (in either orthogonal direction); or (2) a change in centroid location greater than 30% of the wall length measured in the direction of the change.

8.2 Future Studies and Development

The studies described in this report sought to improve the design of new buildings with configuration irregularities, where possible as informed by explicit collapse assessments using the FEMA P695 method. Although this study has been the most comprehensive consideration to date of collapse resistance for several categories of structural irregularity, future studies could be used to further validate the findings and enlarge the scope of issues treated. In particular, improvements can be made in explicit collapse assessment, design sensitivities could be better identified, and several irregularities or systems types could be given more detailed consideration.

8.2.1 Explicit Collapse Assessment Improvements

"To the extent possible, nonlinear models" used in the FEMA P695 method "include explicit simulation of all significant deterioration mechanisms that could lead to structural collapse" (FEMA, 2009). The effects of other behaviors that could trigger collapse can be considered though not simulated explicitly. Non-simulated collapse conditions are often computed using story drift or other indirect metrics. Test results used to establish backbone curves, both for elements that are modeled explicitly and for behaviors that are

assessed indirectly, often characterize behavior to displacements or rotations associated with loss of resistance to lateral loading, rather than loss of gravity-load resistance. The accuracy of collapse assessments could be improved by developing a more robust set of backbone curves that represent behavior to the point of loss of gravity-load resistance. Gravity framing systems are a good example where this improved representation could have a profound effect on collapse predictions, but the same is true of any element that supports gravity loads. ASCE/SEI 41-17 approximates this consideration, in one instance, by doubling life safety and collapse prevention acceptance criteria for coupling beams of reinforced concrete shear wall systems with short spans and bottom reinforcement that is continuous into supporting walls, but a testing-based criterion would be more consistent with the FEMA P695 process.

The shear-flexure-interaction models discussed in Chapter 5 and Appendix B could be further developed to improve collapse assessment predictions.

8.2.2 Design Sensitivity Studies

Recent research has shown that the ELF procedure produces designs that generally have a lower probability of collapse than those designed using modal response spectrum analysis. Future study may be able to validate removal of the prohibition on the ELF procedure for additional irregularities, such as type V3.

ASCE/SEI 7-16 Section C12.9.1.4.1 describes changes made to address unacceptable collapse performance of designs based on modal response spectrum analysis and notes that even those changes do "not necessarily achieve the intended collapse performance." This project's findings for regular baseline structures and irregular variants confirm that ELF designs generally produce better collapse performance than MRSA designs. Further study addressing this disparity is recommended.

The detailed analyses undertaken in this project show that the collapse resistance of "barely code-conforming" designs is more sensitive than expected for more realistic designs of buildings with or without irregularities. A study of standard practice versus minimal design could be informative, especially if accompanied by FEMA P-58 risk assessments to show how much "savings" the minimal designs produce (FEMA, 2012b).

This project has focused on comparing the collapse resistance of properly designed buildings with and without irregularities. It could be useful to study the robustness of designs where possible misinterpretations or errors of application are made.

8.2.3 Strong-Column/Weak-Beam Requirements

The objectives of strong-column/weak-beam (SCWB) requirements in the concrete and steel design standards are consistent. Section R18.7.3 of ACI 318-14 describes the intent "to reduce the likelihood of yielding in columns," which could result "in a column failure mechanism that can lead to collapse." Commentary Section E3.4a of ANSI/AISC 341-16 explains that "the SC/WB concept is more of a global frame concern" because "weak column frames… are likely to exhibit an undesirable response at those stories with the highest column demand-to-capacity ratios." Since the objective is directly related to global system performance associated with the target reliabilities for structural stability set forth in Section 1.3.1.3 of ASCE/SEI 7-16, consideration could be given to adding a general requirement related to strong-column/weak-beam behavior in ASCE/SEI 7.

Reinforced Concrete Moment Frames. The strong-column/weak-beam studies of reinforced concrete moment frames, detailed in Section 6.7.2, suggest that using larger SCWB ratios at lower stories where critical collapse mechanisms usually concentrate and lower ratios in upper stories may have design merit. This approach could be studied further to assess whether it could be refined to improve economy without reducing collapse resistance.

Steel Moment Frames. Like earlier studies, the SCWB studies of steel moment frames, detailed in Section 6.7.2, suggest that yielding in the joint panel zone improves collapse resistance relative to frames with inelastic response concentrated in beams outside the panel zone. However, since the backbone curves commonly used for panel zones reflect no degradation, while those for beams do degrade, it seems that this beneficial effect could be unrealistically overestimated. Further study of the relative importance and consequences of panel zone and beam yielding could inform steel moment frame models that more correctly reflect collapse resistance.

8.2.4 More Detailed Considerations

Additional Structural Systems. Although a range of structural systems was considered in the explicit collapse assessments of this project, further studies could be performed using masonry shear walls, wood frame shear walls, steel concentrically braced frames, and steel eccentrically braced frames. It is expected that the general trends related to configuration irregularity would hold for these systems, but material-specific configuration subtleties could be investigated. For instance, ANSI/AISC 341 limitations on K-bracing and the relative proportion of braces in tension and compression, and requirements for V- and inverted V-braced frames could be better informed by explicit collapse assessments. With respect to reentrant corners or diaphragm

discontinuities, understanding implications of different diaphragm materials and location of vertical elements in the SFRS relative to discontinuities may benefit from more detailed study.

Combinations of Systems. With the exception of the mixed system studies reported in Chapter 4, the archetypes investigated by this project use the same structural system along two orthogonal axes. Section 12.2.2 of ASCE/SEI 7-16 allows combinations of framing systems in different directions, and Section 12.2.3 allows horizontal or vertical combinations of framing systems in the same direction, with direction on the selection of seismic response parameters. The collapse resistance of systems with these configurations has not been assessed explicitly, but could be in future studies.

Buildings with Multiple Irregularities. Although some real buildings include multiple irregularities that could interact, the analyses of this project treat irregularities separately, just as they are defined independently in codes. Future studies could include archetypes with combinations of vertical and/or horizontal irregularities to assess whether performance problems compound. As discussed in Chapter 2, many of the buildings that collapsed in past earthquakes have both soft/weak story irregularity and torsional irregularity. The code rules for buildings with those irregularities were prompted by observations of that damage, but explicit collapse assessments for a broad design space of buildings with multiple irregularities have not yet been performed.

Wall Discontinuity [V8] and In-Plane Discontinuity [V4]. Appendix B reports differences in performance of walls with openings depending on the location of the opening and direction of loading. Additional studies could help to clarify where the introduction of an opening near the end of wall should be classified as an in-plane discontinuity [V4]. Perhaps that classification could be based on the location of neutral axis for the overall wall section with respect to the opening or the anticipated magnitude of localized compressive demands.

Gravity-Induced Lateral Demand. The studies of systems with gravity-induced lateral demand (GILD), detailed in Chapter 6, consider demands induced by all columns at a single story leaning in the same direction by a uniform amount. The same GILD ratio, which is gravity induced story shear (Q_G) divided by story shear capacity (Q_V), could be produced by columns sloping over multiple stories or by one or a few columns leaning more severely. Similarly, a broader set of analyses could help to identify which stories are most sensitive to the GILD effect for various baseline archetypes.

Such further studies could be undertaken with an expanded archetype design space to validate this project's findings.

Consideration of Accidental Torsion Effects in Dynamic Analysis. Chapter 4 and Appendix A report reductions in collapse resistance for torsionally sensitive buildings proportioned for accidental torsion effects by explicit mass offsets in (linear) modal response spectrum analysis. Similar studies should be undertaken to assess whether the explicit mass offset method could be permitted for linear response history analysis and whether it should continue to be required for nonlinear response history analysis (per Section 16.3.4 of ASCE/SEI 7-16).

Appendix A

Torsion Studies

This Appendix documents more detail of the torsion studies, which were completed in support of the findings and recommendations summarized in Chapter 4 of this report. The sections of this Appendix are independent of one another (i.e., they can be read in any order), but they depend on Chapter 4 for context. For detailed results of the torsion studies, see the electronic Supporting Documentation for Appendix A: Torsion Studies Tabulated Designs and Results.

A.1 Development and Validation of Simplified 3D Models

A.1.1 Nonlinear Backbones for Modeling the Seismic-Force-Resisting System

The seismic-force-resisting systems (SFRSs) of the archetype models were modeled with shear springs defined by nonlinear backbones, illustrated in Figure A-1. The short baseline model emulates the global properties of a two-story wood shear wall building for which damage accumulates primarily in the lower story and *P*-Delta effects are small. Data for calibrating the short baseline archetype were taken from a prior study of wood light frame buildings (DeBock et al., 2016).

The mid-rise baseline backbone has characteristics similar to the baseline 12-story reinforced concrete (RC) special moment frame (SMF) that was developed to study vertical irregularities in Chapter 6, which has significant *P*-Delta effects. Key properties of the 12-story baseline building are listed in Table A-1 for the purpose of comparison.

In the mixed system archetypes, lines of lateral resistance representing RC walls used a backbone similar to the backbones computed for RC walls in Chapter 5; the RC wall parallel to the moment frame (Figure A-2) started out stronger than the walls in the wall-only direction, because it is stiffer than the frame and attracts more force. The lines of resistance representing RC SMFs are similar to the 8-story baseline RC SMF developed for the vertical irregularity studies in Chapter 6, except that they are weaker because the frame is softer than the wall and attracts less force.

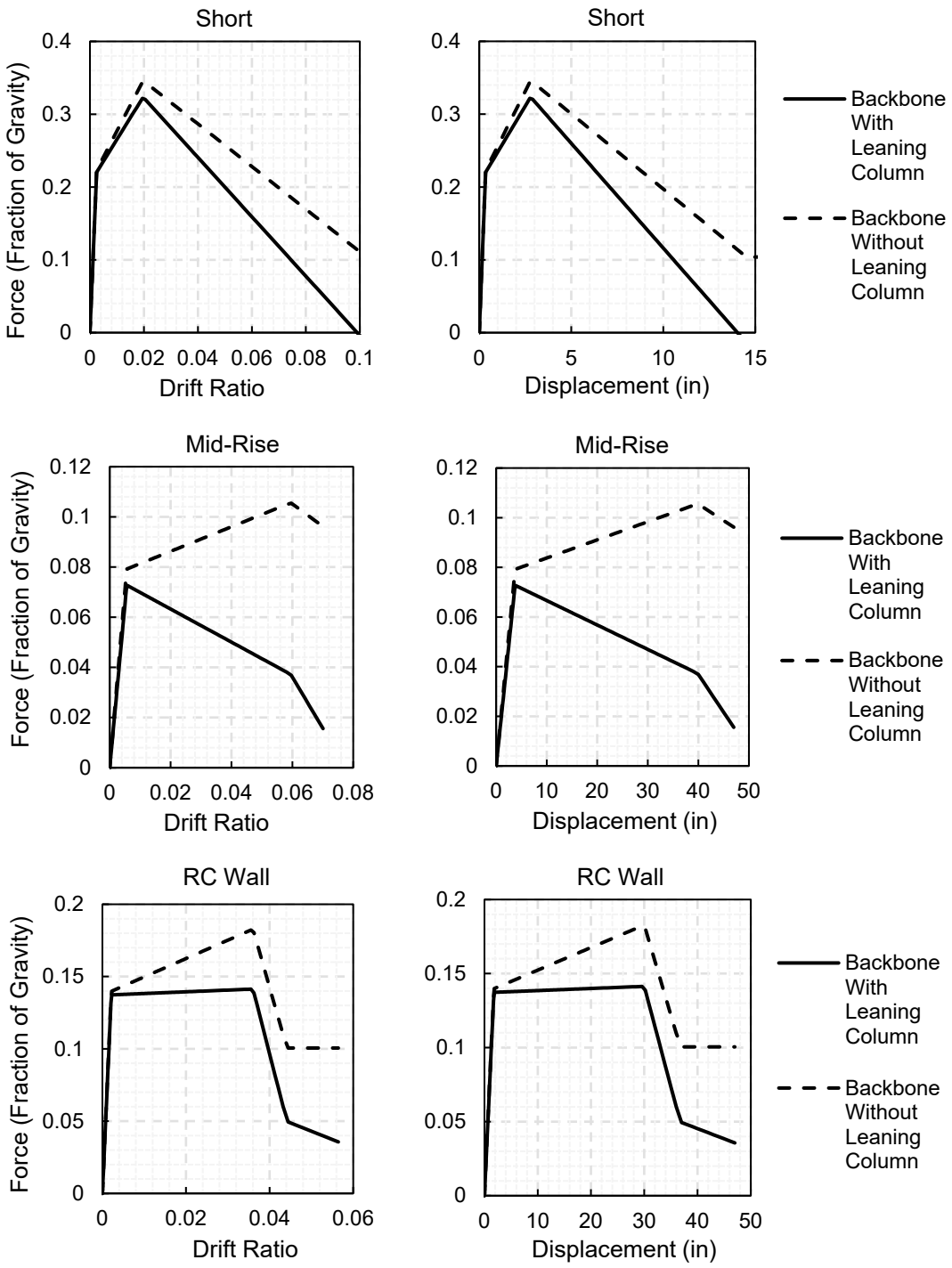

Figure A-1 Backbone properties of the baseline archetypes representing short, mid-rise, and RC wall type buildings.

Table A-1 Model Information for Baseline Archetypes

Baseline Archetype	Height of Model[1] [ft.]	Overstrength (Ω)	Period-Based Ductility (μ)	*ACMR*
"Short"	12	2.11	9.9	1.8
"Mid-rise"	56	1.66	5.3	1.9
Comparison: 12-story RC SMF model	158	1.53	5.2	1.9
"RC Wall"	69	1.33	17	3.0
Comparison: 8-story RC wall models	106	1.11, 1.35	8.6, 12.4	2.9, 3.3

[1] Important for simulating *P*-Delta

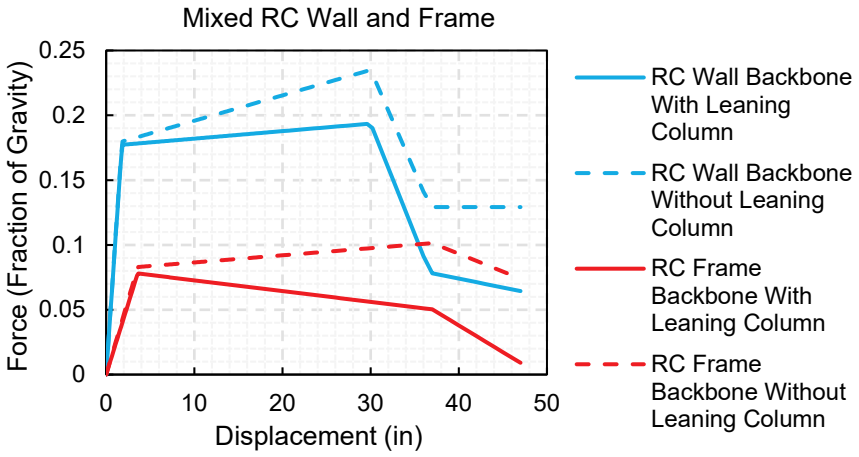

Figure A-2 Backbone properties for lines of lateral resistance representing the "wall" and "frame" that make up the mixed system (in the long direction of the mixed system archetypes).

The heights of the three-dimensional nonlinear models were determined so that *P*-Delta effects approximate those of their multi-story counterparts at story drifts ranging from 3% to 6%, where *P*-Delta effects are critical for determining the onset and progression of collapse. Figure A-1 and Figure A-2 show the nonlinear backbones of the baseline archetypes, with and without leaning columns included in the models. Key properties of the baseline archetypes are summarized in Table A-1. The heights of the *P*-Delta columns in the nonlinear mid-rise model are shorter than the height that is used for drift calculations in the design step because drifts tend to concentrate in fewer stories as the building becomes nonlinear. The drifts shown in Figure A-1 are consistent with maximum story drift ratios observed in the high-end multi-story models, not roof drifts.

The cyclic properties of the nonlinear springs were modeled with peak-oriented material properties having relatively low cyclic deterioration. Cyclic deterioration effects were minimized in the simplified models for the

following reasons: (1) cyclic deterioration is a system/material dependent property and this study is intended to capture torsion effects in a more generic sense; and (2) collapse capacity has been shown to be relatively insensitive to cyclic deterioration properties in comparison with other parameters such as peak strength and negative stiffness (Ibarra, 2003, 2005). Figure A-3 illustrates the cyclic behavior of the short baseline model.

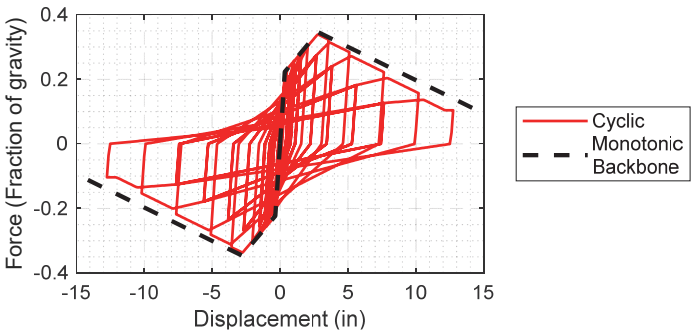

Figure A-3 Cyclic properties of the short baseline backbone (leaning columns excluded).

A.1.2 Scaling of Nonlinear Backbones

The strength and stiffness of the nonlinear backbones that represent lines of lateral resistance were scaled to match the changes in strength and stiffness that were determined in the design step. Scaling of the strength and stiffness were applied to each branch of the nonlinear backbone, therefore ductility did not change. Figure A-4 shows how the backbones change when strength and stiffness are altered: (a) illustrates perfectly coupled strength and stiffness while (b) and (c) illustrate decoupled strength and stiffness.

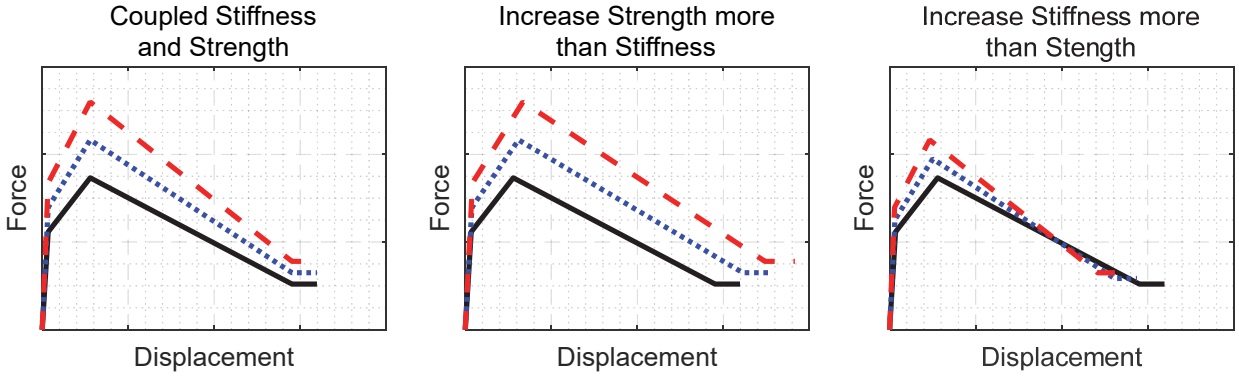

Figure A-4 Effects of scaling strength and stiffness of the nonlinear backbones, illustrated with the short archetype, as follows: (a) identical increases in strength and stiffness (coupled); (b) strength increase greater than stiffness increase (decoupled); and (c) stiffness increase greater than strength increase (decoupled). *P*-Delta effects are excluded for this illustration. The solid black line represents the baseline; blue-dotted and red-dashed lines represent incremental increases in strength and stiffness.

A.1.3 3D Modeling Approach

Three-dimensional single-story models of the archetypes were made in OpenSees (McKenna et al., 2000). The SFRS was modeled with nonlinear shear springs located at each line of lateral resistance. The diaphragm was modeled as rigid with a lumped mass located at its center. For archetypes without inherent eccentricity, the mass was offset by 5% of the building dimension in each orthogonal direction (simultaneously) to produce torsion. The rotational inertia of the building mass was determined assuming an even distribution of the mass across the building plan. Four leaning columns, or *P*-Delta columns, were included in the models, each one radius of gyration away from the center of plan. Figure A-5 shows a plan view of a 3D model.

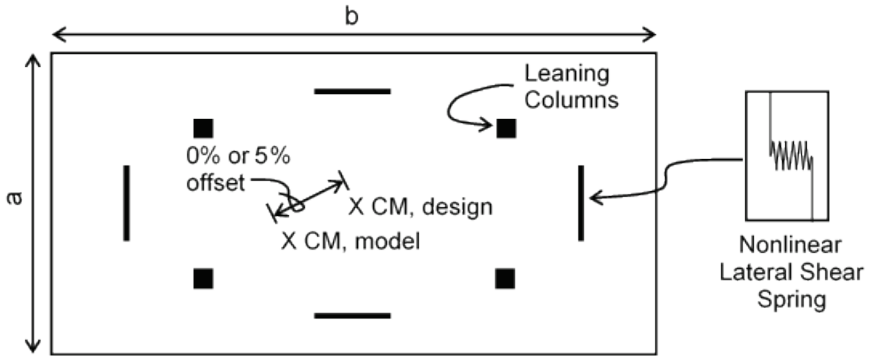

Figure A-5 Plan view of a single story model including placement of leaning (*P*-Delta) columns, mass offset, and SFRS.

Incremental dynamic analysis (IDA) was performed for the 22 FEMA far-field ground motions. Both components of the ground motion were applied simultaneously to the model. Two IDAs were performed for each pair of ground motions—one with the ground motion in its original orientation and another with the ground motion rotated 90 degrees, so a total of 44 IDAs were performed for each archetype. Buildings were considered collapsed if the drift ratio exceeded 10% at any location in plan due to failure of the gravity system.

A.1.4 Validation of Single-Story 3D Models

The single-story 3D models were intended to represent the macro-behavior of multi-story buildings. Therefore, a subset of multi-story models were used to validate their performance. The "high-end" multi-story models are similar in plan to the single-story models, but they are 12 stories tall and use the 12-story RC SMF baseline for their lines of lateral resistance. The lines of lateral resistance were moved systematically to introduce torsional irregularity, but they were not redesigned.

Figure A-6 shows the reduction in collapse resistance that occurs for a 2:1 aspect ratio variant when one line of lateral resistance is moved away from the perimeter, but the SFRS is not re-designed to resist torsion forces. Figure A-7 shows a trend similar to the one observed in Figure A-6, but for the case when all four lines of lateral resistance are moved toward the center of the building plan.

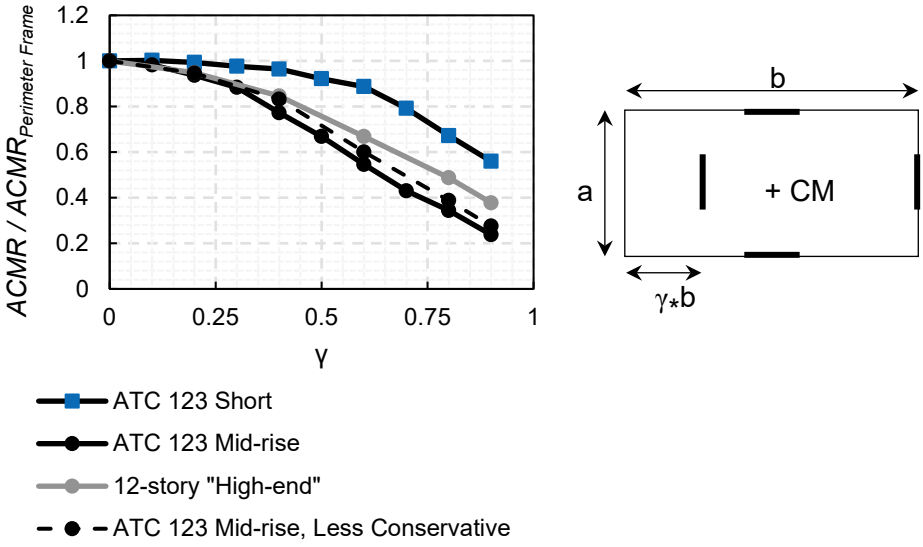

Figure A-6 Trends in collapse resistance of 2:1 aspect ratio single asymmetric archetypes with increasing eccentricity, but no re-proportioning of the SFRS for torsion demands.

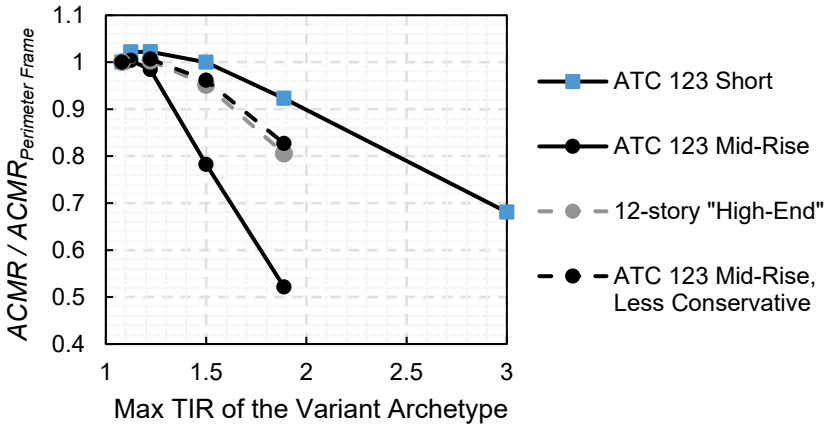

Figure A-7 Trends in collapse resistance of 2:1 aspect ratio symmetric archetypes with increasing torsional irregularity (*TIR*), but no re-proportioning of the SFRS for torsion demands.

Performance of the short archetypes declines less quickly, because they are less sensitive to rotational *P*-Delta effects (or *P*-θ). The mid-rise archetype, which is intended to represent buildings similar to the "high-end" 12-story model, is conservative for predicting the effects of torsional response on

collapse. It is conservative, because the height of the leaning columns is calibrated to match the *P*-Delta effects in the multi-story building during the onset and progression of collapse, when maximum story drifts are high (3% to 5%) and have localized to a few stories. Therefore, *P*-Delta effects at lower drifts are over-estimated in the simplified mid-rise models. As a result, *P-θ* effects are overestimated when torsional responses cause significant displacement of the leaning columns prior to the lines of lateral resistance degrading.

Based on these comparisons, it is concluded that the simplified 3D models for short archetypes are adequate for assessing torsion design provisions. However, the mid-rise variants with leaning columns one radius of gyration from the center of mass (CM) would lead to conservative conclusions when torsional *P-θ* effects play a significant role in the collapse mechanism. Therefore, a modified, less conservative, version of mid-rise archetype models were created by modeling the leaning columns at 70% of the radius of gyration from the CM to compensate for their over-estimation of *P-θ*; the results in Chapter 4 and in this Appendix are obtained from the archetypes with the conservatism reduced.

A.2 Torsional Strength Irregularity

ASCE/SEI 41 classifies buildings as torsionally irregular if the demand to capacity ratio (*DCR*) is significantly higher on one side of the CM than the other. The potential negative outcome of uneven strength distribution is that yielding on one side of the CM may cause the center of rigidity (CR) to move farther away from the CM, thus increasing the torsional response.

To assess the effects of torsional strength irregularity on collapse performance, a suite of symmetric code-conforming archetypes was developed. Torsional strength irregularities were introduced by increasing the strength of the lines of lateral resistance on one side of the CM in: (a) both orthogonal directions; and (b) one orthogonal direction. This was done for three different aspect ratios and for torsionally-flexible variants (lines of lateral resistance near center of plan, high *TIR*) and for torsionally stiff variants (lines of lateral resistance at the perimeter, low *TIR*).

Collapse resistance, relative to the baseline model, for the short and mid-rise archetypes with torsional strength irregularity is shown in Figure A-8 and Figure A-9, respectively. For these archetypes, torsional strength irregularity does not decrease collapse resistance, as long as the building is code-conforming, but it sometimes will increase the collapse resistance.

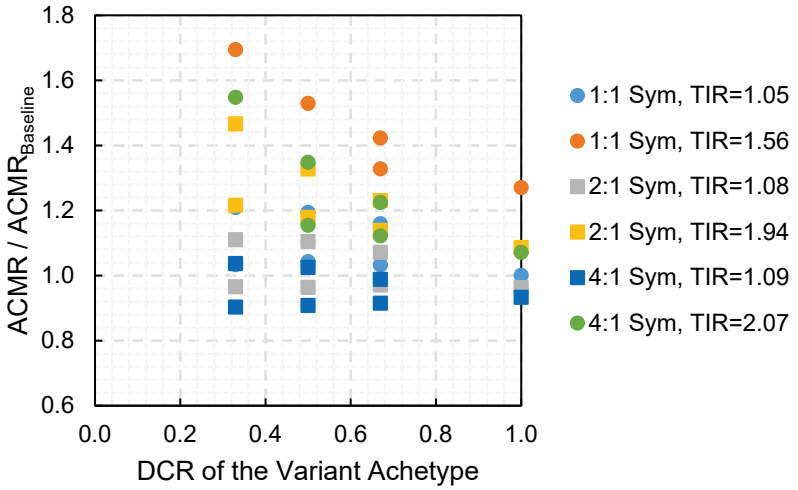

Figure A-8 Relative collapse resistance of symmetric short archetypes having strength irregularities due to lower *DCR* on one side of the center of mass.

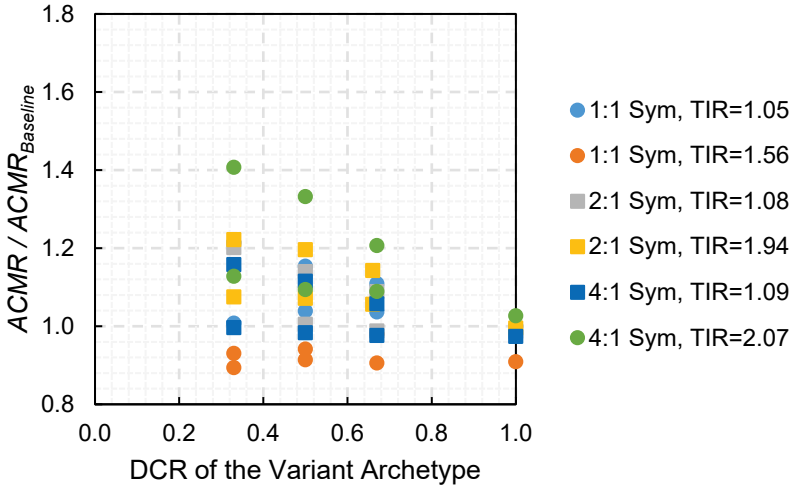

Figure A-9 Relative collapse resistance of symmetric mid-rise archetypes having strength irregularities due to lower *DCR* on one side of the center of mass.

A.3 Importance of Checking Drift and Stability Requirements at the Building's Edge for Torsionally Irregular Buildings

An important finding of the torsional irregularity studies is that enforcing drift and stability limits at the building edge (rather than CM) is critical for providing adequate collapse resistance for torsionally sensitive buildings. Figure A-10 shows steady declines in collapse resistance for the mid-rise archetypes when drift and stability checks are performed at the CM rather than the building edge. Comparing the trends to Figure 4-8, it is seen that

collapse resistance is sometimes nearly as poor as when torsion is neglected entirely in the design process (e.g., the 1:1 Single Asymmetric archetypes).

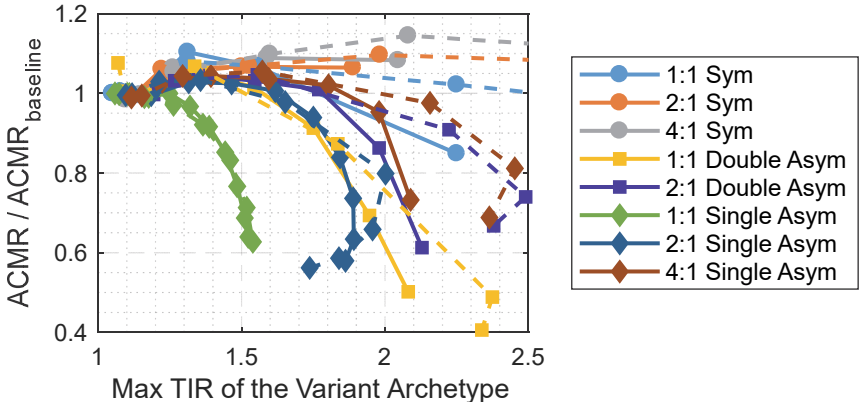

Figure A-10 Trends in collapse resistance for mid-rise archetypes proportioned according to ASCE/SEI 7-16 to resist seismic forces, but with a redundancy (ρ) of 1.0 and drift/stability checks performed at the CM, rather than the edge of the building. Archetypes with decoupled strength and stiffness are represented by solid lines; dashed lines represent archetypes with coupled strength and stiffness.

A.4 Rationale for Triggering Type 1a Torsional Irregularity When >75% of Strength is on One Side of the CM

In Chapter 4, it is recommended that buildings with more than 75% of their strength on one side of the CM be classified as torsionally irregular. The reason for this recommendation is to invoke the 100%-30% orthogonal earthquake load combination rule for buildings with significant inherent eccentricity. The 100%-30% orthogonal load combination rule is necessary to account for the coupling of dynamic responses in the two orthogonal directions. Specifically, lines of resistance orthogonal to the direction with inherent eccentricity have to resist seismic forces in their own direction in addition to torsional moments caused by shaking in the eccentric direction; failure to account for this coupling effect when designing the SFRS results in under-designing lines of resistance perpendicular to the direction with eccentricity.

In many cases, buildings with significant inherent eccentricity are already classified as torsionally irregular due to having $TIR > 1.2$. However, buildings that are rectangular in plan can have significant eccentricity in the long direction and still have $TIR < 1.2$. For example, the three-sided and mixed system archetype buildings all have TIR less than 1.2 for the cases where lines of resistance in the short-direction are at or near the perimeter. The circled data points in Figure A-11 through Figure A-13 show the

performance of these buildings if all of the proposed modifications from Chapter 4 are used, except that torsional irregularity is based solely on *TIR* (as in ASCE/SEI 7-16). The 3-sided archetypes were designed with a redundancy factor, ρ, of 1.3 in the long direction, which is triggered by having all of the lines of resistance on the same side of the CM. A redundancy factor of 1.3 would not be triggered under current ASCE/SEI 7-16 design procedures, so the three-sided archetypes with *TIR* < 1.2 would perform even worse than observed in Figure A-11 and Figure A-12 if they were proportioned according to ASCE/SEI 7-16.

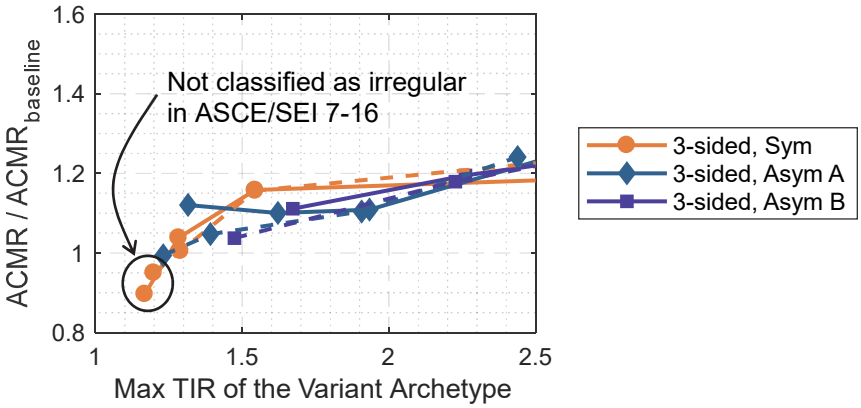

Figure A-11 Trends in collapse resistance for short 3-sided variants designed with all of the recommended torsion provisions from Chapter 4, except that torsional irregularity is determined only by *TIR* (as in ASCE/SEI 7-16).

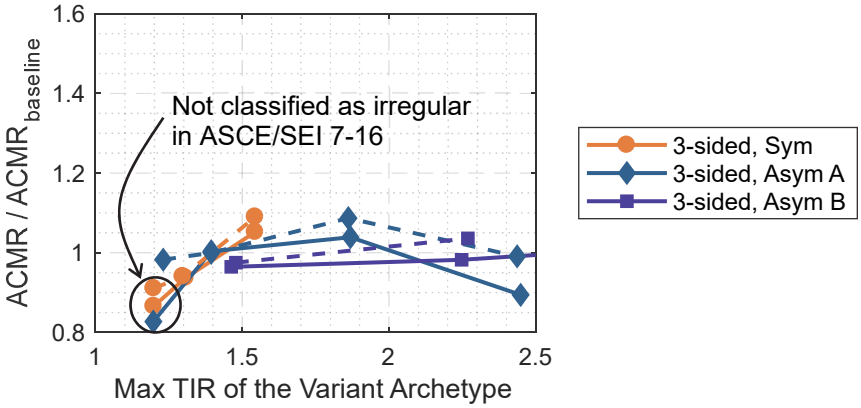

Figure A-12 Trends in collapse resistance for mid-rise 3-sided variants designed with all of the recommended torsion provisions from Chapter 4, except that torsional irregularity is determined only by *TIR* (as in ASCE/SEI 7-16).

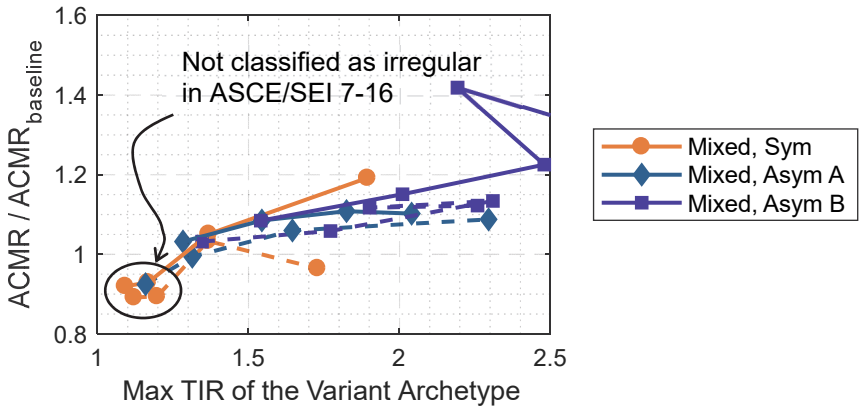

Figure A-13 Trends in collapse resistance for mixed system variants designed with all of the recommended torsion provisions from Chapter 4, except that torsional irregularity is determined only by *TIR* (as in ASCE/SEI 7-16).

A.5 Application of 5% Mass Offsets to Simulate Accidental Torsion with Modal Response Spectrum Analysis

Applying 5% mass offsets in lieu of the static accidental torsion moments set forth in Section 12.8.4 of ASCE/SEI 7-16 is insufficient for some building configurations. The most negatively affected configurations are those whose fundamental mode of vibration is a torsional mode with relatively little modal mass in the lateral direction. This is caused by the torsion mode having too little effect on the analysis due to its small participation factor. The symmetric archetypes are examples of buildings with torsional modes that have little modal participation in their lateral directions.

Table A-2 shows the effects on the required strength and stiffness for plan-symmetric torsionally irregular archetypes when the two design methods for accidental torsion are used. At moderate levels of torsional irregularity, the 5% mass offset method significantly increases force and drift demands. However, at high levels of torsional irregularity, offsetting the mass 5% makes very little difference in the design values. This finding is consistent with a previous study by De la Llera and Chopra (1994); they showed that simulating accidental torsion with 5% mass offsets in modal response spectrum analysis amplifies accidental torsion when the lateral and torsional modes have similar periods, but the amplifying effect of the dynamic analysis diminishes as the torsional period becomes significantly longer than the translational period. For reference, the torsional periods for the buildings in Table A-2 are >140% of the lateral periods.

Table A-2 Differences in Strength and Stiffness Required When 5% Mass Offsets are Used in Lieu of Static Accidental Torsion Moments for Torsionally Irregular Symmetric Archetype Buildings (in the More Critical Direction)

Plan Aspect Ratio	*TIR*[1]	Required Strength Relative to Baseline			Required Stiffness Relative to Baseline[2]		
		Static Accidental Torsion	5% Mass Offsets	Difference	Static Accidental Torsion	5% Mass Offsets	Difference
1	1.31	1.15	1.12	-3%	1.05	1.05	0%
	1.56	1.66	1.40	-16%	1.47	1.00	-32%
	2.25	2.71	1.41	-48%	4.42	1.00	-77%
2	1.22	1.14	1.45	27%	1.00	1.40	40%
	1.53	1.35	1.20	-11%	1.42	1.20	-15%
	2.04	2.27	1.14	-50%	3.74	1.12	-70%
4	1.26	1.17	1.55	32%	1.00	1.50	50%
	1.60	1.43	1.24	-13%	1.65	1.30	-21%
	2.09	2.37	1.17	-51%	3.99	1.20	-70%

[1] Due to differences in stiffness, *TIR* (torsional irregularity ratio) is slightly different between the versions with static accidental torsion moments versus those designed with modal response spectrum analysis and 5% mass offsets. The reported *TIR* values are for the latter.

[2] The stability coefficient and story drift of the baseline are 0.07 and 1.2%, respectively, so the required stiffness does not increase immediately as torsional irregularity is introduced.

Figure A-14 shows the performance of symmetric archetypes when they are designed using modal response spectrum analysis with mass offsets equal to (+/–)5% of the perpendicular direction. The results show that directly accounting for accidental torsion in the modal response spectrum analysis procedure using 5% mass offsets in the structural model can lead to poor performance in extremely torsionally irregular buildings.

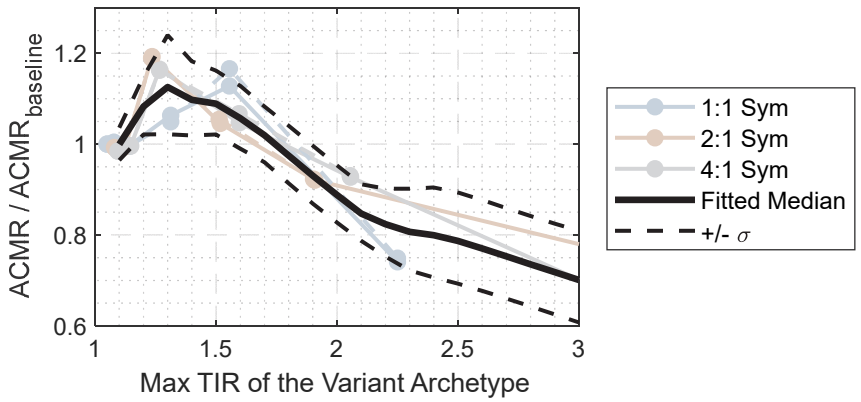

Figure A-14 Collapse performance of symmetric archetypes designed with modal analysis and accidental torsion applied directly by offsetting the mass (+/–) 5% of the perpendicular building dimension in the structural model.

A.6 Explanation of Why Some Trends in the Results Plots Double Back on Themselves

Some of the trends in the results plots "double back" because the *TIR* that is used to gauge torsional irregularity in ASCE/SEI 7-16 Table 12.3-1 saturates and eventually declines at large levels of torsional irregularity. Figure A-15 illustrates this phenomenon for the single asymmetric archetype configuration. Saturation (and eventual reduction) of *TIR* only occurs when inherent eccentricity becomes very large, and it is observed to a greater degree if the building dimension perpendicular to the applied lateral load is larger than the building dimension parallel to the applied lateral load.

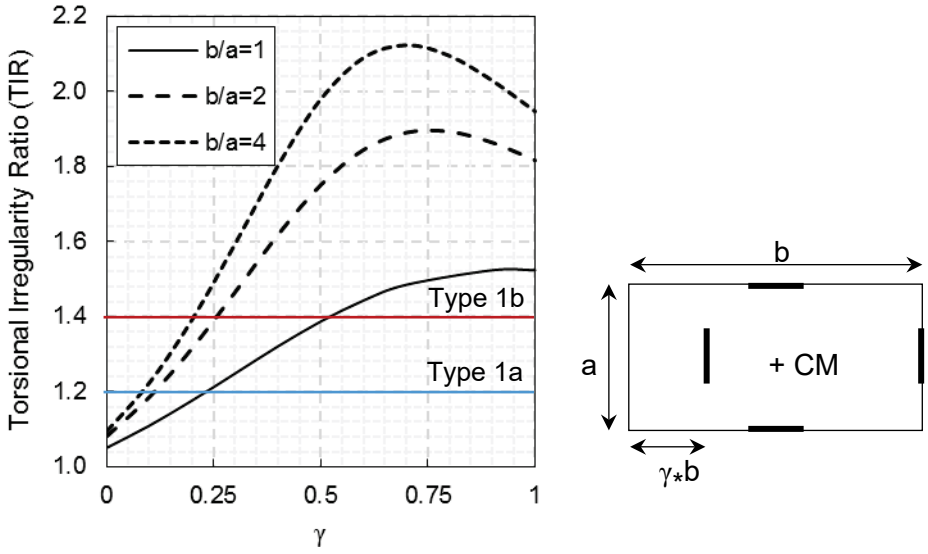

Figure A-15 Illustration of how the torsional irregularity ratio (*TIR*) computed in ASCE/SEI 7-16 Table 12.3-1 varies with plan aspect ratio and eccentricity (after Korolyk and Wagner, 2016). The horizontal lines show the ASCE/SEI 7-16 thresholds for Type 1a Torsional Irregularity and Type 1b Extreme Torsional Irregularity. The thickened lines in the building plan (right) represent lines of lateral resistance. All lines of lateral resistance are equally stiff for computing *TIR* in this example.

Appendix B
Concrete Wall Studies

This Appendix supports and supplements the information and results presented in Chapter 5. Section B.1 provides a summary of past investigations of reinforced concrete (RC) walls with irregularities. Section B.2 provides information on a limited study that was conducted to investigate wall discontinuity (V8) irregularities in RC wall buildings. Section B.3 provides details of the process to design the RC wall buildings used to assess the impact of openings on building performance. Section B.4 and Section B.5 describe validation and comparison studies of analytical methods used in the RC wall building studies. Section B.6 presents all the analysis results generated as part of the study on RC wall buildings, including tables summarizing collapse probabilities, results from pushover analyses, and results from the dynamic response history analysis.

Design calculations and detailed RC wall designs are provided in the electronic Supporting Documentation for Appendix B: Part 1, Concrete Shear Wall Detailed Design Information and Part 2, Concrete Shear Wall Building Drawings.

B.1 Past Investigations of Concrete Walls with Irregularities

The following sections provide an overview of past investigations of RC shear walls with irregularities from observed damage in past earthquakes, quantification studies, and laboratory test results.

B.1.1 Damage of Concrete Walls with Irregularities in Past Earthquakes

Damage to RC wall buildings during recent earthquakes demonstrates the potential for vertical irregularities to impact earthquake performance. Observed damage also suggests which vertical irregularities are highly correlated with damage and are particularly detrimental to building performance.

2010 Maule Earthquake. Evaluation of buildings damaged during the 2010 M8.8 Maule earthquake identified a number of building system design and configuration issues that could be expected to result in poor earthquake performance. These issues include discontinuities in walls; coupling of walls

via slabs, beams, and spandrels; wall demands induced by nonstructural elements; and wall axial demands. These issues are described in detail in Appendix D of NIST GCR 14-917-25, *Recommendations for Seismic Design of Reinforced Concrete Wall Buildings Based on Studies of the 2010 Maule, Chile Earthquake* (NIST, 2014), and addressed in Birely (2012). The following provides a brief description of the building configuration issues considered to be most highly correlated with earthquake damage.

Many of the RC wall buildings damaged during the 2010 Maule earthquake were observed to have significant vertical discontinuities in walls that were primary elements of the lateral load resisting system. Figure B-1 and Figure B-2 show vertical discontinuities in which a significant length of wall is lost from an upper to a lower story. Appendix D of NIST GCR 14-917-25 discusses vertical discontinuities in detail and provides vertical discontinuity data for the Chilean buildings that were studied.

Figure B-1 Coupled walls in upper stories do not continue to lower story (Plaza del Rio Building, Concepción, Chile). Photo courtesy of Ken Elwood.

A vertical discontinuity also arises when coupled walls terminate in a solid wall panel either below or above the coupled region, or both, as shown in Figure B-3a. The solid panel constitutes a discontinuity region that can be subjected to large shear stresses when the coupled walls are loaded laterally. Figure B-3b shows a typical reinforcement layout in the vicinity of this discontinuity and damage observed following the 2010 Maule earthquake. Figure B-4 shows similar damage patterns in a wall system with a similar discontinuity observed following the Loma Prieta earthquake (Moehle,

2015). Detailed descriptions of this particular discontinuity are provided in NIST (2014) and Moehle (2015).

Figure B-2 A change in the wall section from the upper to lower story results in a loss of wall area and localization of flexural yielding (Plaza del Rio Building, Concepción, Chile). Photo courtesy of Ken Elwood.

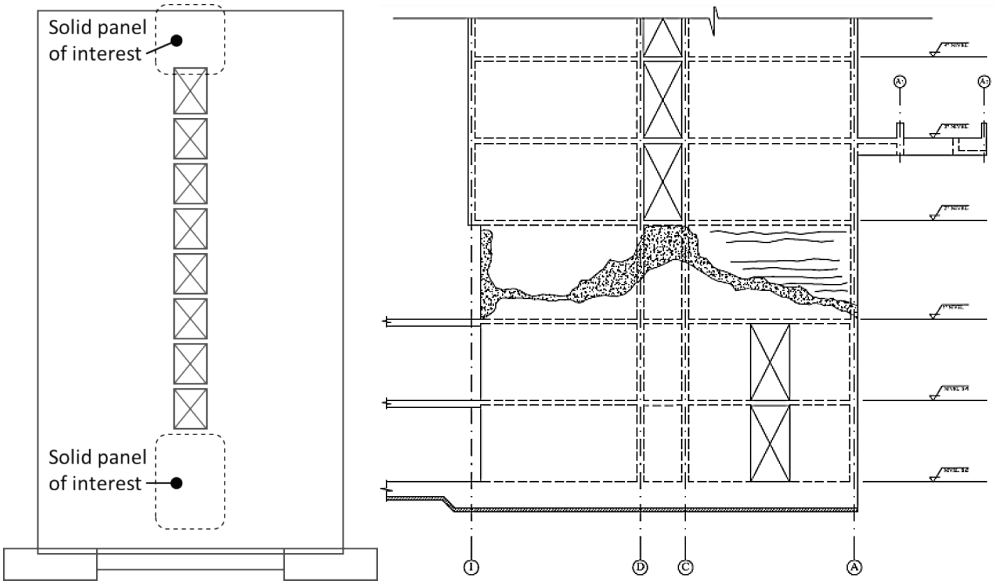

Figure B-3 Vertical discontinuity(ies) in coupled wallsL (a) Coupled walls with stack of openings terminating in a solid wall; and (b) damage map from axis 8 of the Alto Rio Building in Concepción, Chile following the 2010 Maule earthquake (image from NIST, 2014).

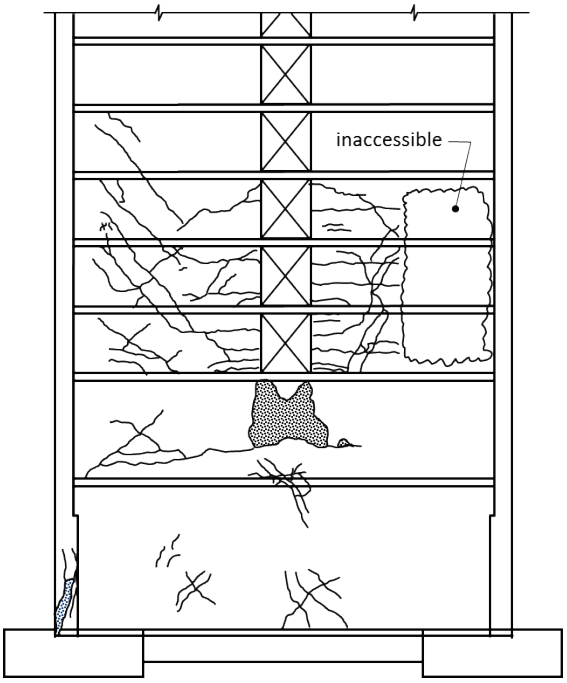

Figure B-4 Damage to building sustained during the 1989 Loma Prieta earthquake (image from Moehle, 2015).

2016 Meinong Earthquake. The 2016 M6.7 Meinong earthquake in southern Taiwan resulted in severe damage to reinforced concrete buildings. For the majority of the damaged buildings, lateral loads were primarily resisted by moment resisting frames. However, a couple of high-rise buildings with reinforced concrete walls and frames were damaged. Figure B-5 shows an example of a reinforced concrete wall with openings. As shown in the figure, the primary damage was to a "column" at the exterior of the wall. It is likely that the large axial force on the column resulted in the compression damage.

Overview of Findings. Based on review of earthquake damage following the 2010 Maule earthquake, and supported by other damage data presented above, primary findings with respect to the impact of building configuration, design, and detailing on earthquake performance are as follows (Birely, 2012):

- Damaged walls often did not have a clearly defined location where a plastic hinge could form.
- Detailing was poor in damaged buildings. Wall confining reinforcement was light, widely spaced, did not have 135-degree hooks and, in some cases, was nonexistent.

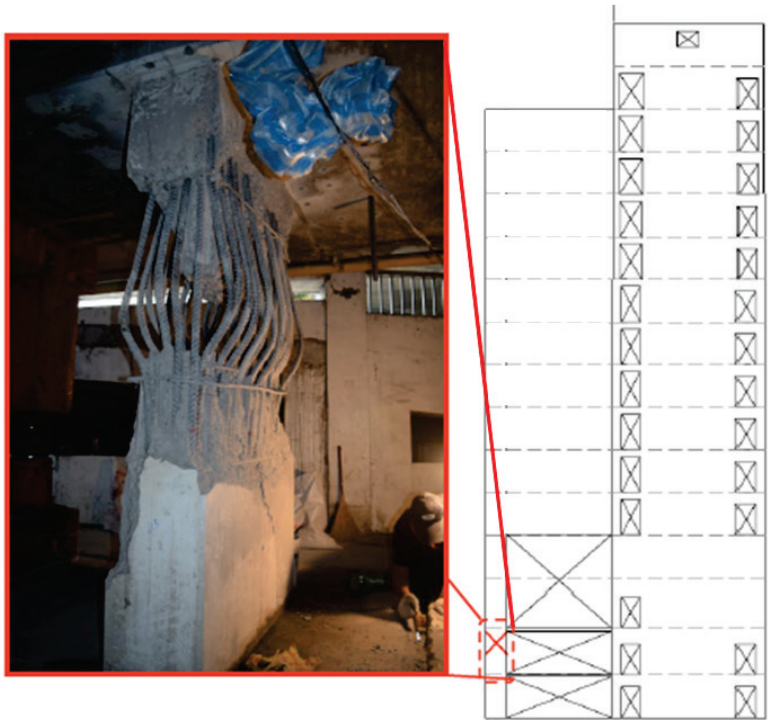

Figure B-5 Damage to "column" at wall discontinuity in a 20-story high-rise building (2016 Meinong earthquake; image from Pujol et al., 2017).

- Wall longitudinal bars that terminated into a lower region without sufficient vertical and horizontal reinforcement resulted in damage between the two terminated bar regions.
- The location of wall reinforcement splices affected the location and concentration of damage.
- Lateral load can be transferred through severe vertical discontinuities in a wall. However, this requires adequate detailing around the discontinuity in the individual wall and adequate detailing and strength in the components (beams or slab) that contribute to the load transfer.
- Several damaged buildings had relatively thin walls (6-in. thickness). It is expected that performance of a building with well-detailed, thick, but fewer walls would be superior to that of a building with many poorly-detailed thin walls. However, minor damage was observed in a wall constructed of relatively poorly-detailed 6-in. thick walls.
- Damage consistent with wall coupling, such as crushing of wall concrete due to high compressive loads and cracking and crushing of concrete in coupling beams and slabs, was observed; however, the extent of the impact from coupling requires further evaluation.
- Buildings that were essentially undamaged typically had a thick, well-reinforced mat foundation and a continuous core.

B.1.2 Quantification of Vertical Discontinuities in Concrete Walls Using Field Data

Vertical discontinuity is used to describe a significant change in the cross-sectional area or reinforcement layout of a wall from one story to the next. Typically, a reduction in cross-sectional or reinforcement area from an upper story to a lower story is more critical than a reduction from a lower to an upper story. A study conducted by Birely (2012) sought to quantify discontinuities for inclusion in evaluation methods, such as the Tier 1 Procedure of ASCE/SEI 31, *Seismic Evaluation of Existing Buildings* (ASCE, 2003).

The ASCE 31 Tier 1 checklists consider vertical discontinuities in buildings by considering the load path, verifying that all lateral load resisting elements are continuous to the foundation, and by considering the relative stiffness and strength of a floor relative to the floor above and below it. However, damage to mid-rise RC wall buildings in the 2010 Maule earthquake suggests that local changes in the stiffness and strength of individual building components may be highly correlated with damage. In Birely (2012), a discontinuity was considered to be any location where the cross-section of a wall at any given floor (referred to as the upper wall) differed from the cross-section of the wall at the floor below (referred to as the lower wall). In the four buildings studied, discontinuities typically fell into one of the following categories:

- Termination of a wall from the upper floor to the lower floor;
- Openings present in the lower section of the wall (Figure B-6a);
- Shift in the centroid of the cross-section, including a relocation of a wall flange(s) (Figure B-6b); or
- Flag-shaped wall, where the upper wall is larger than the lower wall (Figure B-6c).

When assessing the damage levels for the discontinuities, the difference between the damage in the lower and upper floors was considered. Thus, for the wall in Figure B-6c, the damage level is equal to 4 (i.e., 4 (lower floor) – 0 (upper floor) = 0) and for the wall in Figure B-6a, the damage level is equal to 3 (i.e., 4 (lower floor) – 1 (upper floor) = 3). For walls where there is no change in the level of damage at the discontinuity or where the damage level is higher in the upper wall, such as the wall in Figure B-6b, the damage level is defined as zero (0).

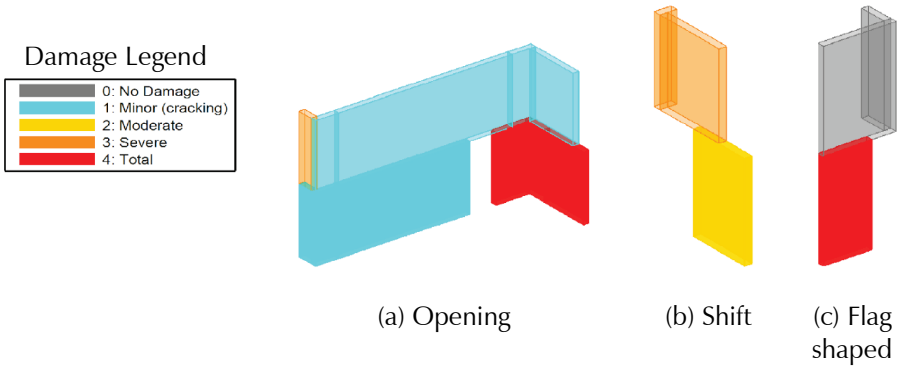

Figure B-6 Discontinuities observed in walls in Chilean buildings and corresponding damage.

The following measures were used to quantify the discontinuities observed in the walls:

- The change in wall area, normalized by the area of upper wall and reported as a percentage.
- The change in the maximum east-west and north-south dimensions of the wall, normalized by the dimension of the upper wall in that direction and reported as a percentage. This is calculated by the dimensions of the rectangle in which the wall is inscribed.
- The change in the centerline length of the wall normalized by that of the upper wall and reported as a percentage. The centerline length, L_{cl}, of the wall is the total length of wall as measured along the centerline of the cross-section. Distinction is also made in the total length of wall in the x- and y-directions.
- The change in the in-plane coordinates of the geometric centroid of the wall, normalized by the length of the wall in the same direction and reported as a percentage. This number is always reported as a negative number to facilitate comparison with the measures defined above.

The complexity of the discontinuities ranged from simple, isolated flag-shaped walls (for which damage was easily attributed to the reduced wall length and area) to walls with multiple adjacent discontinuities (for which damage was not easily attributed to any individual discontinuity). On the basis of these data, it was recommended that in concrete shear walls that are continuous to the foundation, local discontinuities caused by changes in cross-sectional geometry from one story to the story below shall not exceed: (1) a reduction in centerline length greater than 30% (in either orthogonal direction); or (2) a change in the centroid location greater than 30% of the wall length measured in the direction of the change.

B.1.3 Laboratory Test Results for Concrete Walls with Vertical Irregularities

A number of laboratory test programs have studied the earthquake performance of slender, flexure-controlled walls with vertical discontinuities resulting from the introduction of openings. Test programs reviewed for this study are listed and briefly described below. The studies have mixed results, with some studies suggesting that openings have minimal impact on wall performance (e.g., Yanez et al., 1992; Taylor, 1995; Shiu et al., 1981; Noda et al., 1997; Kato et al., 1999; Wu, 2005) and others indicating that openings can reduce drift capacity (Ali and Wight, 1991; Wu, 2005) or improve drift capacity (Wu, 2005). These mixed results are likely due to the wide variation in the design procedures and detailing employed in the different studies. In most cases, the results of these experimental studies support those of the simulation-based studies presented in Section B.2, in that well-detailed walls with openings placed near the middle of the wall exhibit deformation capacities similar to, or slightly larger than, those exhibited by solid walls, while walls with openings placed close to the perimeter of the wall exhibit reduced deformation capacity as the openings increase compressive demands at the perimeter of the wall.

Experimental investigations of the impact of openings on wall performance that were reviewed are briefly summarized below:

- *RC Structural Walls with Staggered Openings* (Ali and Wight, 1991). Ali and Wight tested four barbell concrete walls. The first specimen was solid and served as the reference. The other three specimens had staggered openings placed within the web region of the wall, with each of the three specimens having openings placed progressively further from the boundary element and closer to the center of the wall. The staggered openings had minimal impact on wall response up to a drift of approximately 1%, beyond which the openings resulted in premature compression-shear failure of the web region of the wall, as the solid wall exhibited a drift capacity of 3%.
- *Seismic Behavior of Walls with Irregular Openings* (Yanez et al., 1992). Yanez et al. tested six walls with different opening sizes and arrangements, including staggered openings and stacked openings centered on the centerline of the wall. On the basis of the experimental data, Yanez et al. concluded that performance was not affected by the size and arrangement of openings, with all wall specimens exhibiting a drift capacity of 2.5% to 3.0%.

- *Design of Slender Reinforced Concrete Walls with Openings* (Taylor, 1995). Taylor tested two walls, each with a single opening placed at the base of the wall within the unconfined and lightly reinforced web region of wall. The specimens represent a planar wall (Thomsen and Wallace, 1995) and a barbell wall (Ali and Wight, 1991) tested as part of other studies, with a single opening placed at the base of the solid reference walls used in the other studies. Experimental data show the opening having minimal impact on performance for the planar wall and, similar to the results obtained by Ali and Wight, resulting in significant reduction in deformation capacity for the barbell wall.
- *Earthquake Resistant Structural Walls: Test of Walls with and without Openings* (Shiu et al., 1981). Shiu et al. tested a solid wall and a wall with stacked openings centered on the centerline of the wall. Walls exhibited similar deformation capacity, but different failure modes.
- *Tests of Reinforced Concrete Cantilever Walls with Openings* (Noda et al., 1997) and *Strength and Deformation Capacity of Cantilever Structural Walls with Openi*ngs (Kato et al., 1999). Six two-story walls with different opening sizes, reinforcement ratios, and configurations (stacked at the centerline of the wall or stacked at the perimeter of the wall) were tested to investigate the impact of openings on wall performance. The research team concluded that: (1) walls with openings can behave in a ductile manner and fail in flexure similar to solid walls provided sufficient reinforcement is added to both sides of the opening; and (2) diagonal reinforcement around the openings had a major influence in increasing the shear strength of these walls.
- *Design of Reinforced Concrete Walls with Openings for Strength and Ductility* (Wu, 2005). Wu tested six I-shaped walls including a solid wall, three walls with openings located in one half of the wall, and two walls with openings centered on the centerline of the wall. Wall openings varied in length. In the best cases, walls with openings centered on the centerline of the wall exhibited substantially greater drift capacity than the solid wall. A wall with an opening located very close to the wall flange exhibited reduced deformation capacity in comparison with the solid wall.
- *Seismic Behavior of Reinforced Concrete Shear Walls with Regular and Staggered Openings after the Strong Earthquakes between 2009 and 2011* (Marius, 2013). Marius tested five walls—one solid wall, three walls with staggered openings, and one coupled wall—to investigate the potential for staggered wall openings to improve wall performance. The research team concluded that: (1) walls with staggered openings are

stiffer than coupled walls; (2) walls with staggered openings that result in a small and a large pier at the wall base exhibit compression-shear failure of the small pier; (3) coupled walls with inadequately detailed coupling beams exhibit wall failure due to coupling beam failure; and (4) walls with staggered openings exhibit diagonal shear cracking between openings.

B.2 Investigation of Vertical Irregularity Using Nonlinear Continuum Analysis

Nonlinear continuum-type analysis using ATENA software was conducted to investigate the impact on wall performance of the horizontal location of an opening introduced in the bottom story of a mid-rise wall. The study used modeling recommendation per Whitman (2015) for simulating the response of reinforced concrete walls using ATENA. Whitman (2015) demonstrates, using an experimental data set comprising approximately twenty planar wall test specimens, that these recommendations result in accurate and precise simulation of strength, deformation capacity, and failure mode for concrete walls with varying design parameters subjected to cyclic lateral loading. In the Whitman study, as in the study conducted for this project, simulations applied constant gravity load and lateral load under monotonically increasing displacement demand.

An 8-story wall (30 ft. long, 2 ft. thick, 106 ft. tall) with uniformly distributed vertical and horizontal reinforcement was used as the reference wall configuration for this study. Four opening locations were considered: (1) no opening (reference configuration); (2) openings at the center of the wall; (3) openings on the right side of the wall; and (4) openings on the left side of the wall. In the simulation, lateral loading was applied at the top of the wall to produce monotonically increasing lateral displacement; thus, walls with openings on the left and right sides of the wall exhibited different behavior depending on whether the opening was in the tension or compression region of the wall. Figure B-7 shows the reference wall configuration with openings (7.5 ft. long by 10 ft. tall), as well as the supplemental horizontal reinforcement added above the opening to prevent damage directly above the opening.

All analyses employed a lateral load at the top of the wall to produce monotonically increasing displacement of the wall to the right such that an opening on the right side of the wall affected the compression region of the wall while an opening on the left affected the tension region. Figure B-8 shows base shear, normalized by $\sqrt{f_c'}A_g$ with f_c' = 6500 psi and A_g equal to the area of the reference wall (A_g = 60 ft.^{2}), versus drift at the point of the

applied load. Figure B-8 shows that introducing an opening in the middle of the wall has minimal impact on the stiffness, strength, and deformation capacity of the wall while introducing an opening near the edge of a wall has significant impact on wall strength and deformation capacity. Reduction in wall strength results when an opening reduces the area of reinforcing steel near the edge of the wall that is available to carry tension. Reduction in wall deformation capacity results when an opening reduces the area of concrete and reinforcing steel near the edge of the wall that is available to carry compressive load, triggering early onset of a compression failure at the edge of the wall.

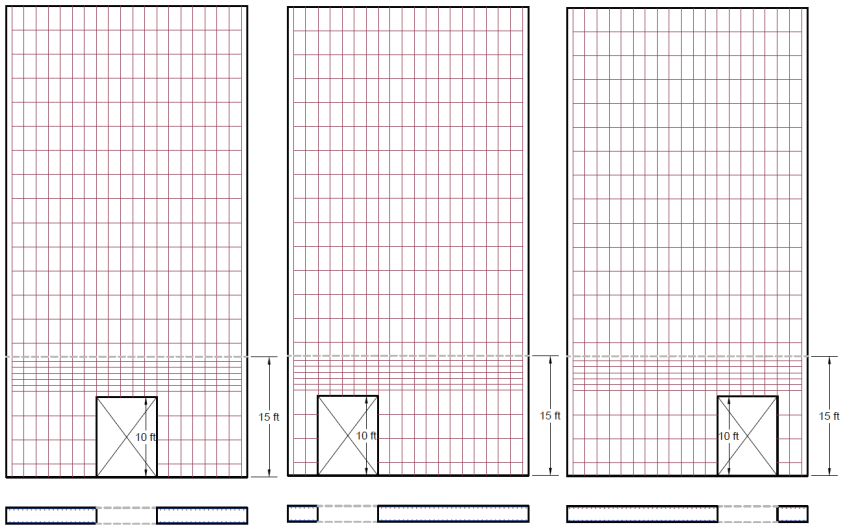

Figure B-7 Wall configurations and designs used for ATENA analyses to investigate the impact of opening location. Wall is 30 ft. long by 2 ft. thick by 106 ft. tall.

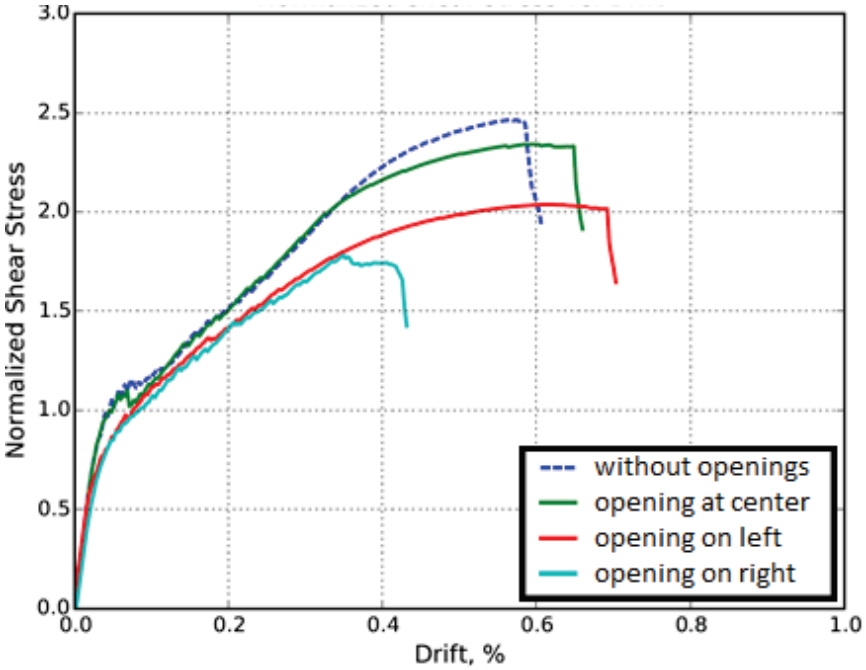

Figure B-8 Normalized base shear stress $\left(V_{base} / \left(A_g \sqrt{f'_c}\right)\right.$ with f'_c in psi$\left.\right)$ versus drift at the effective height.

B.3 RC Wall Building Design Process

A series of RC wall buildings were designed in which lateral loads are resisted by planar reinforced concrete walls. Walls were designed without openings and with openings located at the 1st, 1st and 2nd, and an upper story. Opening length was determined to achieve a stiffness for the stories with the opening that was either 75% or 50% of the stiffness of the baseline building. Story stiffness was computed as $K = V/\Delta$ with V and Δ defined as shown in Figure B-9. This approach was established early in the project and differs from the approach recommended in Appendix G. Wall demands were determined using the ELF procedure per ASCE/SEI 7-16, *Minimum Design Loads and Associated Criteria for Buildings and Other Structures* (ASCE, 2017a) and for the case of the D_{max} design spectrum, using the results of a modal response spectrum analysis (MRSA). When using MRSA, 10 modes considered for each analysis and a mass participation of more than 97% was achieved in all cases.

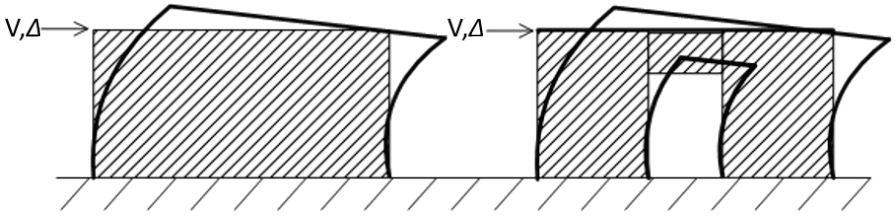

Figure B-9 Story stiffness calculation ($K = V/\Delta$).

B.3.1 Building Prototype

The walls designed represent a structural RC wall as part of an 8-story and a 12-story building. The prototypes of the buildings are shown in Figure B-10. For the 8-story building, two walls are used in each direction and for the 12-story building four walls are used in each direction to resist lateral loads. ASCE/SEI 7-16 and ACI 318-14, *Building Code Requirements for Structural Concrete* (ACI, 2014), were used to design the shear walls with the following assumptions:

- Wind loading:
  - Exposure category B
  - Wind speed for strength = 130 mph
  - Wind speed for stiffness = 100 mph
- Earthquake loading:
  - Seismic Design Categories B and D; for each category the maximum spectral acceleration was used.
  - Site Class: C - Very dense soil and soft rock
  - Risk Category: II
- Gravity loading:
  - Dead load (materials + mechanical) = 175 psf (floors)
= 140 psf (roof)
  - Live load (area load + partitions) = 50 psf + 15 psf (partitions)
= 65 psf (floors)
= 20 psf + 0 psf (partitions)
= 20 psf (roof)
- ASCE/SEI 7-16 load cases were considered:

  Load Case 4: $1.2D + 1.0W + 0.5L$

  Load Case 5: $0.9D + 1.0W$

  Load Case 6: $(1.2 + 0.2S_{DS})D + \rho Q_E + 0.5L$

  Load Case 7: $(0.9 - 0.2S_{DS})D + \rho Q_E$

  with $\rho = 1.0$ used for all designs.
- Figure B-10 shows plan view for 8- and 12-story buildings and:
  - Footprint is 120 ft. × 120 ft.
  - Center of stiffness and mass coincide (no eccentricity)

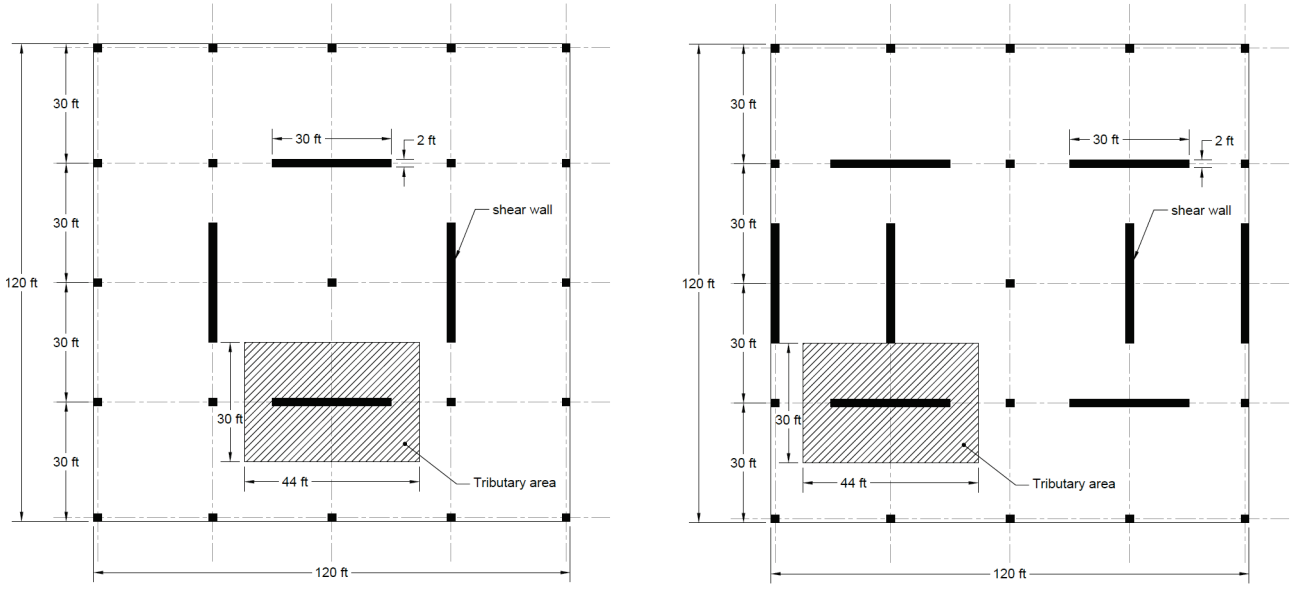

(a) 8-story building (b) 12-story building

Figure B-10 Building prototypes. Shown wall length (30 ft.) is for D_{max} designs; wall length is 20 ft. for B_{max} designs.

- For both 8-story and 12-story building designs:
  - Walls were designed for gravity load on the basis of assumed dead and live loads and the framing patterns shown in Figure B-10. The dead loads above are assumed to be distributed over the entire area.
  - Earthquake demands were increased by 5% to account for accidental torsion.
- For the 8-story building (Figure B-10a):
  - Two planar walls were located in each direction.
  - For D_{max} designs, Load Case 7 controlled strength design. Wall longitudinal and horizontal reinforcement was designed to meet moment and shear demands associated with earthquake loads. Two 30 ft. walls were required to meet flexural strength requirements for earthquake load without excessive longitudinal reinforcement ratios. Two 30 ft. walls provide adequate stiffness to meet seismic drift requirements.
  - For B_{max} designs, two 20 ft. walls were required to meet seismic drift limits. Load Case 5 (wind) controlled strength design. Minimum reinforcement ratios were adequate to meet flexure and shear demands associated with wind loading.
- 12-story building (Figure B-10b):
  - Four planar walls were located in each direction.

- For D_{max} designs, Load Case 7 controlled strength design. Wall longitudinal and horizontal reinforcement were designed to meet moment and shear demands associated with earthquake loads. Four 20 ft. walls were required to meet flexural strength requirements for earthquake load, without excessive longitudinal reinforcement ratios. Four 30 ft. walls provide adequate stiffness to meet seismic drift requirements.
- For B_{max} designs, four 20 ft. walls were required to meet wind drift limits. Load Case 5 (wind) controlled strength design. Minimum reinforcement ratios were adequate to meet flexure and shear demands associated with wind loading.

B.3.2 Wall Design

All walls were designed per ACI 318-14. The longitudinal reinforcements were designed such that the wall was tension-controlled for flexure. The design was based on the following:

- Specified concrete compressive strength, f_c' = 5000 psi
- Yield strength of steel bars, f_y = 60 ksi
- Length of the wall, l_w = 30 ft. (D_{max}) = 20 ft. (B_{max})
- Thickness of the wall, t_w = 2 ft.

For wall regions with boundary elements, the cross-section configuration shown in Figure B-11 was assumed. Per ACI 318-14, the nominal flexural strength, M_n, was defined by the compression strain in the extreme concrete fiber reaching a magnitude of -0.003 in/in. The maximum longitudinal reinforcement ratio considered for wall boundary elements, $\rho_{v.BE}$, was 3%. This limit was chosen based on the practical constraint that in splice regions the longitudinal reinforcement ratio would double to 6%, and reinforcement ratios in excess of 6% can impair concrete placement and significantly reduce constructability. For calculation of the wall nominal flexural strength, a fiber-type section model and the OpenSees software platform were used. The OpenSees Concrete01 and Steel01 material models were employed to simulate the stress strain response of concrete and steel. Concrete and steel models employed the material strengths listed above; the the impact on steel confinement on concrete response and steel hardening were not included in the analysis.

Wall sections were designed such that ϕM_n exceeded the flexural demand. Per ACI 318-14 Section 21.2.2, ϕ = 0.9 in was used, as allowed for the case of steel strain in excess of 0.005 in./in. at M_n. Spacing of longitudinal

reinforcement and reinforcement detailing were according to Section 11.7 and Chapter 25 of ACI 318-14 (ACI, 2014).

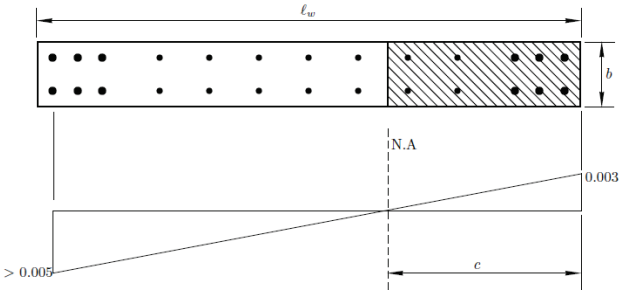

Figure B-11 Typical wall section and assumed strain distribution.

Shear design was in accordance with ACI 318-14 Sections 18.10.2 and 18.10.4. Shear demand was as defined by ASCE/SEI 7-16, with no amplification to account for dynamic response of yielding structure. In almost all web regions of the walls, shear demands were such that minimum shear reinforcement requirements of Section 18.10.2.1 controlled the design, and horizontal and vertical reinforcement ratios within the web region were 0.0025 ($\rho_l = \rho_t = 0.0025$). In the vicinity of wall openings, where shear demands increased due to the discontinuity, horizontal and vertical reinforcement ratios increased significantly. Design of these regions was in accordance with ACI 318-14 Sections 11.7 and Chapter 25.

The transverse reinforcement in the boundary elements was designed in accordance with ACI 318-14 Sections 18.10.6.4, 11.7 and Chapter 25.

B.3.3 Design of Wall Panel Zone

According to Moehle (2015), "panel zone" is the region or element of a structural wall subjected to relatively uniform shear which can be with or without normal stresses. The forces from adjacent wall segments are resolved and as a result the nominal shear stress in the panel zone may be bigger than the ones in the adjacent wall segments. Moehle uses a useful solution by assuming no weights for the walls and equal dimensions (l_w) as shown in Figure B-12. After assuming $T_2 = C_2$, and from horizontal equilibrium of the chord along **ab**, $T_2 = C_2 = v_1 l_h b_w/2$. And from horizontal equilibrium of chords along **ef** and **ij**, $T_2 = C_2 = v_2 l_w b_w$. Both quantities should be equal and after rearranging it is found that:

$$v_2 = \frac{l_h}{2l_w} v_1$$

This relation indicates how different and bigger v_1 is relative to v_2. To find that, the vertical equilibrium of forces were taken in the vertical chords and that required:

$$T_1 = (v_1 + v_2)h_s b_w = \left(1 + \frac{l_h}{2l_w}\right) v_1 h_s b_w$$

Hence the shear stress in the panel zone can be found:

$$v_1 = \frac{1}{1 + \frac{l_h}{2l_w}} \left(\frac{T_1}{h_s b_w}\right)$$

The shear reinforcement above and below the punches, which resembles a panel zone, is designed both in accordance with ACI 318-14 and using the method suggested by Moehle (2015). In almost all the cases, Moehle's method controls the design of shear reinforcement for the region above the punch. However, the depth of the panel zone, h_s, is extended whenever it would not meet the requirements of Section 18.10.4 of ACI 318-14 for shear strength. Consequently, the amount of reinforcement in the chord is calculated by considering the moment induced by the couple from the two boundary elements on each side of the opening (tension and compression). In other words, the two horizontal chords above the opening, have the same or larger moment capacity as the ones from the boundary reinforcements on each side of the punch.

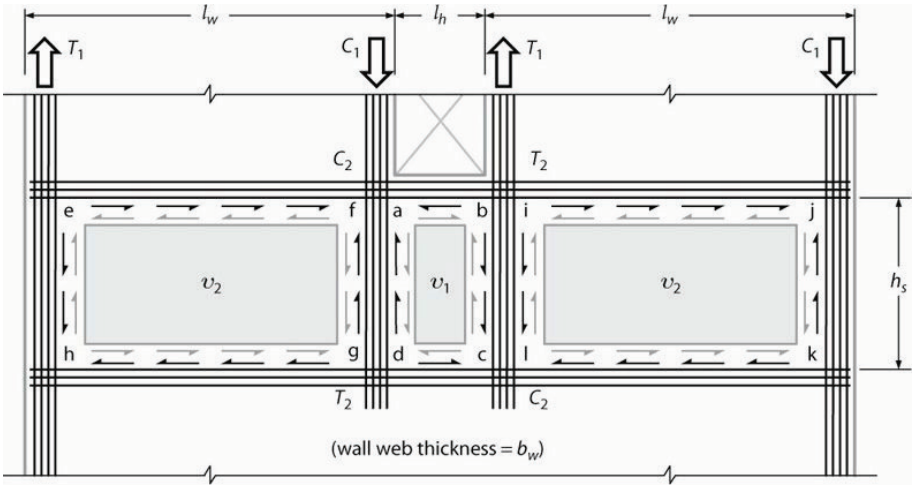

Figure B-12 Forces in the panel zone (Moehle, 2015).

B.3.4 Design of Coupling Beams

The coupling beams were designed according to Section 18.7 of ACI 318-14. Shear forces in the coupling beams were found using "Section Cut" in SAP2000. For each coupling beam, two groups of diagonally placed bars

were used symmetric about the midspan. ACI 318-14 requires transverse reinforcement to be provided for either diagonal bars or for the entire beam cross section according to Section 18.7.5.2 of ACI 318-14. Transverse reinforcement was provided in the entire beam cross section.

B.3.5 RC Wall Building Design Summaries

Table B-1 Summary of Parameters Used in the Design and Analysis (8-Story Building – D_{max})

8-story, Special Concrete Wall (8-D-0-0-ELF)	
Design Parameters	
Dead Load:	Typical = 175 psf; Roof = 140 psf
Live Load:	Typical = 65 psf; Roof = 20 psf
Seismic Weight:	Typical = 190 psf; Roof = 147.5 psf
Total building seismic weight:	W = 21276 kips
Wind Speed:	110 mph (strength); 85 mph (service)
Risk Category:	II
Importance Factor:	I_e = 1.0
Special Concrete Walls:	R = 6; C_d = 5
Site Class C Seismic Design Category D:	S_{DS} = 1.5; S_{D1} = 0.6
Material properties:	$f'_{c,beam}$ = 5 ksi; f_y = 60 ksi
Analysis	
Centerline modeling of beams and columns Rigid diaphragms	$I_{wall} = 0.5I_g$
Design based on Equivalent Lateral Force Procedure	
Calculated period: Upper limit period: Seismic response coefficient: Controlling equation: Seismic base shear (two walls):	T_x = 1.14 s C_uT_x = 0.925 s $C_{s,x}$ = 0.108 Equation 12.8-3, ASCE/SEI 7-16 V_x = 2300 kips = 0.108W (Load Case 7)
Drift limits considered:	0.020h_x (seismic); h/400(wind)
Design base shear (including accidental torsion) (two walls):	V = 2358 kips = 0.18W
Controlling lateral design criteria:	Two 30 ft. walls required to provide adequate flexural strength to meet earthquake demands. Two 30 ft. walls in each direction provide adequate strength without excessive longitudinal reinforcement ratios (boundary element longitudinal reinforcement ratio = 2.5%). Two 30 ft. walls in each direction provide adequate stiffness to meet drift limits for seismic demands (max. interstory drift = 0.55%).

Table B-2 Summary of Parameters Used in the Design and Analysis (12-story Building – D_{max})

12-story, Special Concrete Wall (12-D-0-0-ELF)	
Design Parameters	
Dead Load:	Typical = 175 psf; Roof = 140 psf
Live Load:	Typical = 65 psf; Roof = 20 psf
Seismic Weight:	Typical = 190 psf; Roof = 147.5 psf
Total building seismic weight:	W = 32220 kips
Wind Speed:	110 mph (strength); 85 mph (service)
Risk Category:	II
Importance Factor:	I_e = 1.0
Special Concrete Walls:	R = 6; C_d = 5
Site Class C Seismic Design Category D:	S_{DS} = 1.5; S_{D1} = 0.6
Material properties:	$f'_{c,beam}$ = 5 ksi; f_y = 60 ksi
Analysis	
Centerline modeling of beams and columns Rigid diaphragms	$I_{wall} = 0.5I_g$
Design based on Equivalent Lateral Force Procedure	
Calculated period: Upper limit period: Seismic response coefficient: Controlling equation: Seismic base shear (four walls):	T_x = 1.69 s C_uT_x = 1.25 s $C_{s,x}$ = 0.08 (Equation 12.8-3, ASCE/SEI 7-16) V_x = 2582 kips = 0.080W (Load Case 7)
Drift limits considered:	0.020h_x (seismic); h/400 (wind)
Design base shear (including accidental torsion) (two walls):	V = 2647 kips = 0.082W
Controlling lateral design criteria:	Four 30 ft. walls required to provide adequate flexural strength to meet earthquake demands. Four 30 ft. walls in each direction provide adequate strength without excessive longitudinal reinforcement ratios (boundary longitudinal reinforcement ratio = 2.1%). Four 30 ft. walls in each direction provide adequate stiffness to meet drift limits for seismic demands (max. interstory drift = 0.9%).

Table B-3 Summary of Parameters Used in the Design and Analysis (8-Story Building – B_{max})

8-story, Ordinary Concrete Wall (8-D-0-0)	
Design Parameters	
Dead Load:	Typical = 175 psf; Roof = 140 psf
Live Load:	Typical = 65 psf; Roof = 20 psf
Seismic Weight:	Typical = 190 psf; Roof = 147.5 psf
Total building seismic weight:	W = 21276 kips
Wind Speed:	110 mph (strength); 85 mph (service)
Risk Category:	II
Importance Factor:	I_e = 1.0
Special Concrete Walls:	R = 5; C_d = 4
Site Class C Seismic Design Category B:	S_{DS} = 0.22; S_{D1} = 0.055
Material properties:	$f'_{c,beam}$ = 5 ksi; f_y = 60 ksi
Analysis	
Centerline modeling of beams and columns Rigid diaphragms	$I_{wall} = 0.5I_g$
Design based on Equivalent Lateral Force Procedure	
Calculated period: Upper limit period: Seismic response coefficient: Controlling equation: Seismic base shear (two walls): Wind base shear (two walls): 	T_x = 2.03 s C_uT_x = 1.12 s $C_{s,x}$ = 0.01 Equation 12.8-5, ASCE/SEI 7-16 V_x = 210 kips = 0.010W (Load Case 7) V_x = 350 kips = 0.016W (Load Case 5)
Drift limits considered:	0.020h_x (seismic); h/400 (wind)
Design base shear (including accidental torsion) (two walls):	V = 350 kips = 0.016W
Controlling lateral design criteria:	Two 20 ft. walls required to provide adequate stiffness under earthquake loading. Max. story drift under earthquake loading is 1.63%. Two 20 ft. walls in each direction provide adequate flexural strength with minimum longitudinal reinforcement (ρ = 0.25%) to meet wind load demands.

Table B-4 Summary of Parameters Used in the Design and Analysis (12-Story Building – B_{max})

12-story, Ordinary Concrete Wall (12-D-0-0)	
Design Parameters	
Dead Load:	Typical = 175 psf; Roof = 140 psf
Live Load:	Typical = 65 psf; Roof = 20 psf
Seismic Weight:	Typical = 190 psf; Roof = 147.5 psf
Total building seismic weight:	W = 21276 kips
Wind Speed:	110 mph (strength); 85 mph (service)
Risk Category:	II
Importance Factor:	I_e = 1.0
Special Concrete Walls:	R = 5; C_d = 4
Site Class C Seismic Design Category B:	S_{DS} = 0.22; S_{D1} = 0.055
Material properties:	$f'_{c,beam}$ = 5 ksi; f_y = 60 ksi
Analysis	
Centerline modeling of beams and columns Rigid diaphragms	$I_{wall} = 0.5I_g$
Design based on Equivalent Lateral Force Procedure	
Calculated period: Upper limit period: Seismic response coefficient: Controlling equation: Seismic base shear (four walls): Wind base shear (four walls): 	T_x = 3.07 s C_uT_x = 1.52 s $C_{s,x}$ = 0.01 (Equation 12.8-5, ASCE/SEI 7-16) V_x = 322 kips = 0.010W (Load Case 7) V_x = 590 kips = 0.018W (Load Case 5)
Drift limits considered:	0.020h_x (seismic); h/400 (wind)
Controlling lateral design:	Seismic Strength
Design base shear (including accidental torsion) (two walls):	V = 590 kips = 0.018W
Controlling lateral design criteria:	Four 20 ft. walls required to provide adequate stiffness under earthquake loading. Max. story drift under earthquake loading is 1.35%. Four 20 ft. walls in each direction provide adequate flexural strength with minimum longitudinal reinforcement (ρ = 0.25%) to meet wind demands.

B.4 Modeling Wall Response

To investigate the impact of vertical irregularities on RC wall building collapse risk, the FEMA P695 methodology was used with nonlinear dynamic analyses using OpenSees. For all building designs, nonlinear dynamic analyses were conducted using both the displacement- and the force-based distributed-plasticity, beam-column elements with fiber-type cross-section models. For an 8-story planar and an 8-story coupled wall, collapse assessments were conducted also using the using the shear-flexure-interaction multi-vertical-line-elements model (SFI-MVLEM) (Kolozvari et al., 2015a,b; 2018). For all of these analyses the concrete and steel constitutive models available in OpenSees were employed. To validate the use of OpenSees for simulation of the nonlinear response of walls with openings, OpenSees analysis results were compared with those from nonlinear quasi-static analysis conducted using continuum-type solid element models and the ATENA software platform. ATENA and OpenSees analysis methods have been shown, using large experimental data sets, to provide accurate stimulation of stiffness, strength, and deformation capacity for *planar* walls exhibiting flexure-controlled response in the laboratory (Marafi et al., 2018; Pugh et al., 2015; Whitman, 2015). Figure B-13 shows simulated and measured normalized base shear versus drift at the point of applied lateral load for a typical flexure-controlled wall specimen. OpenSees element formulations are computationally efficient, and thus ideal for use in assessing collapse risk via the FEMA P695 procedure, which requires numerous nonlinear time-history analyses. The following sections summarize the different modeling approaches.

B.4.1 ATENA

Overview. The ATENA software was selected for continuum-type analysis of the model RC walls because: (1) the ATENA concrete constitutive model provides automatic regularization of material softening in both tension and compression using an element characteristic length, which minimizes mesh sensitivity resulting from localization of damage and enables accurate simulation of onset of strength loss; and (2) the ATENA concrete constitutive model simulates concrete dilation under compressive loading such that the impact of confining reinforcement is explicitly simulated.

Constitutive Modeling. The concrete constitutive model used: (1) continuum damage theory with fixed cracks to define concrete tensile response; and (2) plasticity theory with non-associated flow to define concrete compressive response. For tension, concrete fracture energy and a mesh-dependent length were used to define the tensile post-peak stress

versus cracking strain response. For compression, the concrete stress versus plastic strain curve is parabolic to maximum strength with linear softening to produce zero compressive strength at a user-defined plastic *deformation*; plastic *strain* at zero compressive strength is defined as the plastic deformation divided by a mesh-dependent length. Calibration of the NC2 model to simulate the response of concrete was conducted by Whitman (2015).

A relatively simple reinforcing steel model was used for the analyses. Boundary element longitudinal steel and confining steel were modeled using truss elements embedded in the concrete matrix with perfect bond. Web region vertical and horizontal steel was modeled as "smeared" across individual concrete elements with perfect bond. The stress-strain response of reinforcement was modeled using a phenomenological model in which the envelope to the stress-strain history is defined as either bilinear or multilinear based on coupon test data, and unload-reload response was modeled using Menegotto-Pinto curves to simulate the Bauschinger effect. Neither bar buckling nor bar fracture are modeled as ATENA does not support tracking of strain as required to determine onset of buckling and post-buckling fracture. Non-simulated failure criteria were established by Whitman (2015) to enable accurate prediction of onset of lateral strength loss in the event that this is controlled by bar buckling or fracture. To enhance numerical stability and robustness, a small volume (0.1%) of *elastic*, smeared horizontal and vertical reinforcement was added in the regions of the wall that were expected to sustain nonlinear deformation demands

Comparison of Simulated and Measured Response. The ATENA modeling approach was validated using 21 planar wall specimens (Whitman, 2015). Figure B-13 shows normalized base shear versus drift as simulated using the ATENA modeling approach and as measured in the laboratory for two specimens.

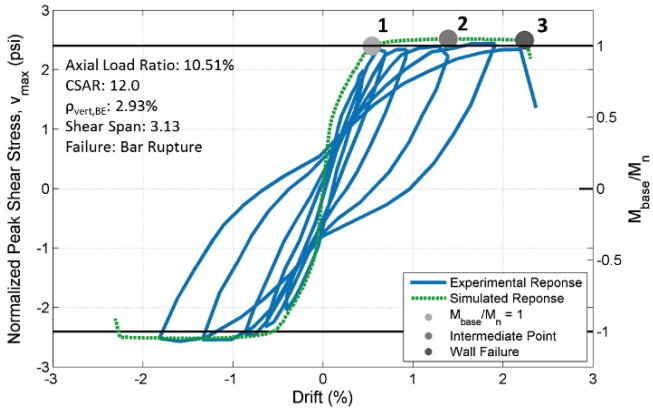

(a) Response as measured and as simulated using ATENA (Whitman, 2015)

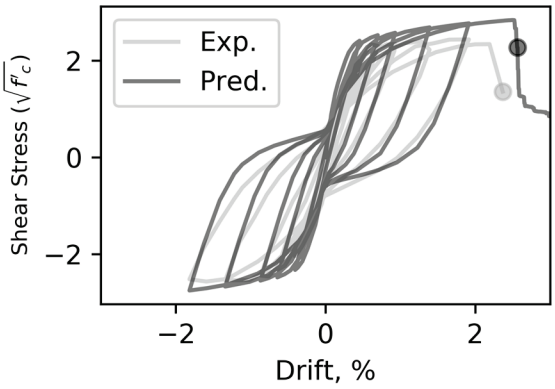

(b) Response as measured and as simulated using OpenSees displacement-based element

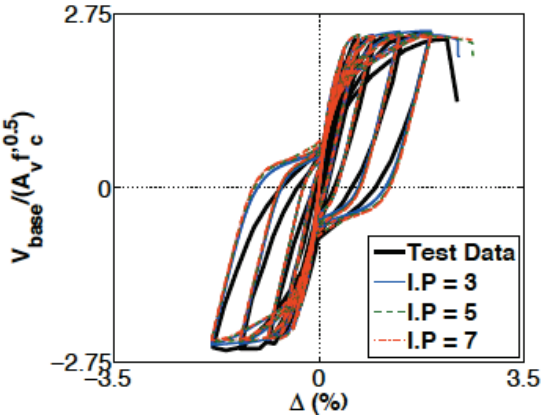

(c) Response as measured and as simulated using OpenSees force-based elements (Pugh, 2012)

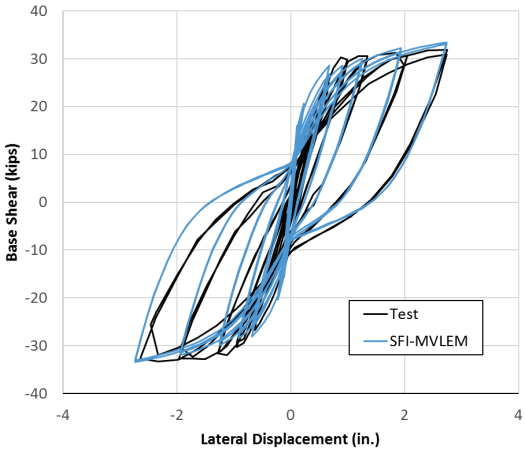

(d) Response as measured and as simulated using OpenSees SFI-MVLEM

Figure B-13 Wall response histories as measured and as simulated using OpenSees and ATENA specimen RW1 – bar fracture failure (Cross-Section Aspect Ratio [CSAR] = 12; Axial Load Ratio = 10.5, $V_{max} = 2.6\sqrt{f_c}A_g$).

B.4.2 OpenSees

Dynamic analyses of RC wall buildings to investigate collapse risk were conducted using OpenSees with walls modeled using: (1) the force-based beam-column element (FBE) with fiber-type section models and the modeling approach developed by Pugh et al. (2015); (2) the displacement-based beam-column element (DBE) with fiber-type section models and the modeling approach developed by Pugh et al. (2015) and updated by Marafi et al. (2018); and (3) the SFI-MVLEM developed by Kolozvari et al. (2015a,b; 2018). The modeling approaches developed by Pugh et al. (2015) and Marafi et al. (2018) employ regularization of material softening to achieve mesh-objective simulation of strength loss and have been verified, using a large database of planar and non-planar wall tests, to provide accurate, mesh-objective, simulation of onset of strength loss, which is required for accurate

assessment of collapse risk. For this study, concrete and steel material response models used in the SFI-MVLEM were calibrated such that the SFI-MVLEM predicted drift capacities for the wall designs that were equal to those predicted using models comprising distributed-plasticity beam-column elements.

Elements and Mesh Size. Displacement- and force-based fiber-type beam-column elements as well as the SFI-MVLEM were used to assess collapse risk. Figure B-14 and Figure B-15 show the models used to represent the walls, the RC wall buildings, and wall cross-sections.

The FBE employs the assumption of a linear moment distribution and constant axial load distribution along the length of the element, as well as the assumption that flexure and shear response are decoupled. As such, one FBE per story provides a highly accurate representation of the moment and axial load distributions that develop in a wall, in which lateral earthquake loads and axial loads may be approximated as being applied to the wall at the floor level. Using the FBE, multiple fiber-type section models are employed along the length of the element to provide accurate simulation of deformations in regions in which flexural yielding occurs. Fiber-section models employ multiple confined and unconfined concrete fibers and steel fibers to provide accurate simulation of the flexural response of sections. One FBE with five fiber sections per element is used vertically per story. Fiber sections employ 150 concrete and steel fibers to provide accurate simulation of section response. Figure B-14 and Figure B-15 show models with one FBE used per story.

The DBE employs the assumptions of a linear curvature field and a constant axial strain field. Thus, multiple elements are required, per story, to provide an accurate representation of the curvature and strain fields that develop in regions of the wall in which nonlinear flexural behavior occurs. As with the FBE, multiple fiber-type sections models are employed within each element. Six DBEs were used per story, each with five fiber section models. Figure B-14 and Figure B-15 show models of the walls and buildings with six DBEs used per story.

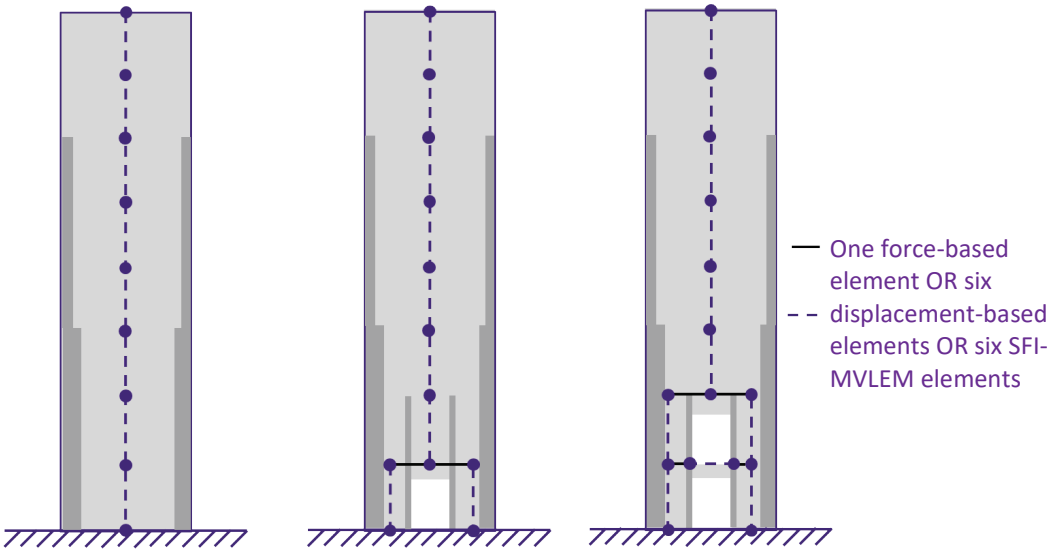

Figure B-14 OpenSees model configurations for walls with and without openings.

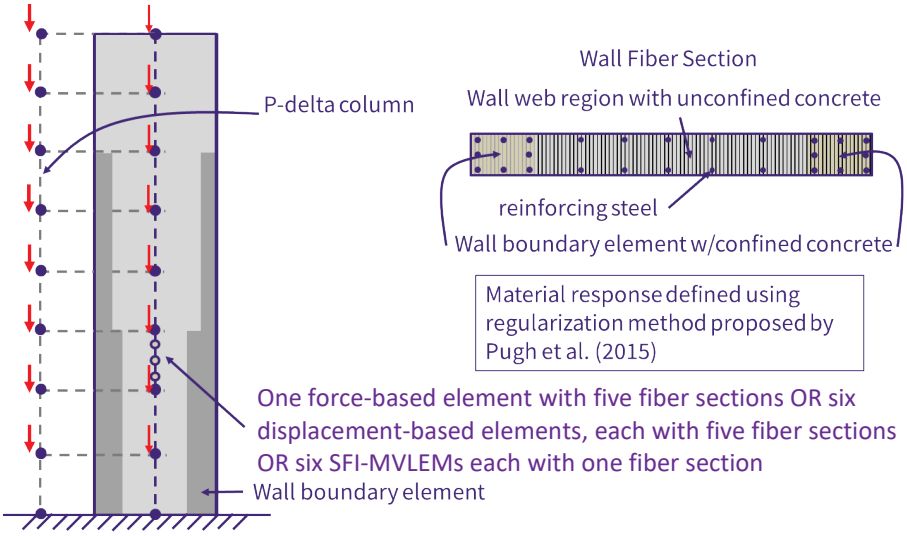

Figure B-15 OpenSees model configuration for RC wall building.

The SFI-MVLEM employs the fixed-strut angle approach (Orakcal et al., 2012) to characterize the biaxial constitutive response of the two-dimensional RC panel fibers that compose the SFI-MVLEM (Orakcal et al., 2004). Axial-shear coupling is achieved within each two-dimensional fiber through the two-dimensional RC panel constitutive model. Integration of fiber stresses to determine element response results in simulation of coupled axial-flexural-shear responses at the element level. All material models are cyclic in nature, such that the SFI-MVLEM also represents cyclic response. A constant distribution of curvature is assumed over the element height such that biaxial stresses and strains are constant within each fiber. Since element shear strength and stiffness are determined from integration of the two-dimensional fiber stresses and stiffnesses, explicit definition of shear

response is not required. For simulation of RC wall buildings, SFI-MVLEM building models employed the same number of elements as were used for the DBE models and the same number of cross-section fibers as were used for the DBE and FBE models. Figure B-14 and Figure B-15 show models of the walls and buildings with six SFI-MVLEM elements used per story.

Constitutive Models for Displacement- and Force-Based Beam-Column Element Models. Concrete response was simulated using the OpenSees Concrete02 material mode. In compression, this model represents a quadratic response to peak strength with linear deterioration to a residual compressive strength. In tension, the model represents a linear response history to tensile strength with linear strength loss to zero tensile capacity. Tensile strength for unconfined and confined concrete was defined as $4\sqrt{f_c'}$ psi. Regularization of post-peak response in tension is not required as concrete cracking does not result in section or element softening. Unconfined concrete was assumed to reach peak strength at a strain of -0.002. Confined concrete strength and strain at maximum strength were defined using the model by Saatcioglu and Razvi (1992). Per the recommendations of Pugh et al. (2015) and Marafi et al. (2018), concrete post-peak response was defined by the unconfined or confined concrete crushing energy and a mesh-dependent length; this was required to ensure that simulation of onset of strength loss was accurate and did not depend on mesh size. Concrete residual strength is defined as 20% of peak strength for confined concrete and 10% of peak strength for unconfined concrete.

For reinforcing steel, the OpenSees Steel02 model was used. Reinforcing steel is assumed to lose compressive and tensile strength, due to buckling, at the regularized strain at which concrete strength deteriorates to the residual compressive strength.

Figure B-16 shows concrete and steel material model response under cyclic loading. Figure B-17 shows regularization of concrete and steel response using unconfined, G_{fc}, and confined concrete, G_{fcc}, crushing energies and L, which is the element length associated with the fiber section in which the material model is used. For the FBE, when strength loss occurs, deformation localizes in a section and L is taken equal to the length assigned to each fiber section. For the DBE, when strength loss occurs, deformation localizes in an element and L is taken equal to the element length. The red 'X' in Figure B-17 shows the strain at which reinforcing steel loses strength due to buckling. Pugh et al. (2015) and Marafi et al. (2018) provide additional information on the material regularization method used for modeling.

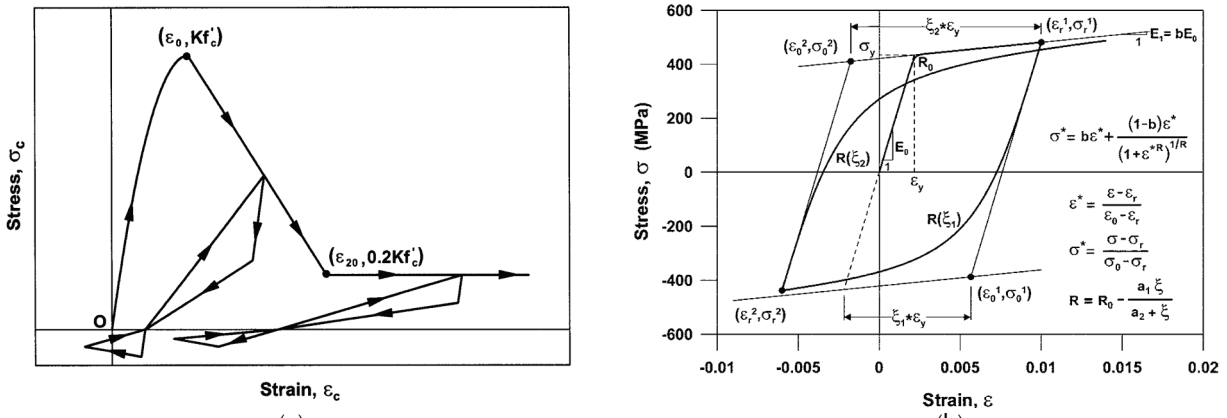

Figure B-16 Nonlinear 1D cyclic material models. (a) Yassin cyclic concrete model, which employs the monotonic Modified Kent-Park model (Yassin, 1994; Scott et al., 1982) as presented by Orakcal et al. (2006). Note that compressive stress-strain is positive. (b) Menegotto-Pinto-Filippou reinforcing steel model (Filippou et al., 1983) as presented by Orakcal et al. (2006).

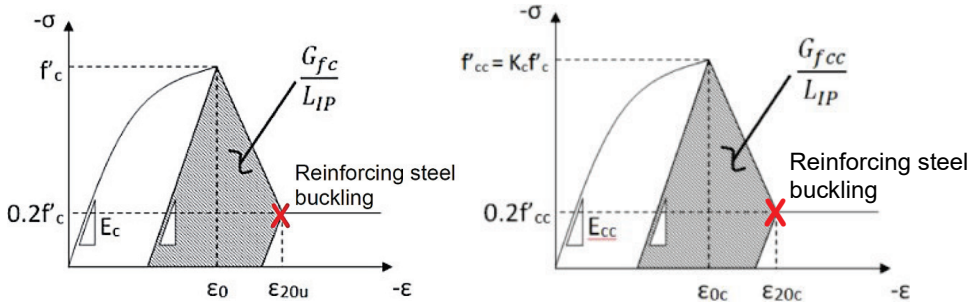

Figure B-17 Regularization of concrete material response using mesh dependent length. Note that steel buckling occurs at ε_{20u} and ε_{20c}. (Figure adapted from Pugh et al., 2015)

Constitutive Models for SFI-MVLEM. Material models for concrete and steel and all parameters necessary to define the constitutive models used in the SFI-MVLEM were identical to the one used in the DBE, to ensure consistent comparison between the modeling approaches.

B.5 Preliminary Analyses to Investigate Modeling Assumptions and Identify a Preferred Modeling Approach

OpenSees and ATENA analyses were conducted to investigate modeling assumptions and assess the performance of the 8-story RC wall buildings designed for the D_{max} spectrum using the ASCE/SEI 7-16 ELF procedure. These analyses comprised pushover analyses using both software platforms as well as dynamic analyses using the OpenSees models.

Significant observations and conclusions of the analyses are described in the following sections.

B.5.1 Modeling Assumptions Employed for OpenSees and ATENA Analyses

Analyses conducted to investigate wall performance and the impact of various modeling assumptions employed the modeling procedures described in this Appendix and in Chapter 3.

All nonlinear analyses employed expected material properties. Expected material strengths were defined following the recommendations of the *Guidelines for Performance-Based Seismic Design of Tall Buildings* (PEER, 2010). Following these recommendations, unconfined concrete compressive strength was increased by 30% from 5000 psi to 6500 psi and reinforcing steel yield strength was increased by 17% from 60 ksi to 72 ksi. Longitudinal reinforcing steel was assumed to reach an ultimate strength of 105 ksi at a fracture strain of 0.20.

Gravity load was applied for all pushover and dynamic analyses. Following the recommendations of FEMA P695, gravity load was defined by:

$$1.05D + 0.25L$$

where D is the nominal dead load of the structure and L is the nominal live load, defined as follows:

- Dead load (materials and mechanical) on all floors = 175 psf
- Dead load (materials and mechanical) on roof = 140 psf
- Live load (area load plus partitions) on all floors = 50 + 15 psf = 65 psf
- Live load (area load plus partitions) on roof = 20 + 0 psf = 20 psf

The wall tributary area was used to determine the gravity load applied to the wall.

For dynamic OpenSees analyses the total gravity load that could be expected to destabilize the wall was included in the analysis via use of a *P*-Delta column (Figure B-15). The total building gravity load attributed to the wall (half the total gravity load applied to the building), less the gravity load applied directly to the wall, was applied to a "*P*-Delta" column adjacent to the wall. The *P*-Delta column was assigned a flexural stiffness approximately equal to the sum of the flexural stiffnesses of all of the gravity columns attributed to the wall (half the total number of gravity columns) and an axial stiffness that was similarly defined. The *P*-Delta column was linked to the wall via essentially rigid, axial-only elements. Initially the *P*-Delta

column was included in pushover analyses; however, essentially no difference was observed between results with and without the *P*-Delta column. Thus, the *P*-Delta column was subsequently included only in dynamic analyses.

Where monotonic pushover analyses were conducted in OpenSees, the ASCE/SEI 7-16 ELF lateral load distribution was applied under generalized displacement control. For ATENA analyses, lateral load was applied as a single point load at the effective height associated with the ELF load distribution.

B.5.2 Pushover Analyses to Compare OpenSees and ATENA Models

ATENA and all three OpenSees modeling approaches described in Section 5.4 were used to perform pushover analyses of the 8-story RC wall buildings designed by the D_{max} spectrum using the ELF procedure (walls with no openings, openings at the 1st story, openings at the 1st and 2nd stories, and openings at the 5th story). Pushover analyses were performed using the modeling procedure described in Section 5.4 and the model configurations shown in Figure B-14 and Figure B-15. Lateral load was applied as a point load (series of point loads for the ATENA model) under displacement control at the effective height of the ELF lateral load distribution. Simulated base shear versus drift at the effective height is presented in Figure B-18.

The data in Figure B-18 support the following observations:

- OpenSees models predict approximately the same strength and stiffness for all of the wall configurations.
- The OpenSees SFI-MVLEM model predicts different drift capacity and/or post-peak response than is predicted using the OpenSees DBE and FBE models.
- The ATENA model predicts approximately the same pre-peak response as is predicted using the OpenSees models; though it predicts greater strength for three of five wall configurations and greater stiffness for two of five wall configurations.
- OpenSees DBE and FBE models predict approximately the same response.
- OpenSees DBE/FBE models, OpenSees SFI-MVLEM and ATENA models all predict different drift capacities and post-peak stiffnesses.

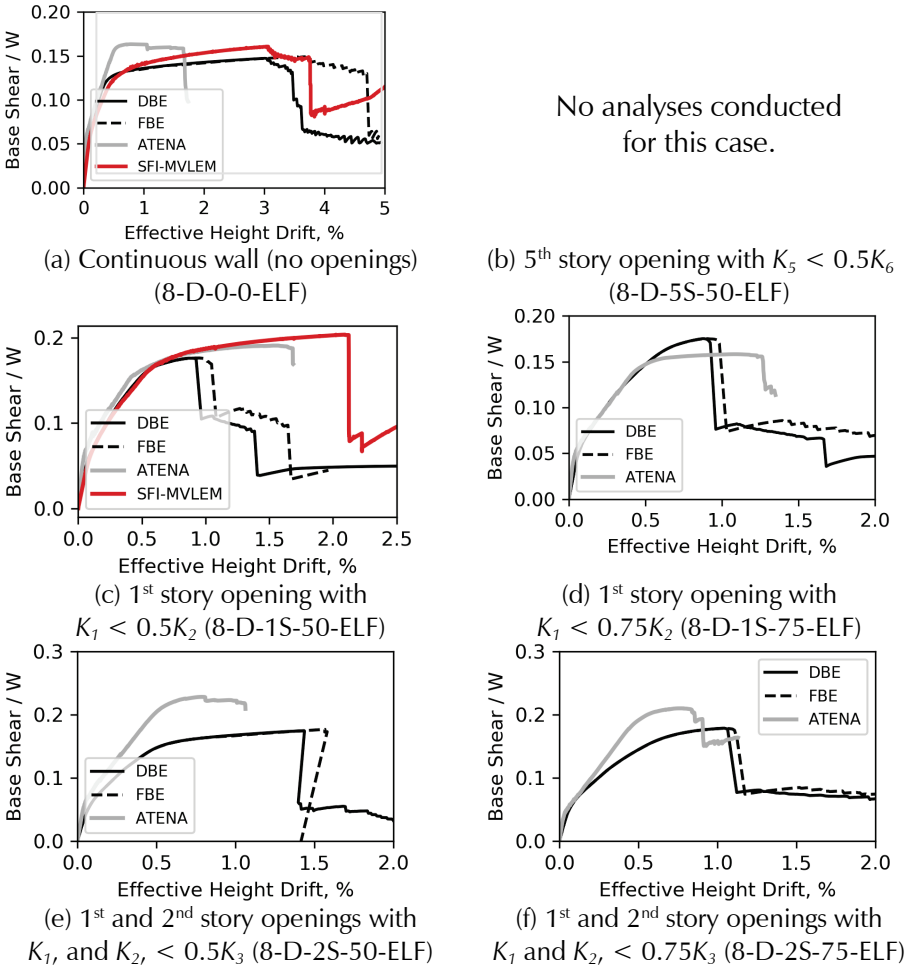

Figure B-18 Base shear versus drift at effective height for 8-story walls as simulated using ATENA (grey), OpenSees DBE (black), and SFI-MVLEM (red) models. Note that lateral load is applied as a point load at the effective height of the ELF load distribution. K_i indicates stiffness of story i defined per Section B.3.

Differences in simulated strength and stiffness are attributed to difference in the way that shear-flexure interaction is simulated, with the DBE/FBE elements simulating no flexure-shear interaction, the SFI-MVLEM simulating constrained flexure-shear interaction (shear strain constrained to be constant over the cross-section), and the ATENA model providing simulation of unconstrained flexure-shear interaction.

Ultimately the differences between the individual OpenSees models and between the OpenSees and ATENA models suggest the potential for: (1) the OpenSees line-element models to provide inaccurate simulation of response for walls with irregular configurations for which response is not entirely flexure-controlled; and (2) the potential the deformation capacities predicted

using DBE, FBE, and SFI-MVLEM models to result in significant differences in assessment of collapse risk.

B.5.3 Dynamic Analyses to Compare OpenSees Displacement-Based and Force-Based Beam-Column Element Models

Incremental dynamic analyses of the 8-story RC wall buildings were conducted to investigate the difference in collapse risk resulting from use of OpenSees DBE versus FBE to simulate wall response. Figure B-19 shows incremental dynamic analysis results for the 8-story archetype without openings (8-0-0-ELF) modeled using the DBEs (Figure B-19a) and using the FBEs (Figure B-19b). Figure B-19 shows spectra acceleration at the fundamental period of the structure, S_a, versus maximum interstory drift for the suite of far-field motions provided for use with the FEMA P695 procedure. Red dots in the figures indicate the "last converged analysis" achieved prior to an increase in the ground motion amplitude resulting in a "non-converged" solution; black dots indicate a non-simulated collapse at a maximum interstory drift of 5%. The black line indicates median spectral acceleration, S_{CT} is the spectral acceleration for which 50% of the records result in building collapse, and S_{MT} is the spectral acceration at the design period of the structure for the MCE. Figure B-20 shows similar data for the 8-story archetype with an opening at the 1st-story resulting in a 50% reduction in stiffness for that story.

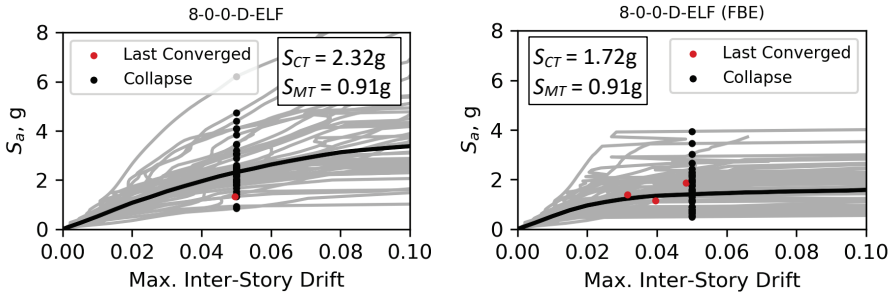

(a) DBE model (b) FBE model

Figure B-19 Earthquake spectral acceleration at the design period of the structure, S_a, versus maximum interstory drift for the 8-story continuous wall building designed for D_{max} spectrum using the ASCE/SEI 7-16 ELF procedure.

The data in Figure B-19 and Figure B-20 show that when the FBE is used, there are many more analyses that "fail to converge" at intensity levels less than that resulting in collapse, defined by a maximum interstory drift of 5%. These failures to converge result from either instability of the global structural system, suggesting a true building collapse due to development of a side-sway mechanism, or, for the models comprising FBEs, a failure of the FBE intra-element solution algorithm, which may or may not be indicative of

a true building collapse. These failures to converge at lower intensity levels result in a lower S_{CT} value and calculation of a higher collapse risk for the models comprising FBE. Thus, the model comprising FBEs is considered to over-predict the true collapse risk, and models comprising DBEs are preferred to those comprising FBEs.

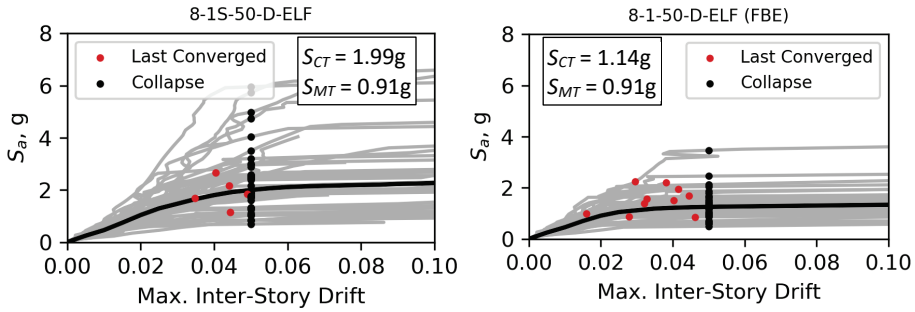

(a) DBE model (b) FBE model

Figure B-20 Earthquake intensity at design period, S_a, versus maximum interstory drift for 8-story RC wall building with opening at 1st story resulting in 50% stiffness loss and designed for D_{max} spectrum using the ASCE/SEI 7-16 ELF procedure.

B.5.4 Dynamic Analyses to Compare Models Comprising OpenSees Displacement-Based Beam-Column Elements and SFI-MVLEM

Incremental dynamic analyses of the 8-story RC wall buildings were also conducted to investigate the difference in collapse risk resulting from use of a model comprising DBEs, which assume a linear shear model and decoupling of flexure and shear action, versus the SFI-MVLEs, which assume flexure and shear response are coupled and thus result in simulation of a nonlinear shear response. Figure B-21 shows dynamic analysis results for a single ground motion for the 8-story RC wall building archetype without openings (8-0-0-ELF) for models comprising DBEs and SFI-MVLEMs. The same ground motion was used for both models which resulted in collapse (maximum interstory drift in excess of 5%) for the building model comprising SFI-MVLEMs. The data in Figure B-21 enable comparison of the DBE and SFI-MVLEM models on the basis of simulated: (1) roof displacement history (Figure B-21a); (2) base shear history (Figure B-21b); (3) the vertical interstory drift profile of the RC wall building at the timestep corresponding to the maximum interstory drift for each model (Figure B-21c); and (4) shear forces and moments (Figure B-21d,e). In addition, local (first story) wall hysteretic responses are compared to assess the behavior of the models within the plastic hinge region including (Figure B-21f): (1) shear force versus total displacement; (2) shear force versus shear displacement; and (3) moment versus rotation.

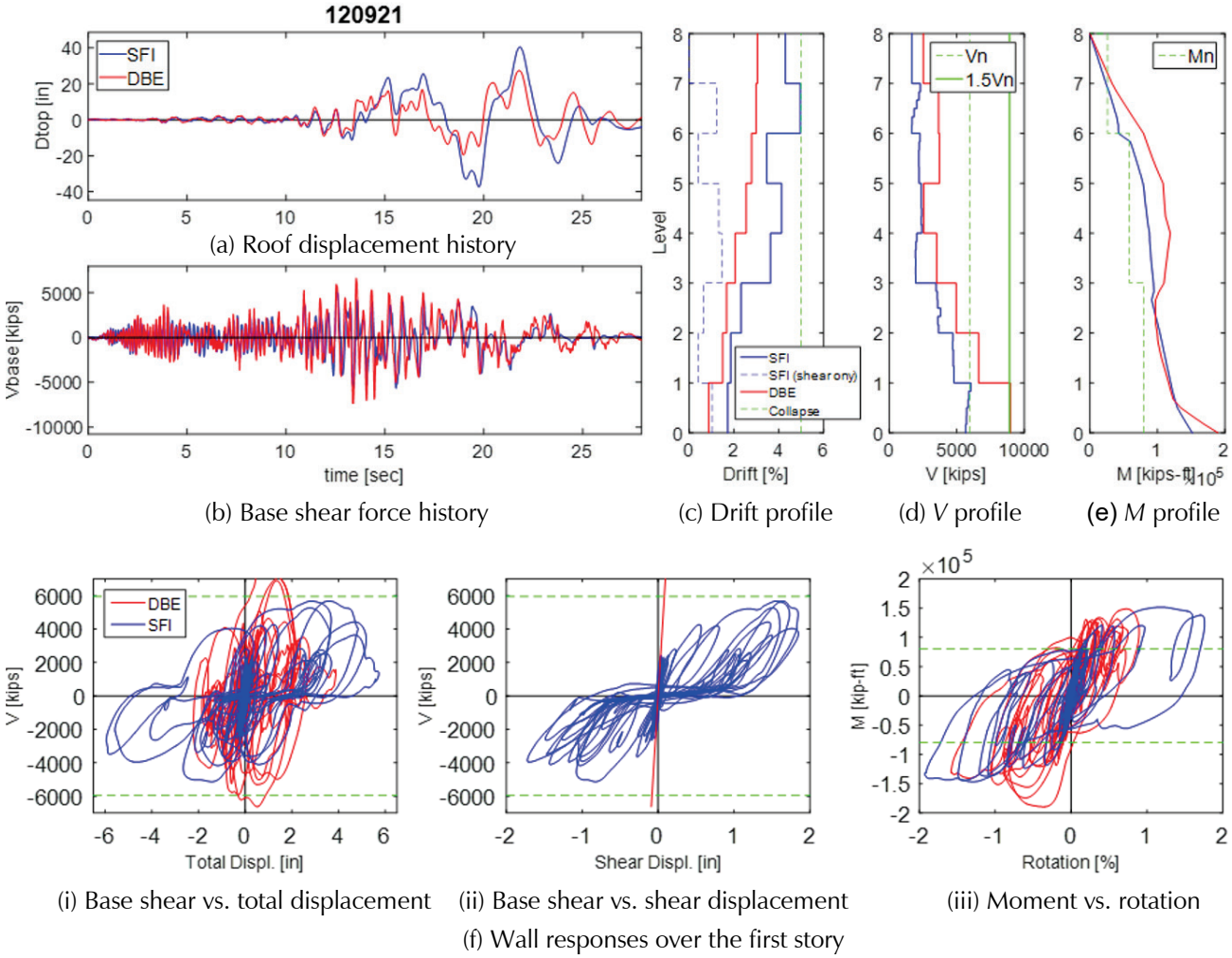

Figure B-21 Simulated response quantities for models comprising SFI-MVLEM and displacement-based beam-column element responses for collapse-level of shaking.

Results presented in Figure B-21 show that the model comprising SFI-MVLEM predicts substantially larger roof drifts and interstory drifts than does the model comprising DBEs (Figure B-21a,c), while the DBE model predicts substantially larger shear forces than does the SFI-MVLEM model the history of base shear (Figure B-21b,d). Differences in the maximum base moments predicted using the two models are substantially less, with the DBE model predicting a maximum base moment that is approximately 25% larger than that predicted using the SFI-MVLEM (Figure B-21e). Vertical profiles of predicted interstory drifts (Figure B-21c) and story shear (Figure B-21d) show that maximum base shear and interstory drift predicted using the two models differ by as much as 50%. The data in Figure B-21c show that a significant portion (20-60%) of the interstory drift over the wall height is associated with nonlinear shear deformations (dashed blue line in Figure B-21c) that are not captured using the DBE.

The data in Figure B-21f show force-displacement response, as predicted using the two models, in the bottom story of the wall where inelastic deformation is greatest. These data clearly highlight the differences between the two models. In particular, the data show the highly nonlinear shear response that is predicted using the SFI-MVLEM. This nonlinear shear response results from nonlinear flexural yielding and coupling of the shear and flexural response through the multi-dimensional concrete model. The nonlinear shear response predicted using the SFI-MVLEM differs substantially from the linear shear response predicted using the DBE model. These data also show that the DBE model predicts a larger moment capacity and smaller flexural deformations than are predicted using the SFI-MVLEM. The difference in predicted moment capacity likely results from differences in axial load distributions that result from the different model formulations; larger flexural deformations in the SFI-MVLEM model are likely due to the flexure-shear interaction with shear demand resulting in increased inelastic deformation that produces larger flexural, as well as large, shear deformations.

Figure B-22 compares data from incremental dynamic analysis (IDA) of the 8-story RC wall building without openings (8-0-0-ELF) for a selected ground motion as obtained using the SFI-MVLEM and DBE models. These data show that for all ground motion intensity levels beyond those that are associated with essentially elastic wall response, the SFI-MVLEM model predicts maximum interstory drifts that are larger than those predicted using the DBE model. The difference in predicted maximum interstory drift increases with increasing ground motion intensity. The larger drifts predicted by the SFI-MVLEM are attributed to the nonlinear shear response and are consistent with the data shown in Figure B-22.

Figure B-23 provides the IDA data for the 8-story RC wall building archetype without openings (8-0-0-ELF) for the FEMA P695 far-field ground motion suite as obtained using the SFI-MVLEM and DBE wall models. With collapse defined by a maximum interstory drift greater than 5%, the Collapse Margin Ratio (*CMR*) predicted using the SFI-MVLEM (CMR_{SFI} = 2.36) is less than that predicted using the DBE model (CMR_{DBE} = 2.75), due to the larger deformations and interstory drifts predicted using the SFI-MVLEM.

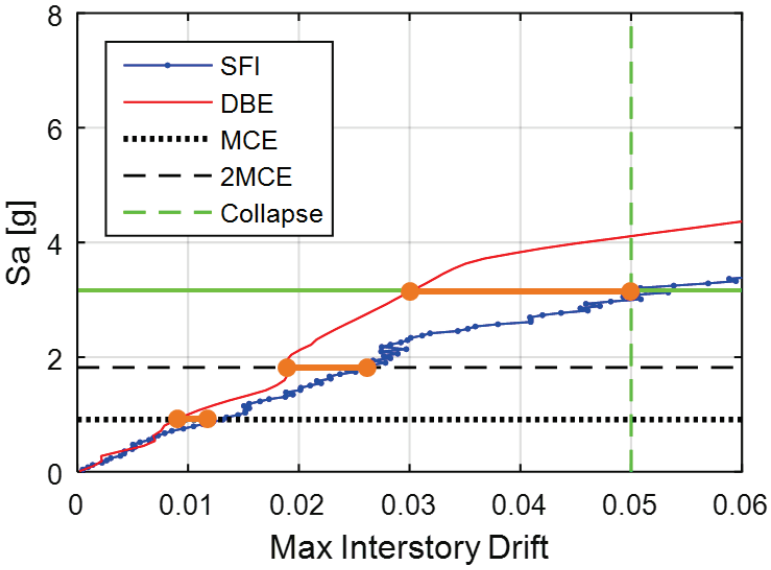

Figure B-22 Comparison of SFI-MVLEM and displacement-based beam column element IDA results for selected ground motion.

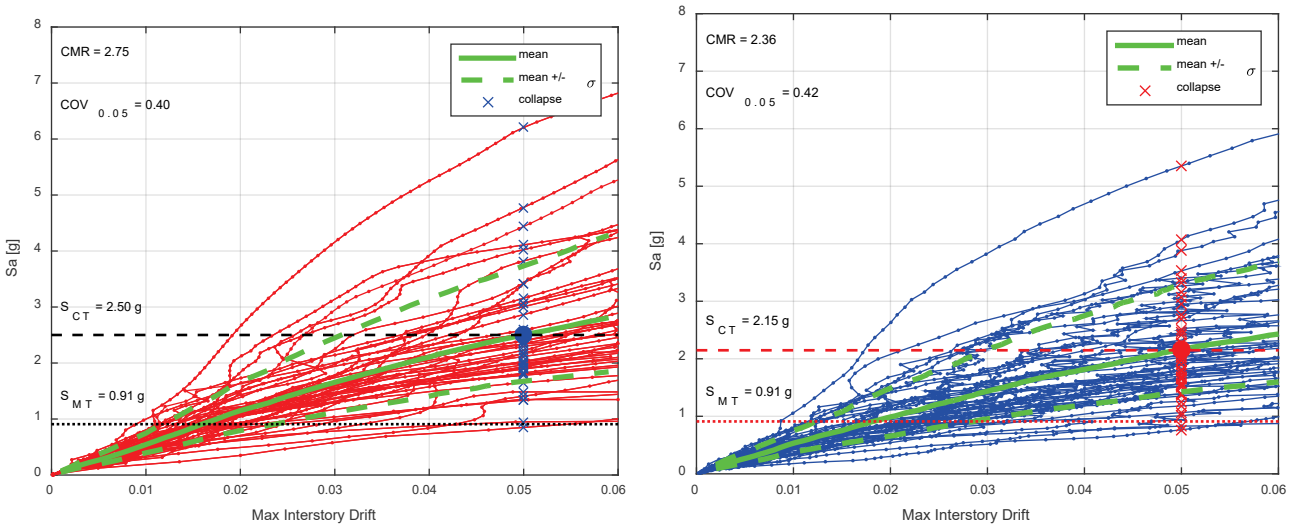

(a) DBE (8-0-0-DBE-ELF) (b) SFI-MVLEM (8-0-0-SFI-ELF)

Figure B-23 Comparison of SFI-MVLEM and displacement-based IDA analysis results for 8-story RC wall building without openings (8-0-0-ELF).

Figure B-24 provides IDA data for the 8-story RC wall building with an opening in the first story that reduces story stiffness to 50% of the adjacent story stiffness. These IDA data were created using the FEMA P695 far-field ground motion suite as obtained using the SFI-MVLEM and DBE wall models. Due to presence of the opening, the *CMR* is slightly reduced (3-4% reduction) for both models.

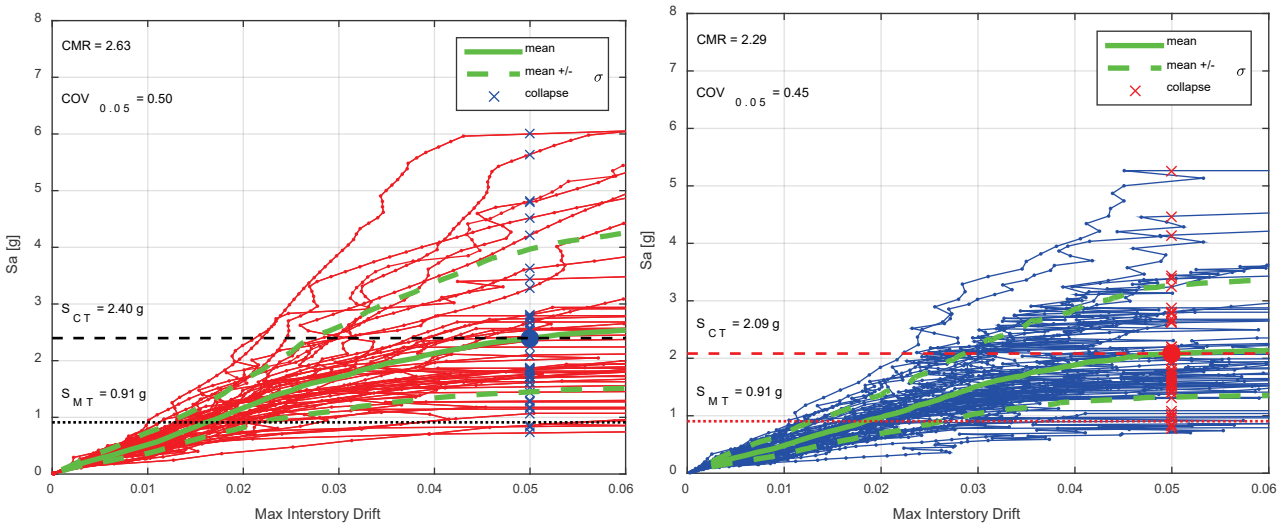

(a) DBE (8-1S-50-DBE-ELF) (b) SFI-MVLEM (8-1S-50-SFI-ELF)

Figure B-24 Comparison of SFI-MVLEM and displacement-based IDA analysis results for 8-story archetype with opening at the first floor (8-1S-50-ELF).

Comparison of the SFI-MVLEM and DBE model results for simulation of the nonlinear response of concrete RC wall buildings subjected to monotonically increasing as well as dynamic lateral loading shows:

- SFI-MVLEM predicts larger interstory drifts and smaller base shear demands than does the DBE model;
- Use of the SFI-MVLEM results in prediction of larger collapse risk and smaller *CMR*s than are predicted using the DBE; and
- Both models predict approximately the same, small change in collapse risk associated with introduction of an opening in the 1st story of a RC wall building.

B.5.5 Identification of a Preferred Modeling Approach for Assessing the Impact of Vertical Irregularities on the Collapse Risk Posed by RC Wall Buildings

The data in Section B.5.2 through Section B.5.4 show significant differences in drift capacity, and to a lesser extent stiffness and strength of a RC wall buildings, predicted using the OpenSees and ATENA models discussed above. These differences could be expected to affect the assessment of collapse risk for RC wall buildings and, in particular, the impact of vertical irregularities resulting from the introduction of openings on this risk. The OpenSees DBE modeling approach was selected for the use in the study because:

- The ATENA model, which likely provides the most accurate simulation of response, cannot be used for dynamic analyses.

- The OpenSees FBE modeling approach exhibits failures of the numerical solution algorithm that result inaccurate, reduced calculation of collapse risk.
- The OpenSees SFI-MVLEM has not be extensively validated for use in simulating response beyond onset of strength loss.
- The OpenSees DBE modeling approach has been extensively validated for simulation of onset of strength loss, provides plausible simulation of response following onset of strength loss (minimal experimental data exist for validation), and provides the greatest numerical robustness and the greatest numerical efficiency.

B.6 Analysis Results

Results of analyses conducted to assess collapse risk of the archetype RC wall building designs are presented in Tables B-5 and B-6 and Figures B-25 through B-34; for these analyses, collapse is defined by a maximum interstory drift greater than 10%, except for Figures B-29 and B-31 where it is defined by a maximum interstory drift greater that 5%. Figures B-35 through B-37 present the ratios of the *ACMR*s for buildings comprising walls with openings to those comprising walls without openings ($ACMR/ACMR_{baseline}$) and thereby provide understanding of the impact on collapse risk of introducing the openings. The data in these figures show the following:

- Collapse probabilities for all of the RC wall building designs, including those comprising walls with and without openings that significantly reduced story stiffness, are low (less than 2%).
- Collapse probabilities are very low (less than 0.11%) and *ACMR*s very large (greater than 5.0) for the baseline RC wall building designs that comprise walls without openings.

For RC wall buildings designed for Seismic Design Category B, for which wall strength was determined by wind loads, collapse probabilities for the baseline RC wall building comprising walls without openings were extremely small (less than 0.02%) and *ACMR*s extremely large (greater than 6.5). For these designs, the introduction of openings that reduced story stiffness by more than 25% had minimal impact on the *ACMR* (less than 10% change). For these designs, the introduction of openings in the bottom two stories that reduced story stiffness by more than 50%, resulted in significant changes in the *ACMR* (greater than 30% for the 12-story building). However, resulting collapse probabilities remained extremely low (0.11% or less); thus, the data were not considered to warrant additional study or code revisions.

Table B-5 Collapse Probabilities for RC Wall Building Archetypes Designed for the D_{max} Spectrum for the Case of Collapse at Maximum Story Drifts in Excess of 10%

Archetype	$\hat{S}_{CT}$	S_{MT}	*CMR*	μ_T	*SSF*	*ACMR*	*ACMR* / $ACMR_{baseline}$	*SSF* (μ=8)	*ACMR* (μ=8)	Collapse Prob. (μ=8)	*ACMR* / $ACMR_{baseline}$ (μ=8)
8-story walled buildings designed for D_{max} spectrum using ELF											
8-0-0-D-ELF	3.29	0.91	3.60	12.40	1.45	5.20	-	1.40	5.20	0.08	-
8-1S-50-D-ELF	2.18	0.91	2.40	2.70	1.22	2.90	0.56	1.40	3.50	0.88	0.67
8-1S-75-D-ELF	2.09	0.91	2.30	2.50	1.21	2.80	0.54	1.40	3.30	1.10	0.63
8-2S-50-D-ELF	2.08	0.91	2.30	5.90	1.37	3.10	0.60	1.40	3.30	1.13	0.63
8-2S-75-D-ELF	2.08	0.91	2.30	4.60	1.32	3.00	0.58	1.40	3.30	1.14	0.63
8-5S-50-D-ELF	3.06	0.91	3.40	10.00	1.45	4.90	0.94	1.40	4.90	0.13	0.94
8-story walled buildings designed for D_{max} spectrum using MRSA											
8-0-0-D-MRSA	3.15	0.91	3.50	15.80	1.45	5.00	-	1.40	5.00	0.11	-
8-1S-50-D-MRSA	2.19	0.91	2.40	5.60	1.36	3.30	0.66	1.40	3.50	0.87	0.70
8-1S-75-D-MRSA	2.11	0.91	2.30	5.40	1.35	3.10	0.62	1.40	3.40	1.04	0.68
8-2S-50-D-MRSA	2.05	0.91	2.30	7.10	1.41	3.20	0.64	1.40	3.30	1.22	0.66
8-2S-75-D-MRSA	2.07	0.91	2.30	6.60	1.39	3.20	0.64	1.40	3.30	1.16	0.66
8-5S-50-D-ELF	-	-	-	-	-	-	-	-	-	-	-
12-story walled buildings designed for D_{max} spectrum using ELF											
12-0-0-D-ELF	2.69	0.67	4.00	8.70	1.53	6.10	-	1.50	6.10	0.03	-
12-1S-50-D-ELF	1.88	0.67	2.80	3.30	1.30	3.60	0.85	1.50	4.30	0.28	0.70
12-1S-75-D-ELF	1.92	0.67	2.90	3.20	1.30	3.70	0.85	1.50	4.40	0.24	0.72
12-2S-50-D-ELF	1.85	0.67	2.80	2.40	1.25	3.40	0.82	1.50	4.20	0.30	0.69
12-2S-75-D-ELF	1.89	0.67	2.80	2.30	1.23	3.50	0.80	1.50	4.30	0.27	0.70
12-5S-50-D-ELF	-	-	-	-	-	-	-	-	-	-	-
12-story walled buildings designed for D_{max} spectrum using MRSA											
12-0-0-D-MRSA	2.44	0.67	3.60	20.40	1.53	5.60	-	1.50	5.60	0.05	-
12-1S-50-D-MRSA	1.56	0.67	2.30	7.30	1.50	3.50	0.98	1.50	3.60	0.78	0.64
12-1S-75-D-MRSA	1.68	0.67	2.50	7.20	1.50	3.70	0.98	1.50	3.80	0.53	0.68
12-2S-50-D-MRSA	1.31	0.67	1.90	3.60	1.33	2.60	0.87	1.50	3.00	1.83	0.54
12-2S-75-D-MRSA	1.48	0.67	2.20	3.60	1.33	2.90	0.87	1.50	3.40	1.01	0.61
12-5S-50-D-MRSA	-	-	-	-	-	-	-	-	-	-	-

Table B-6 **Collapse Probabilities for RC Wall Building Archetypes Designed for the B_{max} Spectrum for the Case of Collapse at Maximum Story Drifts in Excess of 10%**

Archetype	$\hat{S}_{CT}$	S_{MT}	*CMR*	μ_T	*SSF*	*ACMR*	*ACMR* / $ACMR_{baseline}$	*SSF* (μ=8)	*ACMR* (μ =8)	Collapse Prob. (%) (μ =8))	*ACMR* / $ACMR_{baseline}$ (μ =8)
8-story RC wall buildings designed for B_{max} spectrum using ELF											
8-0-0-B-ELF	0.97	0.22	4.5	16.4	1.45	6.5	-	1.4	6.5	0.02	-
8-1S-50-B-ELF	0.91	0.22	4.2	11.6	1.45	6.1	0.94	1.4	6.1	0.03	0.94
8-1S-75-B-ELF	0.92	0.22	4.3	12.4	1.45	6.2	0.95	1.4	6.2	0.03	0.95
8-2S-50-B-ELF	0.81	0.22	3.8	11.2	1.45	5.4	0.83	1.4	5.4	0.06	0.83
8-2S-75-B-ELF	0.89	0.22	4.1	8.8	1.45	5.9	0.91	1.4	5.9	0.04	0.91
8-5S-50-B-ELF	-	-	-	-	-	-	-	-	-	-	-
12-story RC wall buildings designed for B_{max} spectrum using ELF											
12-0-0-B-ELF	0.79	0.16	4.9	7.7	1.52	7.5	-	1.5	7.5	0.01	-
12-1S-50-B-ELF	0.78	0.16	4.8	6.7	1.48	7.2	0.96	1.5	7.4	0.01	0.99
12-1S-75-B-ELF	0.79	0.16	4.9	6.5	1.47	7.3	0.97	1.5	7.6	0.01	1.01
12-2S-50-B-ELF	0.52	0.16	3.3	5.6	1.43	4.7	0.63	1.5	5.0	0.11	0.67
12-2S-75-B-ELF	0.75	0.16	4.7	4.9	1.40	6.5	0.87	1.5	7.1	0.01	0.95
12-5S-50-B-ELF	-	-	-	-	-	-	-	-	-	-	-

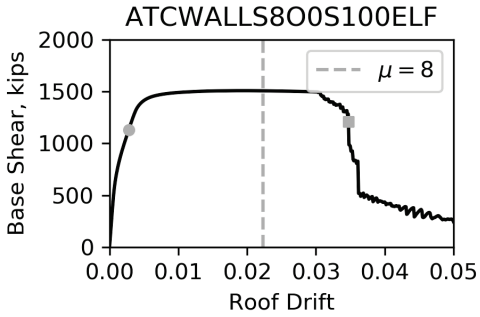

(a) Continuous wall (8-D-0-0-ELF)

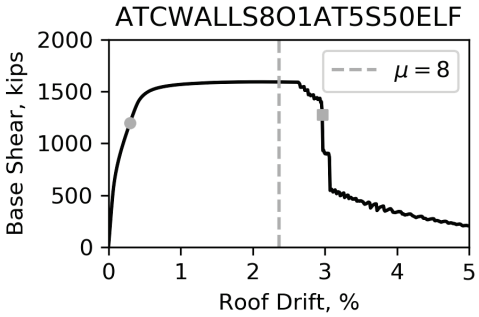

(b) 5th story opening with $K_5 < 0.5K_6$ (8-D-5S-50-ELF)

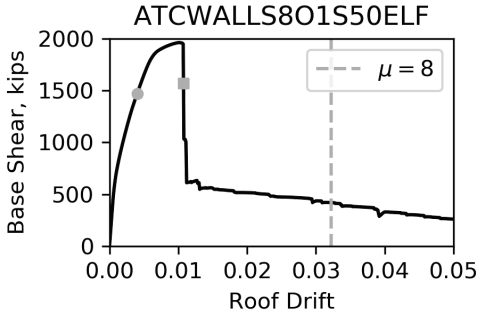

(c) 1st story opening with $K_1 < 0.5K_2$ (8-D-1S-50-ELF)

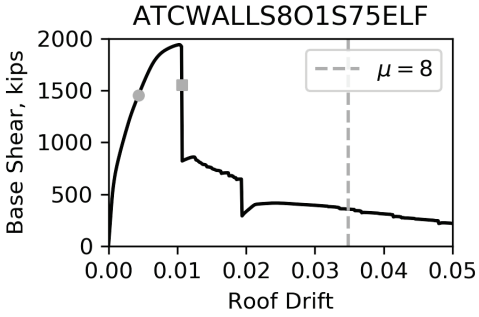

(d) 1st story opening, with $K_1 < 0.75K_2$ (8-D-1S-75-ELF)

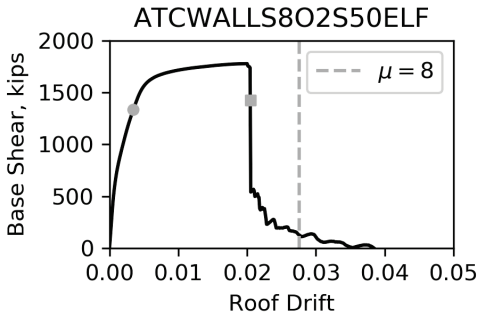

(e) 1st and 2nd story openings with K_1 and $K_2 < 0.5K_3$ (8-D-2S-50-ELF)

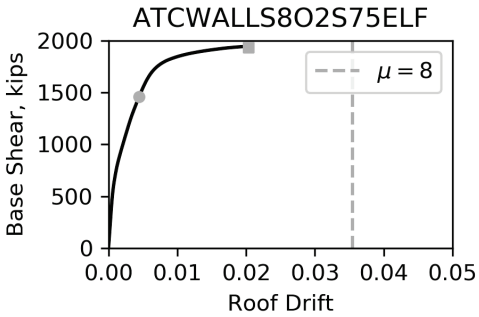

(f) 1st and 2nd story openings with K_1 and $K_2 < 0.75K_3$ (8-D-2S-75-ELF)

Figure B-25 Base shear versus roof drift for 8-story walls designed for D_{max} spectrum using the ASCE/SEI7-16 ELF procedure. Grey marker indicates yield drift (circle) and drift at 20% strength loss (square); dashed grey line indicates ductility of 8. K_i indicates stiffness of story i defined per Section B.3.

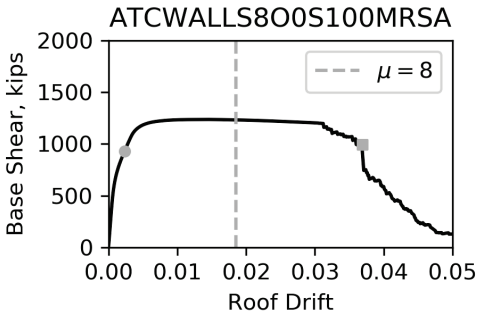

(a) Continuous wall (8-D-0-0- MRSA)

No analysis conducted for this case.

(b) 5th story opening with $K_5 < 0.5K_6$

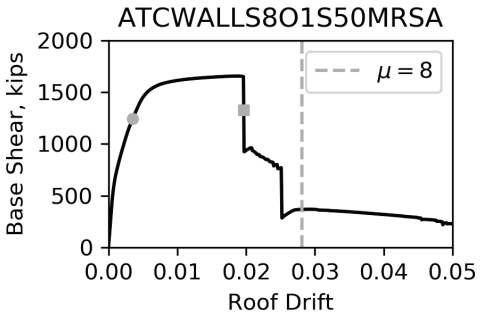

(c) 1st story opening with $K_1 < 0.5K_2$ (8-D-1S-50-MRSA)

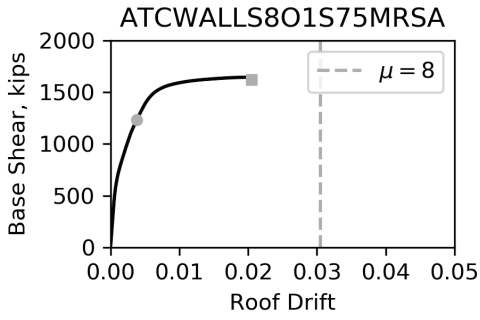

(d) 1st story opening, with $K_1 < 0.75K_2$ (8-D-1S-75-MRSA)

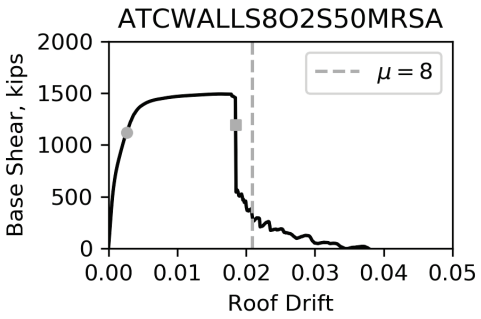

(e) 1st and 2nd story openings with K_1 and $K_2 < 0.5K_3$ (8-D-2S-50-MRSA)

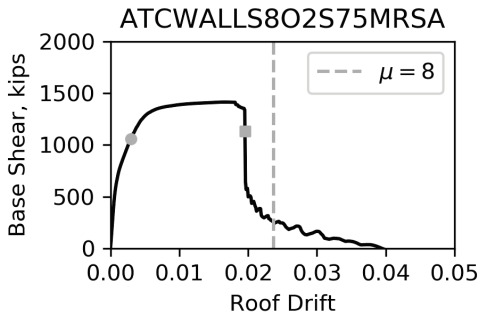

(f) 1st and 2nd story openings with K_1 and $K_2 < 0.75K_3$ (8-D-2S-75-MRSA)

Figure B-26 Base shear versus roof drift for 8-story walls designed for D_{max} spectrum using the ASCE/SEI 7-16 MRSA procedure. Grey marker indicates yield drift (circle) and drift at 20% strength loss (square); dashed grey line indicates ductility of 8. K_i indicates stiffness of story i defined per Section B.3.

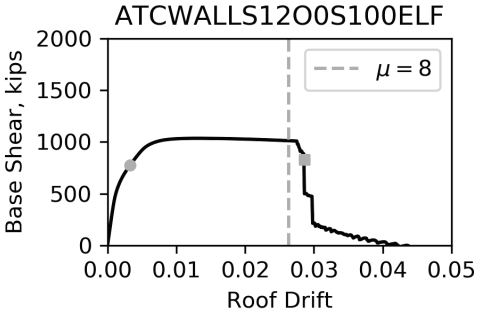

(a) Continuous wall (12-D-0-0-ELF)

No analysis conducted for this case.

(b) 8th story opening with $K_8 < 0.5K_9$

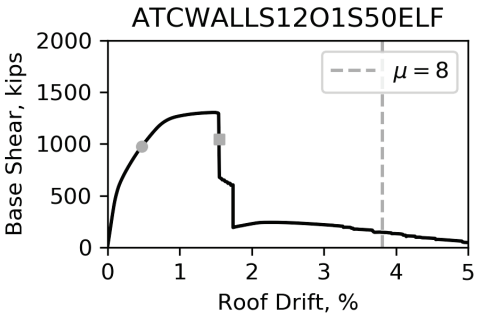

(c) 1st story opening with $K_1 < 0.5K_2$ (12-D-1S-50-ELF)

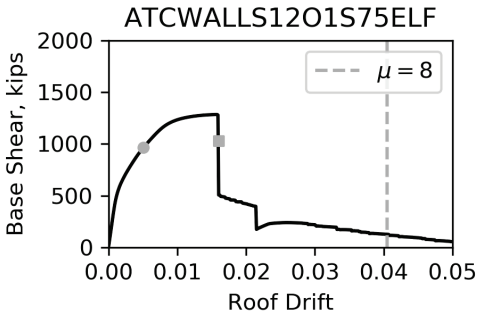

(d) 1st story opening, with $K_1 < 0.75K_2$ (12-D-1S-75-ELF)

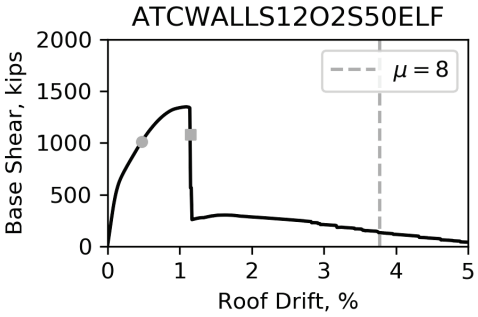

(e) 1st and 2nd story openings with K_1 and $K_2 < 0.5K_3$ (12-D-2S-50-ELF)

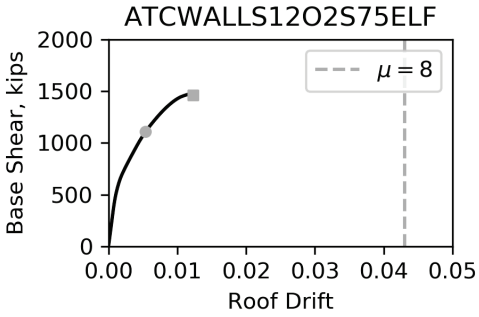

(f) 1st and 2nd story openings with K_1 and $K_2 < 0.75K_3$ (12-D-2S-75-ELF)

Figure B-27 Base shear versus roof drift for 12-story walls designed for D_{max} spectrum using the ASCE/SEI 7-16 ELF procedure. Grey marker indicates yield drift (circle) and drift at 20% strength loss (square); dashed grey line indicates ductility of 8. K_i indicates stiffness of story i defined per Section B.3.

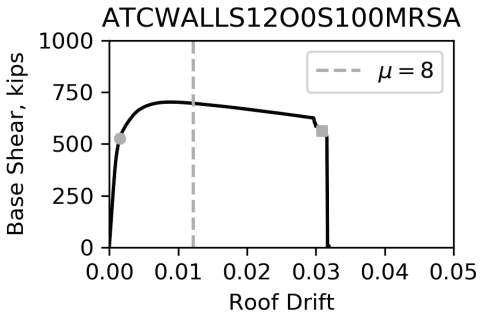

(a) Continuous wall (12-D-0-0-MRSA)

No analysis conducted for this case.

(b) 5th story opening with $K_5 < 0.5K_6$

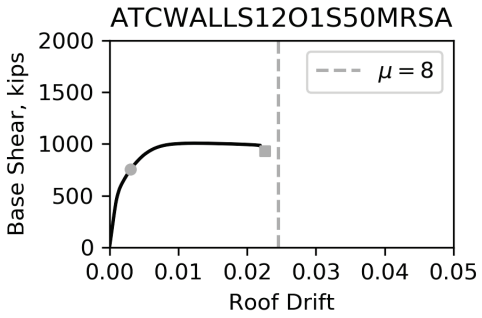

(c) 1st story opening with 50% stiffness (12-D-1S-50-MRSA)

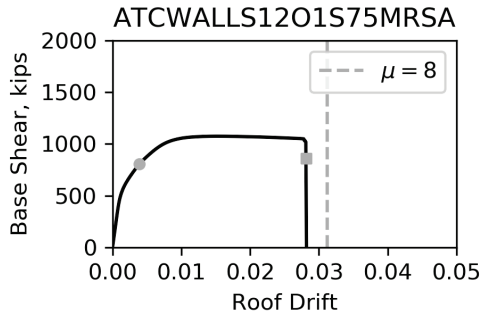

(d) 1st story opening with 75% stiffness (12-D-1S-75-MRSA)

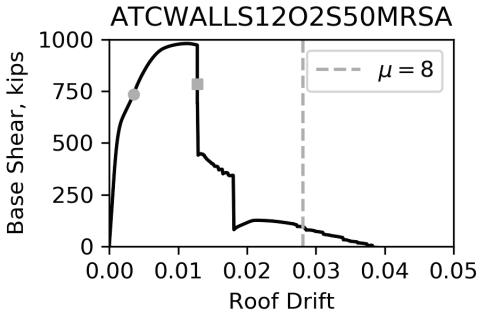

(e) 1st and 2nd story openings with 50% stiffness (12-D-2S-50-MRSA)

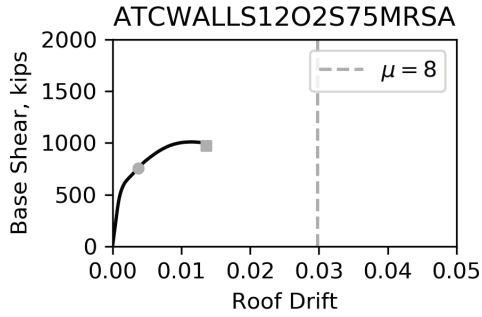

(f) 1st and 2nd story openings with 75% stiffness (12-D-2S-75-MRSA)

Figure B-28 Base shear versus roof drift for 12-story walls designed for D_{max} spectrum using the ASCE/SEI 7-16 MRSA procedure. Grey marker indicates yield drift (circle) and drift at 20% strength loss (square); dashed grey line indicates ductility of 8. K_i indicates stiffness of story i defined per Section B.3.

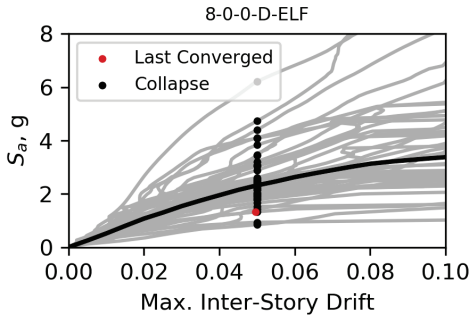

(a) Continuous wall (8-D-0-0-ELF)

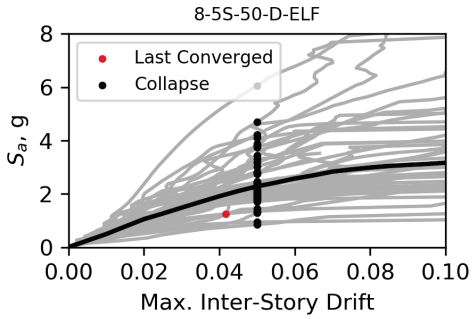

(b) 5th story opening with $K_5 < 0.5K_6$ (8-D-5S-50-ELF)

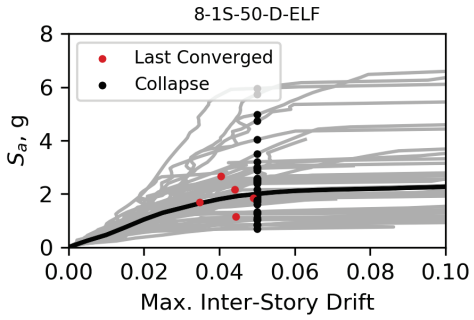

(c) 1st story opening, with $K_1 < 0.5K_2$ (8-D-1S-50-ELF)

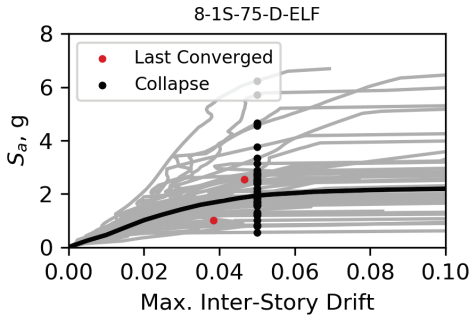

(d) 1st story opening, with $K_1 < 0.75K_2$ (8-D-1S-75-ELF)

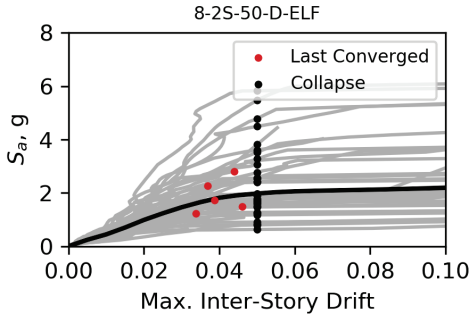

(e) 1st and 2nd story openings with K_1 and $K_2 < 0.5K_3$ (8-D-2S-50-ELF)

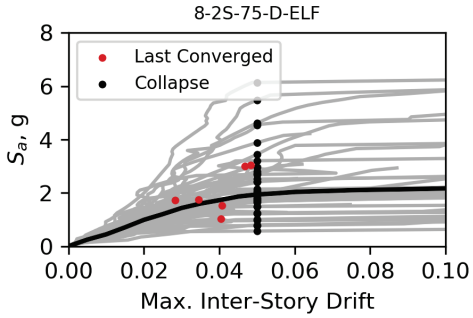

(f)) 1st and 2nd story openings with K_1 and $K_2 < 0.75K_3$ (8-D-2S-75-ELF)

Figure B-29 Earthquake intensity at design period, S_a, versus maximum inter-story drift for 8-story walls designed for D_{max} spectrum using the ASCE/SEI 7-16 ELF procedure. Black line indicates spectral acceleration at which 50% of motions result in collapse defined by maximum inter-story drift in excess of 5%. K_i indicates stiffness of story i defined per Section B.3.

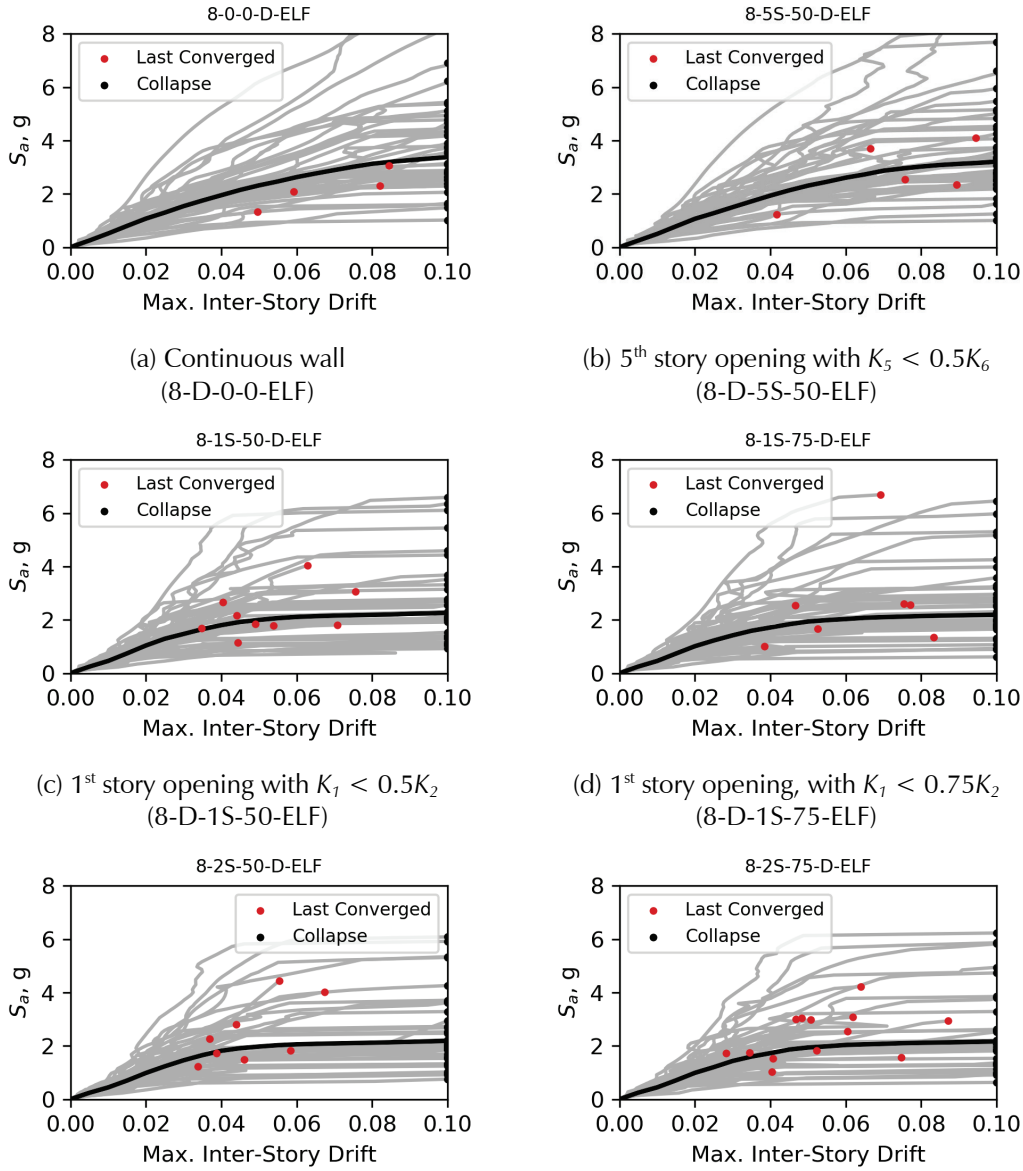

(a) Continuous wall (8-D-0-0-ELF)

(b) 5th story opening with $K_5 < 0.5K_6$ (8-D-5S-50-ELF)

(c) 1st story opening with $K_1 < 0.5K_2$ (8-D-1S-50-ELF)

(d) 1st story opening, with $K_1 < 0.75K_2$ (8-D-1S-75-ELF)

(e) 1st and 2nd story openings with K_1 and $K_2 < 0.5K_3$ (8-D-2S-50-ELF)

(f) 1st and 2nd story openings with K_1 and $K_2 < 0.75K_3$ (8-D-2S-75-ELF)

Figure B-30 Earthquake intensity at design period, S_a, versus maximum interstory drift for 8-story walls designed for D_{max} spectrum using the ASCE/SEI 7-16 ELF procedure. Black line indicates spectral acceleration at which 50% of motions result in collapse defined by maximum interstory drift in excess of 10%. K_i indicates stiffness of story i defined per Section B.3.

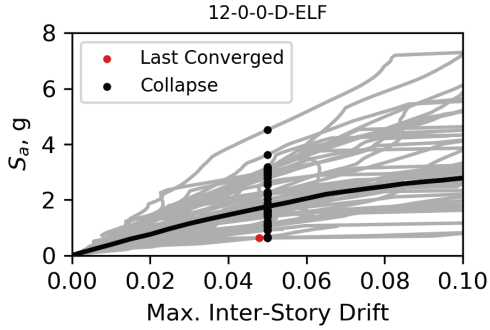

(a) Continuous wall (12-D-0-0-ELF)

No analysis conducted for this case.

(b) 8th story opening with $K_8 < 0.5K_9$

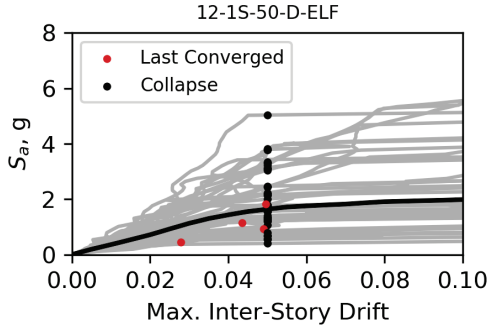

(c) 1st story opening with $K_1 < 0.5K_2$ (12-D-1S-50-ELF)

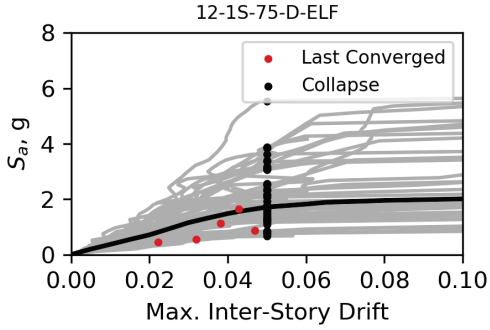

(d) 1st story opening with $K_1 < 0.75K_2$ (12-D-1S-75-ELF)

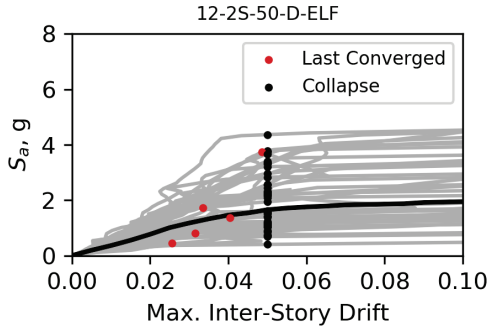

(e) 1st and 2nd story openings with K_1 and $K_2 < 0.5K_3$ (12-D-2S-50-ELF)

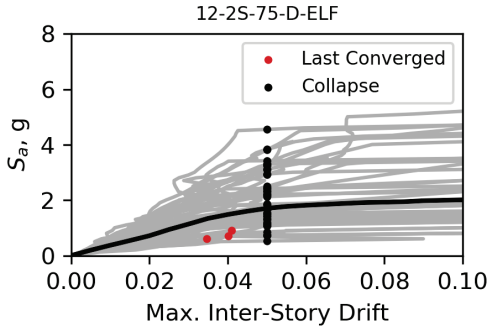

(f) 1st and 2nd story openings with K_1 and $K_2 < 0.75K_3$ (12-D-2S-75-ELF)

Figure B-31 Earthquake intensity at design period, S_a, versus maximum inter-story drift for 12-story walls designed for D_{max} spectrum using the ASCE/SEI 7-16 ELF procedure. Black line indicates spectral acceleration at which 50% of motions result in collapse defined by maximum inter-story drift in excess of 5%. K_i indicates stiffness of story i defined per Section B.3.

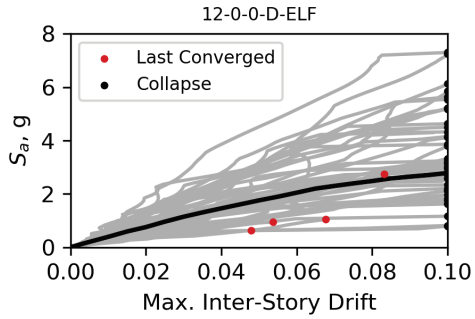

(a) Continuous wall (12-D-0-0-ELF)

No analysis conducted for this case.

(b) 8th story opening with $K_8 < 0.5K_9$

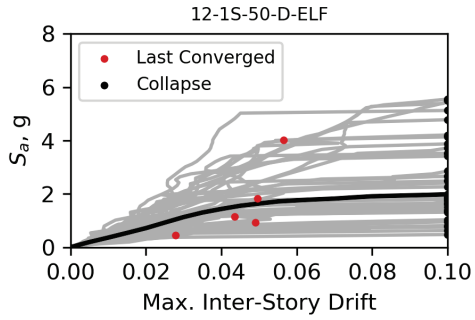

(c) 1st story opening with $K_1 < 0.5K_2$ (12-D-1S-50-ELF)

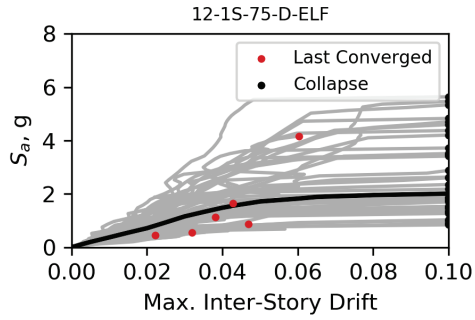

(d) 1st story opening with $K_1 < 0.75K_2$ (12-D-1S-75-ELF)

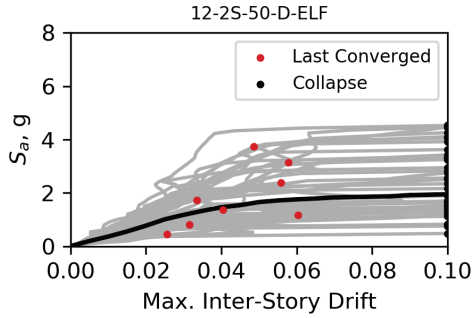

(e) 1st and 2nd story openings with K_1 and $K_2 < 0.5K_3$ (12-D-2S-50-ELF)

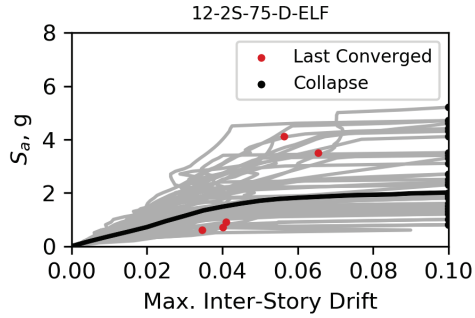

(f) 1st and 2nd story openings with K_1 and $K_2 < 0.75K_3$ (12-D-2S-75-ELF)

Figure B-32 Earthquake intensity at design period, S_a, versus maximum inter-story drift for 12-story walls designed for D_{max} spectrum using the ASCE/SEI 7-16 ELF procedure. Black line indicates spectral acceleration at which 50% of motions result in collapse defined by maximum inter-story drift in excess of 10%. K_i indicates stiffness of story i defined per Section B.3.

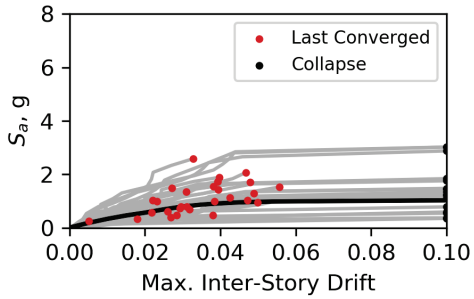

(a) Continuous wall (8-B-0-0-ELF)

No analysis conducted for this case.

(b) 5th story opening with $K_5 < 0.5K_6$ (8-B-5S-50-ELF)

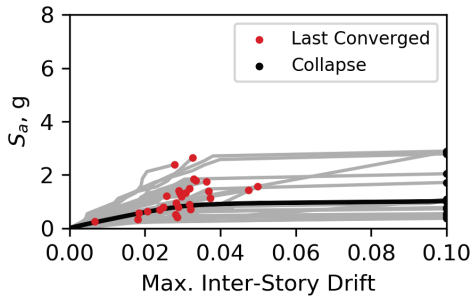

(c) 1st story opening with $K_1 < 0.5K_2$ (8-B-1S-50-ELF)

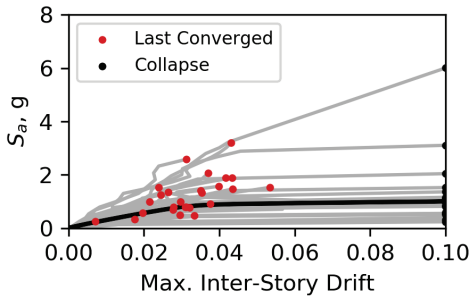

(d) 1st story opening, with $K_1 < 0.75K_2$ (8-B-1S-75-ELF)

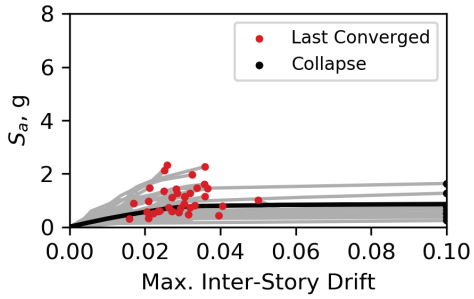

(e) 1st and 2nd story openings with K_1 and $K_2 < 0.5K_3$ (8-B-2S-50-ELF)

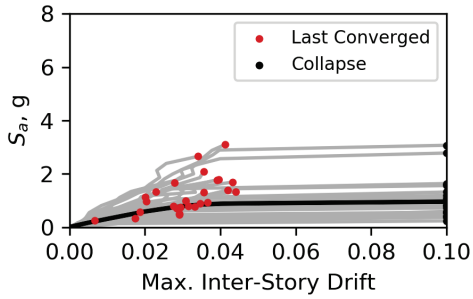

(f) 1st and 2nd story openings with K_1 and $K_2 < 0.75K_3$ (8-B-2S-75-ELF)

Figure B-33 Earthquake intensity at design period, S_a, versus maximum interstory drift for 8-story walls designed for B_{max} spectrum using the ASCE/SEI 7-16 ELF procedure. Black line indicates spectral acceleration at which 50% of motions result in collapse defined by maximum interstory drift in excess of 10%. K_i indicates stiffness of story i defined per Section B.3.

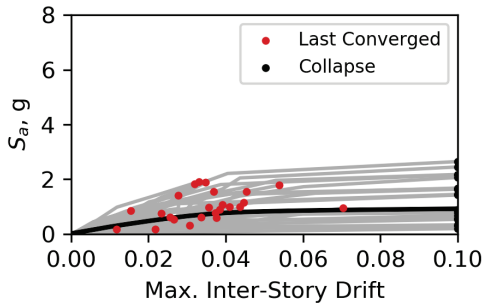

(a) Continuous wall (12-B-0-0-ELF)

No analysis conducted for this case.

(b) 5th story opening with $K_8 < 0.5K_9$ (12-B-5S-50-ELF)

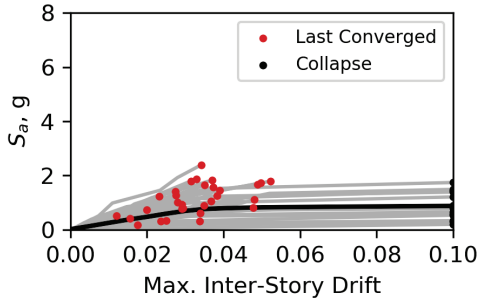

(c) 1st story opening with $K_1 < 0.5K_2$ (12-B-1S-50-ELF)

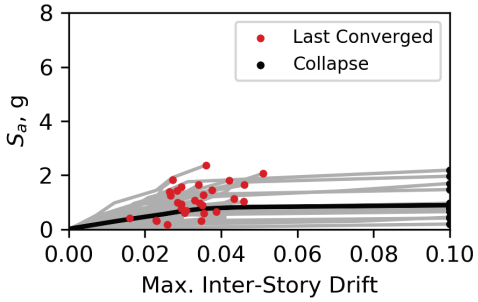

(d) 1st story opening, with $K_1 < 0.75K_2$ (12-B-1S-75-ELF)

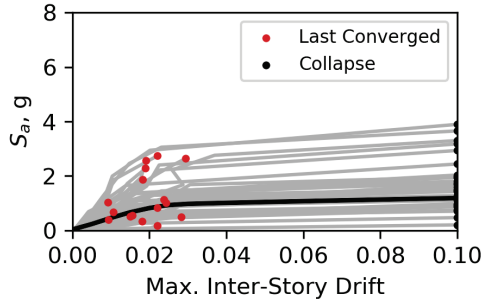

(e) 1st and 2nd story openings with K_1 and $K_2 < 0.5K_3$ (12-B-2S-50-ELF)

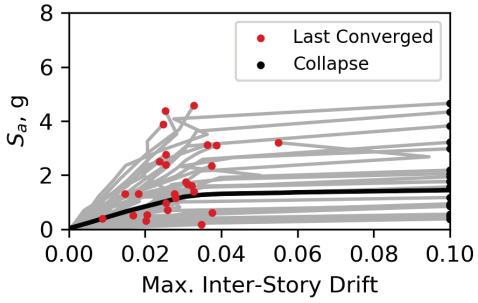

(f) 1st and 2nd story openings with K_1 and $K_2 < 0.75K_3$ (12-B-2S-75-ELF)

Figure B-34 Earthquake intensity at design period, S_a, versus maximum interstory drift for 12-story walls designed for B_{max} spectrum using the ASCE/SEI 7-16 ELF procedure. Black line indicates spectral acceleration at which 50% of motions result in collapse defined by maximum interstory drift in excess of 10%. K_i indicates stiffness of story i defined per Section B.3.

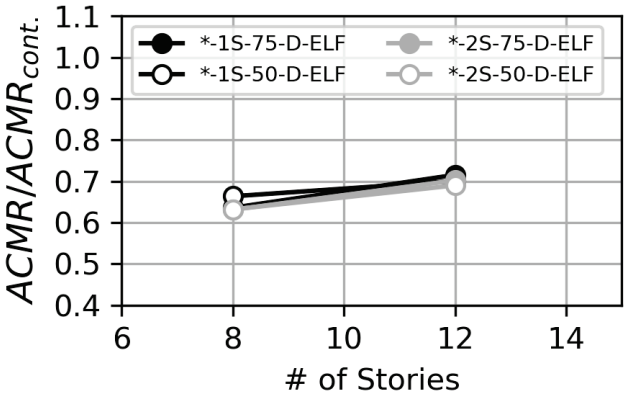

Figure B-35 Impact of vertical irregularity and building height on *ACMR* for walls designed for D_{max} demands using ASCE/SEI 7-16 ELF procedure. Non-simulated collapse at 10% interstory drift.

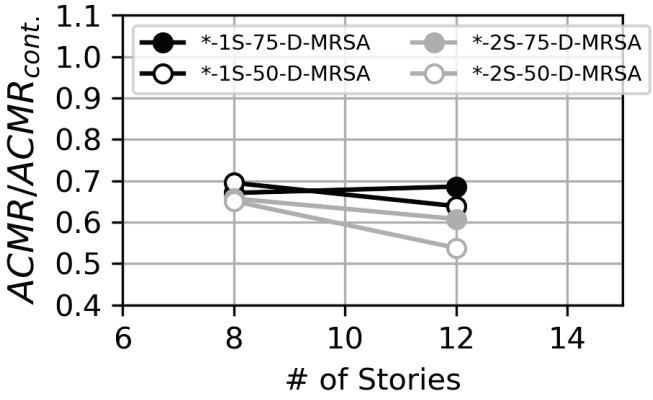

Figure B-36 Impact of vertical irregularity and building height on *ACMR* for walls designed for D_{max} demands using ASCE/SEI 7-16 MRSA procedure. Non-simulated collapse at 10% interstory drift.

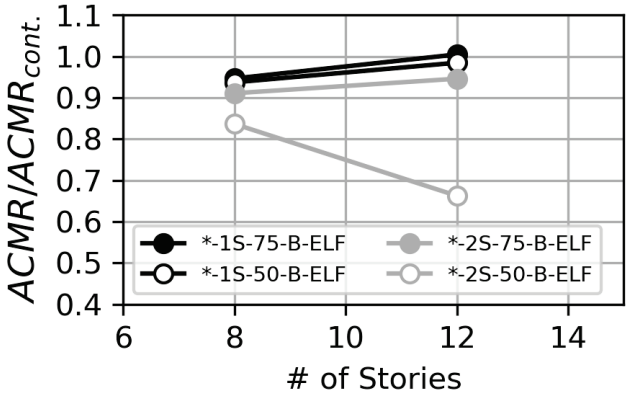

Figure B-37 Impact of vertical irregularity and building height on *ACMR* for walls designed for B_{max} demands using ASCE/SEI 7-16 ELF procedure. Non-simulated collapse at 10% interstory drift.

Appendix C
Steel Moment Frame Studies

This Appendix provides the following information on the steel moment frame studies: (1) B_{max} and D_{max} steel moment frame baseline designs; and (2) summary of the steel moment frame archetype results. For details on the steel moment frame designs with irregularities (i.e., mass irregularity, strong-column/weak-beam, and gravity-induced lateral demand) and for detailed results of the steel moment frame studies, see the electronic Supporting Documentation for Appendix C: Steel Moment Frame Irregularity Designs and Detailed Results.

C.1 Steel Moment Frame Baseline Designs

The archetype space as outlined in Chapter 6 includes 3-, 9-, and 20-story buildings each in a high and low seismicity zone. The high seismicity zone was represented by the Los Angeles region in California (Seismic Design Category D_{max}) and the low seismicity zone was represented by the Boston region in Massachusetts (Seismic Design Category B_{max}).

The steel moment frame buildings were designed per ASCE/SEI 7-16 *Minimum Design Loads and Associated Criteria for Buildings and Other Structures* (ASCE, 2017a) and AISC 341-10, *Seismic Provisions for Structural Steel Buildings* (AISC, 2010b). Dynamic analysis per Section 12.9 in ASCE/SEI 7-16 was used for calculating the member forces and story drifts.

Based upon the analyses undertaken, all the three buildings in the higher seismicity zone are governed by seismic forces and were designed to satisfy a story drift limit of 0.02. Generally, the buildings in the low seismicity zone are governed by wind forces and were designed to satisfy a story drift limit of $H/400$, where H is the building height. This is toward the lower end of the range discussed in ASCE/SEI 7-16 Commentary Appendix C.1.2 (ASCE, 2017a). A wind event of 50-year mean recurrence interval calculated, as discussed in Appendix C of ASCE/SEI 7-16, was used to design for satisfying serviceability requirements.

The post-Northridge SAC Model Buildings of Los Angeles and Boston area, in Appendix B of FEMA 355C (FEMA, 2000b), were used as the base models for the designs. These were selected because they have been used in

a variety of different studies since FEMA 355C was concluded. The building configuration and loading criteria match those of the SAC models, except that the 20-story buildings have a bay width of 30 feet, rather than 20 feet, because the 30-foot bay was judged to be more realistic. Figures C-1 through C-3 show the building configurations and Table C-1 summarizes the loading criteria.

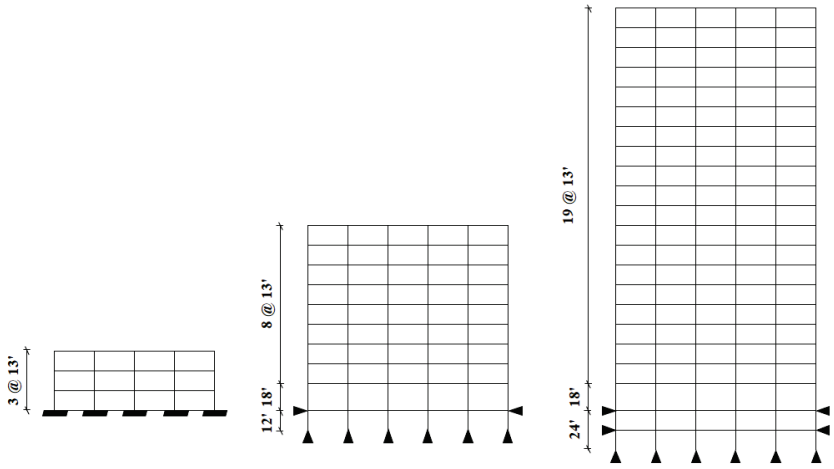

Figure C-1 Baseline steel moment frame building elevations.

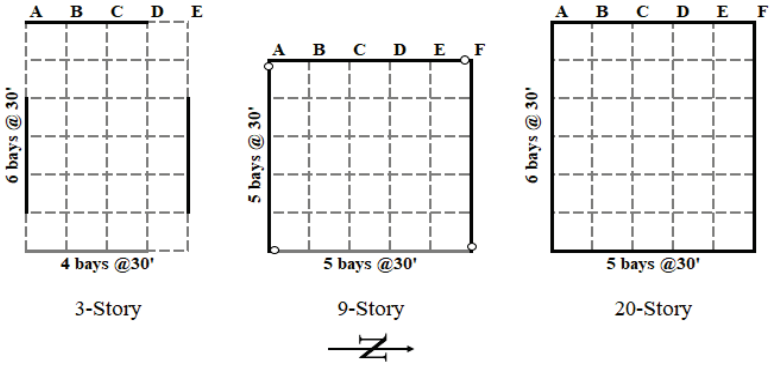

Floor Plans Showing Layout of Moment-resisting Frames for LA Model Buildings

Figure C-2 Baseline SDC D_{max} steel moment frame building plans.

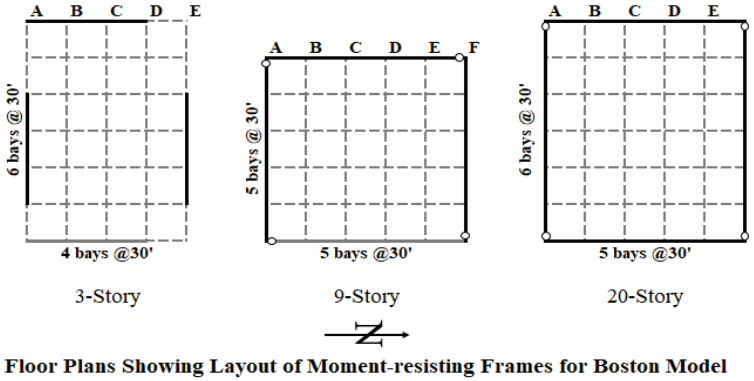

Floor Plans Showing Layout of Moment-resisting Frames for Boston Model Buildings

Figure C-3 Baseline SDC B_{max} steel moment frame building plans.

Table C-1 Typical Design Loading

Typical Floor Loads	Load (psf)
Dead Load	96.0
Seismic Weight	86.0
Seismic Partitions	10.0
Office LL (Reducible)	50.0
Typical Roof Loads	**Load (psf)**
Dead Load	83.0
Seismic Weight	83.0
Roof LL (Reducible)	20.0
Typical Roof Loads at Penthouse	**Load (psf)**
Dead Load	116.0
Seismic Weight	116.0
Roof LL (Reducible)	20.0

As required by the analysis matrix, baseline designs were developed using the modal response spectrum analysis (MRSA) and equivalent lateral force (ELF) methods.

C.1.1 Low Seismicity Zone (SDC B_{max}) – Steel Ordinary Moment Frame Design

Each of the three buildings in the low seismicity zone was designed to satisfy two criteria: most efficient design with deeper girders, and the strong-column/weak-beam design with stronger columns and relatively shallower girders. The code does not mandate satisfaction of the strong-column/weak-beam criterion in an ordinary moment frame building, but it has been investigated in the analyses.

Relevant wind and seismic loading criteria are summarized in Table C-2.

All the buildings in the SDC B_{max} (lower seismicity) region are story drift governed. The wind story drift has been limited to 0.25% (H/400), similar to the original SAC models. Per ASCE/SEI 7-16 (Commentary on Wind Serviceability requirements), story drift of the structure should be limited within H/300 to H/600. This study used the H/400 limit used in the SAC models.

The member sizes in the SDC B_{max} models remained more or less the same as in the SAC models. The base shear charts show that the wind serviceability base shear is almost the same based on either 1993 edition of *The BOCA National Building Code* (BOCA, 1993) or ASCE/SEI 7-16 provisions. Some

of the member sizes were made more efficient in the design by increasing the member depth and reducing the member weight.

Table C-2 Low Seismicity Zone Seismic and Wind Design Values

Wind Design Criteria	
Site Address: SDC B_{max}	
V_Basic Wind Speed (Strength)	130 mph
V_Basic Wind Speed (Serviceability)	100 mph
Wind Importance Factor	1
Wind Exposure	B
Seismic Design Criteria ASCE/SEI 7-16	
Site Address: SDC B_{max}	
T_L	6 s
Site Class	D
S_S	0.480g
S_1	0.198g
F_a	1.000
F_v	1.000
S_{MS}	0.480g
S_{M1}	0.198g
S_{DS}	0.320g
S_{D1}	0.132g
Risk Category	II
SDC	B

The designs of the SDC B_{max} models have two versions:

Model 1: a non-strong-column/weak-beam design, which is the most efficient design satisfying the H/400 story drift limit.

Model 2: a strong-column/weak-beam design, which encourages beam yielding before column yielding, thereby limiting column hinging and potentially poor building performance.

The difference in frame tonnage between the two models varies from about 12% in the 3- and 9-story buildings and about 2% in the 20-story building. Considering that the gravity members form a large part of the total building steel quantity, the increase in frame steel quantities would have a relatively small impact on the overall steel weight.

C.1.1.1 3-Story OMF Building

Figures C-4 and C-5 illustrate the geometry of the 3-story building. The base shear calculated for this building is as follows (seismic governs):

- Seismic: 292 kips (design period, $T = C_u T_a = 0.859$ s)
- Wind: 244 kips

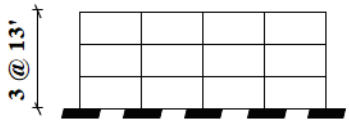

Figure C-4 Baseline SDC B_{max} steel moment frame building typical 3-story elevation.

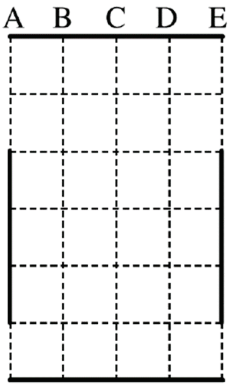

Figure C-5 Baseline SDC B_{max} steel moment frame building typical 3-story plan.

The wind and seismic shears are comparable but the wind story drift limit of h/400 is 8 times more stringent than the seismic story drift limit of 0.02. The structure was designed to satisfy both seismic and wind forces and story drift limits.

The baseline frame designs for the non-strong-column/weak-beam model are summarized in Tables C-3 and C-4 for MRSA and ELF designs, respectively. Using frame sizes from Table C-3 for ELF analysis resulted in a maximum story drift of 2.5% between the third and second floor. The beam sizes were increased as shown in Table C-4 to meet the allowable 2% story drift requirement using ELF analysis.

The baseline frame designs for the strong-column/weak-beam model are summarized in Tables C-5 and C-6 for MRSA and ELF designs, respectively. Using frame sizes from Table C-5 for ELF analysis resulted in a maximum story drift of 2.3% between the third and second floor. The beam sizes were increased as shown in Table C-6 to meet the allowable 2% story drift

requirement using ELF analysis. A variant on the frame designs was developed eliminating doubler plates, as summarized in Table C-7 and Table C-8.

Table C-3 V0030101 Baseline

MRSA Design: Non-Strong-Column/Weak-Beam				
Story/Floor	Columns		Doubler Plates	Girder
	Ext	Int		
Roof	W14×53	W14×99	Yes	W21×44
3rd	W14×53	W14×99	Yes	W21×62
2nd	W14×53	W14×99	Yes	W21×62

Notes: Model 1: MRSA Design, Non-Strong-Column/Weak-Beam
Steel Tonnage 1.85 psf (Columns: 0.81 psf, Beams: 1.04 psf)

Table C-4 V0030102 Baseline

ELF Design: Non-Strong-Column/Weak-Beam								
Story/Floor	Columns		Doubler Plates	Girder	ELF Story Drift		Moment Ratio	
	Ext	Int			Δ_X	Δ_Y	Ext	Int
Roof	W14×53	W14×99	No	W21×57	1.07%	1.48%	0.49	0.49
3rd	W14×53	W14×99	Yes	W24×76	1.48%	2.00%	0.6	0.62
2nd	W14×53	W14×99	Yes	W24×76	1.20%	1.53%	0.53	0.59

Notes: Model 1: ELF Design, Non-Strong-Column/Weak-Beam
Steel Tonnage 2.09 psf (Columns: 0.81 psf, Beams: 1.28 psf)

Table C-5 V0030103 Baseline

MRSA Design: Strong-Column/Weak-Beam				
Story/Floor	Columns		Doubler Plates	Girder
	Ext	Int		
Roof	W14×82	W14×145	Yes	W21×44
3rd	W14×82	W14×146	Yes	W21×50
2nd	W14×82	W14×147	Yes	W21×50

Notes: Model 2: MRSA Design, Strong-Column/Weak-Beam
Steel Tonnage 2.09 psf (Columns: 1.20 psf, Beams: 0.89 psf)

Table C-6 V0030104 Baseline

ELF Design: Strong-Column/Weak-Beam								
Story/Floor	Columns		Doubler Plates	Girder	ELF Story Drift		Moment Ratio	
	Ext	Int			Δ_X	Δ_Y	Ext	Int
Roof	W14×53	W14×99	No	W21×44	1.10%	1.51%	1.07	1.03
3rd	W14×53	W14×99	No	W24×62	1.37%	1.81%	1.29	1.25
2nd	W14×53	W14×99	No	W24×62	0.95%	1.20%	1.2	1.2

Notes: Model 2: ELF Design, Strong-Column/Weak-Beam
Steel Tonnage 1.84 psf (Columns: 0.81 psf, Beams: 1.03 psf)

Table C-7 V0030105 Baseline

MRSA Design: Strong-Column/Weak-Beam Design				
Story/Floor	Columns		Doubler Plates	Girder
	Ext	Int		
Roof	W14×120	W14×211	No	W21×44
3rd	W14×132	W14×233	No	W21×50
2nd	W14×132	W14×233	No	W21×50

Notes: Model 3: MRSA Design, Strong-Column/Weak-Beam, No Doubler Plates
Steel Tonnage 2.76 psf (Columns: 1.87 psf, Beams: 0.89 psf)

Table C-8 V0030106 Baseline

ELF Design: Strong-Column/Weak-Beam Design						
Story/Floor	Columns		Doubler Plates	Girder	ELF Story Drift	
	Ext	Int			Δ_X	Δ_Y
Roof	W14×120	W14×211	No	W21×44	1.21%	1.62%
3rd	W14×132	W14×233	No	W21×50	1.37%	1.77%
2nd	W14×132	W14×233	No	W21×50	0.80%	1.00%

Notes: Model 2: ELF Design, Strong-Column/Weak-Beam
Steel Tonnage 2.76 psf (Columns: 1.87 psf, Beams: 0.89 psf)

C.1.1.2 9-Story OMF Building

Figures C-6 and C-7 illustrate the geometry of the 9-story building. The base shear calculated for this building is as follows (wind governs):

- Seismic: 358 kips (design period, $T = C_u T_a = 2.138$ s)
- Wind: 950 kips

Corner columns were oriented such that the pinned connection frames into the column web. Other column sections were oriented with their strong axis parallel to the longitudinal direction of the frame.

The baseline frame designs are summarized in Tables C-9 and C-10 for the ELF design for non-strong-column/weak-beam frames and strong-column/weak-beam frames, respectively. The frame sizes designed for the 9-story building in Boston satisfying wind and seismic demands also satisfy story drift levels for ELF analysis.

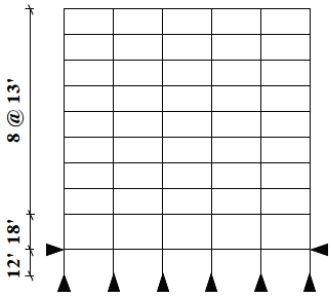

Figure C-6 Baseline SDC B_{max} steel moment frame building typical 9-story elevation.

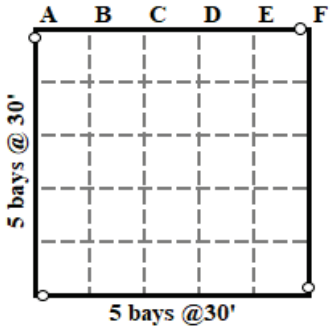

Figure C-7 Baseline SDC B_{max} steel moment frame building typical 9-story plan.

Table C-9 V0090101 Baseline

MRSA Design: Non-Strong-Column/Weak-Beam Design						
	Columns		Doubler Plates	Girder	ELF Story Drift	
Story/Floor	Ext	Int			Δ_X	Δ_Y
Roof	W14×48	W14×90	No	W21×44	0.70%	0.71%
9th	W14×48	W14×90	No	W24×84	0.93%	0.93%
8th	W14×74	W14×145	No	W27×84	0.86%	0.86%
7th	W14×74	W14×145	No	W30×108	0.87%	0.87%
6th	W14×120	W14×211	No	W33×118	0.74%	0.74%
5th	W14×120	W14×211	No	W33×118	0.74%	0.74%
4th	W14×145	W14×311	No	W33×130	0.60%	0.60%
3rd	W14×145	W14×311	No	W33×141	0.57%	0.57%
2nd	W14×193	W14×398	No	W36×194	0.56%	0.56%
1st	W14×193	W14×398	No	W21×44	-	-

Notes: Model 1: Non-Strong-Column/Weak-Beam Design
(Design is governed by drift due to wind ≤ 0.25% limit)
Steel Tonnage 5.10 psf (Columns: 2.40 psf, Beams: 2.70 psf)

Table C-10 V0090102 Baseline

MRSA Design: Strong-Column/Weak-Beam Design								
	Columns		Doubler Plates	Girder	ELF Story Drift		Moment Ratio	
Story/Floor	Ext	Int			Δ_X	Δ_Y	Ext	Int
Roof	W14×99	W14×176	No	W21×44	0.82%	0.83%	1.39	1.29
9th	W14×99	W14×176	No	W21×44	0.97%	0.97%	2.72	2.55
8th	W14×145	W14×283	No	W24×68	0.85%	0.85%	1.79	1.82
7th	W14×145	W14×283	No	W27×84	0.80%	0.80%	1.52	1.65
6th	W14×211	W14×398	No	W30×90	0.72%	0.72%	1.61	1.74
5th	W14×211	W14×398	No	W30×90	0.66%	0.66%	1.91	2.07
4th	W14×257	W14×455	No	W33×118	0.58%	0.58%	1.44	1.51
3rd	W14×257	W14×455	No	W33×118	0.58%	0.58%	1.57	1.62
2nd	W14×283	W14×500	No	W33×118	0.54%	0.54%	1.63	1.7
1st	W14×283	W14×00	No	W21×44	-	-		

Notes: Model 3: Strong-Column/Weak-Beam Design
(Design is governed by drift due to wind ≤ 0.25% limit while satisfying moment ratio < 1.0)
Steel Tonnage 5.84 psf (Columns: 3.77 psf, Beams: 2.07 psf)

C.1.1.3 20-Story OMF Building

Figures C-8 and C-9 illustrate the geometry of the 20-story building. The base shear calculated for this building is as follows (wind governs):

- Seismic: 750 kips (design period, $T = C_u T_a = 3.977$ s)
- Wind: 3116 kips (east-west); 2580 kips (north-south)

Corner columns were oriented such that the pinned connection frames into the column web. Other column sections were oriented with their strong axis parallel to the longitudinal direction of the frame. The basement floor (-1 Level) has simple connections.

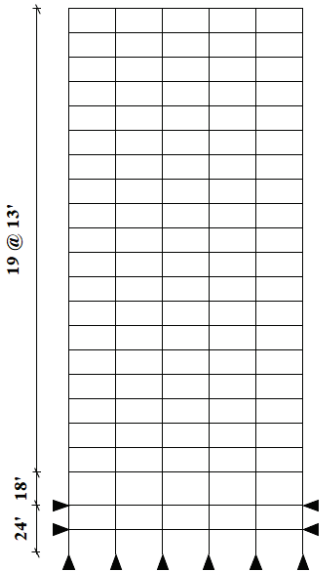

Figure C-8 Baseline SDC B_{max} steel moment frame building typical 20-story elevation.

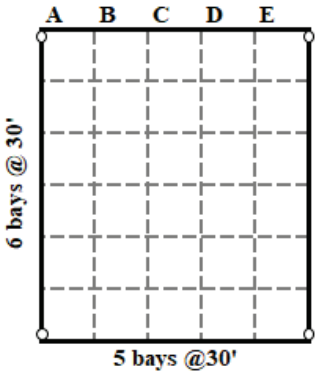

Figure C-9 Baseline SDC B_{max} steel moment frame building typical 20-story plan.

Table C-11 V0200101 Baseline

MRSA Design: Non-Strong-Column/Weak-Beam Design					
	Columns			Doubler Plates	Girder
Story/Floor	Ext	Next to Ext	Int		
Roof	W14×109	W24×117	W24×131	No	W21×48
20th	W14×109	W24×117	W24×131	No	W24×76
19th	W14×159	W36×150	W36×150	No	W27×84
18th	W14×159	W36×150	W36×150	No	W30×99
17th	W14×193	W36×182	W36×210	No	W30×108
16th	W14×193	W36×182	W36×210	No	W33×118
15th	W14×283	W36×262	W36×282	No	W33×118
14th	W14×283	W36×262	W36×282	No	W36×135
13th	W14×283	W36×262	W36×302	No	W36×135
12th	W14×283	W36×262	W36×302	No	W36×182
11th	W14×311	W36×262	W36×302	No	W36×182
10th	W14×311	W36×262	W36×302	No	W36×182
9th	W14×342	W36×302	W36×361	No	W36×210
8th	W14×342	W36×302	W36×361	No	W36×210
7th	W14×342	W36×302	W36×361	No	W36×256
6th	W14×342	W36×302	W36×361	No	W36×256
5th	W14×370	W36×330	W36×395	No	W36×256
4th	W14×370	W36×330	W36×395	No	W36×282
3rd	W14×455	W36×395	W36×487	No	W36×282
2nd	W14×455	W36×395	W36×487	No	W36×302
Level 1	W14×455	W36×395	W36×487	No	W24×62
Basement	W14×455	W36×395	W36×487	No	W24×84

Notes: Model 1: Non Strong-Column/Weak-Beam Design
Steel Tonnage 6.92 psf (Columns: 3.03 psf, Beams: 3.89 psf)

Table C-12 V0200102 Baseline

MRSA Design: Strong-Column/Weak-Beam Design					
	Columns			Doubler Plates	Girder
Story/Floor	Ext	Next to Ext	Int		
Roof	W14×109	W24×117	W24×117	No	W18×35
20th	W14×109	W24×117	W24×117	No	W24×76
19th	W14×159	W36×150	W36×150	No	W27×84
18th	W14×159	W36×150	W36×150	No	W30×99
17th	W14×193	W36×210	W36×182	No	W30×108
16th	W14×311	W36×210	W36×182	No	W33×118
15th	W14×311	W36×302	W36×282	No	W33×118
14th	W14×370	W36×302	W36×282	No	W36×135
13th	W14×370	W36×330	W36×302	No	W36×135
12th	W14×370	W36×330	W36×302	No	W36×160
11th	W14×426	W36×361	W36×302	No	W36×170
10th	W14×426	W36×361	W36×302	No	W36×170
9th	W14×455	W36×395	W36×361	No	W36×194
8th	W14×455	W36×395	W36×361	No	W36×194
7th	W14×500	W36×441	W36×395	No	W36×232
6th	W14×500	W36×441	W36×395	No	W36×232
5th	W14×605	W36×487	W36×441	No	W36×232
4th	W14×605	W36×487	W36×441	No	W36×247
3rd	W14×665	W36×487	W36×487	No	W36×247
2nd	W14×665	W36×487	W36×487	No	W36×262
Level 1	W14×665	W36×487	W36×487	No	W24×55
Basement	W14×665	W36×487	W36×487	No	W24×84

Notes: Model 2: Strong-Column/Weak-Beam Design
Steel Tonnage 7.12 psf (Columns: 3.53 psf, Beams: 3.59 psf)

C.1.2 High Seismicity Zone (SDC D_{max}) – Steel Special Moment Frame Design

The 3-, 9-, and 20-story buildings were designed for SDC D_{max}, as well. The 3- and 9-story buildings were designed to satisfy two criteria: (1) code design meeting the minimum code requirements for special moment frames per AISC 341-10; and (2) performance-based plastic design, also called the Energy Method, which calculates the demand on the seismic members based on the ultimate story drift to which the structure is subjected. The energy method provides a parallel design to the code design.

The buildings were designed to a story drift limit of 2% for a design based earthquake and to a story drift limit of 3% for a maximum-considered earthquake (MCE). The columns in the code design were designed to satisfy the strong-column/weak-beam principle with M_{pc}*/ M_{pb}*>1.00; in the energy method the beams and the columns are designed to sustain seismic demands generated due to the story drift of the structure (Goel and Chao, 2008).

The frame elements designed using the energy method are heavier than those designed by code design because the buildings in the code design do not reach the 2% story drift limit under a design based earthquake.

Reduced beam section (RBS) connections per AISC 358-10 were used as the prequalified connections for the steel special moment frames. The RBS dimensions, shown in Figure C-10, were considered explicitly when evaluating the frame story drift.

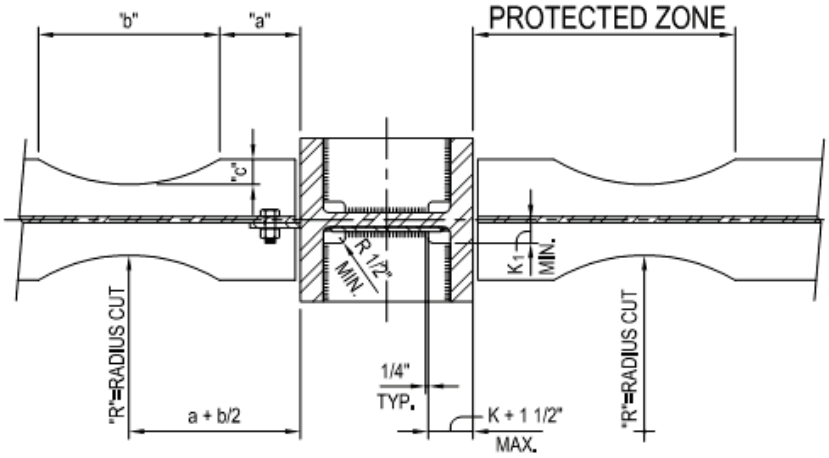

Figure C-10 Reduced beam section profiles.

As required by the analysis matrix, baseline designs were developed using MRSA and ELF methods. Relevant wind and seismic loading criteria are summarized in Table C-13. Table C-14 indicates RBS profiles used in the high seismicity zone studies.

During the course of baseline frame design, it was observed that the member sizes of the SDC D_{max} 3- and 9-story buildings could be reduced compared to the SAC models. The original SAC model for the Los Angeles 9-story building was used to study this.

Even accounting for the shift in design methodology between the 1994 *Uniform Building Code* (UBC-94; International Conference of Building Officials, 1994) (working) and ASCE/SEI 7-16 (strength), it was observed that the base shear for the Los Angeles 9-story building increased from the original SAC design parameters. On the other hand, the story drift limit also

relaxed from $h/400$ or 0.25% in UBC-94 (working/elastic) to 2% in ASCE/SEI 7-16 (strength/inelastic). For some frame members, it was possible to reduce the sizes in the SDC D_{max} 3- and 9-story buildings.

Table C-13 High Seismicity Zone Seismic and Wind Design Values

Wind Design Criteria	
Site Address: SDC D_{max}	
V_Basic Wind Speed (Strength)	110 mph
V_Basic Wind Speed (Serviceability)	85 mph
Wind Importance Factor	1
Wind Exposure	B
Seismic Design Criteria ASCE/SEI 7-16	
Site Address: SDC D_{max}	
T_L	8 s
Site Class	D
S_S	2.250g
S_1	0.600g
F_a	1.000
F_v	1.500
S_{MS}	2.250g
S_{M1}	0.900g
S_{DS}	1.500g
S_{D1}	0.600g
Risk Category	II
SDC	D

Table C-14 Reduced Beam Section Profiles Used in SDC D_{max} Buildings

Beam Size	*a* (in.)	*b* (in.)	*c* (in.)	*R* (in.)
W24×76 to W34×103	6	18	2.00	21.25
W24×131 to W24×229	8	18	2.75	16.10
W27×94 to W27×129	6	20	2.25	23.35
W27×146 to W27×217	8	20	2.75	19.56
W30×108 to W30×148	7	22	2.25	28.01
W30×173 to W30×261	9	22	3.00	21.67
W33×130 to W33×169	7	24	2.50	30.05
W33×201 to W33×291	9	24	3.25	23.78
W36×150 to W36×256	8	27	2.75	34.51
W36×230 to W36×282	10	27	3.50	27.79

This phenomenon was not observed in the 20-story building. The seismic base shear of the 20-story building increased by about 110%, which is significant, and even the relaxation in the story drift limit from UBC-94 to ASCE/SEI 7-10 did not help and the sizes had to be increased to meet all code provisions.

C.1.2.1 3-Story SMF Building

Figure C-11 and Figure C-12 illustrate the geometry of the 3-story building from which the baseline moment frame designs were developed. The base shear calculated for this building is as follows (seismic governs):

- Seismic: 679 kips (design period, $T = C_u T_a = 0.735$ s)
- Wind: 346 kips

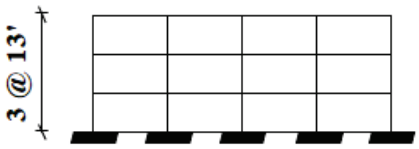

Figure C-11 Baseline SDC D_{max} steel moment frame building typical 3-story elevation.

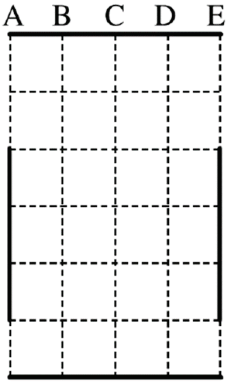

Figure C-12 Baseline SDC D_{max} steel moment frame building typical 3-story plan.

Table C-15 V0300201 Baseline

MRSA Design								
Story/ Floor	Columns		Doubler Plates	Girder	MRSA Story Drift		Moment Ratio	
	Ext	Int			Δ_X	Δ_Y	Ext	Int
Roof	W14×159	W14×176	No	W24×55	1.75%	1.77%	2.00	1.15
3rd	W14×159	W14×176	Yes	W27×94	1.86%	1.88%	1.89	1.09
2nd	W14×159	W14×176	Yes	W27×94	1.36%	1.37%	1.75	1.05

Notes: Model 1: Code Design
Steel Tonnage 2.81 psf (Columns: 1.53 psf, Beams: 1.28 psf)

The MRSA frame sizes in Table C-16, when subjected to ELF analysis, resulted in drifts exceeding the allowable 2% limit. The frame sizes were increased as shown in Table C-17 to meet the allowable 2% story drift requirement.

Table C-16 V0300202 Baseline

MRSA Design								
	Columns		Doubler Plates	Girder	MRSA Story Drift		Moment Ratio	
Story/Floor	Ext	Int			Δ_X	Δ_Y	Ext	Int
Roof	W14×132	W14×159	No	W24×55	1.90%	1.91%	1.62	1.03
3rd	W14×176	W14×283	No	W27×94	1.65%	1.66%	1.82	1.43
2nd	W14×176	W14×283	No	W27×94	1.11%	1.12%	1.99	1.84

Notes: Model 2: Code Design, No Doubler Plates
Steel Tonnage 3.12 psf (Columns: 1.84 psf, Beams: 1.28 psf)

Table C-17 V0300203 Baseline

ELF Design								
	Columns		Doubler Plates	Girder	ELF Story Drift		Moment Ratio	
Story/Floor	Ext	Int			Δ_X	Δ_Y	Ext	Int
Roof	W14×211	W14×311	No	W27×94	1.79%	1.80%	1.33	1.06
3rd	W14×311	W14×370	No	W33×130	1.98%	1.98%	1.88	1.32
2nd	W14×311	W14×370	No	W33×130	1.33%	1.33%	2.2	1.43

Notes: Model 2: ELF Design, No Doubler Plates
Steel Tonnage 4.74 psf (Columns: 2.87psf, Beams: 1.87 psf)

Table C-18 V0300204 Baseline

Energy Method				
	Columns		Doubler Plates	Girder
Story/Floor	Ext	Int		
Roof	W14×257	W14×455	No	W24×94
3rd	W14×257	W14×455	No	W30×108
2nd	W14×311	W14×500	No	W33×130

Notes: Model 3: Energy Method
Steel Tonnage 5.43 psf (Columns: 3.59 psf, Beams: 1.84 psf)

C.1.2.2 9-Story SMF Building

Figures C-13 and C-14 illustrate the geometry of the 9-story building. The base shear calculated for this building is as follows (seismic governs):

- Seismic: 1341 kips (design period, $T = C_u T_a = 1.830$ s)
- Wind: 816 kips

Corner columns were oriented such that the pinned connection frames into the column web. Other column sections were oriented with their strong axis parallel to the longitudinal direction of the frame.

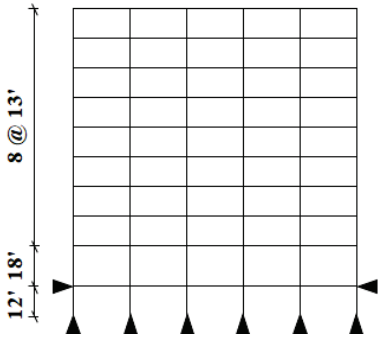

Figure C-13 Baseline SDC D_{max} steel moment frame building typical 9-story elevation.

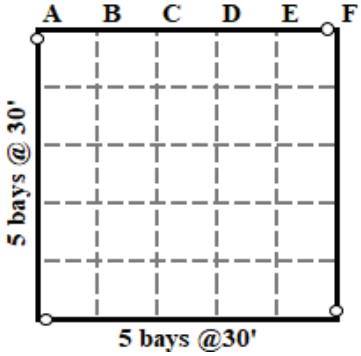

Figure C-14 Baseline SDC D_{max} steel moment frame building typical 9-story plan.

The baseline frame designs are summarized in Tables C-19 and C-20 for the code-complying baseline MRSA design and for design without doubler plates (i.e., column sizes were increased), respectively.

The frame sizes in Tables C-19 and C-20, when analyzed with the ELF method, resulted in story drifts substantially exceeding the 2% allowable story drift limit at all story levels. The frame sizes were increased as shown in Table C-21 in order to meet the allowable 2% story drift requirement using ELF analysis. Optimal sizes were chosen that simultaneously satisfy story drift and strong-column/weak-beam requirements. Conforming to ELF-based frame sizes results in a steel tonnage that is 1.7 times the weight per square foot tonnage using MRSA-based design.

Table C-22 summarizes the results from the energy-based design methodology. Deep column section were selected inasmuch as the method

generally results in larger column sizes than do designs based on MRSA or ELF methods.

Table C-19 V0900201 Baseline

MRSA Design				
Story/Floor	Columns		Doubler Plates	Girder
	Ext	Int		
Roof	W14×132	W14×145	Yes	W21×50
9th	W14×132	W14×145	Yes	W24×76
8th	W14×193	W14×211	Yes	W24×84
7th	W14×193	W14×211	Yes	W27×94
6th	W14×233	W14×257	Yes	W27×94
5th	W14×233	W14×257	Yes	W30×108
4th	W14×257	W14×283	Yes	W30×108
3rd	W14×257	W14×283	Yes	W30×108
2nd	W14×283	W14×370	No	W33×130
1st	W14×283	W14×370	No	W33×130

Notes: Model 1: Code Design
Steel Tonnage 5.32 psf (Columns: 2.83 psf, Beams: 2.49 psf)

Table C-20 V0900202 Baseline

MRSA Design				
Story/Floor	Columns		Doubler Plates	Girder
	Ext	Int		
Roof	W14×145	W14×159	No	W21×50
9th	W14×145	W14×159	No	W24×76
8th	W14×193	W14×283	No	W24×84
7th	W14×193	W14×283	No	W27×94
6th	W14×233	W14×311	No	W27×94
5th	W14×233	W14×311	No	W30×108
4th	W14×257	W14×311	No	W30×108
3rd	W14×257	W14×311	No	W30×108
2nd	W14×283	W14×370	No	W33×130
1st	W14×283	W14×370	No	W33×130

Notes: Model 2: Code Design, No Doubler Plates
Steel Tonnage 5.6 psf (Columns: 3.1 psf, Beams: 2.49 psf)

Table C-21 V0900203 Baseline

ELF Design								
Story/ Floor	Columns		Doubler Plates	Girder	ELF Story Drift		Moment Ratio	
	Ext	Int			Δ_X	Δ_Y	Ext	Int
Roof	W14×233	W14×311	No	W27×94	1.28%	1.30%	1.47	1.06
9th	W14×233	W14×311	No	W30×116	1.67%	1.67%	2.06	1.48
8th	W14×370	W14×398	No	W36×150	1.74%	1.74%	1.79	1.1
7th	W14×370	W14×398	No	W36×150	1.92%	1.92%	2.23	1.24
6th	W14×398	W14×426	No	W36×182	1.95%	1.95%	1.87	1.04
5th	W14×398	W14×426	No	W36×194	1.96%	1.95%	1.8	1
4th	W14×455	W14×500	No	W36×232	1.80%	1.80%	1.6	0.99
3rd	W14×455	W14×500	No	W36×232	1.90%	1.90%	1.7	0.99
2nd	W14×455	W14×550	No	W36×232	1.92%	1.92%	1.67	1.04
1st	W14×455	W14×550	No	W36×232	-	-	1.64	1.09

Notes: Model 2 Revised: ELF Design, No Doubler Plates
Steel Tonnage 9.44 psf (Columns: 4.85 psf, Beams: 4.59 psf)

Table C-22 V0900204 Baseline

Energy Method				
Story/Floor	Columns		Doubler Plates	Girder
	Ext	Int		
Roof	W27×336	W27×539	No	W30×108
9th	W27×336	W27×539	No	W33×130
8th	W27×336	W27×539	No	W40×149
7th	W27×368	W36×652[(1)]	No	W40×167
6th	W27×368	W36×652[(1)]	No	W40×183
5th	W27×539	W36×652[(1)]	No	W40×199
4th	W27×539	W36×652[(1)]	No	W40×199
3rd	W27×539	W36×652[(1)]	No	W40×199
2nd	W27×539	W36×652[(1)]	No	W40×199
1st	W27×539	W36×652[(1)]	No	W33×130

[(1)] Section deeper than 30 in.
Notes: Model 3: Energy Method
Steel Tonnage 12.46 psf (Columns: 8.03 psf, Beams: 4.43 psf)

C.1.2.3 20-Story SMF Building

Figures C-15 and C-16 illustrate the geometry of the 20-story building. The base shear calculated for this building is as follows (seismic governs):

- Seismic: 3500 kips (design period, $T = C_u T_a = 3.403$ s)
- Wind: 2155 kips (east-west); 1810 kips (north-south)

Corner columns are box sections because they participate in orthogonal frames. The orthogonal load combinations in ASCE/SEI 7-16 were used to determine demands on the corner columns. Other column sections oriented with their strong axis parallel to the longitudinal direction of the frame. The basement floor (-1 Level) has simple connections.

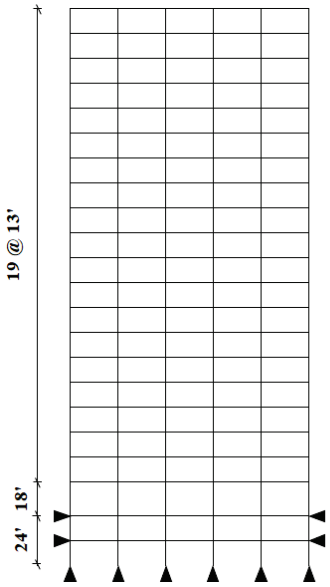

Figure C-15 Baseline SDC D_{max} steel moment frame building typical 20-story elevation.

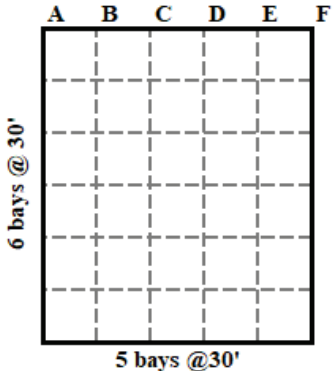

Figure C-16 Baseline SDC D_{max} steel moment frame building typical 20-story plan.

Designs based on MRSA and the ELF method were developed, with and without doubler plates (i.e., the columns were upsized). Tables C-23 through C-26 summarize the resulting baseline designs.

Table C-23 V02002011 Baseline

MRSA Design					
	Columns			Doubler Plates	Girder
	Ext	North-South Frame			
Story/Floor	[HSS Section]	Next to Ext	Int		
Roof	15×15×1.00	W27×129	W27×129	Yes	W24×76
20th	15×15×1.00	W27×129	W27×129	Yes	W33×130
19th	15×15×1.00	W27×235	W27×235	Yes	W33×130
18th	15×15×1.00	W27×235	W27×235	Yes	W33×130
17th	15×15×1.00	W27×235	W27×235	Yes	W33×130
16th	15×15×1.00	W27×235	W27×235	Yes	W36×150
15th	15×15×1.00	W27×235	W27×235	Yes	W36×150
14th	15×15×1.00	W27×281	W27×258	Yes	W36×150
13th	15×15×1.00	W27×281	W27×258	Yes	W36×150
12th	15×15×1.25	W27×368	W27×336	Yes	W36×170
11th	15×15×1.25	W27×368	W27×336	Yes	W36×170
10th	15×15×1.25	W27×368	W27×336	Yes	W36×182
9th	15×15×1.50	W27×539	W27×539	No	W36×182
8th	15×15×1.50	W27×539	W27×539	No	W36×194
7th	15×15×1.50	W27×539	W27×539	No	W36×194
6th	15×15×1.50	W27×539	W27×539	No	W36×210
5th	15×15×2.00	W27×539	W27×539	No	W36×210
4th	15×15×2.00	W27×539	W27×539	No	W36×210
3rd	15×15×2.00	W27×539	W27×539	No	W36×210
2nd	15×15×2.00	W27×539	W27×539	Yes	W36×262
Level 1	15×15×2.00	W27×539	W27×539	No	W30×116
Basement	15×15×2.00	W27×539	W27×539	No	W27×94

Notes: Model 1: MRSA Design
Steel Tonnage 6.68 psf (Columns: 3.28 psf, Beams: 3.40 psf)

Table C-24 V02002012 Baseline

MRSA Design					
	Columns				
		East-West Frame		Doubler Plates	Girder
Story/Floor	Ext [HSS Section]	Next to Ext	Int		
Roof	15×15×1.00	W27×129	W27×129	Yes	W24×76
20th	15×15×1.00	W27×129	W27×129	Yes	W24×76
19th	15×15×1.00	W27×129	W27×129	Yes	W30×108
18th	15×15×1.00	W27×161	W27×161	Yes	W30×108
17th	15×15×1.00	W27×161	W27×161	Yes	W30×108
16th	15×15×1.00	W27×194	W27×194	Yes	W30×116
15th	15×15×1.00	W27×194	W27×194	Yes	W30×116
14th	15×15×1.00	W27×217	W27×217	Yes	W33×130
13th	15×15×1.00	W27×217	W27×217	Yes	W33×130
12th	15×15×1.25	W27×258	W27×258	Yes	W33×130
11th	15×15×1.25	W27×258	W27×258	Yes	W36×150
10th	15×15×1.25	W27×258	W27×258	Yes	W36×150
9th	15×15×1.50	W27×336	W27×307	Yes	W36×150
8th	15×15×1.50	W27×336	W27×307	Yes	W36×150
7th	15×15×1.50	W27×336	W27×307	Yes	W36×150
6th	15×15×1.50	W27×336	W27×307	Yes	W36×150
5th	15×15×2.00	W27×368	W27×336	No	W36×150
4th	15×15×2.00	W27×368	W27×336	No	W36×160
3rd	15×15×2.00	W27×539	W27×539	No	W36×170
2nd	15×15×2.00	W27×539	W27×539	No	W36×182
Level 1	15×15×2.00	W27×539	W27×539	No	W30×116
Basement	15×15×2.00	W27×539	W27×539	No	W27×94

Notes: Model 1: MRSA Design
Steel Tonnage 6.68 psf (Columns: 3.28 psf, Beams: 3.40 psf)

Table C-25 V02002021 Baseline

MRSA Design					
	Columns			Doubler Plates	Girder
		North-South Frame			
Story/Floor	Ext [HSS Section]	Next to Ext	Int		
Roof	15×15×1.00	W27×307	W27×307	No	W24×76
20th	15×15×1.00	W27×307	W27×307	No	W33×130
19th	15×15×1.00	W27×307	W27×307	No	W33×130
18th	15×15×1.00	W27×307	W27×307	No	W33×130
17th	15×15×1.00	W27×307	W27×307	No	W33×130
16th	15×15×1.00	W27×336	W27×336	No	W36×150
15th	15×15×1.00	W27×336	W27×336	No	W36×150
14th	15×15×1.00	W27×336	W27×336	No	W36×150
13th	15×15×1.00	W27×336	W27×336	No	W36×150
12th	15×15×1.00	W27×368	W27×368	No	W36×170
11th	15×15×1.25	W27×368	W27×368	No	W36×170
10th	15×15×1.25	W27×539	W27×539	No	W36×182
9th	15×15×1.25	W27×539	W27×539	No	W36×182
8th	15×15×1.50	W27×539	W27×539	No	W36×194
7th	15×15×1.50	W27×539	W27×539	No	W36×194
6th	15×15×1.50	W27×539	W27×539	No	W36×210
5th	15×15×2.00	W27×539	W27×539	No	W36×210
4th	15×15×2.00	W27×539	W27×539	No	W36×210
3rd	15×15×2.00	W27×539	W27×539	No	W36×210
2nd	15×15×2.00	W27×539	W27×539	No	W36×262
Level 1	15×15×2.00	W27×539	W27×539	No	W30×116
Basement	15×15×2.00	W27×539	W27×539	No	W27×94

Notes: Model 2: MRSA Design, No Doubler Plates
Steel Tonnage 7.04 psf (Columns: 3.67 psf, Beams: 3.37 psf)

Table C-26 V02002022 Baseline

MRSA Design					
	Columns				
		East-West Frame		Doubler Plates	Girder
Story/Floor	Ext [HSS Section]	Next to Ext	Int		
Roof	15×15×1.00	W27×194	W27×194	No	W24×76
20th	15×15×1.00	W27×194	W27×194	No	W24×76
19th	15×15×1.00	W27×281	W27×281	No	W30×108
18th	15×15×1.00	W27×281	W27×281	No	W30×108
17th	15×15×1.00	W27×281	W27×281	No	W30×108
16th	15×15×1.00	W27×307	W27×307	No	W30×116
15th	15×15×1.00	W27×307	W27×307	No	W30×116
14th	15×15×1.00	W27×307	W27×307	No	W33×130
13th	15×15×1.00	W27×307	W27×307	No	W33×130
12th	15×15×1.00	W27×307	W27×307	No	W33×130
11th	15×15×1.25	W27×336	W27×336	No	W36×150
10th	15×15×1.25	W27×336	W27×336	No	W36×150
9th	15×15×1.25	W27×336	W27×336	No	W36×150
8th	15×15×1.50	W27×336	W27×336	No	W36×150
7th	15×15×1.50	W27×336	W27×336	No	W36×150
6th	15×15×1.50	W27×336	W27×336	No	W36×150
5th	15×15×2.00	W27×336	W27×336	No	W36×150
4th	15×15×2.00	W27×368	W27×368	No	W36×160
3rd	15×15×2.00	W27×368	W27×368	No	W36×170
2nd	15×15×2.00	W27×539	W27×539	No	W36×182
Level 1	15×15×2.00	W27×539	W27×539	No	W30×116
Basement	15×15×2.00	W27×539	W27×539	No	W27×94

Notes: Model 2: MRSA Design, No Doubler Plates
Steel Tonnage 7.04 psf (Columns: 3.67 psf, Beams: 3.37 psf)

C.2 Summary of Steel Moment Frame Results

Table C-27 Steel Moment Frame Results

Model ID	Design Configuration					Building Performance Summary			
	No. of Stories	Irregularity	SDC	Design Method	Design Period (C_uT_a) [s]	OpenSees Model Period [s]	Static Over-strength, Ω	*ACMR* (const. *SSF*)	*ACMR*/ $ACMR_{baseline}$
V00301011	3	Baseline_MRS _Non-SCWB	B_{max}	MRSA	0.859	1.55	3.20	4.42	1.00
V00301012	3	Baseline_MRS _Non-SCWB	B_{max}	MRSA	0.859	1.80	2.51	3.76	1.00
V00301021	3	Baseline_ELF _Non-SCWB	B_{max}	ELF	0.859	1.39	3.58	4.07	1.00
V00301022	3	Baseline_ELF _Non-SCWB	B_{max}	ELF	0.859	1.61	2.86	3.43	1.00
V00301031	3	Baseline_MRS _SCWB	B_{max}	MRSA	0.859	1.48	3.25	7.01	1.00
V00301032	3	Baseline_MRS _SCWB	B_{max}	MRSA	0.859	1.72	2.53	6.01	1.00
V00301041	3	Baseline_ELF _SCWB	B_{max}	ELF	0.859	1.66	2.05	3.98	1.00
V00301042	3	Baseline_ELF _SCWB	B_{max}	ELF	0.859	1.93	1.60	3.84	1.00
V00301051	3	Baseline_MRS SCWB (No Doubl. Plates)	B_{max}	MRSA	0.859	1.34	4.32	8.04	1.00
V00301052	3	Baseline_MRS SCWB (No Doubl. Plates)	B_{max}	MRSA	0.859	1.55	3.36	6.84	1.00
V60301011	3	SCWB 0.4	B_{max}	ELF	0.859	1.56	2.21	4.87	1.04
V60301012	3	SCWB 0.4	B_{max}	ELF	0.859	1.81	1.71	4.34	0.99
V60301021	3	SCWB 0.7	B_{max}	ELF	0.859	1.55	2.44	4.45	0.95
V60301022	3	SCWB 0.7	B_{max}	ELF	0.859	1.79	1.87	4.11	0.94
V60301031	3	SCWB 1.0	B_{max}	ELF	0.859	1.47	3.25	4.68	1.00
V60301032	3	SCWB 1.0	B_{max}	ELF	0.859	1.71	2.24	4.37	1.00
V00901011	9	Baseline_Non -SCWB	B_{max}	MRSA	2.138	2.94	4.54	3.93	1.00
V00901012	9	Baseline_Non -SCWB	B_{max}	MRSA	2.138	2.89	4.60	4.41	1.00
V00901021	9	Baseline_SCWB (No Dbl. Plates)	B_{max}	MRSA	2.138	2.84	7.43	5.42	1.00

Table C-27 Steel Moment Frame Results (continued)

Model ID	Design Configuration					Building Performance Summary			
	No. of Stories	Irregularity	SDC	Design Method	Design Period (C_uT_a) [s]	OpenSees Model Period [s]	Static Over-strength, Ω	*ACMR* (const. *SSF*)	*ACMR*/ $ACMR_{baseline}$
V00901022	9	Baseline_SCWB (No Dbl. Plates)	B_{max}	MRSA	2.138	2.71	7.96	5.40	1.00
V60901011	9	SCWB 0.4	B_{max}	MRSA	2.138	2.50	4.82	8.32	1.53
V60901012	9	SCWB 0.4	B_{max}	MRSA	2.138	2.46	4.85	8.93	1.60
V60901021	9	SCWB 0.7	B_{max}	MRSA	2.138	2.76	4.34	5.24	0.97
V60901022	9	SCWB 0.7	B_{max}	MRSA	2.138	2.71	4.40	5.48	0.98
V60901031	9	SCWB 1.0	B_{max}	MRSA	2.138	2.82	4.45	5.43	1.00
V60901032	9	SCWB 1.0	B_{max}	MRSA	2.138	2.77	4.53	5.58	1.00
V02001011	20	Non-SCWB	B_{max}	MRSA	3.977	3.51	8.16	9.16	1.00
V02001012	20	Non-SCWB	B_{max}	MRSA	3.977	3.48	7.90	9.72	1.00
V02001021	20	Baseline	B_{max}	MRSA	3.977	3.41	9.09	5.19	1.00
V02001022	20	Baseline	B_{max}	MRSA	3.977	3.45	8.90	6.27	1.00
V62001011	20	SCWB 0.4	B_{max}	MRSA	3.977	3.33	7.01	5.01	1.02
V62001012	20	SCWB 0.4	B_{max}	MRSA	3.977	3.29	6.62	7.20	1.12
V62001021	20	SCWB 0.7	B_{max}	MRSA	3.977	3.31	7.77	5.55	1.13
V62001022	20	SCWB 0.7	B_{max}	MRSA	3.977	3.29	7.93	6.88	1.08
V62001031	20	SCWB 1.0	B_{max}	MRSA	3.977	3.30	9.59	4.90	1.00
V62001032	20	SCWB 1.0	B_{max}	MRSA	3.977	3.30	9.21	6.40	1.00
V72001011	20	1st Story $\alpha = 0.1$	B_{max}	MRSA	3.98	3.51	8.15	8.47	0.96
V72001021	20	1st Story $\alpha = 0.3$	B_{max}	MRSA	3.98	3.51	8.11	8.10	0.92
V72001031	20	1st Story $\alpha = 0.5$	B_{max}	MRSA	3.98	3.50	8.08	7.71	0.87
V72001041	20	7th Story $\alpha = 0.1$	B_{max}	MRSA	3.98	3.51	8.05	8.33	0.94
V72001051	20	7th Story $\alpha = 0.3$	B_{max}	MRSA	3.98	3.50	7.91	8.12	0.92
V72001061	20	7th Story $\alpha = 0.5$	B_{max}	MRSA	3.98	3.49	8.00	8.70	0.99
V72001071	20	14th Story $\alpha = 0.1$	B_{max}	MRSA	3.98	3.51	8.10	8.70	0.99
V72001081	20	14th Story $\alpha = 0.3$	B_{max}	MRSA	3.98	3.51	7.96	8.14	0.92

Table C-27 Steel Moment Frame Results (continued)

Model ID	Design Configuration					Building Performance Summary			
	No. of Stories	Irregularity	SDC	Design Method	Design Period ($C_u T_a$) [s]	OpenSees Model Period [s]	Static Over-strength, Ω	*ACMR* (const. *SSF*)	*ACMR*/ $ACMR_{baseline}$
V72001091	20	14th Story $\alpha = 0.5$	B_{max}	MRSA	3.98	3.51	7.80	8.34	0.95
V00302011	3	Baseline_MRS	D_{max}	MRSA	0.735	1.18	2.33	2.37	1.00
V00302012	3	Baseline_MRS	D_{max}	MRSA	0.735	1.19	2.26	2.23	1.00
V00302021	3	Baseline_MRS (No Dbl Plates)	D_{max}	MRSA	0.735	1.12	2.68	2.27	1.00
V00302022	3	Baseline_MRS (No Dbl Plates)	D_{max}	MRSA	0.735	1.13	2.60	2.21	1.00
V00302031	3	Baseline_ELF	D_{max}	ELF	0.735	0.80	4.73	2.92	1.00
V00302032	3	ELF	D_{max}	ELF	0.735	0.80	4.61	2.89	1.00
V00302041	3	Energy Method	D_{max}	Energy	0.735	0.79	4.71	3.04	1.00
V00302042	3	Energy Method	D_{max}	Energy	0.735	0.80	4.59	3.05	1.00
V20302011	3	Baseline_MRS	D_{max}	MRSA	0.735	1.09	2.74	2.39	1.00
V20302012	3	Baseline_MRS	D_{max}	MRSA	0.735	1.11	2.66	2.28	1.00
V20302021	3	MR 1.5_FLR2 _MRS	D_{max}	MRSA	0.735	1.11	2.47	2.18	0.91
V20302022	3	MR 1.5_FLR2 _MRS	D_{max}	MRSA	0.735	1.12	2.38	2.07	0.91
V20302031	3	MR2.0_FLR2	D_{max}	MRSA	0.735	1.12	2.25	2.10	0.88
V20302032	3	MR2.0_FLR2 _MRS	D_{max}	MRSA	0.735	1.13	2.17	1.87	0.82
V20302041	3	MR3.0_FLR2	D_{max}	MRSA	0.735	1.15	1.90	1.83	0.77
V20302042	3	MR3.0_FLR2 _MRS	D_{max}	MRSA	0.735	1.16	1.82	1.74	0.77
V20302051	3	MR3.0_FLR3 _MRS	D_{max}	MRSA	0.735	1.16	2.27	1.77	0.74
V20302052	3	MR3.0_FLR3_ MRS	D_{max}	MRSA	0.735	1.17	2.19	1.72	0.76
V20302061	3	Baseline_ELF	D_{max}	ELF	0.735	0.80	4.72	2.87	1.00
V20302062	3	Baseline_ELF	D_{max}	ELF	0.735	0.80	4.60	2.82	1.00
V20302071	3	MR 1.5_FLR2 _ELF	D_{max}	ELF	0.735	0.80	4.24	2.64	0.92
V20302072	3	MR 1.5_FLR2 _ELF	D_{max}	ELF	0.735	0.81	4.13	2.58	0.91
V20302081	3	MR 1.5_FLR2 _ELF (revised)	D_{max}	ELF	0.735	0.77	4.18	2.83	0.99

Table C-27 Steel Moment Frame Results (continued)

Model ID	Design Configuration					Building Performance Summary			
	No. of Stories	Irregularity	SDC	Design Method	Design Period (C_uT_a) [s]	OpenSees Model Period [s]	Static Over-strength, Ω	*ACMR* (const. *SSF*)	$ACMR/ACMR_{baseline}$
V20302082	3	MR 1.5_FLR2 _ELF (revised)	D_{max}	ELF	0.735	0.77	4.08	2.73	0.97
V20302091	3	MR2.0_FLR2 _ELF	D_{max}	ELF	0.735	0.72	3.89	2.59	0.90
V20302092	3	MR2.0_FLR2 _ELF	D_{max}	ELF	0.735	0.72	3.80	2.49	0.88
V20302101	3	MR3.0_FLR2 _ELF	D_{max}	ELF	0.735	0.73	4.08	2.36	0.82
V20302102	3	MR3.0_FLR2 _ELF	D_{max}	ELF	0.735	0.74	3.98	2.31	0.82
V20302111	3	MR3.0_FLR3 _ELF	D_{max}	ELF	0.735	0.76	4.84	2.62	0.91
V20302112	3	MR3.0_FLR3 _ELF	D_{max}	ELF	0.735	0.76	4.74	2.55	0.90
V60302011	3	SCWB 0.5	D_{max}	MRSA	0.735	1.65	2.05	2.01	0.88
V60302012	3	SCWB 0.5	D_{max}	MRSA	0.735	1.66	1.95	1.92	0.85
V60302021	3	SCWB 1.0	D_{max}	MRSA	0.735	1.32	2.47	2.30	1.00
V60302022	3	SCWB 1.0	D_{max}	MRSA	0.735	1.33	2.40	2.26	1.00
V60302031	3	SCWB 1.2	D_{max}	MRSA	0.735	1.45	2.29	2.44	1.06
V60302032	3	SCWB 1.2	D_{max}	MRSA	0.735	1.46	2.21	2.41	1.07
V60302041	3	SCWB 1.5	D_{max}	MRSA	0.735	1.47	1.98	2.16	0.94
V60302042	3	SCWB 1.5	D_{max}	MRSA	0.735	1.49	1.91	2.10	0.93
V60302051	3	SCWB 2.0	D_{max}	MRSA	0.735	1.38	2.31	2.25	0.98
V60302052	3	SCWB 2.0	D_{max}	MRSA	0.735	1.40	2.24	2.12	0.94
V00902011	9	Baseline _Conforming - AISC 341-10	D_{max}	MRSA	1.83	2.82	1.84	2.08	1.00
V00902012	9	Baseline _Conforming - AISC 341-10	D_{max}	MRSA	1.83	2.86	1.80	1.99	1.00
V00902021	9	Baseline _Conforming - AISC 341-10 No Dbl	D_{max}	MRSA	1.83	2.81	1.84	2.22	1.00
V00902022	9	Baseline _Conforming - AISC 341-10 No Dbl	D_{max}	MRSA	1.83	2.84	1.80	2.08	1.00

Table C-27 Steel Moment Frame Results (continued)

Model ID	Design Configuration					Building Performance Summary			
	No. of Stories	Irregularity	SDC	Design Method	Design Period (C_uT_a) [s]	OpenSees Model Period [s]	Static Over-strength, Ω	*ACMR* (const. *SSF*)	$ACMR/ACMR_{baseline}$
V00902031	9	Baseline_Conforming - ELF No Dbl	D_{max}	ELF	1.83	1.81	4.26	3.07	1.00
V00902032	9	Baseline _Conforming - ELF No Dbl	D_{max}	ELF	1.83	1.83	4.17	2.87	1.00
V00902041	9	Baseline _Conforming - Energy	D_{max}	Energy	1.83	1.28	5.65	4.39	1.00
V00902042	9	Baseline _Conforming - Energy	D_{max}	Energy	1.83	1.30	5.54	4.39	1.00
V60902011	9	SCWB 0.5	D_{max}	MRSA	1.83	2.21	2.55	1.02	0.69
V60902012	9	SCWB 0.5	D_{max}	MRSA	1.83	2.23	2.36	0.93	0.74
V60902021	9	SCWB 1.0	D_{max}	MRSA	1.83	2.87	1.64	1.47	1.00
V60902022	9	SCWB 1.0	D_{max}	MRSA	1.83	2.90	1.56	1.27	1.00
V60902031	9	SCWB 1.2	D_{max}	MRSA	1.83	3.08	1.46	1.42	0.97
V60902032	9	SCWB 1.2	D_{max}	MRSA	1.83	3.11	1.39	1.30	1.03
V60902041	9	SCWB 1.5	D_{max}	MRSA	1.83	3.00	1.57	1.75	1.20
V60902042	9	SCWB 1.5	D_{max}	MRSA	1.83	3.03	1.53	1.65	1.30
V60902051	9	SCWB 2.0	D_{max}	MRSA	1.83	2.95	1.55	1.97	1.34
V60902052	9	SCWB 2.0	D_{max}	MRSA	1.83	2.99	1.51	1.86	1.47
V02002011	20	Baseline _Conforming - AISC 341-10	D_{max}	MRSA	3.403	3.53	1.67	2.01	1.00
V02002012	20	Baseline _Conforming - AISC 341-10	D_{max}	MRSA	3.403	3.11	2.11	1.78	1.00
V02002021	20	Conforming - AISC 341-10 No Dbl	D_{max}	MRSA	3.403	3.58	1.66	1.93	1.00
V02002022	20	Baseline _Conforming - AISC 341-10 No Dbl	D_{max}	MRSA	3.403	3.17	2.09	1.38	1.00
V22002011	20	Baseline - Mass	D_{max}	MRSA	3.403	3.53	1.67	2.12	1.00
V22002012	20	Baseline - Mass	D_{max}	MRSA	3.403	3.11	2.11	2.02	1.00
V22002021	20	1.5_STORY3	D_{max}	MRSA	3.403	3.52	1.65	1.96	0.92

Table C-27 Steel Moment Frame Results (continued)

Model ID	Design Configuration					Building Performance Summary			
	No. of Stories	Irregularity	SDC	Design Method	Design Period ($C_u T_a$) [s]	OpenSees Model Period [s]	Static Over-strength, Ω	*ACMR* (const. *SSF*)	*ACMR*/ $ACMR_{baseline}$
V22002022	20	1.5_STORY3	D_{max}	MRSA	3.403	3.10	2.09	1.96	0.97
V22002031	20	2.0_STORY3	D_{max}	MRSA	3.403	3.52	1.62	1.91	0.90
V22002032	20	2.0_STORY3	D_{max}	MRSA	3.403	3.10	2.05	2.00	0.99
V22002041	20	3.0_STORY3	D_{max}	MRSA	3.403	3.52	1.58	1.75	0.82
V22002042	20	3.0_STORY3	D_{max}	MRSA	3.403	3.10	2.00	1.81	0.90
V22002051	20	1.5_STORY11	D_{max}	MRSA	3.403	3.56	1.66	2.03	0.96
V22002052	20	1.5_STORY11	D_{max}	MRSA	3.403	3.65	1.58	1.72	0.85
V22002061	20	2.0_STORY11	D_{max}	MRSA	3.403	3.58	1.65	1.96	0.93
V22002062	20	2.0_STORY11	D_{max}	MRSA	3.403	3.68	1.55	1.86	0.92
V22002071	20	3.0_STORY11	D_{max}	MRSA	3.403	3.69	1.69	1.92	0.91
V22002072	20	3.0_STORY11	D_{max}	MRSA	3.403	3.80	1.49	1.61	0.80
V22002081	20	1.5_STORY19	D_{max}	MRSA	3.403	3.62	1.63	2.16	1.02
V22002082	20	1.5_STORY19	D_{max}	MRSA	3.403	3.72	1.58	1.90	0.94
V22002091	20	2.0_STORY19	D_{max}	MRSA	3.403	3.68	1.64	2.02	0.95
V22002092	20	2.0_STORY19	D_{max}	MRSA	3.403	3.77	1.55	1.87	0.92
V22002101	20	3.0_STORY19	D_{max}	MRSA	3.403	3.78	1.61	1.89	0.89
V22002102	20	3.0_STORY19	D_{max}	MRSA	3.403	3.80	1.72	1.78	0.88
V62002011	20	SCWB 0.5	D_{max}	MRSA	3.4	3.93	1.09	1.80	0.89
V62002012	20	SCWB 0.5	D_{max}	MRSA	3.4	3.49	1.36	2.10	0.77
V62002021	20	SCWB 1.0	D_{max}	MRSA	3.4	3.75	1.56	2.03	1.00
V62002022	20	SCWB 1.0	D_{max}	MRSA	3.4	3.31	1.96	2.71	1.00
V62002031	20	SCWB 1.2	D_{max}	MRSA	3.4	3.51	1.84	2.08	1.02
V62002032	20	SCWB 1.2	D_{max}	MRSA	3.4	3.10	2.33	1.34	0.50
V62002041	20	SCWB 1.5	D_{max}	MRSA	3.4	3.54	1.79	1.63	0.80
V62002042	20	SCWB 1.5	D_{max}	MRSA	3.4	3.13	2.27	1.24	0.46
V62002051	20	SCWB 2.0	D_{max}	MRSA	3.4	3.50	1.68	1.91	0.94
V62002052	20	SCWB 2.0	D_{max}	MRSA	3.4	3.08	2.13	1.30	0.48
V72002011	20	1st Story $\alpha = 0.1$	D_{max}	MRSA	3.403	3.53	1.67	1.75	0.87
V72002021	20	1st Story $\alpha = 0.3$	D_{max}	MRSA	3.403	3.48	1.69	2.09	1.04

Table C-27 Steel Moment Frame Results (continued)

Model ID	Design Configuration					Building Performance Summary			
	No. of Stories	Irregularity	SDC	Design Method	Design Period ($C_u T_a$) [s]	OpenSees Model Period [s]	Static Over-strength, Ω	*ACMR* (const. *SSF*)	*ACMR*/ $ACMR_{baseline}$
V72002031	20	1st Story $\alpha = 0.5$	D_{max}	MRSA	3.403	3.45	1.71	1.94	0.97
V72002041	20	7th Story $\alpha = 0.1$	D_{max}	MRSA	3.403	3.52	1.69	2.04	1.02
V72002051	20	7th Story $\alpha = 0.3$	D_{max}	MRSA	3.403	3.59	1.77	1.86	0.92
V72002061	20	7th Story $\alpha = 0.5$	D_{max}	MRSA	3.403	3.54	1.81	1.81	0.90
V72002071	20	14th Story $\alpha = 0.1$	D_{max}	MRSA	3.403	3.64	1.67	1.99	0.99
V72002081	20	14th Story $\alpha = 0.3$	D_{max}	MRSA	3.403	3.61	1.67	1.95	0.97
V72002091	20	14th Story $\alpha = 0.5$	D_{max}	MRSA	3.403	3.53	1.69	1.99	0.99
V720020012	20	Baseline - GILD Undesigned	D_{max}	MRSA	3.403	0.00	1.67	2.01	1.00
V720020212	20	1st Story $\alpha = 0.3$	D_{max}	MRSA	3.403	3.53	1.66	1.84	0.92
V720020312	20	1st Story $\alpha = 0.5$	D_{max}	MRSA	3.403	3.53	1.64	1.77	0.88
V720020812	20	14th Story $\alpha = 0.3$	D_{max}	MRSA	3.403	3.53	1.67	1.88	0.94
V720020912	20	14th Story $\alpha = 0.5$	D_{max}	MRSA	3.403	3.53	1.66	1.05	0.52

Appendix D
Concrete Moment Frame Studies

This Appendix provides the following information on the concrete moment frame studies: (1) B_{max} and D_{max} concrete moment frame baseline designs; and (2) summary of the concrete moment frame archetype results. For details on the concrete moment frame designs with irregularities (i.e., soft story, mass ratio irregularity, weak story, strong-column/weak-beam, and gravity-induced lateral demand) and for detailed results of the concrete moment frame studies, see the electronic Supporting Documentation for Appendix D: Concrete Moment Frame Irregularity Designs and Detailed Results.

D.1 Concrete Moment Frame Baseline Designs

The intent of the archetype designs is to create structural models that represent realistic modern structures. In order to achieve that goal, design assumptions and structural properties were selected to represent common building stock and design practice. The archetype space includes 4-, 8-, 12-, and 20-story buildings each in high and low seismicity zones (see Table D-1). Hypothetical B_{max} and D_{max} sites were selected for the low and high seismicity zones respectively. Table D-2 provides a summary of the design values used for all concrete moment frame designs.

Table D-1 Summary of Baseline Reinforced Concrete Frame Archetypes

Baseline Reinforced Concrete Moment Frame Designs				
Model ID	Number of Stories	Frame Detail	SDC	Modification
V104101	4	SMF	D_{max}	Baseline
V104201	4	OMF	B_{max}	Baseline
V108101	8	SMF	D_{max}	Baseline
V112101	12	SMF	D_{max}	Baseline
V112201	12	OMF	B_{max}	Baseline
V120101	20	SMF	D_{max}	Baseline

Table D-2 Common Design Values Used for All RC MF Designs

Common Design Properties	
Dead Load	175 psf
Partition Load	15 psf
Roof Load	140 psf
Live Load	65 psf
f'_c Beams	5000 psi
f'_c Col	7000 psi
Beam Design Stiffness	$0.35EI_g$
Column Design Stiffness	$0.7EI_g$

D.1.1 Low Seismicity Zone (SDC B_{max}) – RC Ordinary Moment Frame Design

D.1.1.1 4-Story OMF Building

Figures D-1 and D-2 illustrate the geometry of the 4-story RC ordinary moment frame (OMF) building. Tables D-3 and D-4 provide design values and a summary of the design, respectively, for the 4-story OMF building.

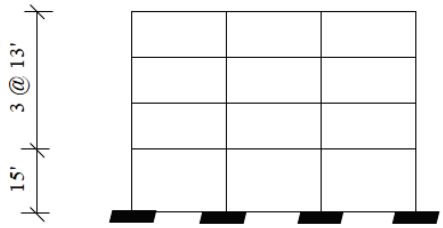

Figure D-1 Baseline RC moment frame building typical 4-story elevation.

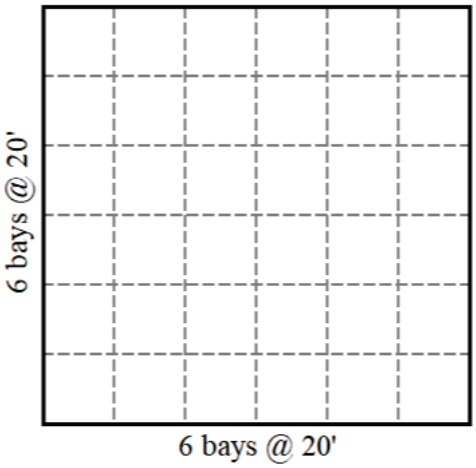

Figure D-2 Baseline RC moment frame building typical 4-story plan.

Table D-3 Design Values – 4-Story RC OMF Baseline

4-story, RC OMF (V104201)	
Design Parameters	
Dead Load:	Typical = 175 psf; Roof = 140 psf
Live Load:	Typical = 65 psf; Roof = 20 psf
Seismic Weight:	Typical = 190 psf; Roof = 147.5 psf
Total Tributary Seismic Weight:	W = 2583 kips
Wind Speed:	110 mph (strength); 85 mph (service)
Risk Category:	II
Importance Factor:	I_e = 1.0
Reinforced Concrete SMFs:	R = 3; C_d = 2.5; Ω_0 = 3
Site Class C Seismic Design Category D:	S_{DS} = 0.32; S_{D1} = 0.132
Material properties:	$f'_{c,\ beam}$ = 4 ksi; $f'_{c,\ col}$ = 4 ksi; f_y = 60 ksi
Analysis	
Centerline modeling of beams and columns Rigid diaphragms:	$I_{beam} = 0.35I_g$; $I_{col} = 0.70I_g$
Design based on Equivalent Lateral Force Procedure	
Calculated period(s):	T_x = 1.933 s; T_y = 1.933 s
Upper limit period:	C_uT_{ax} = 0.93 s; C_uT_{ay} = 0.93 s
Seismic response coefficient:	$C_{s,x}$ = 0.048; $C_{s,x}$ = 0.048
Controlling equation:	(12.8-3)
Seismic base shear:	V_x = 123 kips; V_y = 123 kips
Story drift limits applied:	$0.020h_{sx}$ (seismic); h/400 (wind)
Design base shear:	V_x = 123 kips; V_y = 123 kips
Controlling lateral design:	Seismic strength

Table D-4 4-Story RC OMF Baseline Design Summary: V104201

Level	Columns depth × width [tie spacing] (ρ_{total}, ρ_{sh})		Beams depth × width [hoop spacing] (ρ_{top}, ρ_{bot}, ρ_{sh})		Story Drift Δ	Strength and Stiffness Ratio to Story Above Strength (Stiffness)
	Exterior	Interior	Exterior	Interior		
4	21×18 [9]	21×18 [18]	18×18 [7.5]	18×18 [7.5]	0.05%	N/A
	(0.0125, 0.0014)	(0.0125, 0.0007)	(0.0106, 0.0047, 0.0016)	(0.0106, 0.0047, 0.0016)		(N/A)
3	21×18 [9]	21×18 [9]	18×18 [7.5]	18×18 [7.5]	0.6%	0.89
	(0.0125, 0.0014)	(0.0125, 0.0014)	(0.0121, 0.0047, 0.0016)	(0.0121, 0.0047, 0.0016)		(1.49)
2	21×18 [9]	21×18 [9]	24×18 [10.5]	24×18 [10.5]	0.6%	1.35
	(0.0125, 0.0014)	(0.0125, 0.0014)	(0.0110, 0.0057, 0.0012)	(0.0110, 0.0057, 0.0012)		(1.25)
1	21×18 [9]	21×18 [9]	24×18 [10.5]	24×18 [10.5]	0.5%	1.09
	(0.0208, 0.0014)	(0.0208, 0.0014)	(0.0110, 0.0057, 0.0012)	(0.0110, 0.0057, 0.0012)		(1.15)

D.1.1.2 8-Story OMF Building

No 8-story RC ordinary moment frames were developed for this study.

D.1.1.3 12-Story OMF Building

Figures D-3 and D-4 illustrate the geometry of the 12-story RC OMF building. Tables D-5 and D-6 provide design values and a summary of the design, respectively, for the 12-story OMF building.

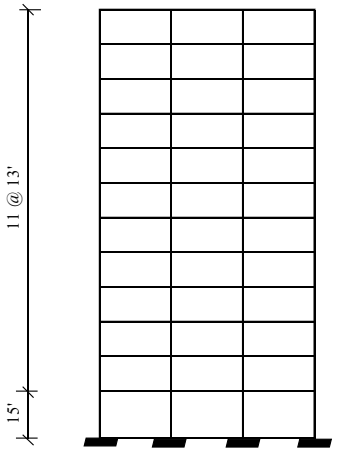

Figure D-3 Baseline RC moment frame building typical 12-story elevation.

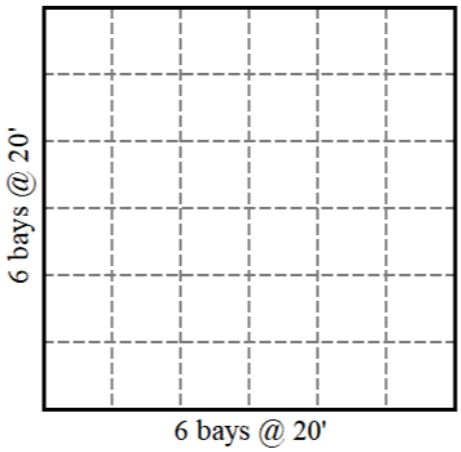

Figure D-4 Baseline RC moment frame building typical 12-story plan.

Table D-5 Design Values – 12-Story RC OMF Baseline

12-story, RC OMF (V112201)	
Design Parameters	
Dead Load:	Typical = 175 psf; Roof = 140 psf
Live Load:	Typical = 65 psf; Roof = 20 psf
Seismic Weight:	Typical = 190 psf; Roof = 147.5 psf
Total Tributary Seismic Weight:	W = 8055 kips
Wind Speed:	110 mph (strength); 85 mph (service)
Risk Category:	II
Importance Factor:	I_e = 1.0
Reinforced Concrete SMFs:	R = 3; C_d = 2.5; Ω_0 = 3
Site Class C Seismic Design Category D:	S_{DS} = 0.32; S_{D1} = 0.132
Material properties:	$f'_{c,\,beam}$ = 4 ksi; $f'_{c,\,col}$ = 4 ksi; f_y = 60 ksi
Analysis	
Centerline modeling of beams and columns Rigid diaphragms:	$I_{beam} = 0.35I_g$; $I_{col} = 0.70I_g$
Design based on Equivalent Lateral Force Procedure	
Calculated period(s):	T_x = 4.506 s; T_y = 4.506 s
Upper limit period:	C_uT_{ax} = 2.44 s; C_uT_{ay} = 2.44 s
Seismic response coefficient:	$C_{s,x}$ = 0.018; $C_{s,x}$ = 0.018
Controlling equation:	(12.8-3)
Seismic base shear:	V_x = 146 kips; V_y = 146 kips
Story drift limits applied:	$0.020h_{sx}$ (seismic); h/400 (wind)
Design base shear:	V_x = 147.5 kips (wind); V_y = 147.5 kips (wind)
Controlling lateral design:	Seismic strength & wind strength

Table D-6 12-Story RC OMF Baseline Design Summary: V112201

Level	Columns depth x width [tie spacing] (ρ_{total}, ρ_{sh})		Beams depth x width [hoop spacing] (ρ_{top}, ρ_{bot}, ρ_{sh})		Story Drift Δ	Strength and Stiffness Ratio to Story Above Strength (Stiffness)
	Exterior	Interior	Exterior	Interior		
12	21×21 [9]	21×21 [18]	21×21 [9]	21×21 [9]	0.2%	NA
	(0.0107, 0.0012)	(0.0107, 0.0006)	(0.0065, 0.0034, 0.0012)	(0.0065, 0.0034, 0.0012)		(NA)
11	21×21 [9]	21×21 [9]	21×21 [9]	21×21 [9]	0.3%	0.97
	(0.0107, 0.0012)	(0.0107, 0.0012)	(0.0087, 0.0034, 0.0012)	(0.0087, 0.0034, 0.0012)		(1.27)
10	21×21 [9]	21×21 [9]	21×21 [9]	21×21 [9]	0.5%	1.02
	(0.0107, 0.0012)	(0.0107, 0.0012)	(0.0099, 0.0034, 0.0012)	(0.0099, 0.0034, 0.0012)		(1.05)
9	21×21 [9]	21×21 [9]	21×21 [9]	21×21 [9]	0.6%	1.08
	(0.0107, 0.0012)	(0.0107, 0.0012)	(0.0110, 0.0045, 0.0012)	(0.0110, 0.0045, 0.0012)		(1.02)
8	21×21 [9]	21×21 [9]	24×21 [10.5]	24×21 [10.5]	0.6%	1.06
	(0.0107, 0.0012)	(0.0107, 0.0012)	(0.0095, 0.0049, 0.0010)	(0.0095, 0.0049, 0.0010)		(1.02)
7	21×21 [9]	21×21 [9]	24×21 [10.5]	24×21 [10.5]	0.7%	1.21
	(0.0142, 0.0012)	(0.0142, 0.0012)	(0.0095, 0.0049, 0.0010)	(0.0095, 0.0049, 0.0010)		(1.1)
6	21×21 [9]	21×21 [9]	27×21 [12]	27×21 [12]	0.6%	1.12
	(0.0142, 0.0012)	(0.0142, 0.0012)	(0.0083, 0.0043, 0.0009)	(0.0083, 0.0043, 0.0009)		(1.11)
5	21×21 [9]	21×21 [9]	27×21 [12]	27×21 [12]	0.6%	1.02
	(0.0142, 0.0012)	(0.0142, 0.0012)	(0.0083, 0.0043, 0.0009)	(0.0083, 0.0043, 0.0009)		(1.15)
4	21×21 [9]	21×21 [9]	33×21 [10]	33×21 [10]	0.5%	1.15
	(0.0142, 0.0012)	(0.0142, 0.0012)	(0.0067, 0.0034, 0.0011)	(0.0067, 0.0034, 0.0011)		(1.16)
3	21×21 [9]	21×21 [9]	33×21 [10.5]	33×21 [10.5]	0.5%	1.03
	(0.0142, 0.0012)	(0.0142, 0.0012)	(0.0067, 0.0034, 0.0010)	(0.0067, 0.0034, 0.0010)		(1.03)
2	21×21 [9]	21×21 [9]	33×21 [10.5]	33×21 [10.5]	0.5%	1.02
	(0.0142, 0.0012)	(0.0142, 0.0012)	(0.0067, 0.0034, 0.0010)	(0.0067, 0.0034, 0.0010)		(1.01)
1	21×21 [9]	21×21 [9]	33×21 [10.5]	33×21 [10.5]	0.5%	0.99
	(0.0178, 0.0012)	(0.0178, 0.0012)	(0.0067, 0.0041, 0.0010)	(0.0067, 0.0041, 0.0010)		(0.94)

D.1.2 High Seismicity Zone (SDC D_{max}) – RC Special Moment Frame Design

D.1.2.1 4-Story SMF

Figures D-5 and D-6 illustrate the geometry of the 4-story RC special moment frame (SMF) building. Tables D-7 and D-8 provide design values and a summary of the design, respectively, for the 4-story SMF building.

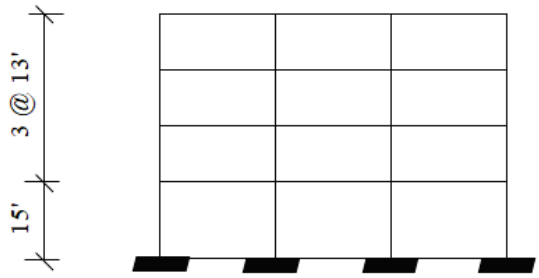

Figure D-5 Baseline RC moment frame building typical 4-story elevation.

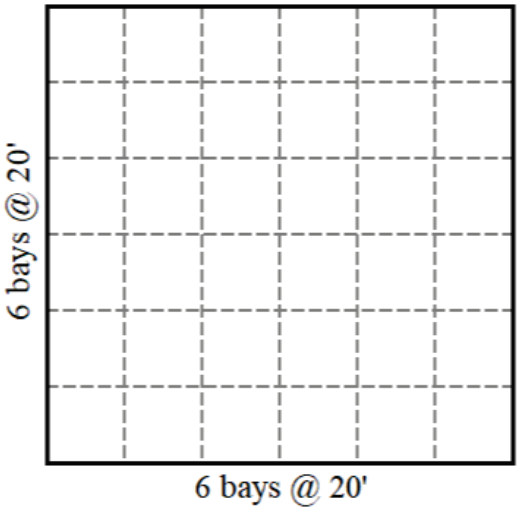

Figure D-6 Baseline RC moment frame building typical 4-story plan.

Table D-7 Design Values – Baseline 4-Story RC SMF

4-story, RC SMF (V104101)	
Design Parameters	
Dead Load:	Typical = 175 psf; Roof = 140 psf
Live Load:	Typical = 65 psf; Roof = 20 psf
Seismic Weight:	Typical = 190 psf; Roof = 147.5 psf
Total Tributary Seismic Weight:	W = 2583 kips
Wind Speed:	110 mph (strength); 85 mph (service)
Risk Category:	II
Importance Factor:	I_e = 1.0

Table D-7 Design Values – Baseline 4-Story RC SMF (continued)

4-story, RC SMF (V104101)	
Design Parameters (continued)	
Reinforced Concrete SMFs:	$R = 8$; $C_d = 5.5$; $\Omega_0 = 3.0$
Site Class C Seismic Design Category D:	$S_{DS} = 1.5$; $S_{D1} = 0.6$
Material properties:	$f'_{c,\,beam} = 5$ ksi; $f'_{c,\,col} = 7$ ksi; $f_y = 60$ ksi
Analysis	
Centerline modeling of beams and columns Rigid diaphragms:	$I_{beam} = 0.35I_g$; $I_{col} = 0.70I_g$
Design based on Equivalent Lateral Force Procedure	
Calculated period(s):	$T_x = 1.12$ s; $T_y = 1.12$ s
Upper limit period:	$C_uT_{ax} = 0.81$ s; $C_uT_{ay} = 0.81$ s
Seismic response coefficient:	$C_{s,x} = 0.092$; $C_{s,x} = 0.092$
Controlling equation:	(12.8-3)
Seismic base shear:	$V_x = 239$ kips; $V_y = 239$ kips
Story drift limits applied:	$0.020h_{sx}$ (seismic); $h/400$ (wind)
Design base shear:	$V_x = 239$ kips; $V_y = 239$ kips
Controlling lateral design:	Seismic strength

Table D-8 4-Story RC SMF Baseline Design Summary: V104101

Level	Columns depth × width [tie spacing] (ρ_{total}, ρ_{sh})		Beams depth × width [hoop spacing] (ρ_{top}, ρ_{bot}, ρ_{sh})		Story Drift Δ	Moment ratio, $\Sigma M_c/\Sigma M_b$ Exterior (Interior)	Strength and Stiffness Ratio to Story Above Strength (Stiffness)
	Exterior	Interior	Exterior	Interior			
4	26×22 [2.5]	26×22 [2.5]	24×18 [5]	24×18 [5]	1.2%	1.16	NA
	(0.0110, 0.0107)	(0.0110, 0.0107)	(0.0081, 0.0046, 0.0044)	(0.0081, 0.0046, 0.0044)		(0.74)	(NA)
3	26×22 [2.5]	26×22 [2.5]	24×18 [5]	24×18 [5]	1.5%	1.96	0.89
	(0.0110, 0.0107)	(0.0165, 0.0107)	(0.0097, 0.0046, 0.0044)	(0.0097, 0.0046, 0.0044)		(1.65)	(1.58)
2	30×22 [3.5]	30×22 [3.5]	34×20 [5]	34×20 [5]	1.2%	1.37	1.75
	(0.0119, 0.0102)	(0.0167, 0.0102)	(0.0069, 0.0048, 0.0039)	(0.0069, 0.0048, 0.0039)		(1.22)	(1.54)
1	30×22 [3.5]	30×22 [3.5]	34×20 [5]	34×20 [5]	1.0%	1.89	0.87
	(0.0167, 0.0102)	(0.0167, 0.0102)	(0.0069, 0.0048, 0.0039)	(0.0069, 0.0048, 0.0039)		(1.44)	(1.22)

D.1.2.2 8-Story SMF

Figures D-7 and D-8 illustrate the geometry of the 8-story RC SMF building. Tables D-9 and D-10 provide design values and a summary of the design, respectively, for the 8-story SMF building.

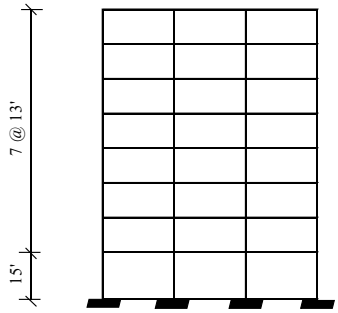

Figure D-7 Baseline RC moment frame building typical 8-story elevation.

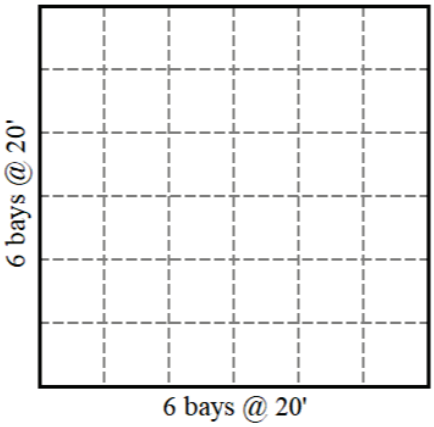

Figure D-8 Baseline RC moment frame building typical 8-story plan.

Table D-9 Design Values – 8-Story RC SMF Baseline

8-story, RC SMF (V108101)	
Design Parameters	
Dead Load:	Typical = 175 psf; Roof = 140 psf
Live Load:	Typical = 65 psf; Roof = 20 psf
Seismic Weight:	Typical = 190 psf; Roof = 147.5 psf
Total Tributary Seismic Weight:	W = 5319 kips
Wind Speed:	110 mph (strength); 85 mph (service)
Risk Category:	II
Importance Factor:	I_e = 1.0
Reinforced Concrete SMFs:	R = 8; C_d = 5.5; Ω_0 = 3.0
Site Class C Seismic Design Category D:	S_{DS} = 1.5; S_{D1} = 0.6
Material properties:	$f'_{c,\,beam}$ = 5 ksi; $f'_{c,\,col}$ = 7 ksi; f_y = 60 ksi

Table D-9 Design Values – 8-Story RC SMF Baseline (continued)

8-story, RC SMF (V108101)	
Analysis	
Centerline modeling of beams and columns Rigid diaphragms:	$I_{beam} = 0.35I_g$; $I_{col} = 0.70I_g$
Design based on Equivalent Lateral Force Procedure	
Calculated period(s):	$T_x = 2.105$ s; $T_y = 2.105$ s
Upper limit period:	$C_uT_{ax} = 1.49$ s; $C_uT_{ay} = 1.49$ s
Seismic response coefficient:	$C_{s,x} = 0.050$; $C_{s,x} = 0.050$
Controlling equation:	(12.8-3)
Seismic base shear:	$V_x = 268$ kips; $V_y = 268$ kips
Story drift limits applied:	$0.020h_{sx}$ (seismic); $h/400$ (wind)
Design base shear:	$V_x = 268$ kips; $V_y = 268$ kips
Controlling lateral design:	Seismic strength

Table D-10 8-Story RC SMF Baseline Design Summary: V108101

Level	Columns depth × width [tie spacing] (ρ_{total}, ρ_{sh})		Beams depth × width [hoop spacing] (ρ_{top}, ρ_{bot}, ρ_{sh})		Story Drift Δ	Moment ratio, $\Sigma M_c/\Sigma M_b$ Exterior (Interior)	Strength and Stiffness Ratio to Story Above Strength (Stiffness)
	Exterior	Interior	Exterior	Interior			
8	26×26 [3]	26×26 [3]	28×20 [6]	28×20 [6]	0.7%	1.01	NA
	(0.0116, 0.0101)	(0.0116, 0.0101)	(0.0073, 0.0047, 0.0033)	(0.0073, 0.0047, 0.0033)		(0.62)	(NA)
7	26×26 [3]	26×26 [3]	28×20 [5.5]	28×20 [5.5]	1.2%	2.04	0.88
	(0.0116, 0.0101)	(0.0116, 0.0101)	(0.0073, 0.0047, 0.0036)	(0.0073, 0.0047, 0.0036)		(1.26)	(1.21)
6	26×26 [3]	26×26 [3]	28×20 [5]	28×20 [5]	1.6%	1.77	0.98
	(0.0116, 0.0101)	(0.0139, 0.0101)	(0.0085, 0.0047, 0.0039)	(0.0085, 0.0047, 0.0039)		(1.31)	(1.06)
5	30×26 [3]	30×26 [3]	28×20 [4.5]	28×20 [4.5]	1.5%	1.68	1.18
	(0.0101, 0.0101)	(0.0121, 0.0101)	(0.0097, 0.0071, 0.0044)	(0.0097, 0.0071, 0.0044)		(1.27)	(1.3)
4	30×26 [3]	30×26 [3]	34×20 [4.5]	34×20 [4.5]	1.4%	1.43	1.24
	(0.0101, 0.0101)	(0.0141, 0.0101)	(0.0078, 0.0057, 0.0044)	(0.0078, 0.0057, 0.0044)		(1.21)	(1.18)
3	30×26 [3]	30×26 [3]	34×20 [4.5]	34×20 [4.5]	1.4%	1.39	1.00
	(0.0101, 0.0101)	(0.0141, 0.0101)	(0.0078, 0.0057, 0.0044)	(0.0078, 0.0057, 0.0044)		(1.36)	(1.04)

Table D-10 8-Story RC SMF Baseline Design Summary: V108101 (continued)

Level	Columns depth × width [tie spacing] (ρ_{total}, ρ_{sh})		Beams depth × width [hoop spacing] (ρ_{top}, ρ_{bot}, ρ_{sh})		Story Drift Δ	Moment ratio, $\Sigma M_c/\Sigma M_b$ Exterior (Interior)	Strength and Stiffness Ratio to Story Above Strength (Stiffness)
	Exterior	Interior	Exterior	Interior			
2	30×26 [3]	30×26 [3]	34×20 [4]	34×20 [4]	1.4%	1.20	1.11
	(0.0101, 0.0101)	(0.0141, 0.0101)	(0.0088, 0.0067, 0.0049)	(0.0088, 0.0067, 0.0049)		(1.24)	(1.05)
1	30×26 [3]	30×26 [3]	34×20 [4]	34×20 [4]	1.0%	1.53	0.90
	(0.0161, 0.0101)	(0.0141, 0.0101)	(0.0088, 0.0067, 0.0049)	(0.0088, 0.0067, 0.0049)		(1.24)	(1.23)

D.1.2.3 12-Story SMF

Figures D-9 and D-10 illustrate the geometry of the 12-story RC SMF building. Tables D-11 and D-12 provide design values and a summary of the design, respectively, for the 12-story SMF building.

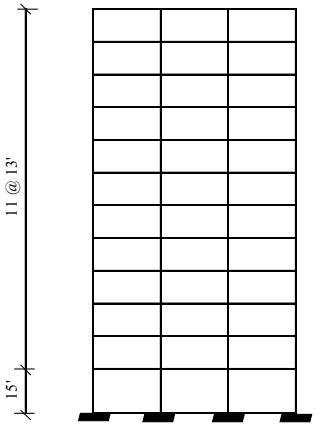

Figure D-9 Baseline RC moment frame building typical 12-story elevation.

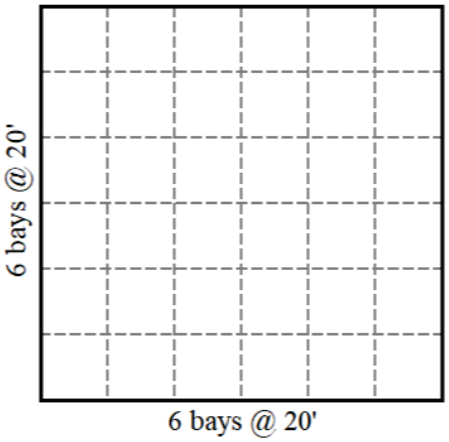

Figure D-10 Baseline RC moment frame building typical 12-story plan.

Table D-11 Design Values – 12-Story RC SMF Baseline

12-story, RC SMF (V112101)	
Design Parameters	
Dead Load:	Typical = 175 psf; Roof = 140 psf
Live Load:	Typical = 65 psf; Roof = 20 psf
Seismic Weight:	Typical = 190 psf; Roof = 147.5 psf
Total Tributary Seismic Weight:	W = 8055 kips
Wind Speed:	110 mph (strength); 85 mph (service)
Risk Category:	II
Importance Factor:	I_e = 1.0
Reinforced Concrete SMFs:	R = 8; C_d = 5.5; Ω_0 = 3.0
Site Class C Seismic Design Category D:	S_{DS} = 1.5; S_{D1} = 0.6
Material properties:	$f'_{c,\ beam}$ = 5 ksi; $f'_{c,\ col}$ = 7 ksi; f_y = 60 ksi
Analysis	
Centerline modeling of beams and columns Rigid diaphragms:	$I_{beam} = 0.35I_g$; $I_{col} = 0.70I_g$
Design based on Equivalent Lateral Force Procedure	
Calculated period(s):	T_x = 2.575 s; T_y = 2.575 s
Upper limit period:	C_uT_{ax} = 2.13 s; C_uT_{ay} = 2.13 s
Seismic response coefficient:	$C_{s,x}$ = 0.044; $C_{s,x}$ = 0.044
Controlling equation:	(12.8-5)
Seismic base shear:	V_x = 354 kips; V_y = 354 kips
Story drift limits applied:	0.020 h_{sx} (seismic); h/400 (wind)
Design base shear:	V_x = 354 kips; V_y = 354 kips
Controlling lateral design:	Seismic strength

Table D-12 12-Story RC SMF Baseline Design Summary: V112101

Level	Columns depth × width [tie spacing] (ρ_{total}, ρ_{sh})		Beams depth × width [hoop spacing] (ρ_{top}, ρ_{bot}, ρ_{sh})		Story Drift Δ	Moment ratio, $\Sigma M_c/\Sigma M_b$ Exterior (Interior)	Strength and Stiffness Ratio to Story Above Strength (Stiffness)
	Exterior	Interior	Exterior	Interior			
12	30×26 [3]	30×26 [3]	26×24 [5.5]	26×24 [5.5]	0.8%	1.27	NA
	(0.0101, 0.0076)	(0.0102, 0.0101)	(0.0066, 0.0043, 0.0030)	(0.0066, 0.0043, 0.0030)		(0.79)	(NA)
11	30×26 [3]	30×26 [3]	26×24 [5.5]	26×24 [5.5]	1.2%	2.56	0.79
	(0.0101, 0.0076)	(0.0102, 0.0101)	(0.0066, 0.0043, 0.0030)	(0.0066, 0.0043, 0.0030)		(1.61)	(1.37)
10	30×26 [3]	30×26 [3]	26×24 [4]	26×24 [4]	1.5%	2.22	1.03
	(0.0101, 0.0076)	(0.0102, 0.0101)	(0.0077, 0.0053, 0.0033)	(0.0077, 0.0053, 0.0033)		(1.42)	(1.13)
9	30×26 [3]	30×26 [3]	26×24 [4.5]	26×24 [4.5]	1.4%	1.95	1.02
	(0.0101, 0.0076)	(0.0161, 0.0101)	(0.0087, 0.0053, 0.0036)	(0.0087, 0.0053, 0.0036)		(1.69)	(1.35)
8	34×26 [3]	34×26 [3]	38×24 [4.5]	38×24 [4.5]	1.1%	1.31	1.78
	(0.0107, 0.0076)	(0.0142, 0.0101)	(0.0065, 0.0042, 0.0036)	(0.0065, 0.0042, 0.0036)		(1.26)	(1.48)
7	34×26 [3]	34×26 [3]	38×24 [4.5]	38×24 [4.5]	1.1%	1.48	1.03
	(0.0107, 0.0076)	(0.0142, 0.0101)	(0.0065, 0.0042, 0.0036)	(0.0065, 0.0042, 0.0036)		(1.38)	(1.06)
6	34×26 [3]	34×26 [3]	38×24 [4]	38×24 [4]	1.2%	1.44	1.05
	(0.0107, 0.0076)	(0.0142, 0.0101)	(0.0065, 0.0049, 0.0041)	(0.0065, 0.0049, 0.0041)		(1.32)	(1.02)
5	34×26 [3]	34×26 [3]	38×24 [4]	38×24 [4]	1.2%	1.39	0.99
	(0.0107, 0.0076)	(0.0142, 0.0101)	(0.0065, 0.0049, 0.0041)	(0.0065, 0.0049, 0.0041)		(1.34)	(1.01)
4	34×26 [3]	34×26 [3]	38×24 [4]	38×24 [4]	1.2%	1.34	0.99
	(0.0107, 0.0076)	(0.0142, 0.0101)	(0.0065, 0.0049, 0.0041)	(0.0065, 0.0049, 0.0041)		(1.37)	(1.01)
3	34×26 [3]	34×26 [3]	38×24 [4]	38×24 [4]	1.2%	1.27	1.05
	(0.0124, 0.0076)	(0.0142, 0.0101)	(0.0072, 0.0049, 0.0041)	(0.0072, 0.0049, 0.0041)		(1.33)	(1.02)
2	34×26 [3]	34×26 [3]	38×24 [4]	38×24 [4]	1.2%	1.32	1.00
	(0.0124, 0.0076)	(0.0142, 0.0101)	(0.0072, 0.0049, 0.0041)	(0.0072, 0.0049, 0.0041)		(1.36)	(1.05)
1	34×26 [3]	34×26 [3]	38×24 [3.5]	38×24 [3.5]	0.8%	1.60	0.95
	(0.0178, 0.0101)	(0.0178, 0.0101)	(0.0072, 0.0056, 0.0047)	(0.0072, 0.0056, 0.0047)		(1.44)	(1.22)

D.1.2.4 20-Story SMF

Table D-13 provides design values and Tables D-14 and D-15 provide summaries of the designs for the 20-story ELF and MRSA design buildings, respectively.

Table D-13 Design Values – 20-Story RC SMF Baseline

20-story, SMF, D_{max} (V120101)	
Design Parameters	
Dead Load:	Typical = 175 psf; Roof = 140 psf
Live Load:	Typical = 65 psf; Roof = 20 psf
Seismic Weight:	Typical = 190 psf; Roof = 147.5 psf
Total effective seismic weight:	W = 13527 kips
Wind Speed:	110 mph (strength); 85 mph (service)
Risk Category:	II
Importance Factor:	I_e = 1.0
Reinforced Concrete SMFs:	R = 8; C_d = 5.5; Ω_0 = 3.0
Site Class C Seismic Design Category D:	S_{DS} = 1.5; S_{D1} = 0.6
Material properties	$f'_{c,\ beam}$ = 5 ksi; $f'_{c,\ col}$ = 7 ksi; f_y = 60 ksi
Analysis	
Centerline modeling of beams and columns Rigid diaphragms:	$I_{beam} = 0.35I_g$; $I_{col} = 0.70I_g$
Design based on Equivalent Lateral Force Procedure	
Calculated period(s):	T_x = 3.657 s; T_y = 3.657 s
Upper limit period:	$C_uT_{a,x}$ = 3.363 s; $C_uT_{a,y}$ = 3.363 s
Seismic response coefficient:	$C_{s,x}$ = 0.044; $C_{s,y}$ = 0.044
Controlling equation:	(12.8-5)
Seismic base shear:	V_x = 595 kips; V_y = 595 kips
Story drift limits applied:	0.020 h_{sx}(seismic); h/400 (wind)
Design base shear:	V_x = 595 kips; V_y = 595 kips
Controlling lateral design:	Seismic strength

Table D-14 20-Story RC SMF Baseline ELF Design Summary: V120101

Level	Columns depth × width [tie spacing] (ρ_{total}, ρ_{sh})		Beams depth × width [hoop spacing] (ρ_{top}, ρ_{bot}, ρ_{sh})		Story Drift Δ	Moment ratio, $\Sigma M_c/\Sigma M_b$ Exterior (Interior)	Strength and Stiffness Ratio to Story Above Strength (Stiffness)
	Exterior	Interior	Exterior	Interior			
20	28×28 [2.5]	28×28 [2.5]	28×26 [5.5]	28×26 [5.5]	0.7%	0.90	NA
	(0.0100, 0.0112)	(0.0100, 0.0112)	(0.0070, 0.0036, 0.0027)	(0.0070, 0.0036, 0.0027)		(0.58)	(NA)

Table D-14 20-Story RC SMF Baseline ELF Design Summary: V120101 (continued)

Level	Columns depth × width [tie spacing] (ρ_{total}, ρ_{sh})		Beams depth × width [hoop spacing] (ρ_{top}, ρ_{bot}, ρ_{sh})		Story Drift Δ	Moment ratio, $\Sigma M_c/\Sigma M_b$ Exterior (Interior)	Strength and Stiffness Ratio to Story Above Strength (Stiffness)
	Exterior	Interior	Exterior	Interior			
19	28×28 [2.5]	28×28 [2.5]	28×26 [5]	28×26 [5]	0.9%	1.80	0.90
	(0.0100, 0.0112)	(0.0140, 0.0112)	(0.0070, 0.0036, 0.0030)	(0.0070, 0.0036, 0.0030)		(1.4)	(1.72)
18	32×28 [2.5]	32×28 [2.5]	34×26 [4.5]	34×26 [4.5]	1.0%	1.48	1.31
	(0.0105, 0.0112)	(0.0140, 0.0112)	(0.0066, 0.0038, 0.0034)	(0.0066, 0.0038, 0.0034)		(1.26)	(1.38)
17	32×28 [2.5]	32×28 [2.5]	34×26 [4]	34×26 [4]	1.0%	1.69	1.04
	(0.0105, 0.0112)	(0.0158, 0.0112)	(0.0066, 0.0048, 0.0038)	(0.0066, 0.0048, 0.0038)		(1.42)	(1.22)
16	36×28 [2.5]	36×28 [2.5]	40×26 [3.5]	40×26 [3.5]	1.0%	1.41	1.38
	(0.0109, 0.0112)	(0.0156, 0.0112)	(0.0064, 0.0048, 0.0043)	(0.0064, 0.0048, 0.0043)		(1.23)	(1.24)
15	36×28 [2.5]	36×28 [2.5]	40×26 [3.5]	40×26 [3.5]	1.1%	1.57	1.07
	(0.0109, 0.0112)	(0.0156, 0.0112)	(0.0064, 0.0056, 0.0043)	(0.0064, 0.0056, 0.0043)		(1.29)	(1.07)
14	36×28 [2.5]	36×28 [2.5]	40×26 [3.5]	40×26 [3.5]	1.1%	1.52	0.99
	(0.0109, 0.0112)	(0.0156, 0.0112)	(0.0064, 0.0056, 0.0043)	(0.0064, 0.0056, 0.0043)		(1.3)	(1.05)
13	36×28 [2.5]	36×28 [2.5]	40×26 [3.5]	40×26 [3.5]	1.1%	1.30	1.05
	(0.0109, 0.0112)	(0.0171, 0.0112)	(0.0072, 0.0056, 0.0043)	(0.0072, 0.0056, 0.0043)		(1.29)	(1.07)
12	40×32 [2.5]	40×32 [2.5]	42×26 [3]	42×26 [3]	1.1%	1.32	1.19
	(0.0110, 0.0098)	(0.0135, 0.0098)	(0.0076, 0.0061, 0.0050)	(0.0076, 0.0061, 0.0050)		(1.22)	(1.15)
11	40×32 [2.5]	40×32 [2.5]	42×26 [3]	42×26 [3]	1.1%	1.51	1.00
	(0.0110, 0.0098)	(0.0135, 0.0098)	(0.0076, 0.0061, 0.0050)	(0.0076, 0.0061, 0.0050)		(1.3)	(1.04)
10	40×32 [2.5]	40×32 [2.5]	42×26 [2.5]	42×26 [2.5]	1.1%	1.44	0.99
	(0.0110, 0.0098)	(0.0135, 0.0098)	(0.0076, 0.0061, 0.0050)	(0.0076, 0.0061, 0.0050)		(1.31)	(1.03)
9	40×32 [2.5]	40×32 [2.5]	42×26 [3]	42×26 [3]	1.1%	1.37	1.00
	(0.0110, 0.0098)	(0.0135, 0.0098)	(0.0076, 0.0061, 0.0050)	(0.0076, 0.0061, 0.0050)		(1.32)	(1.03)
	(0.0245, 0.0123)	(0.0135, 0.0098)	(0.0076, 0.0069, 0.0060)	(0.0076, 0.0069, 0.0060)		(1.38)	(1.34)
8	40×32 [2.5]	40×32 [2.5]	42×26 [2.5]	42×26 [2.5]	1.1%	1.29	1.05
	(0.0110, 0.0098)	(0.0135, 0.0098)	(0.0076, 0.0069, 0.0060)	(0.0076, 0.0069, 0.0060)		(1.26)	(1.03)

Table D-14 20-Story RC SMF Baseline ELF Design Summary: V120101 (continued)

Level	Columns depth × width [tie spacing] (ρ_{total}, ρ_{sh})		Beams depth × width [hoop spacing] (ρ_{top}, ρ_{bot}, ρ_{sh})		Story Drift Δ	Moment ratio, $\Sigma M_c/\Sigma M_b$ Exterior (Interior)	Strength and Stiffness Ratio to Story Above Strength (Stiffness)
	Exterior	Interior	Exterior	Interior			
7	40×32 [2.5]	40×32 [2.5]	42×26 [2.5]	42×26 [2.5]	1.1%	1.29	1.00
	(0.0123, 0.0098)	(0.0135, 0.0098)	(0.0076, 0.0069, 0.0060)	(0.0076, 0.0069, 0.0060)		(1.28)	(1.03)
6	40×32 [2.5]	40×32 [2.5]	42×26 [2.5]	42×26 [2.5]	1.1%	1.29	1.00
	(0.0123, 0.0098)	(0.0135, 0.0098)	(0.0076, 0.0069, 0.0060)	(0.0076, 0.0069, 0.0060)		(1.29)	(1.03)
5	40×32 [2.5]	40×32 [2.5]	42×26 [2.5]	42×26 [2.5]	1.1%	1.30	1.00
	(0.0135, 0.0098)	(0.0135, 0.0098)	(0.0076, 0.0069, 0.0060)	(0.0076, 0.0069, 0.0060)		(1.3)	(1.03)
4	40×32 [2.5]	40×32 [2.5]	42×26 [2.5]	42×26 [2.5]	1.0%	1.30	1.00
	(0.0135, 0.0098)	(0.0135, 0.0098)	(0.0076, 0.0069, 0.0060)	(0.0076, 0.0069, 0.0060)		(1.32)	(1.03)
3	40×32 [2.5]	40×32 [2.5]	42×26 [2.5]	42×26 [2.5]	1.0%	1.29	1.00
	(0.0147, 0.0098)	(0.0135, 0.0098)	(0.0076, 0.0069, 0.0060)	(0.0076, 0.0069, 0.0060)		(1.34)	(1.05)
2	40×32 [2.5]	40×32 [2.5]	42×26 [2.5]	42×26 [2.5]	0.9%	1.39	1.00
	(0.0160, 0.0098)	(0.0135, 0.0098)	(0.0076, 0.0069, 0.0060)	(0.0076, 0.0069, 0.0060)		(1.36)	(1.09)
1	40×32 [2.5]	40×32 [2.5]	42×26 [2.5]	42×26 [2.5]	0.9%	2.04	0.91
	(0.0245, 0.0123)	(0.0135, 0.0098)	(0.0076, 0.0069, 0.0060)	(0.0076, 0.0069, 0.0060)		(1.38)	(1.34)

Table D-15 20-Story RC SMF Baseline MRSA Design Summary: V120301

Level	Columns depth × width [tie spacing] (ρ_{total}, ρ_{sh})		Beams depth × width [hoop spacing] (ρ_{top}, ρ_{bot}, ρ_{sh})		Story Drift Δ	Moment ratio, $\Sigma M_c/\Sigma M_b$ Exterior (Interior)	Strength and Stiffness Ratio to Story Above Strength (Stiffness)
	Exterior	Interior	Exterior	Interior			
20	28×28 [2.5]	28×28 [2.5]	26×26 [5.5]	26×26 [5.5]	0.8%	0.98	NA
	(0.0100, 0.0112)	(0.0100, 0.0112)	(0.0076, 0.0039, 0.0027)	(0.0076, 0.0039, 0.0027)		(0.64)	(NA)
19	28×28 [2.5]	28×28 [2.5]	26×26 [5]	26×26 [5]	1.0%	1.98	0.84
	(0.0100, 0.0112)	(0.0120, 0.0112)	(0.0076, 0.0039, 0.0030)	(0.0076, 0.0039, 0.0030)		(1.41)	(1.71)
18	28×28 [2.5]	28×28 [2.5]	30×26 [4.5]	30×26 [4.5]	1.1%	1.69	1.12
	(0.0100, 0.0112)	(0.0120, 0.0112)	(0.0065, 0.0044, 0.0034)	(0.0065, 0.0044, 0.0034)		(1.21)	(1.3)

Table D-15 20-Story RC SMF Baseline MRSA Design Summary: V120301 (continued)

Level	Columns depth × width [tie spacing] (ρ_{total}, ρ_{sh})		Beams depth × width [hoop spacing] (ρ_{top}, ρ_{bot}, ρ_{sh})		Story Drift Δ	Moment ratio, $\Sigma M_c/\Sigma M_b$	Strength and Stiffness Ratio to Story Above
	Exterior	Interior	Exterior	Interior		Exterior (Interior)	Strength (Stiffness)
17	28×28 [2.5]	28×28 [2.5]	30×26 [4.5]	30×26 [4.5]	1.2%	1.70	0.96
	(0.0100, 0.0112)	(0.0140, 0.0112)	(0.0065, 0.0044, 0.0034)	(0.0065, 0.0044, 0.0034)		(1.33)	(1.24)
16	32×28 [2.5]	32×28 [2.5]	36×26 [4.5]	36×26 [4.5]	1.1%	1.41	1.33
	(0.0105, 0.0112)	(0.0140, 0.0112)	(0.0062, 0.0036, 0.0034)	(0.0062, 0.0036, 0.0034)		(1.25)	(1.27)
15	32×28 [2.5]	32×28 [2.5]	36×26 [4.5]	36×26 [4.5]	1.2%	1.61	1.01
	(0.0105, 0.0112)	(0.0140, 0.0112)	(0.0062, 0.0036, 0.0034)	(0.0062, 0.0036, 0.0034)		(1.43)	(1.05)
14	32×28 [2.5]	32×28 [2.5]	36×26 [4.5]	36×26 [4.5]	1.3%	1.60	0.99
	(0.0105, 0.0112)	(0.0140, 0.0112)	(0.0062, 0.0036, 0.0034)	(0.0062, 0.0036, 0.0034)		(1.46)	(1.02)
13	32×28 [2.5]	32×28 [2.5]	36×26 [4]	36×26 [4]	1.3%	1.58	1.07
	(0.0105, 0.0112)	(0.0140, 0.0112)	(0.0062, 0.0045, 0.0038)	(0.0062, 0.0045, 0.0038)		(1.37)	(1.07)
12	40×32 [2.5]	40×32 [2.5]	40×26 [3.5]	40×26 [3.5]	1.1%	1.41	1.40
	(0.0110, 0.0098)	(0.0110, 0.0098)	(0.0080, 0.0040, 0.0043)	(0.0080, 0.0040, 0.0043)		(1.21)	(1.24)
11	40×32 [2.5]	40×32 [2.5]	40×26 [3.5]	40×26 [3.5]	1.2%	2.26	0.95
	(0.0110, 0.0098)	(0.0110, 0.0098)	(0.0064, 0.0048, 0.0043)	(0.0064, 0.0048, 0.0043)		(1.53)	(1.02)
10	40×32 [2.5]	40×32 [2.5]	40×26 [3]	40×26 [3]	1.2%	2.22	0.99
	(0.0110, 0.0098)	(0.0110, 0.0098)	(0.0064, 0.0048, 0.0043)	(0.0064, 0.0048, 0.0043)		(1.55)	(1)
9	40×32 [2.5]	40×32 [2.5]	40×26 [3.5]	40×26 [3.5]	1.3%	2.16	1.00
	(0.0110, 0.0098)	(0.0110, 0.0098)	(0.0064, 0.0048, 0.0043)	(0.0064, 0.0048, 0.0043)		(1.57)	(0.99)
8	40×32 [2.5]	40×32 [2.5]	40×26 [3]	40×26 [3]	1.3%	1.87	1.14
	(0.0110, 0.0098)	(0.0110, 0.0098)	(0.0072, 0.0056, 0.0050)	(0.0072, 0.0056, 0.0050)		(1.39)	(0.98)
7	40×32 [2.5]	40×32 [2.5]	40×26 [3]	40×26 [3]	1.4%	1.80	1.00
	(0.0110, 0.0098)	(0.0110, 0.0098)	(0.0072, 0.0056, 0.0050)	(0.0072, 0.0056, 0.0050)		(1.41)	(0.98)
6	40×32 [2.5]	40×32 [2.5]	40×26 [3]	40×26 [3]	1.4%	1.72	1.00
	(0.0110, 0.0098)	(0.0110, 0.0098)	(0.0072, 0.0056, 0.0050)	(0.0072, 0.0056, 0.0050)		(1.43)	(0.98)
5	40×32 [2.5]	40×32 [2.5]	40×26 [3]	40×26 [3]	1.5%	1.63	1.06
	(0.0110, 0.0098)	(0.0110, 0.0098)	(0.0072, 0.0064, 0.0050)	(0.0072, 0.0064, 0.0050)		(1.37)	(0.98)

Table D-15 20-Story RC SMF Baseline MRSA Design Summary: V120301 (continued)

Level	Columns depth × width [tie spacing] (ρ_{total}, ρ_{sh})		Beams depth × width [hoop spacing] (ρ_{top}, ρ_{bot}, ρ_{sh})		Story Drift Δ	Moment ratio, $\Sigma M_c/\Sigma M_b$ Exterior (Interior)	Strength and Stiffness Ratio to Story Above Strength (Stiffness)
	Exterior	Interior	Exterior	Interior			
4	40×32 [2.5]	40×32 [2.5]	40×26 [3]	40×26 [3]	1.5%	1.39	1.06
	(0.0110, 0.0098)	(0.0110, 0.0098)	(0.0080, 0.0064, 0.0050)	(0.0080, 0.0064, 0.0050)		(1.31)	(0.99)
3	40×32 [2.5]	40×32 [2.5]	40×26 [3]	40×26 [3]	1.5%	1.30	1.00
	(0.0110, 0.0098)	(0.0110, 0.0098)	(0.0080, 0.0064, 0.0050)	(0.0080, 0.0064, 0.0050)		(1.34)	(1.01)
2	40×32 [2.5]	40×32 [2.5]	40×26 [3]	40×26 [3]	1.4%	1.40	1.00
	(0.0135, 0.0098)	(0.0110, 0.0098)	(0.0080, 0.0064, 0.0050)	(0.0080, 0.0064, 0.0050)		(1.36)	(1.06)
1	40×32 [2.5]	40×32 [2.5]	40×26 [3]	40×26 [3]	0.9%	2.10	0.91
	(0.0209, 0.0098)	(0.0123, 0.0098)	(0.0080, 0.0064, 0.0050)	(0.0080, 0.0064, 0.0050)		(1.44)	(1.35)

D.2 Summary of Reinforced Concrete Moment Frame Results

Table D-16 Reinforced Concrete Moment Frame Results

Model ID	Design Configuration						Building Performance Summary		
	No. of Stories	Irregularity	SDC	Design Method	Design Period ($C_u T_a$) [s]	OpenSees Model Period [s]	Static Overstrength, Ω	*ACMR* (const. SSF)	*ACMR*/ $ACMR_{baseline}$
V104101	4	Baseline	D_{max}	ELF	0.81	1.12	1.63	2.80	1.00
V104102	4	0.8 SS 1	D_{max}	ELF	0.85	1.22	1.65	2.91	1.04
V104103	4	0.7 SS 1	D_{max}	ELF	0.89	1.40	1.61	2.75	0.98
V104104	4	0.6 SS 1	D_{max}	ELF	0.95	1.57	1.57	2.48	0.88
V104105	4	0.8 SS 1&2	D_{max}	ELF	0.92	1.41	1.67	2.86	1.02
V104106	4	0.7 SS 1&2	D_{max}	ELF	1.00	1.56	1.70	2.98	1.06
V104107	4	0.6 SS 1&2	D_{max}	ELF	1.10	1.91	1.59	2.81	1.00
V604102	4	0.5 SCWB	D_{max}	ELF	0.81	1.12	1.60	2.69	0.96
V604103	4	1.0 SCWB	D_{max}	ELF	0.81	1.12	1.60	2.73	0.97
V604104	4	1.5 SCWB	D_{max}	ELF	0.81	1.12	1.66	2.94	1.05
V604105	4	2.0 SCWB	D_{max}	ELF	0.81	0.97	1.81	3.17	1.13
V604107	4	0.5 SCWB Exact	D_{max}	ELF	0.81	1.12	2.19	2.20	1.06
V604108	4	1.0 SCWB Exact	D_{max}	ELF	0.81	1.12	1.99	2.17	1.04
V604106	4	1.2 SCWB Exact	D_{max}	ELF	0.81	1.12	1.98	2.08	1.00

Table D-16 Reinforced Concrete Moment Frame Results (continued)

Model ID	Design Configuration						Building Performance Summary		
	No. of Stories	Irregularity	SDC	Design Method	Design Period ($C_u T_a$) [s]	OpenSees Model Period [s]	Static Overstrength, Ω	*ACMR* (const. SSF)	$ACMR/ACMR_{baseline}$
V604109	4	1.5 SCWB Exact	D_{max}	ELF	0.81	1.12	1.95	3.02	1.45
V604110	4	2.0 SCWB Exact	D_{max}	ELF	0.81	0.97	1.97	3.30	1.59
V108101	8	Baseline	D_{max}	ELF	1.49	2.04	1.63	2.28	1.00
V108102	8	0.8 SS 1	D_{max}	ELF	1.53	2.13	1.53	2.12	0.93
V108103	8	0.7 SS 1	D_{max}	ELF	1.57	2.30	1.51	2.02	0.89
V108104	8	0.6 SS 1	D_{max}	ELF	1.62	2.40	1.55	2.09	0.92
V108105	8	0.8 SS 1&2	D_{max}	ELF	1.59	2.37	1.50	1.97	0.87
V108106	8	0.7 SS 1&2	D_{max}	ELF	1.67	2.45	1.51	1.94	0.85
V108107	8	0.6 SS 1&2	D_{max}	ELF	1.76	2.69	1.54	2.17	0.95
V108108	8	0.8 SS 5	D_{max}	ELF	1.55	2.13	1.65	2.33	1.02
V108109	8	0.7 SS 5	D_{max}	ELF	1.59	2.14	1.72	2.25	0.99
V108110	8	0.6 SS 5	D_{max}	ELF	1.64	1.96	1.98	2.56	1.13
V608102	8	0.5 SCWB	D_{max}	ELF	1.49	2.04	1.63	2.17	0.96
V608103	8	1.0 SCWB	D_{max}	ELF	1.49	2.04	1.63	2.17	0.96
V608104	8	1.5 SCWB	D_{max}	ELF	1.49	2.04	1.65	2.55	1.12
V608105	8	2.0 SCWB	D_{max}	ELF	1.49	1.81	1.82	3.03	1.33
V112101	12	Baseline	D_{max}	ELF	2.13	2.44	1.53	1.93	1.00
V112102	12	0.8 SS 1	D_{max}	ELF	2.17	2.57	1.47	1.73	0.90
V112103	12	0.7 SS 1	D_{max}	ELF	2.17	2.58	1.50	1.84	0.95
V112104	12	0.6 SS 1	D_{max}	ELF	2.25	2.70	1.48	1.83	0.95
V112105	12	0.8 SS 1&2	D_{max}	ELF	2.23	2.64	1.46	1.89	0.98
V112106	12	0.7 SS 1&2	D_{max}	ELF	2.30	2.69	1.45	1.96	1.02
V112107	12	0.6 SS 1&2	D_{max}	ELF	2.40	2.90	1.47	2.19	1.14
V112108	12	0.8 SS 5	D_{max}	ELF	2.19	2.54	1.60	2.11	1.09
V112109	12	0.7 SS 5	D_{max}	ELF	2.23	2.55	1.62	2.24	1.16
V112110	12	0.6 SS 5	D_{max}	ELF	2.28	2.49	1.72	2.49	1.29
V512102	12	0.8 WS 1	D_{max}	ELF	2.13	2.39	1.60	1.91	0.99
V512103	12	0.6 WS 1	D_{max}	ELF	2.13	2.36	1.68	2.09	1.09
V512104	12	0.8 WS 1&2	D_{max}	ELF	2.13	2.32	1.77	2.13	1.10
V512105	12	0.6 WS 1&2	D_{max}	ELF	2.13	2.04	1.87	2.51	1.30
V512106	12	0.8 WS 5	D_{max}	ELF	2.13	2.41	1.56	1.87	0.97
V512107	12	0.6 WS 5	D_{max}	ELF	2.13	2.39	1.58	1.93	1.00

Table D-16 Reinforced Concrete Moment Frame Results (continued)

Model ID	Design Configuration						Building Performance Summary		
	No. of Stories	Irregularity	SDC	Design Method	Design Period ($C_u T_a$) [s]	OpenSees Model Period [s]	Static Overstrength, Ω	*ACMR* (const. SSF)	$ACMR/ACMR_{baseline}$
V612102	12	0.5 SCWB	D_{max}	ELF	2.13	2.54	1.51	1.73	0.90
V612103	12	1.0 SCWB	D_{max}	ELF	2.13	2.44	1.52	1.79	0.93
V612104	12	1.5 SCWB	D_{max}	ELF	2.13	2.44	1.53	1.98	1.03
V612105	12	2.0 SCWB	D_{max}	ELF	2.13	2.14	1.65	2.25	1.16
V612107	12	0.5 SCWB Exact	D_{max}	ELF	2.13	2.54	2.27	1.51	0.81
V612108	12	1.0 SCWB Exact	D_{max}	ELF	2.13	2.44	1.67	1.65	0.88
V612106	12	1.2 SCWB Exact	D_{max}	ELF	2.13	2.44	1.56	1.87	1.00
V612109	12	1.5 SCWB Exact	D_{max}	ELF	2.13	2.44	1.55	1.99	1.07
V612110	12	2.0 SCWB Exact	D_{max}	ELF	2.13	2.14	1.70	2.30	1.23
V612111	12	2.0, 1.5, 1.0 Stepped SCWB	D_{max}	Design Min	2.13	2.41	1.51	2.06	1.07
V612112	12	1.5, 1.0, 0.8 Stepped SCWB	D_{max}	Design Min	2.13	2.53	1.54	1.97	1.02
V612113	12	2.0, 1.5, 1.0 Stepped SCWB Exact	D_{max}	Exact	2.13	2.41	1.51	1.63	0.87
V612114	12	1.5, 1.0, 0.8 Stepped SCWB Exact	D_{max}	Exact	2.13	2.53	1.54	1.50	0.81
V612116	12	1.5, 1.2 Stepped SCWB Exact	D_{max}	Exact	2.13	2.44	1.56	1.95	1.04
V7121011	12	SMF - GILD 0.5 at 1	D_{max}	ELF	2.13	2.44	1.43	1.64	0.85
V7121021	12	SMF - GILD 0.5 at 2	D_{max}	ELF	2.13	2.44	1.39	1.63	0.85
V120101	20	Baseline	D_{max}	ELF	3.36	3.22	1.41	2.00	1.00
V120103	20	0.6 SS 1	D_{max}	ELF	3.43	3.39	1.40	1.88	0.94
V120104	20	0.7 SS 1	D_{max}	ELF	3.48	3.44	1.43	1.94	0.97
V120301	20	Baseline	D_{max}	MRSA	3.36	3.46	1.23	1.93	1.00
V520102	20	0.8 WS 1	D_{max}	ELF	3.36	3.19	1.45	2.07	1.07
V520103	20	0.6 WS 1	D_{max}	ELF	3.36	3.19	1.51	2.24	1.16
V220102	20	2.0 MR 3rd Flr	D_{max}	ELF	3.36	3.20	1.43	1.99	1.03
V220103	20	3.0 MR 3rd Flr	D_{max}	ELF	3.36	3.19	1.39	1.95	1.01
V220104	20	2.0 MR 11th Flr	D_{max}	ELF	3.36	3.27	1.42	2.12	1.10
V220105	20	3.0 MR 11th Flr	D_{max}	ELF	3.36	3.20	1.39	2.22	1.15
V220302	20	2.0 MR 3rd Flr	D_{max}	MRSA	3.36	3.46	1.19	1.90	0.99
V220303	20	3.0 MR 3rd Flr	D_{max}	MRSA	3.36	3.41	1.39	1.91	0.99

Table D-16 Reinforced Concrete Moment Frame Results (continued)

Model ID	Design Configuration						Building Performance Summary		
	No. of Stories	Irregularity	SDC	Design Method	Design Period ($C_u T_a$) [s]	OpenSees Model Period [s]	Static Overstrength, Ω	*ACMR* (const. SSF)	*ACMR*/ $ACMR_{baseline}$
V220304	20	2.0 MR 11th Flr	D_{max}	MRSA	3.36	3.47	1.21	2.11	1.10
V220305	20	3.0 MR 11th Flr	D_{max}	MRSA	3.36	3.54	1.20	2.21	1.14
V104201	4	Baseline	B_{max}	ELF	0.93	2.28	1.41	3.97	1.00
V104202	4	0.8 SS 1	B_{max}	ELF	0.97	2.55	1.30	3.72	0.94
V104203	4	0.7 SS 1	B_{max}	ELF	1.02	2.77	1.28	3.81	0.96
V104204	4	0.6 SS 1	B_{max}	ELF	1.08	2.92	1.36	4.40	1.11
V104205	4	0.8 SS 1&2	B_{max}	ELF	1.05	2.88	1.29	4.05	1.02
V104206	4	0.7 SS 1&2	B_{max}	ELF	1.14	3.25	1.23	4.25	1.07
V104207	4	0.6 SS 1&2	B_{max}	ELF	1.26	3.40	1.30	4.88	1.23
V604202	4	0.4 SCWB	B_{max}	ELF	0.93	2.28	1.41	3.76	0.97
V604203	4	0.7 SCWB	B_{max}	ELF	0.93	2.28	1.41	3.76	0.97
V604204	4	1.0 SCWB	B_{max}	ELF	0.93	2.28	1.46	3.88	1.00
V604205	4	0.4 SCWB Exact	B_{max}	ELF	0.93	2.28	1.62	3.46	0.92
V604206	4	0.7 SCWB Exact	B_{max}	ELF	0.93	2.28	1.55	3.39	0.90
V604207	4	1.0 SCWB Exact	B_{max}	ELF	0.93	2.28	1.54	3.78	1.00
V112201	12	Baseline	B_{max}	ELF	2.44	5.22	1.45	2.36	1.00
V112202	12	0.8 SS 1	B_{max}	ELF	2.48	5.27	1.49	2.53	1.07
V112203	12	0.7 SS 1	B_{max}	ELF	2.52	5.33	1.49	2.35	0.99
V112204	12	0.6 SS 1	B_{max}	ELF	2.58	5.46	1.47	2.38	1.01
V112205	12	0.8 SS 1&2	B_{max}	ELF	2.55	5.30	1.39	2.66	1.13
V112206	12	0.7 SS 1&2	B_{max}	ELF	2.63	5.63	1.58	2.55	1.08
V112207	12	0.6 SS 1&2	B_{max}	ELF	2.74	5.84	1.52	2.60	1.10
V112208	12	0.8 SS 5	B_{max}	ELF	2.51	5.16	1.50	2.51	1.06
V112209	12	0.7 SS 5	B_{max}	ELF	2.55	5.11	1.47	2.86	1.21
V112210	12	0.6 SS 5	B_{max}	ELF	2.60	5.15	1.45	2.64	1.12
V512202	12	0.8 WS 1	B_{max}	ELF	2.44	5.03	1.46	2.16	0.92
V512203	12	0.65 WS 1	B_{max}	ELF	2.44	4.92	1.46	2.17	0.92
V512204	12	0.8 WS 1 & 2	B_{max}	ELF	2.44	4.95	1.47	2.03	0.86
V512205	12	0.65 WS 1 & 2	B_{max}	ELF	2.44	4.65	1.55	2.50	1.06
V512206	12	0.8 WS 5	B_{max}	ELF	2.44	5.04	1.46	2.32	0.98
V512207	12	0.65 WS 5	B_{max}	ELF	2.44	4.90	1.46	2.28	0.96
V7122011	12	OMF - GILD 0.5 at 1	B_{max}	ELF	2.44	0.00	1.06	1.16	0.49

Table D-16 Reinforced Concrete Moment Frame Results (continued)

Model ID	Design Configuration						Building Performance Summary		
	No. of Stories	Irregularity	SDC	Design Method	Design Period ($C_u T_a$) [s]	OpenSees Model Period [s]	Static Overstrength, Ω	*ACMR* (const. SSF)	*ACMR*/ $ACMR_{baseline}$
V7122021	12	OMF - GILD 0.5 at 2	B_{max}	ELF	2.44	5.22	1.09	1.34	0.57
V612202	12	0.4 SCWB	B_{max}	ELF	2.44	5.22	1.47	2.36	0.93
V612203	12	0.7 SCWB	B_{max}	ELF	2.44	5.22	1.37	2.36	0.93
V612204	12	1.0 SCWB	B_{max}	ELF	2.44	5.22	1.45	2.54	1.00
V612205	12	0.4 SCWB Exact	B_{max}	ELF	2.44	5.22	1.79	1.71	0.84
V612206	12	0.7 SCWB Exact	B_{max}	ELF	2.44	5.22	1.55	1.95	0.96
V612207	12	1.0 SCWB Exact	B_{max}	ELF	2.44	5.22	1.47	2.04	1.00

Appendix E

Results of Quality Control Review

E.1 Overview of Quality Control Review

Quality control review work was conducted for each of the analytical studies reflected this report, which include: (1) torsional studies; (2) concrete shear wall studies; (3) steel moment frame studies; and (4) concrete moment frame studies. The following were the focus areas of each of the reviews:

- **Archetype Design.** This work included checking the: (1) layout of elements; (2) design base shear; (3) appropriateness of limit states and controlling criteria; and (4) element proportioning and reinforcement.
- **FEMA P695 Analysis Input.** This work included checking: (1) the models for consistency with the design (e.g., layout, proportioning, backbone curves, cyclic performance criteria); (2) that irregularities were modeled as intended (e.g., strength ratios, stiffness ratios, strong-column/weak-beam ratios); (3) *P*-Delta for the gravity system; and (4) the appropriateness of the boundary conditions.
- **FEMA P695 Analysis Results.** This work included checking: (1) trends in metadata (e.g., normalized *ACMR*, *P*(*Collapse*|*MCE*)); (2) structural period(s) (e.g., design period, T_1 from the models); (3) peak pushover strength factor; (4) static overstrength factor; (5) trends in the distribution of mean story drifts (e.g., 33% MCE, 66% MCE, MCE, and near collapse); (6) controlling response parameters and mechanisms; (7) trends for special versus ordinary systems; and (8) hysteresis results (spot-checking only). In addition to this, a complementary analysis was conducted for a reinforced concrete shear wall archetype for the purposes of comparing analysis results.

E.2 Results from Quality Control Review

E.2.1 Torsional Studies

Review work of the torsional studies included: (1) review of backbone behavior of the archetype models; (2) review of cyclic deterioration behavior of the archetype models; (3) a check of the FEMA P695 analysis process, including a comparison of the differences between the typical FEMA P695

analysis and the modified method used for the studies in this report; and (4) a check of the archetype structural design process spreadsheets. The following were noted from this work:

- Observation: Mid-rise archetype models had a higher *P*-Delta when compared to similar models from previous studies. Resolution: This is reflected in Appendix A. Also, this finding indicates that the torsion studies cast a wider net between short and mid-rise models.
- Observation: The capping point was slightly higher in the archetype model when compared to models from prior studies (i.e., failure at 6% roof drift versus ~2-3% from prior studies). Resolution: Effective building heights are different so failure deflections are actually similar.
- Observation: Cyclic deterioration behavior of the archetype models is low. Resolution: The cyclic properties of the nonlinear springs were modeled with peak-oriented material properties having relatively low cyclic deterioration. Cyclic deterioration effects were minimized in the simplified models for the following reasons: (1) cyclic deterioration is a system/material dependent property and the study was intended to capture torsion effects in a more generic sense; and (2) collapse capacity has been shown to be relatively insensitive to cyclic deterioration properties in comparison with other parameters such as peak strength and negative stiffness (Haselton et al., 2011). As such, it was determined that this finding does not significantly impact the conclusions and recommendations resulting from the torsion studies. This finding is reflected in Chapter 4.

All findings from the review work for the torsion studies were addressed and are reflected in this report.

E.2.2 Concrete Shear Wall Studies

Review work of the concrete shear wall studies included review of the: (1) analysis techniques and possible implications; (2) archetype design; (3) structural calculations; and (4) analysis results. In particular, the following were noted:

- **Limitations of Analysis Techniques.**
  - Failure modes modeling was limited in that: (1) compression flexural failure were assessed and modeled, but out-of-plane instability of the compression boundary and tension failure were not considered; (2) shear failure was not considered and could have been assessed by post-processing; and (3) loss of axial load carrying capacity in the

concrete shear walls was not considered (i.e., the approach used was associated with slab rotation and could have some considerable bias).

  - System-level modeling included planar walls that were only subjected to 2D loading, where the effect of biaxial loading was not considered. Wall-slab interaction was also not considered.

- **Limitations of Design Space.** The design space was limited in that the archetypes: (1) only covered planar walls, leaving out flanged walls (e.g., T-shaped walls); (2) only considered two building heights (8- and 12-story buildings) and did not cover building heights (e.g., 3- and 5-story buildings) that might have a more significant stiffness reduction; (3) only considered one type of wall detailing; and (4) only covered walls with low shear stress.

E.2.3 Steel Moment Frame Studies

Review work of the steel moment frame studies included review of the: (1) archetype designs; (2) analytical models used in the collapse analyses; and (3) collapse analysis results used to evaluate vertical irregularities V2 (weight or mass), V6 (strong-column/weak-beam), and V7 (gravity-induced lateral demand). In particular, the following were conducted:

- **Archetype Designs.** Inputs were checked for appropriate seismic parameters for the given seismic design category, material strength, frame geometry, and wind load and gravity load distribution for the given design case. The resulting frame designs were checked for strength, drift, and strong-column/weak-beam compliance for the given design case. Details of the steel moment frame design process and final frame designs are found in Appendix C.

- **Analytical Models for Collapse Analysis.** Quality control review of the OpenSees models used for collapse analyses included a review of a typical frame design and the routines used to produce the various OpenSees models required for the different analytical cases. The review included checking material nonlinear modeling parameters, damping model, frame geometry, and gravity load distribution for the given design case. Tool Command Language (TCL) subroutines used to generate the TCL files for the OpenSees models were also reviewed.

- **Collapse Analysis Results.** Quality control review of the analytical results included scrutiny of the methodology used to estimate collapse fragilities (i.e., the Baker method), the solution method for direct integration (i.e., Newton Raphson), and the impact of the time-step used for direct integration and methodology used to scale the geometric mean

spectra to produce collapse. A sensitivity study was performed that confirmed that the 0.02-second time-step used in the nonlinear analyses was sufficiently short to capture all significant peaks in the response (i.e., the 4% response increase using a shorter time step was judged to be not significant). Lastly, the results were reviewed to confirm that they appeared reasonable with respect to drift (e.g., comparing expected increases between the 33% and 66% MCE runs or lateral displacement distribution up the height of the building), the shape and trend of the incremental dynamic analyses (e.g., a search for illogical results from non-convergence or collapse), and the general shape of the pushover curves.

Overall, the quality control review work demonstrated that the steel moment frame studies and corresponding conclusions were reasonable and did not require any modifications.

E.2.4 Concrete Moment Frame Studies

Review work of the concrete moment frame studies included the following:

- **Archetype Designs.** Inputs were checked for appropriate seismic parameters for the given seismic design category, material strength, frame geometry, wind load and gravity load distribution for the given design case. The resulting frame designs were checked for strength, drift and strong-column/weak-beam compliance, using standard ASCE/SEI 7-16 load combinations and standard envelope design procedures. No accidental torsion was included and the 3D ETABS models described below were completely symmetrical. Details of the concrete moment frame design process and final frame designs are found in Appendix D.
- **Comparison Studies.** Independent 3D ETABS analysis and design runs for the 8- and 12-story baseline buildings were conducted for comparison to the 2D plane frame runs used in the studies. Reasonably good agreement was observed for the reinforcement ratios. It was concluded that these 2D tables used a "broad brush" for the selection of the respective flexural reinforcement ratios. ETABS output indicated different required reinforcement ratios for each story level, whereas the 2D design grouped as many as five levels with the same beam flexural rebar. The beam hoops follow the specified beam flexural reinforcement grouping and many levels list the same hoop reinforcement ratios. Tabulated 2D design column longitudinal rebar and confinement reinforcement were also in general agreement with the 3D ETABS design runs. Typically, reinforcement ratios agreement was on the order

of +/-10% between the results from the 3D ETABS study and the 2D study described in this report.

Overall, the quality control review work demonstrated that the concrete moment frame studies and corresponding conclusions were reasonable and did not require any modifications.

Appendix F

Global Behavior of Buildings with Mass Irregularity (V2)

This Appendix documents a series of analyses performed to test the generality of the observation made in Section 6.5.3 that, in terms of collapse resistance for buildings with mass irregularity, modal response spectrum analysis (MRSA) provides no advantage over the equivalent lateral force (ELF) procedure. For Figures F-29 through F-124 referenced in this Appendix, see the electronic Supporting Documentation for Appendix F: Additional Figures.

F.1 Background

ASCE/SEI 7-16 defines a mass irregularity to exist where the effective mass of a story is more than 150% of that of an adjacent story; the only design consequence is that use of the ELF procedure is prohibited for structures with mass irregularity. Chapter 6 reports the results of explicit collapse assessment of 20-story and 3-story concrete special moment frame (SMF) buildings and steel SMF buildings with mass ratios that might be realistically expected in practice (1.5, 2.0, and 3.0) at selected stories. Those archetypes were proportioned using MRSA with designs being adjusted as needed to satisfy all design requirements, including the effects of actual mass ratios. For a few archetypes separately proportioned using the ELF procedure, it was found that their collapse resistance exceeded that of the systems proportioned using MRSA. Based on this finding, it is proposed that the ELF procedure could be permitted for structures with mass irregularity, such that that irregularity need not be assessed when selecting a suitable analysis procedure for system proportioning.

Since explicit collapse assessments were performed only for moment frame buildings and for mass ratios that do not exceed 3.0, there is some question of the generality of the findings. The concern is that "stiffness and mass irregularities may significantly affect the vertical distribution of forces" making the "modal analysis procedure, which can account for these discontinuities, … necessary" (SEAOC, 2013).

F.2 Expanded Design Space and Assessment Method

F.2.1 Expanded Design Space

An expanded design space was developed to test the sensitivity of the vertical distribution of forces used in proportioning the overall system. The expanded design space includes systems with shear-type response (typical of moment frames) and cantilever-type response (typical of shear walls). Systems of 3-, 10-, and 20-stories are considered in a regular configuration (identical mass at all stories) and with a severe mass irregularity (mass ratio of 3.0, 5.0, or 10.0) at a single story; a variety of locations are considered for the irregular story.

Figure F-1 and Table F-1 show the design space. The archetype perimeter frame building has a plan area of 120 feet by 120 feet, with story heights of 12'-6" and 30'-0" bays. The design is for Seismic Design Category D_{max} with $S_{DS} = 1.5$, $S_{D1} = 0.6$, and $C_u = 1.4$. All archetypes are proportioned using the results of the ELF procedure. Figure F-2 through Figure F-4 show member sizes for the moment frame archetypes. Reinforced concrete (RC) shear wall (SW) archetypes have 30-ft-long walls on each side with wall thicknesses of 24 inches, 18 inches, and 12 inches, respectively, for the 20-story, 10-story, and 3-story buildings.

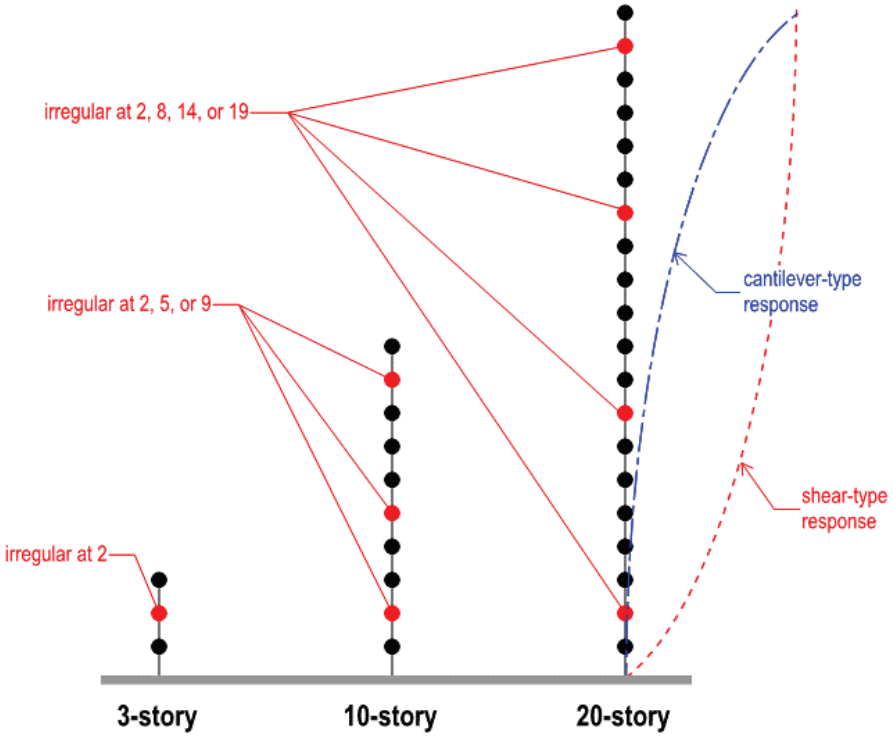

Figure F-1 Expanded design space for assessment of global behavior of buildings with mass irregularity.

Table F-1 System Properties for Expanded Design Space

	Stories	$T = C_u T_a$ (s)	R	C_s	(per framing line)		
					w (kip)	W (kip)	V (kip)
Baseline							
Steel SMF (shear)	3	0.712	8	0.105	700	2100	221
	10	1.866	8	0.066	700	7000	462
	20	3.248	8	0.066	700	14000	924
RC SW (cantilever)	3	0.424	5	0.283	900	2700	764
	10	1.047	5	0.115	900	9000	1032
	20	1.760	5	0.068	900	18000	1227
Irregular (x3)							
Steel SMF (shear)	3	0.712	8	0.105	700	3500	369
	10	1.866	8	0.066	700	8400	554
	20	3.248	8	0.066	700	15400	1016
RC SW (cantilever)	3	0.424	5	0.283	900	4500	1273
	10	1.047	5	0.115	900	10800	1238
	20	1.760	5	0.068	900	19800	1350
Irregular (x5)							
Steel SMF (shear)	3	0.712	8	0.105	700	4900	516
	10	1.866	8	0.066	700	9800	647
	20	3.248	8	0.066	700	16800	1109
RC SW (cantilever)	3	0.424	5	0.283	900	6300	1782
	10	1.047	5	0.115	900	12600	1444
	20	1.760	5	0.068	900	21600	1472
Irregular (x10)							
Steel SMF (shear)	3	0.712	8	0.105	700	8400	885
	10	1.866	8	0.066	700	13300	878
	20	3.248	8	0.066	700	20300	1340
RC SW (cantilever)	3	0.424	5	0.283	900	10800	3054
	10	1.047	5	0.115	900	17100	1960
	20	1.760	5	0.068	900	26100	1779

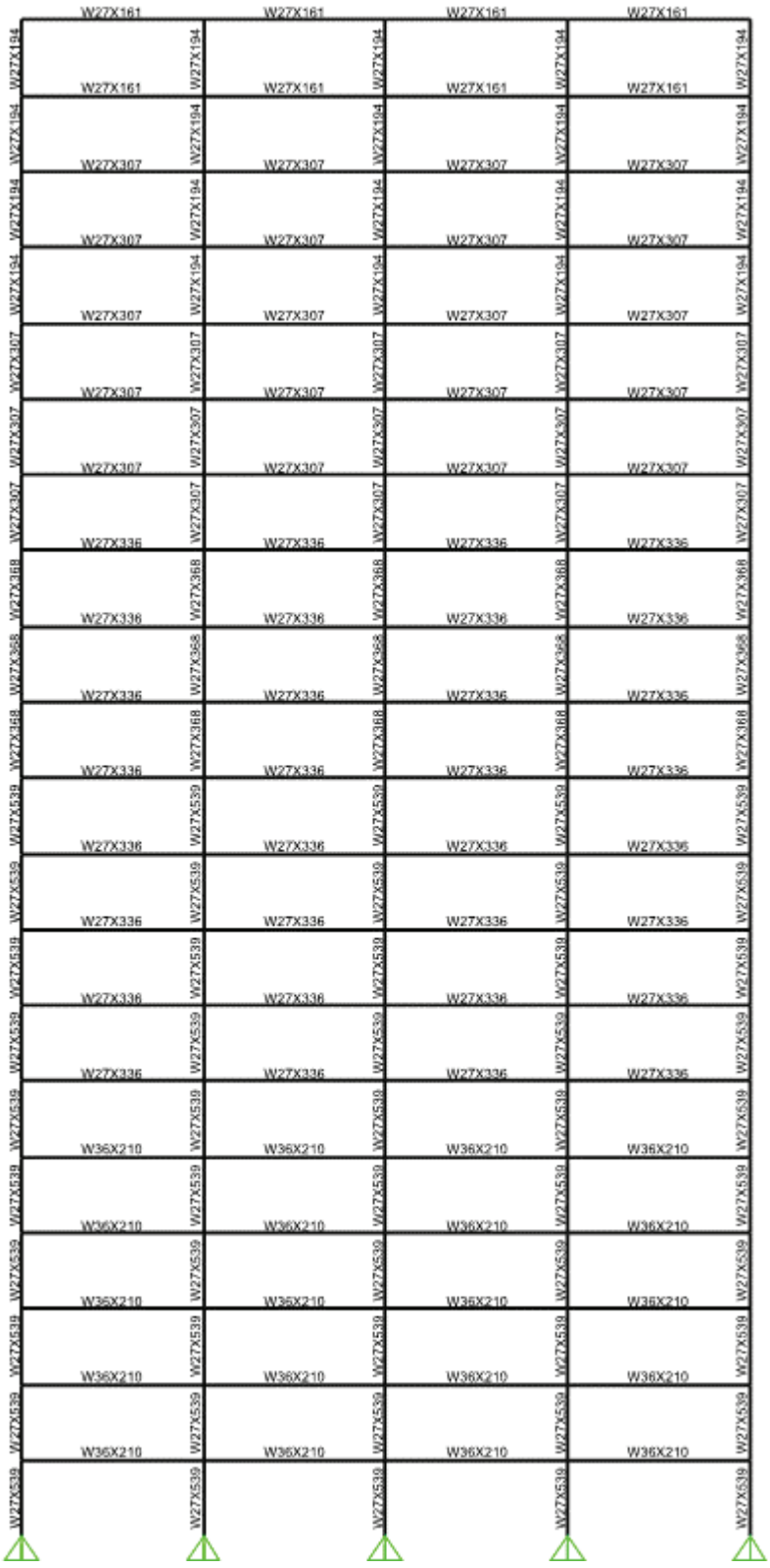

Figure F-2 Member sizes for the 20-story steel SMF baseline archetype.

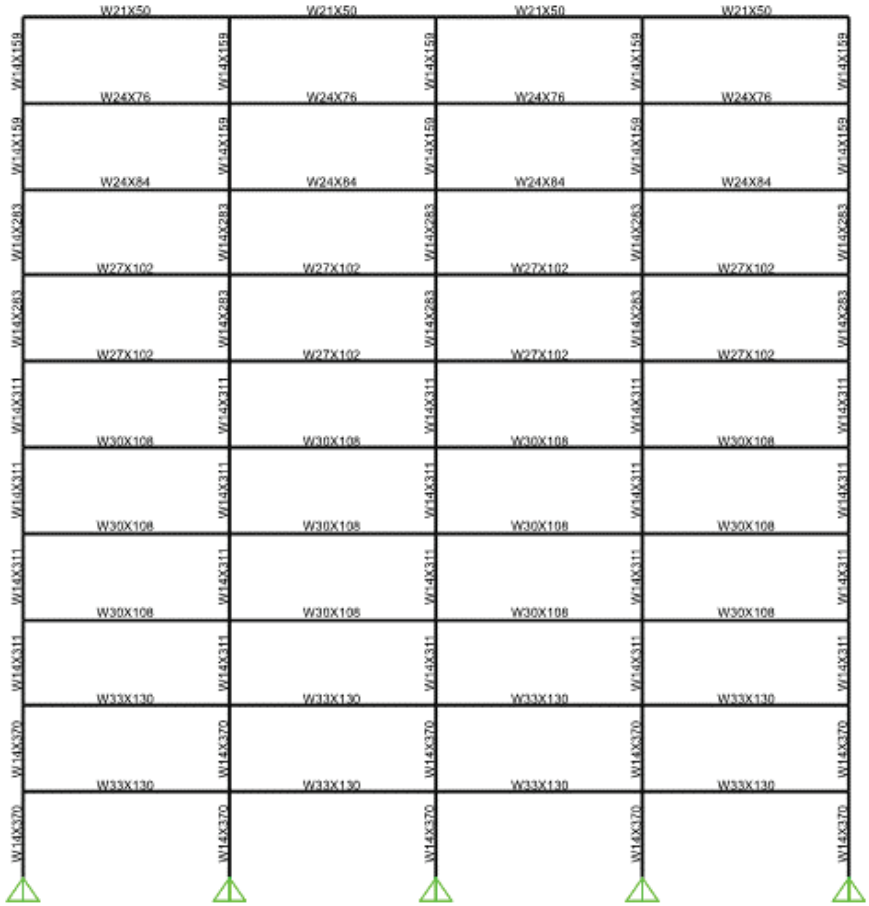

Figure F-3 Member sizes for the 10-story steel SMF baseline archetype.

Figure F-4 Member sizes for the 3-story steel SMF baseline archetype.

Figure F-5 shows that the RC SW archetypes have cantilever-type response. Figure F-6 shows that the SMF archetypes have shear-type response.

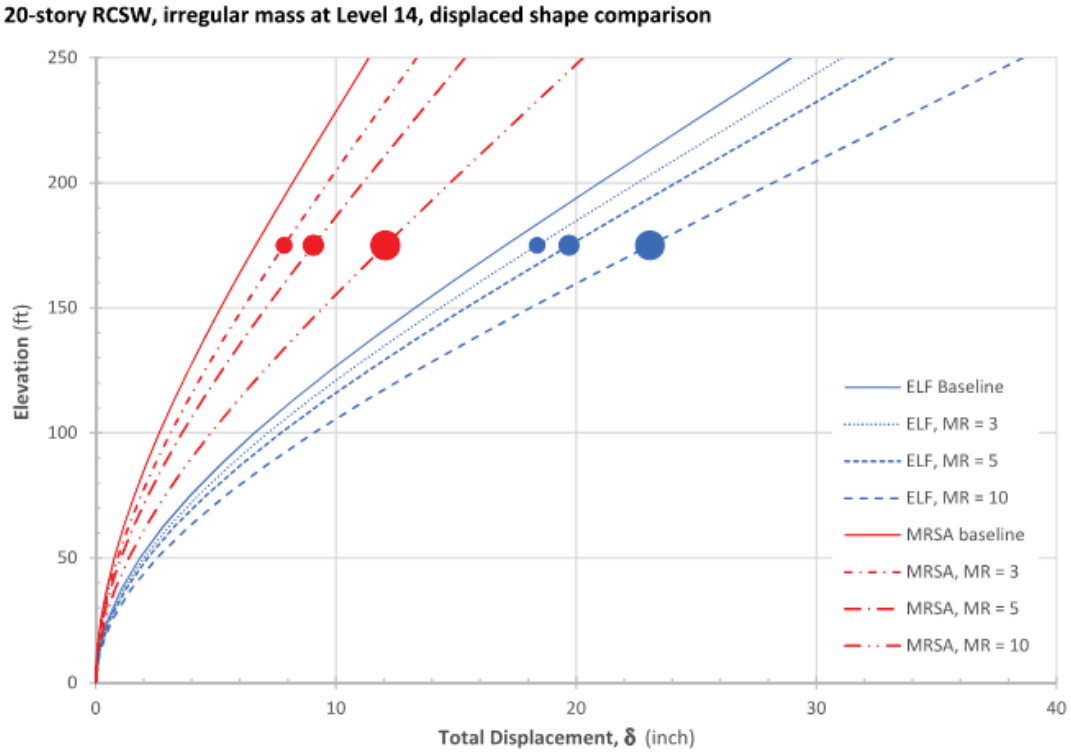

Figure F-5 Cantilever-type response of RC SW archetypes.

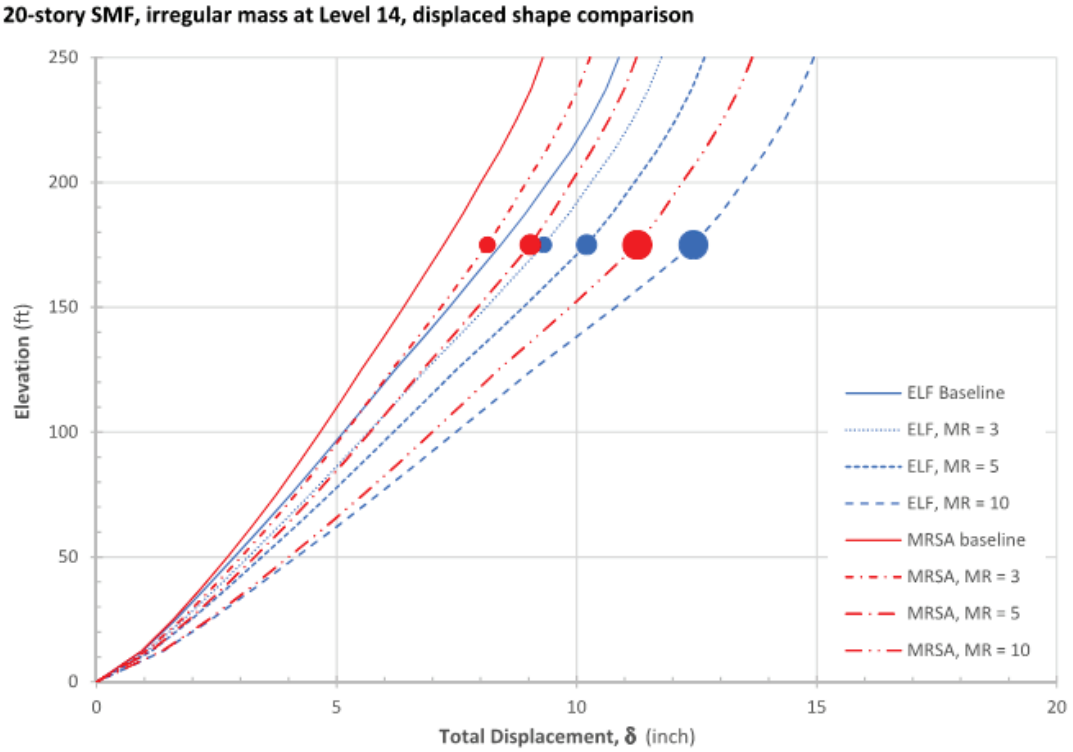

Figure F-6 Shear-type response of steel SMF archetypes.

F.2.2 Assessment Method for Global Behavior

Rather than completing the detailed design of each archetype and explicitly assessing its collapse resistance using the FEMA P695 method, the MRSA and ELF procedures are used to determine differing vertical distributions of story forces so that the related global behavior metrics of story shear, story overturning moment, and story drift (which would drive the detailed design) can be compared. For the ELF procedure story forces are determined in accordance with Section 12.8.3 of ASCE/SEI 7-16, including the exponent, k, related to structure period, which varies from 1.0 to 2.0 for structures with periods from 0.5 to 2.5 seconds. For the MRSA response parameters are computed in accordance with Section 12.9.1 of ASCE/SEI 7-16, including scaling of forces to 100% of the ELF base shear. For all analyses section cuts are used to compute story shear and story overturning moment, and generalized displacements are used to compute maximum story drift in accordance with Section 12.8.6 of ASCE/SEI 7-16.

For each archetype, the distribution of story shear, story overturning moment, and maximum story drift from MRSA and the ELF procedure can be compared. The simplest assessment of the conservatism of the ELF procedure can be made by comparing the shear ratio and moment ratio (ELF/MRSA) for each story to 1.0. Where the ELF/MRSA ratio exceeds 1.0, the ELF procedure global demands, which would drive detailed design and thus collapse resistance, are conservative. Where the ELF/MRSA ratio is less than 1.0, ratios for the baseline (regular) condition should be considered to determine whether mass irregularity is the cause of the smaller values. Even where mass irregularity appears to reduce conservatism compared to the baseline condition, detailed results should be compared to assess whether the reduction has practical significance to the design; for instance, where story shear or moment at the top of a building is very small compared to the base shear or moment, the computed story shear or story moment ratios may exaggerate the significance of the difference.

F.3 Findings

In all cases, except for the 3-story reinforced concrete shear wall (RC SW) archetypes (where the difference is inconsequential), the story drifts computed using the ELF procedure exceed those computed using MRSA. The ELF story shear and story moment for the baseline (regular) buildings exceed those from MRSA, except at the top of 10- or 20-story archetypes and for the 3-story RC SW archetypes. Differences for the 3-story RC SW baseline archetype are inconsequential, and the shear and moment ratios actually improve as the mass ratio increases (Figure F-7 and Figure F-8).

As discussed in Section C12.8.3 of ASCE 7-16, the exponent *k* used in the ELF procedure "is intended to approximate the effect of higher modes" and the horizontal forces computed "are intended to provide lateral seismic forces at individual levels that are consistent with enveloped results from more accurate analyses." Although the ELF/MRSA shear and moment ratios at the top of the 10- and 20-story baseline archetypes can be well below 1.0, the story shears and moments at those levels are so much smaller than the base shear and base moment that the differences are unlikely to be significant for practical designs.

In some cases, the conservatism of the ELF procedure increases as irregular mass ratio increases. For instance, the 20-story RC SW and SMF archetypes exhibit this behavior where the mass irregularity occurs at Level 2 (Figure F-9 and Figure F-10).

In other cases, the increasing mass ratio reduces the conservatism of the ELF procedure, but the ELF/MRSA shear and moment ratios still exceed 1.0 or are no worse than the ratios for the baseline (regular) building. For instance, the 20-story RC SW and SMF archetypes exhibit this behavior where the mass irregularity occurs at Level 8 (Figure F-11, Figure F-12, and Figure F-13).

For three archetypes (20-story SMF with irregular mass at Level 14, 20-story RC SW with irregular mass at Level 14, and 10-story RC SW with irregular mass at Level 5), reductions in ELF/MRSA ratio for increasing mass ratio identify areas where detailed results should be compared.

For the 20-story SMF with irregular mass at Level 14 (Figure F-14 and Figure F-15) ELF/MRSA ratios are less than 1.0 in stories above the mass irregularity. However, the detailed results (Figure F-16 through Figure F-18) show that this is an artifact of very small story shears and moments at the top of the building. When compared with the base shear and base moment, those differences are inconsequential.

For the 20-story RC SW with irregular mass at Level 14 and the 10-story RC SW with irregular mass at Level 5 (Figure F-19, Figure F-20, Figure F-21, and Figure F-22) ELF/MRSA ratios are less than 1.0 in stories above the mass irregularity. However, the detailed results (Figure F-23 through Figure F-25, and Figure F-26 through Figure F-28) show that the story shears and moments above the mass irregularity have similar trends and are small compared to the base shear and base moment. Those differences would not significantly affect the detailed design unless the horizontal dimension of the seismic-force-resisting system were also reduced at those levels; if that were

the case irregularity V3 would exist and MRSA would be required by Table 12.3-2 of ASCE/SEI 7-16.

F.4 Recommendations

Comparison of the global behavior metrics of story shear, story overturning moment, and story drift (which would drive detailed design) for systems with shear-type response or cantilever-type response show that the ELF procedure produces results that would be appropriate for design. In most cases the ELF demands for systems with large mass ratios (up to 10) are greater than or close to the MRSA demands. In the few cases where ELF demands are noticeably less than MRSA demands, practical designs would still be conservative unless the horizontal dimension of the seismic-force-resisting system were greatly reduced above the mass irregularity; such a reduction would produce a V3 (vertical geometric) irregularity, thus requiring use of the MRSA method for design of the system. These analyses, together with the results of the explicit collapse assessments reported in Chapter 6, suggest that there is no need to define mass irregularity in ASCE/SEI 7-16 for buildings and nonbuilding structures similar to buildings. If there are nonbuilding structures whose mass distribution requires special consideration (such as MRSA), appropriate requirements for those structures should be provided in Chapter 15 of ASCE/SEI 7.

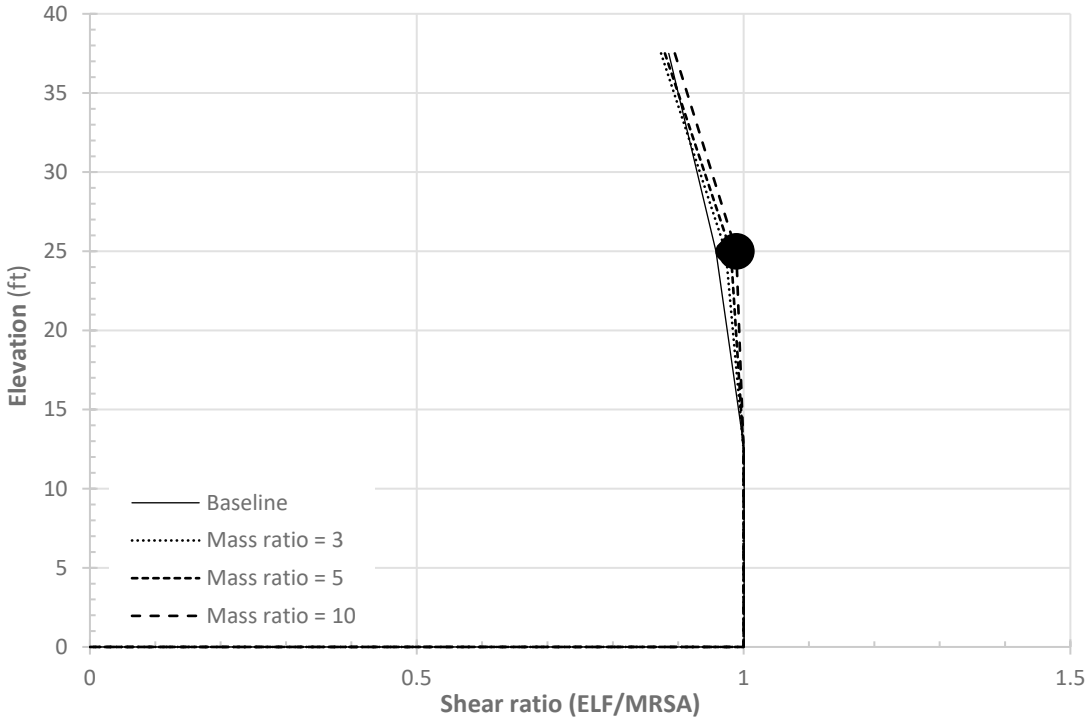

Figure F-7 3-story RC SW, irregular mass at Level 2, story shear ratios (ELF/MRSA). This figure is reproduced as Figure F-75 in the electronic Supporting Documentation for Appendix F: Additional Figures.

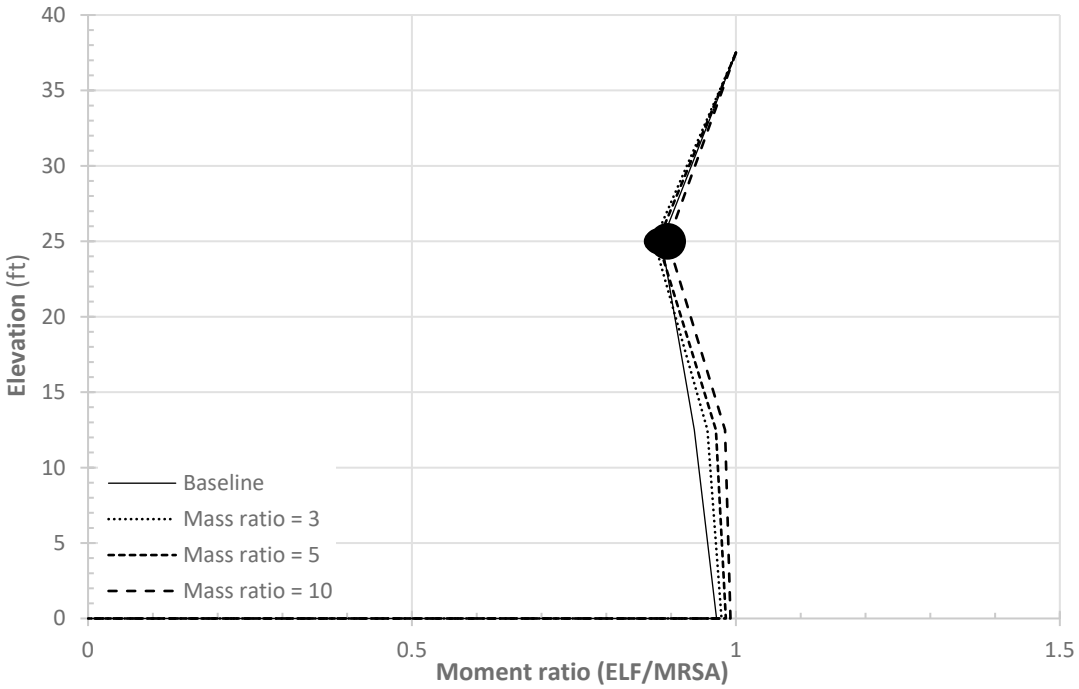

Figure F-8 3-story RC SW, irregular mass at Level 2, story moment ratios (ELF/MRSA). This figure is reproduced as Figure F-76 in the electronic Supporting Documentation for Appendix F: Additional Figures.

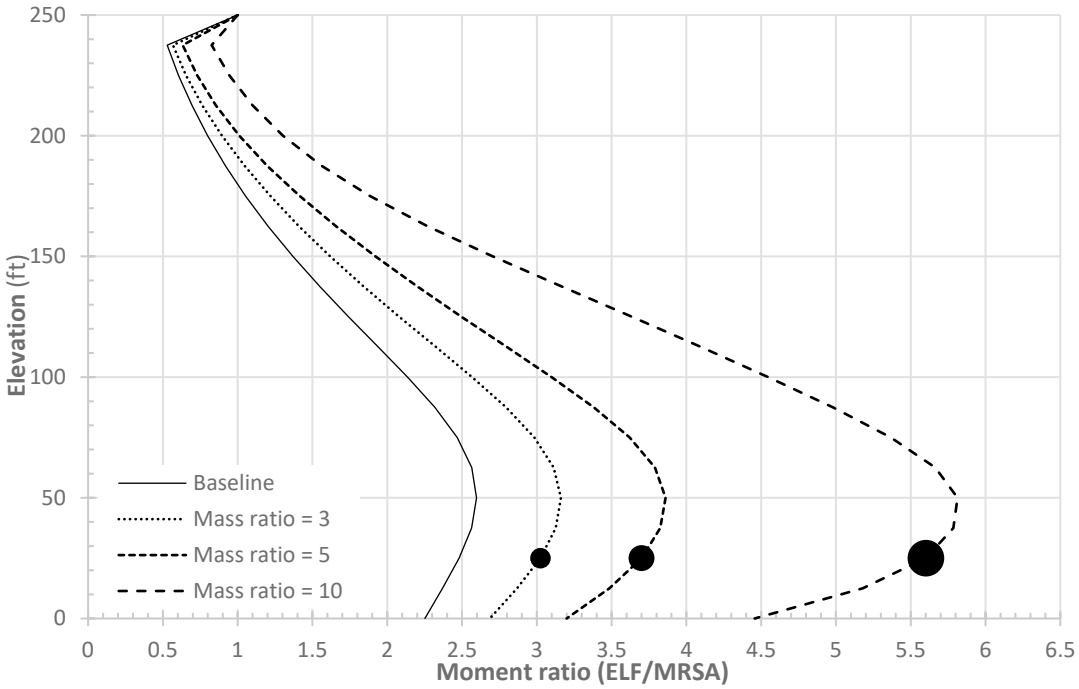

Figure F-9 20-story RC SW, irregular mass at Level 2, story moment ratios (ELF/MRSA). This figure is reproduced as Figure F-34 in the electronic Supporting Documentation for Appendix F: Additional Figures.

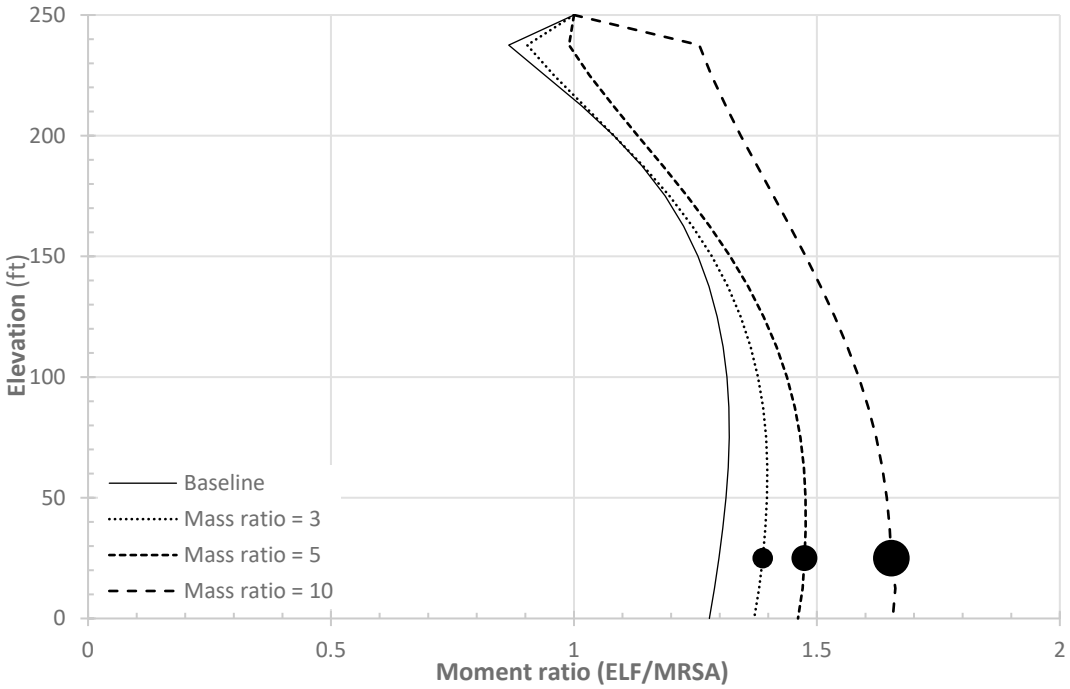

Figure F-10 20-story SMF, irregular mass at Level 2, story moment ratios (ELF/MRSA). This figure is reproduced as Figure F-82 in the electronic Supporting Documentation for Appendix F: Additional Figures.

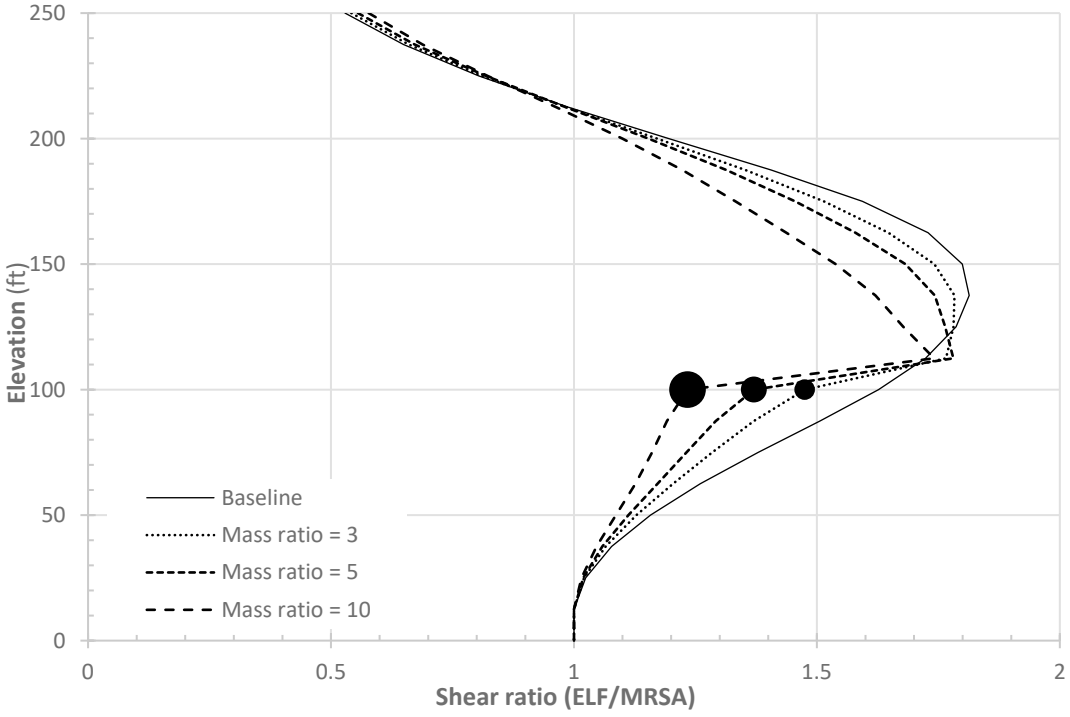

Figure F-11 20-story RC SW, irregular mass at Level 8, story shear ratios (ELF/MRSA). This figure is reproduced as Figure F-39 in the electronic Supporting Documentation for Appendix F: Additional Figures.

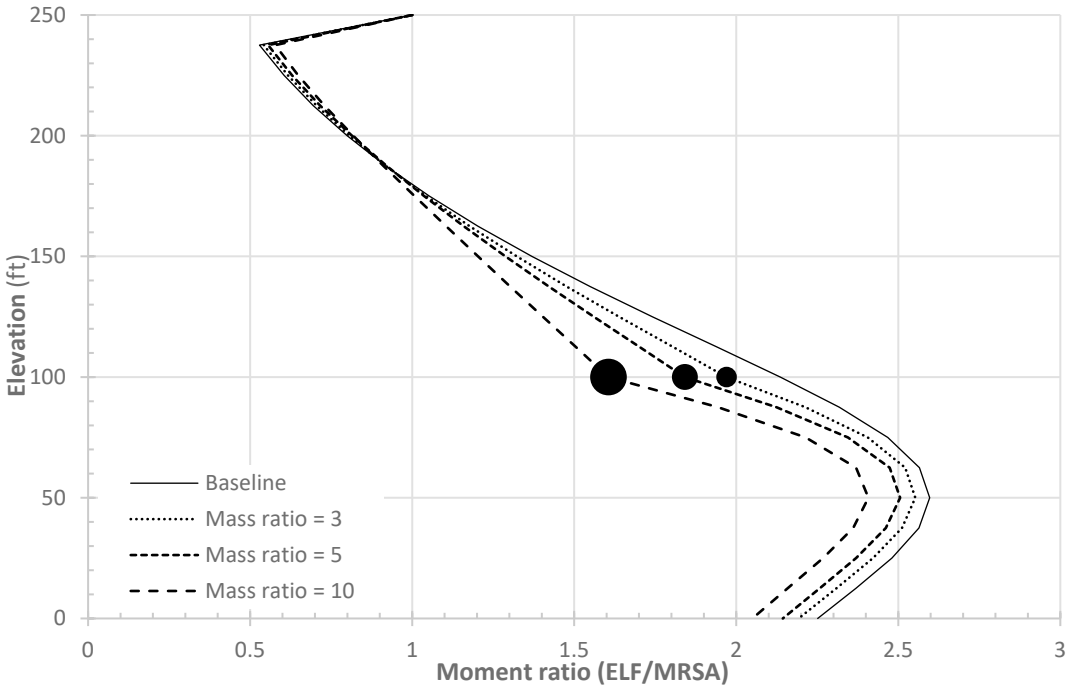

Figure F-12 20-story RC SW, irregular mass at Level 8, story moment ratios (ELF/MRSA). This figure is reproduced as Figure F-40 in the electronic Supporting Documentation for Appendix F: Additional Figures.

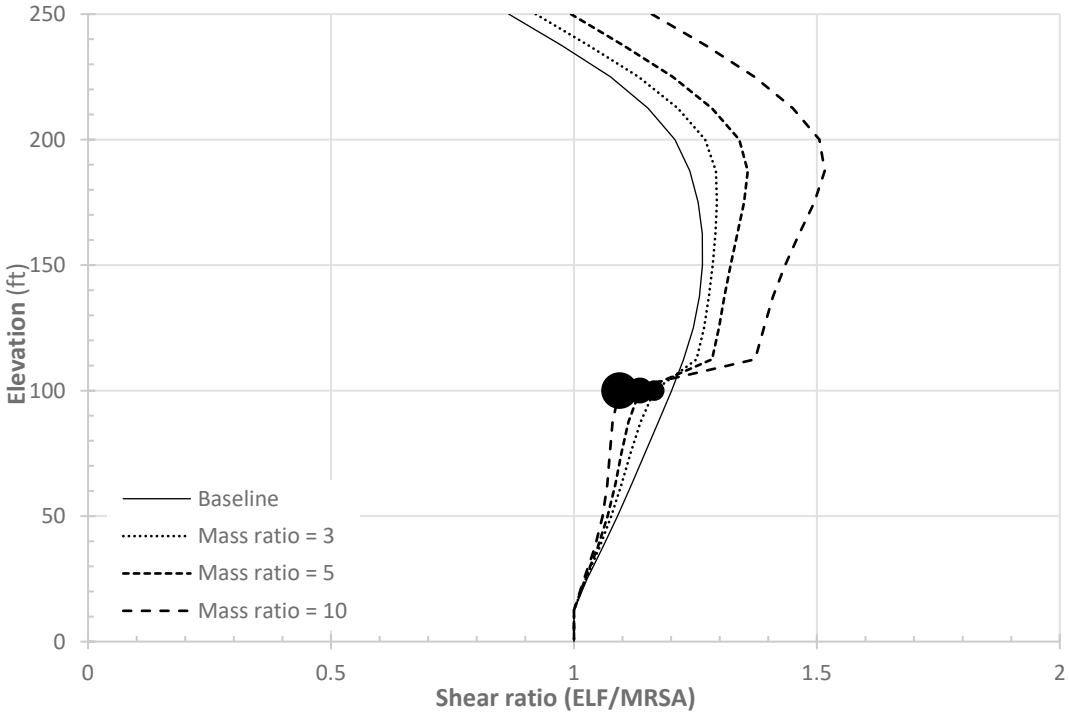

Figure F-13 20-story SMF, irregular mass at Level 8, story shear ratios (ELF/MRSA). This figure is reproduced as Figure F-87 in the electronic Supporting Documentation for Appendix F: Additional Figures.

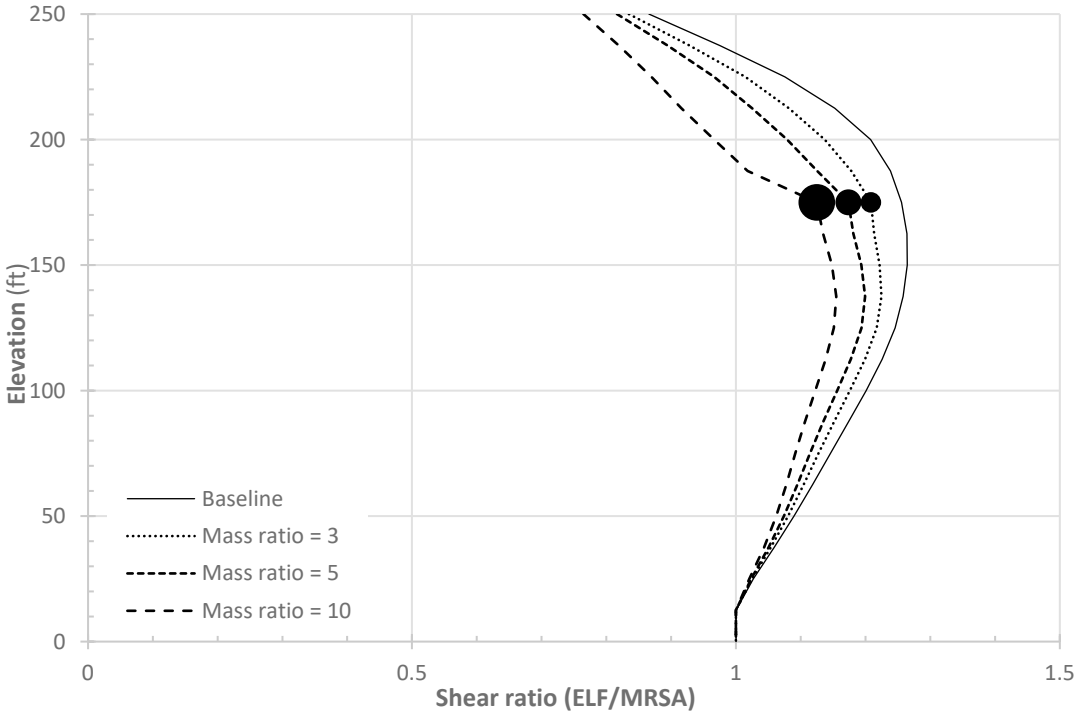

Figure F-14 20-story SMF, irregular mass at Level 14, story shear ratios (ELF/MRSA). This figure is reproduced as Figure F-93 in the electronic Supporting Documentation for Appendix F: Additional Figures.

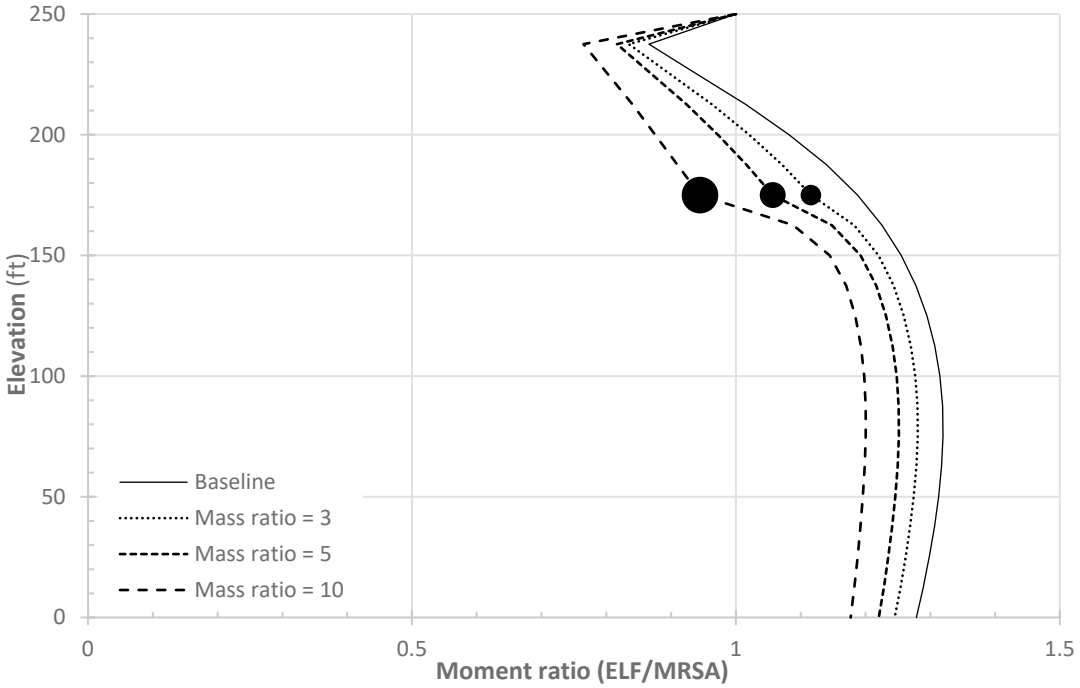

Figure F-15 20-story SMF, irregular mass at Level 14, story moment ratios (ELF/MRSA). This figure is reproduced as Figure F-94 in the electronic Supporting Documentation for Appendix F: Additional Figures.

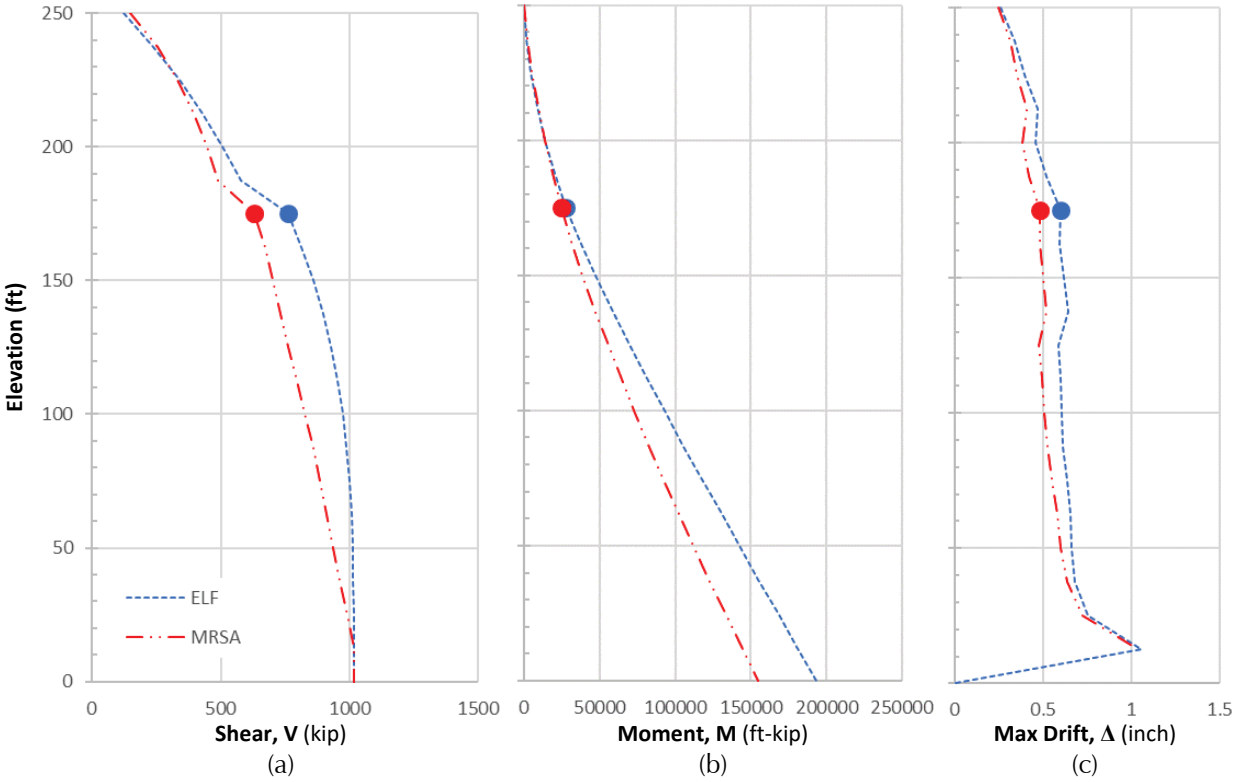

Figure F-16 20-story SMF, irregular mass at Level 14, mass ratio = 3. This figure is reproduced as Figure F-90 in the electronic Supporting Documentation for Appendix F: Additional Figures.

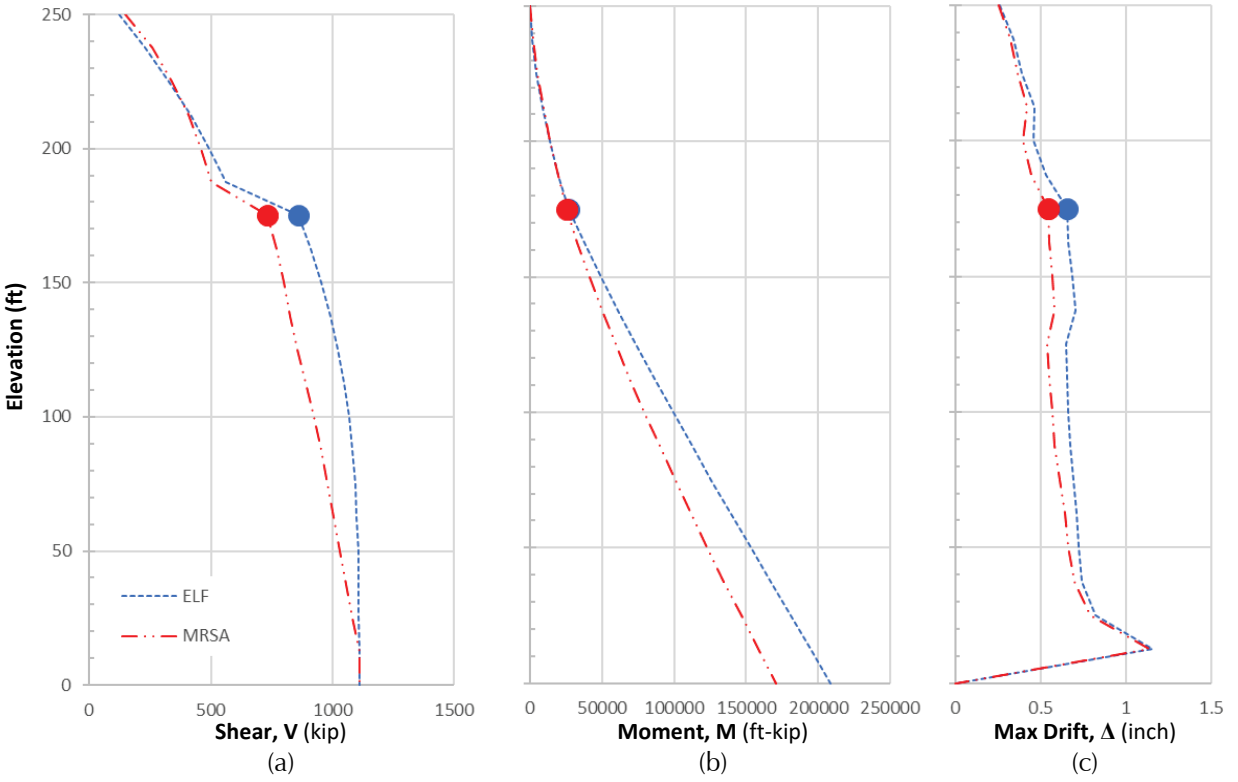

Figure F-17 20-story SMF, irregular mass at Level 14, mass ratio = 5. This figure is reproduced as Figure F-91 in the electronic Supporting Documentation for Appendix F: Additional Figures.

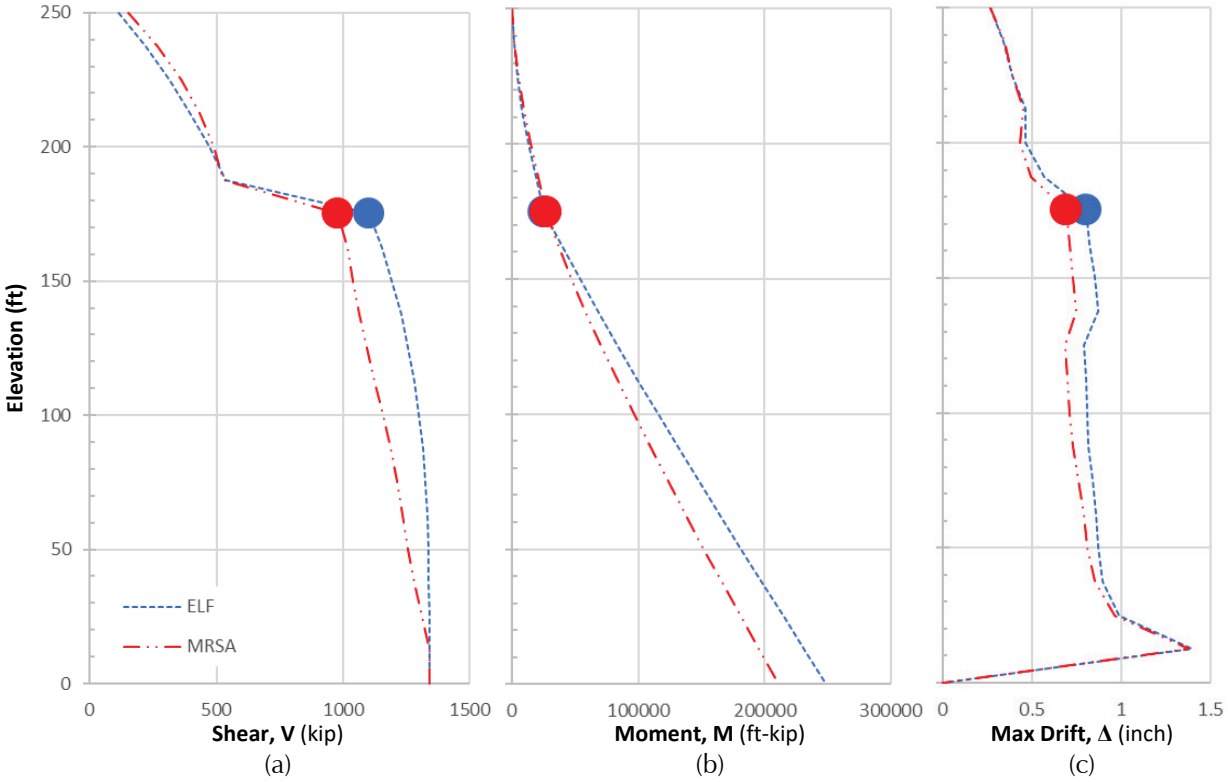

Figure F-18 20-story SMF, irregular mass at Level 14, mass ratio = 10. This figure is reproduced as Figure F-92 in the electronic Supporting Documentation for Appendix F: Additional Figures.

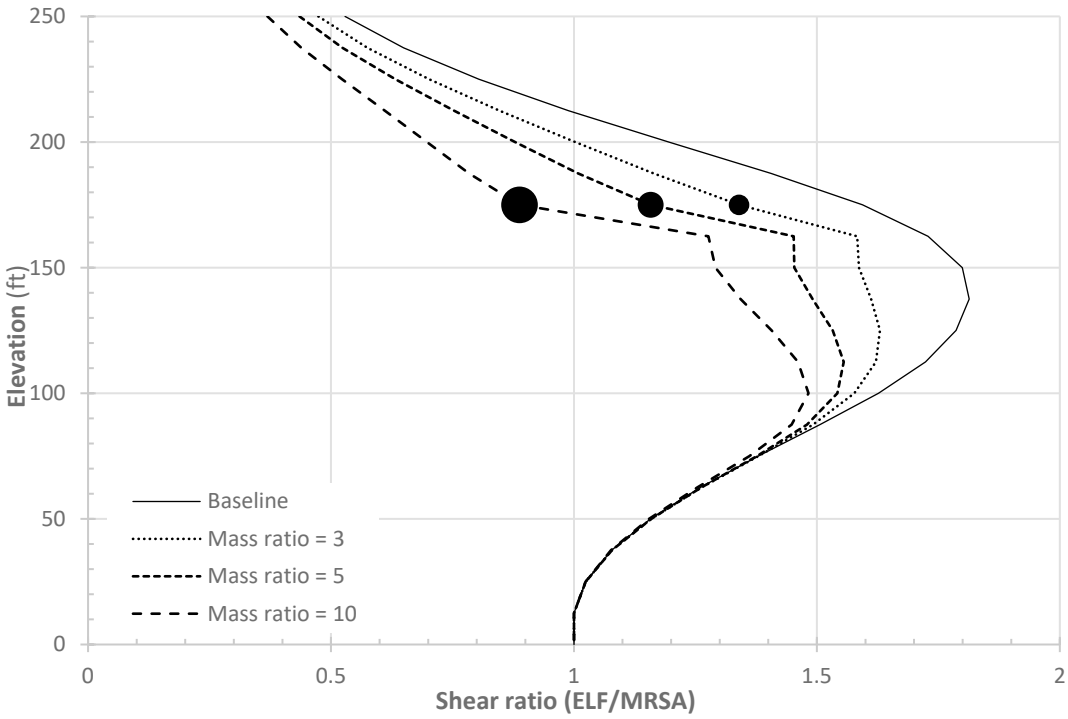

Figure F-19 20-story RC SW, irregular mass at Level 14, story shear ratios (ELF/MRSA). This figure is reproduced as Figure F-45 in the electronic Supporting Documentation for Appendix F: Additional Figures.

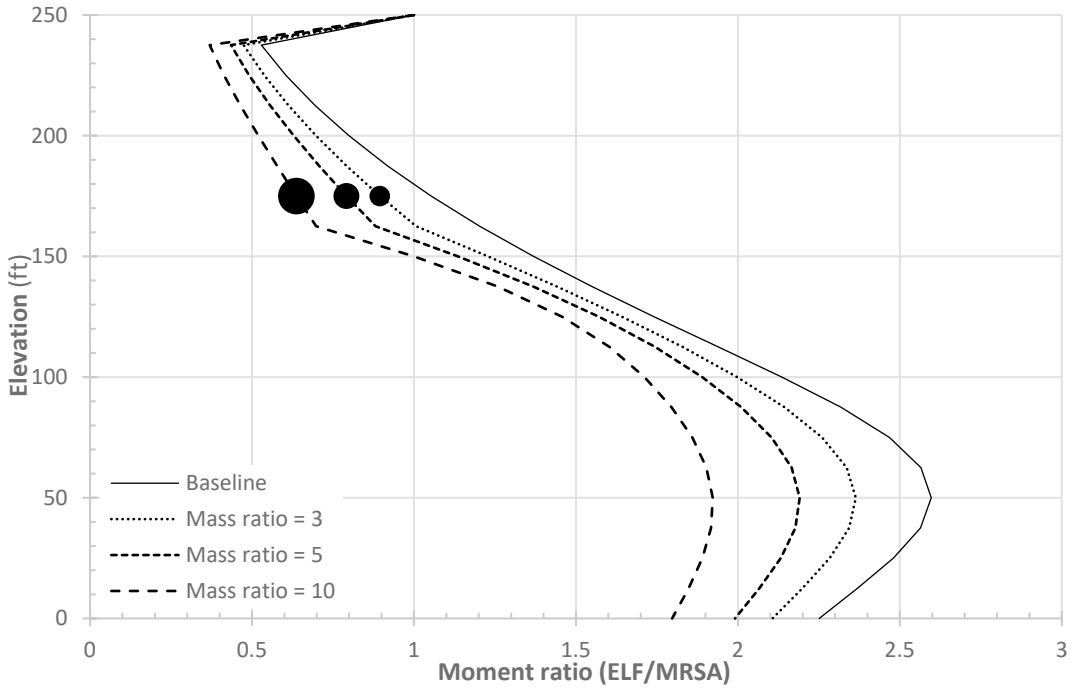

Figure F-20 20-story RC SW, irregular mass at Level 14, story moment ratios (ELF/MRSA). This figure is reproduced as Figure F-46 in the electronic Supporting Documentation for Appendix F: Additional Figures.

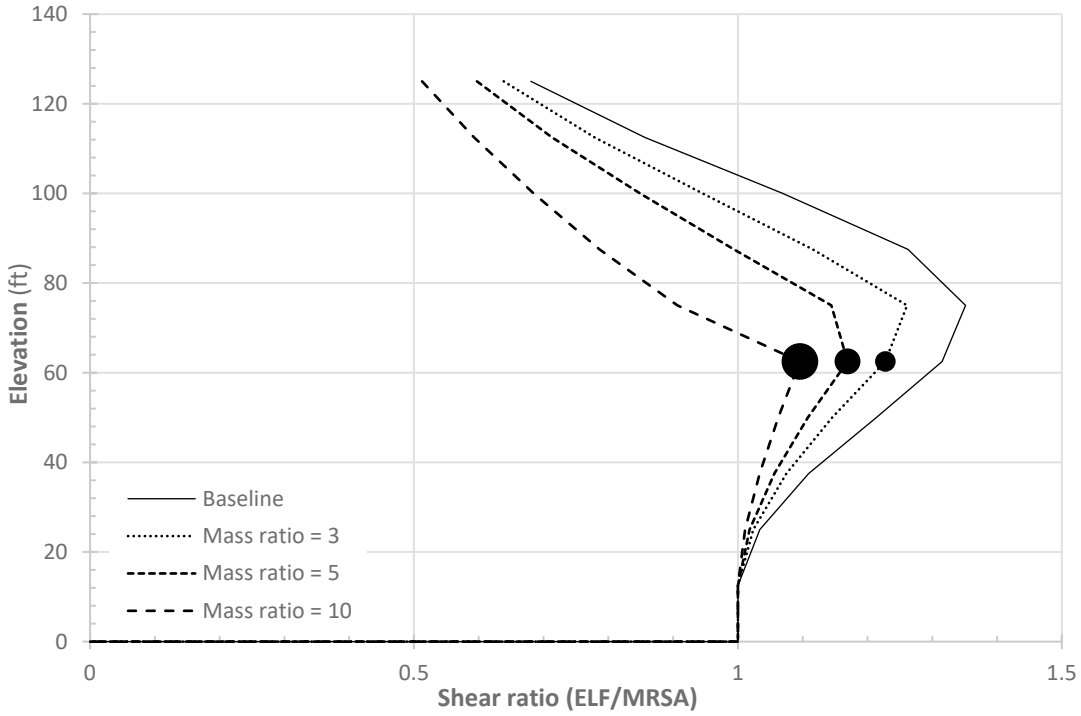

Figure F-21 10-story RC SW, irregular mass at Level 5, story shear ratios (ELF/MRSA). This figure is reproduced as Figure F-63 in the electronic Supporting Documentation for Appendix F: Additional Figures.

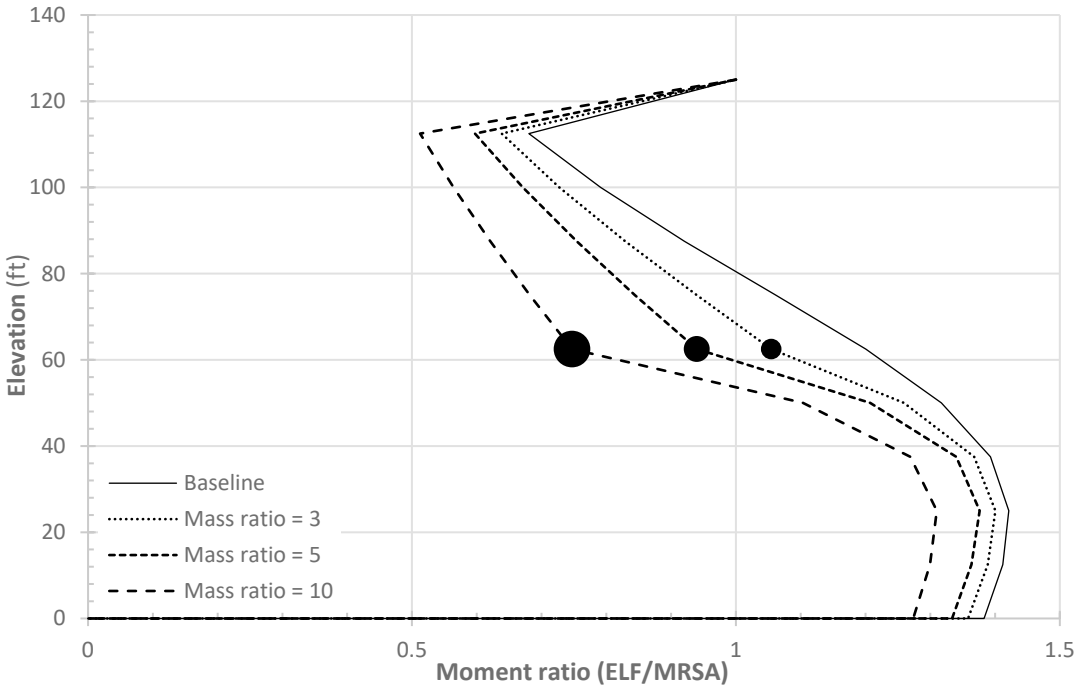

Figure F-22 10-story RC SW, irregular mass at Level 5, story moment ratios (ELF/MRSA). This figure is reproduced as Figure F-64 in the electronic Supporting Documentation for Appendix F: Additional Figures.

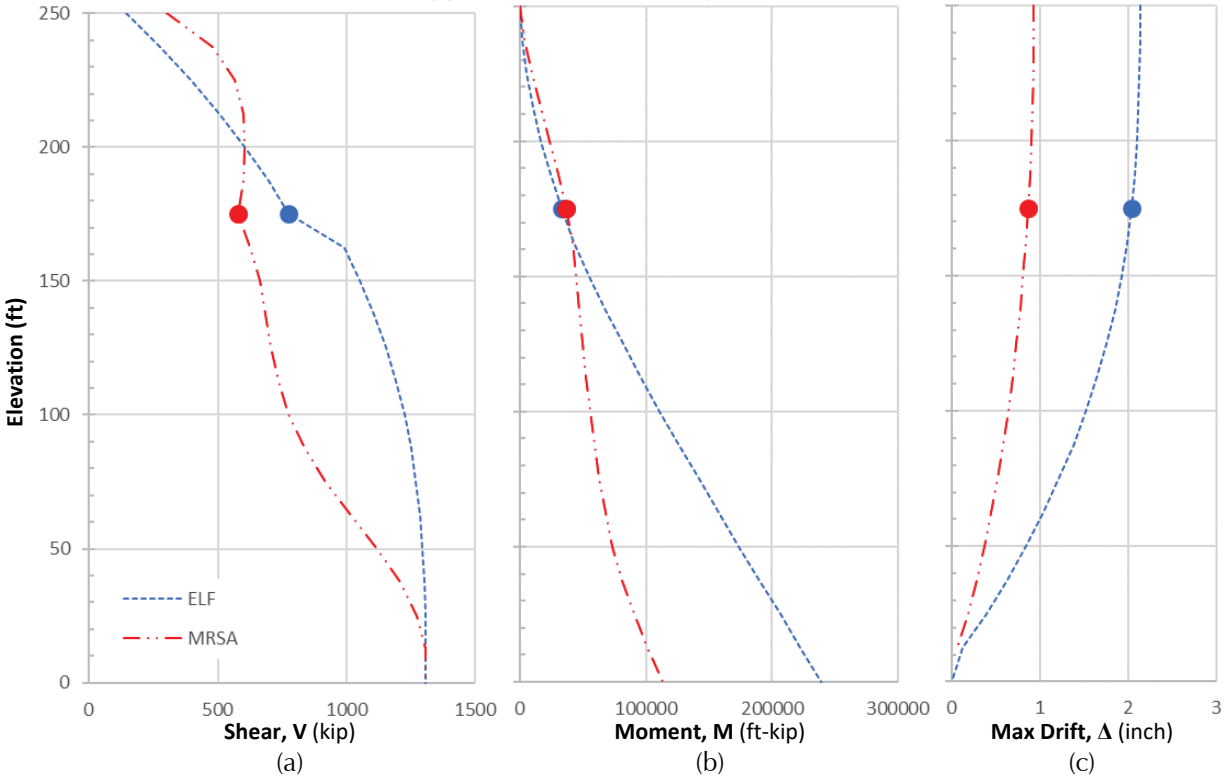

Figure F-23 20-story RC SW, irregular mass at Level 14, mass ratio = 3. This figure is reproduced as Figure F-42 in the electronic Supporting Documentation for Appendix F: Additional Figures.

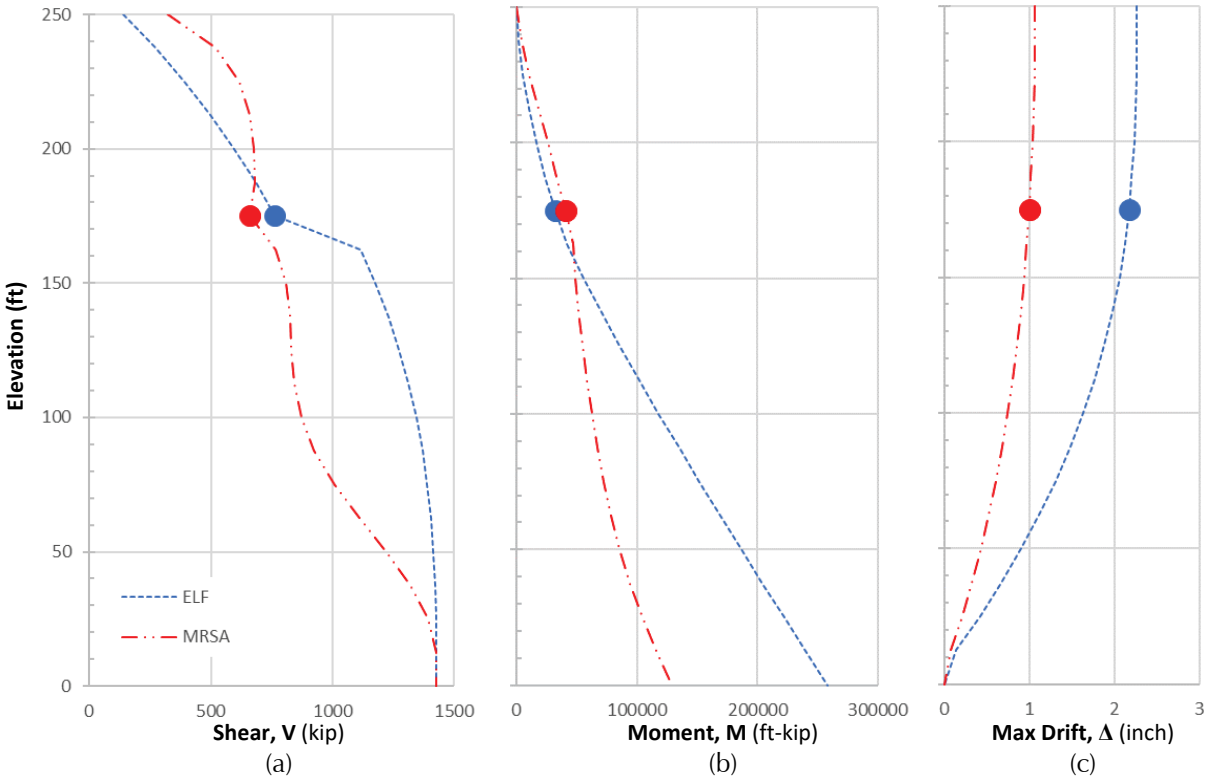

Figure F-24 20-story RC SW, irregular mass at Level 14, mass ratio = 5. This figure is reproduced as Figure F-43 in the electronic Supporting Documentation for Appendix F: Additional Figures.

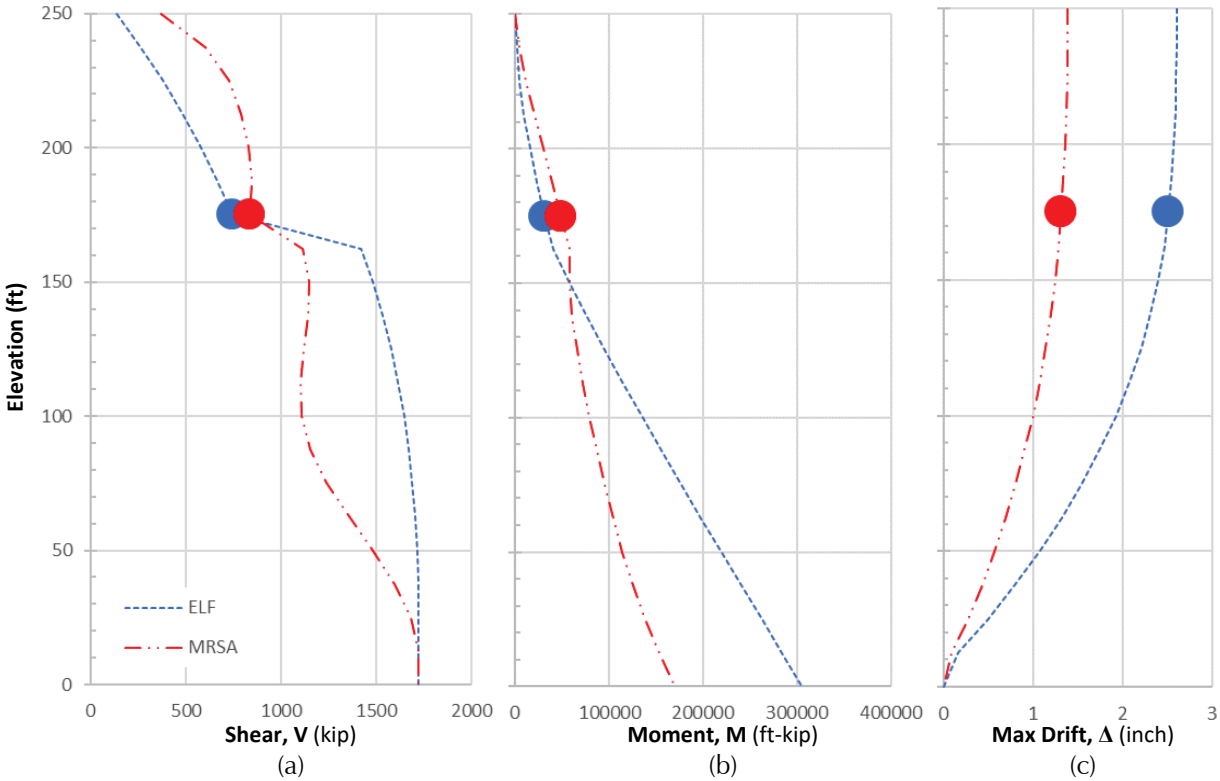

Figure F-25 20-story RC SW, irregular mass at Level 14, mass ratio = 10. This figure is reproduced as Figure F-44 in the electronic Supporting Documentation for Appendix F: Additional Figures.

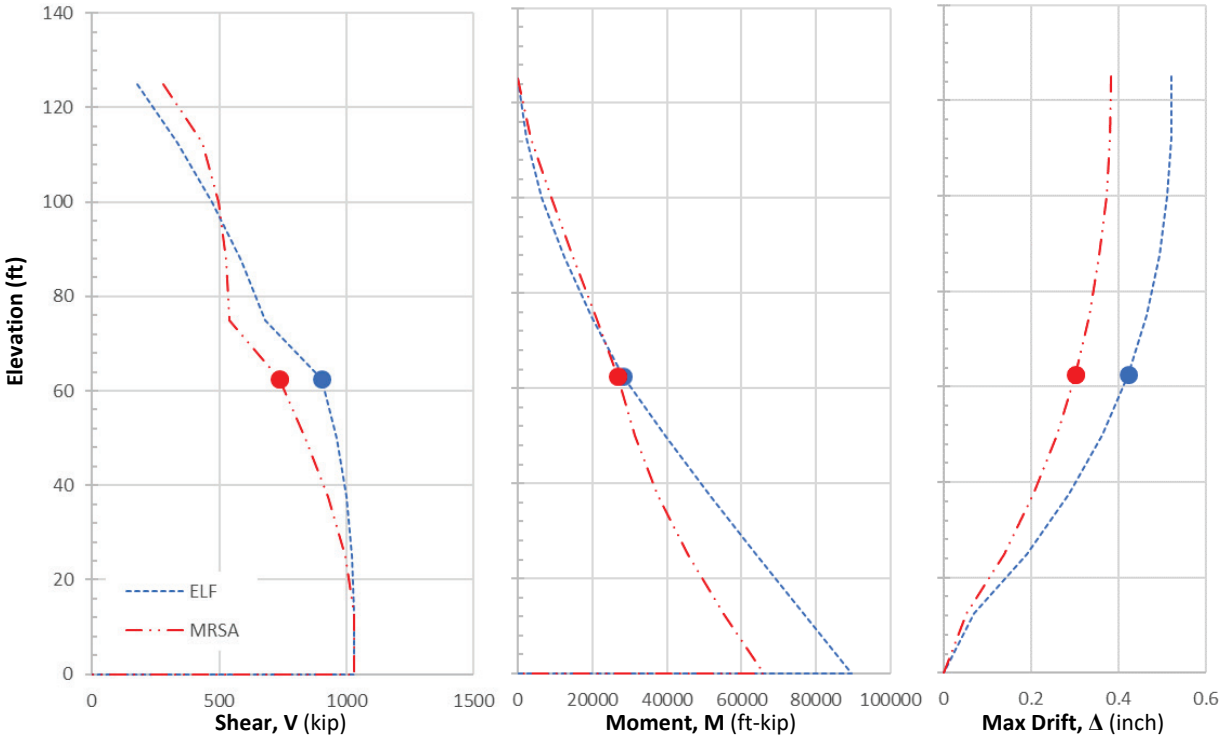

Figure F-26 10-story RC SW, irregular mass at Level 5, mass ratio = 3. This figure is reproduced as Figure F-60 in the electronic Supporting Documentation for Appendix F: Additional Figures.

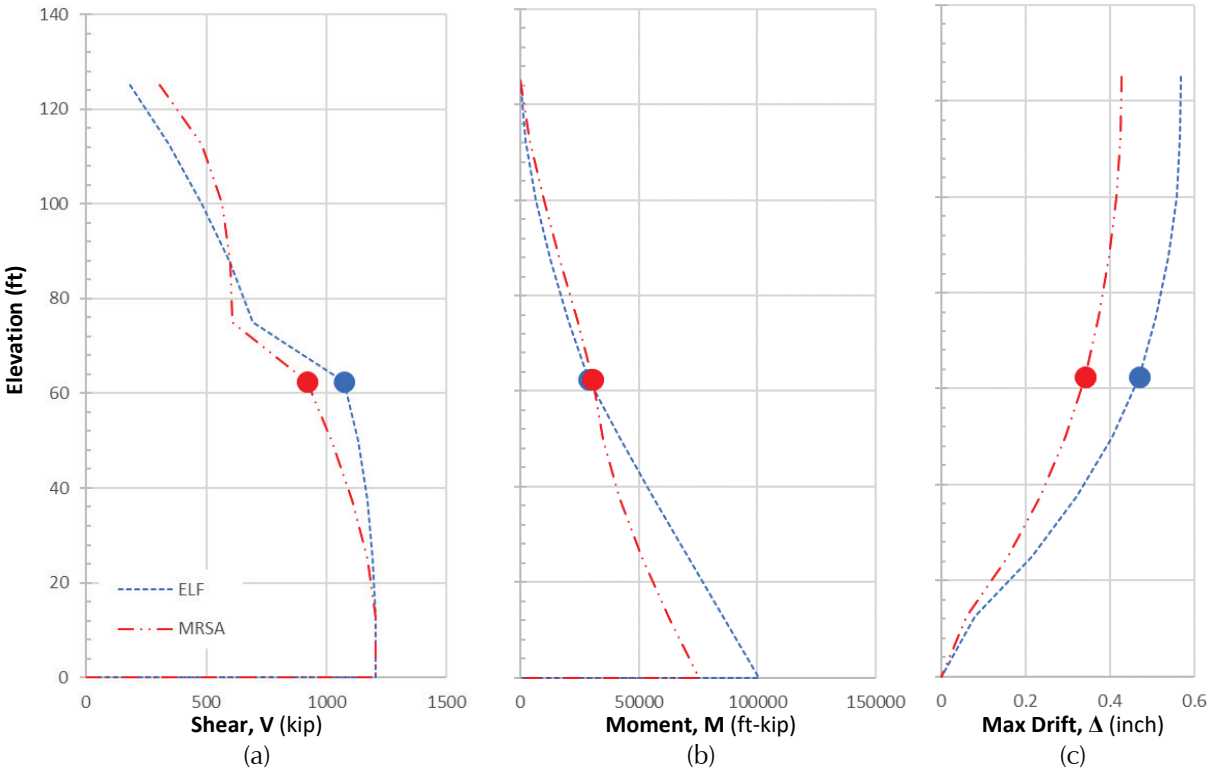

Figure F-27 10-story RC SW, irregular mass at Level 5, mass ratio = 5. This figure is reproduced as Figure F-61 in the electronic Supporting Documentation for Appendix F: Additional Figures.

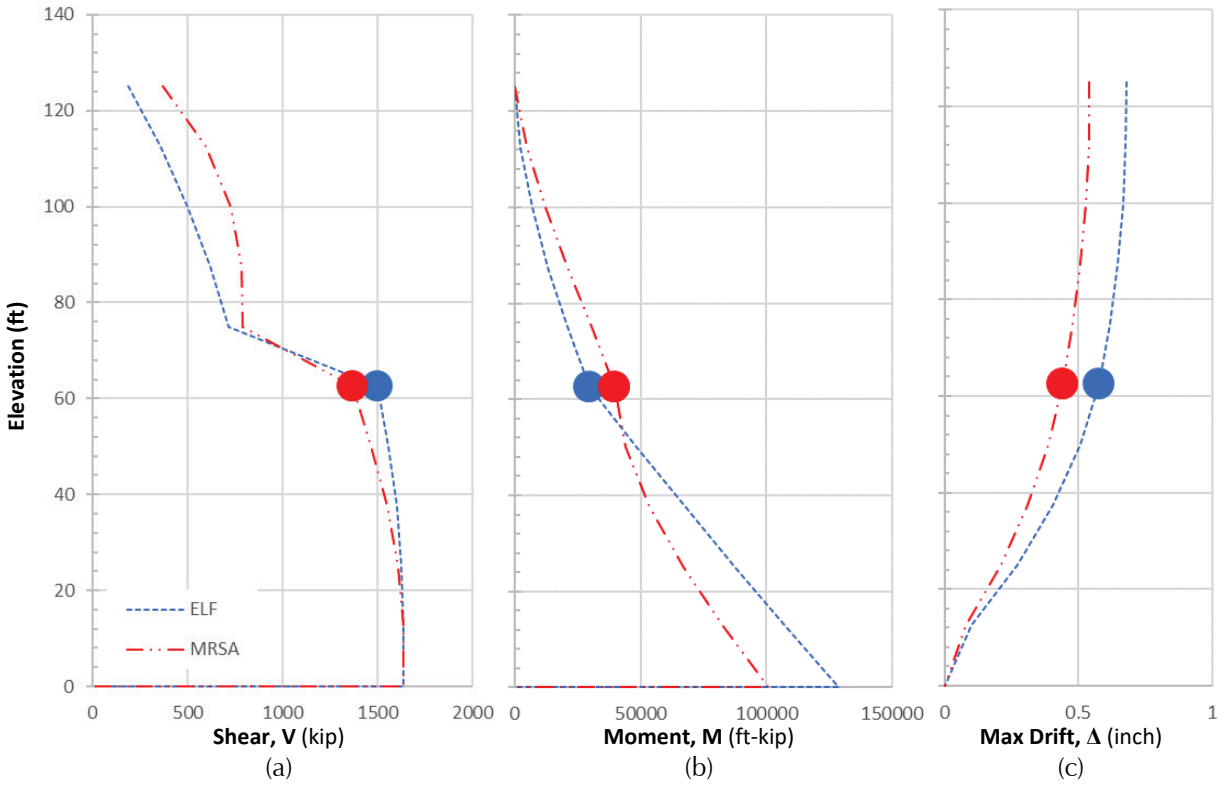

Figure F-28 10-story RC SW, irregular mass at Level 5, mass ratio = 10. This figure is reproduced as Figure F-62 in the electronic Supporting Documentation for Appendix F: Additional Figures.

Appendix G

Story Stiffness and Strength Calculation

This Appendix provides recommendations for the calculation of story stiffness and story strength. Such calculations are required to assess soft story and weak story vertical configuration irregularities [V1 and V5] and to determine the redundancy factor, ρ, in accordance with Table 12.3-3 of ASCE/SEI 7-16.

In addition to summarizing recommendations from the available literature, this appendix presents findings from analysis of a design space of 3-, 10-, and 20-story systems with shear-type response (typical of moment frames) and cantilever-type response (typical of shear walls) in a regular configuration (identical mass at all stories) and with a severe mass irregularity (mass ratio of 3.0, 5.0, or 10.0) at a single story. A few moment frame archetypes with unusual story heights were also investigated. Figure G-1 shows the design space used for these assessments. Archetypes were developed for shear-type response (representative of moment frames) and cantilever-type response (representative of shear walls) for baseline conditions (uniform story heights and story masses). Additional archetypes have uniform story heights but irregular masses of 3, 5, and 10 times the standard mass separately at each location indicated. Other archetypes were developed with uniform masses but with tall story height at an intermediate level. Appendix F provides the design details for each baseline archetype.

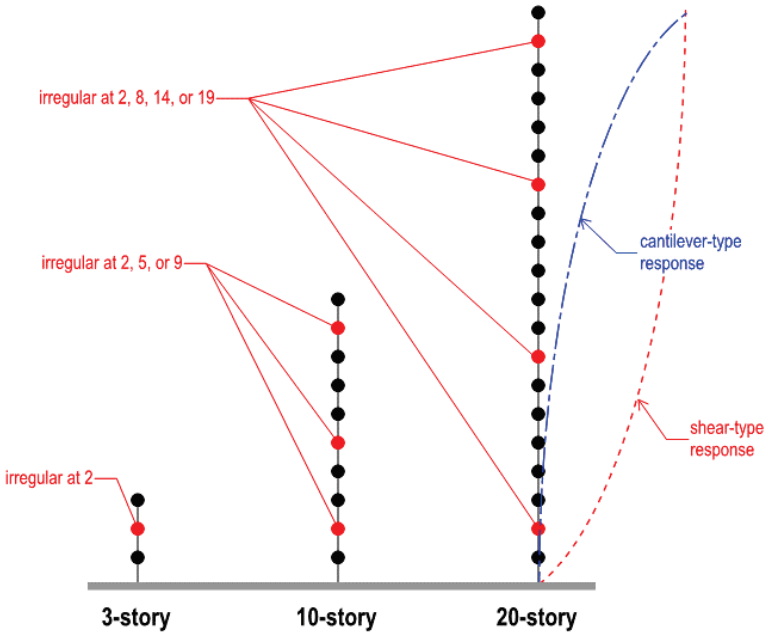

Figure G-1 Design space for story stiffness calculations.

G.1 Background

The equivalent lateral force (ELF) "procedure is based on an assumption of a gradually varying distribution of … stiffness along the height" (ASCE, 2017a). "Stiffness … discontinuities may significantly affect the vertical distribution of forces and, for this reason, the modal analysis procedure, which can account for these discontinuities," has been deemed necessary in such circumstances (SEAOC, 2013). The triggers provided in Table 12.3-2 of ASCE/SEI 7-16 for soft story and extreme soft story irregularity reflect stiffness ratios between adjacent stories that would not be considered "gradually varying." These judgment-based trigger values were established at a time when it was common for designers to use hand calculations for structures with simple configurations. Even for simple structures, the limitations of those calculations are quite severe, as discussed in Section G.2.1.

The *R*-factors used in ASCE/SEI 7-16 Chapter 12 design procedures are appropriate for structural configurations that will result in a reasonably uniform distribution of inelastic behavior in elements throughout the seismic-force-resisting system. "Buildings with a weak-story irregularity [V5] tend to develop all of their inelastic behavior and consequent damage at the weak story, possibly leading to collapse" (ASCE, 2017a). The triggers provided in Table 12.3-2 of ASCE/SEI 7-16 for weak story and extreme weak story irregularity reflect strength ratios where an undesirable concentration of

inelastic response may be expected. As discussed in Section G.3, simple calculations are sufficient to identify this concern.

G.2 Calculation of Story Stiffness

Assessment of stiffness regularity requires computation of lateral stiffness for each story in each direction. "Generally, it is not practical to use stiffness properties unless these can be easily determined. There are many structural configurations where the evaluation of story stiffness is complex and is often not an available output from computer programs" (SEAOC, 2013).

Two methods to perform calculations for story stiffness comparisons are described in Sections G.2.2 and G.2.3.

G.2.1 Simple Hand Calculations and Their Limitations

In recent decades use of the finite element method has become common for structural analysis. Prior to that time simple hand calculations were routinely used. The following expressions for lateral stiffness of moment frames and shear walls have a long history of use. Though not addressed here, simple expressions are also available for concentrically or eccentrically braced frames.

For a moment frame column at an intermediate story:

$$K = \frac{12EI_c}{h^3}\beta$$

$$\beta = \frac{\gamma}{2+\gamma}$$

$$\gamma = \frac{I_{b1}/l_1 + I_{b2}/l_2 + I_{b3}/l_3 + I_{b4}/l_4}{I_c/h}$$

where b_1 and b_2 are the beams above, and b_3 and b_4 are the beams below.

For an elastic, cantilevered shear wall:

$$K = \frac{E_c t}{\frac{h}{L}\left[4\left(\frac{h}{L}\right)^2 + 3\right]}$$

For an elastic wall fixed against rotation below and above:

$$K = \frac{E_c t}{\frac{h}{L}\left[\left(\frac{h}{L}\right)^2 + 3\right]}$$

The expressions above are used for the "hand calculations" reported for the design space analyzed as part of this project. The shear wall calculations generally use the stiffness for a cantilevered wall and treat multiple stories as springs in series; for a bounding comparison the fixed-fixed expression is also used.

While these simple expressions have a long history of use, their shortcomings are numerous and include the following (Shultz, 1992; Eroglu and Akkar, 2010):

- By focusing on one story at a time, they neglect off-diagonal stiffness terms associated with global overturning and even shear and flexure in adjacent stories. Rigorous analysis yields stiffness matrices for frames that have contributions from adjacent minor diagonals and nonzero coefficients outside the tridiagonal band. Neglecting these terms tends to overpredict stiffness irregularities.
- Where story heights differ, the independent story-by-story approach breaks down. Adjustment factors in the literature for this effect are complex and not comprehensive.
- The expression for moment frames, being based on flexural flexibility, neglects the contribution of shear flexibility.
- While the expressions for shear walls include both shear and flexural deformations, they assume the same degree of cracking for both contributions and cannot reflect realistic conditions for multi-story walls that are between the pure cantilever and pure fixed-fixed conditions.
- These methods are not suitable to reflect abrupt changes in stiffness at boundary conditions (especially at top and bottom stories). Adjustment factors in the literature for these boundary effects are complex and not comprehensive.
- The expressions for shear walls do not reflect the effect of openings. There are several design aids compiled for practicing structural engineers that recommend a simplified hand procedure to account for openings in shear walls by treating them as a system of piers and spandrel beams. Neuenhofer (2006) reports that the recommended hand method is highly approximate and consistently underestimates the impact of the opening on the reduction of stiffness, thus producing a lateral stiffness larger than that obtained from detailed finite-element analysis.

Figure G-2 shows that when story stiffnesses for regular (baseline) moment frames are normalized, hand methods produce similar trends and may have reasonable correlation to results from the finite element method. The scatter

introduced by the hand methods would only worsen for nonuniform conditions. For the design space analyzed as part of this project (which uses a typical story height of 12.5 ft.), hand calculations would identify a soft story for an unusual story with height of 14.5 ft. and an extreme soft story for an unusual story with height of 15.5 ft. By comparison, the rigorous finite element analyses identify triggering story heights of approximately 16 ft. and 18 ft., respectively.

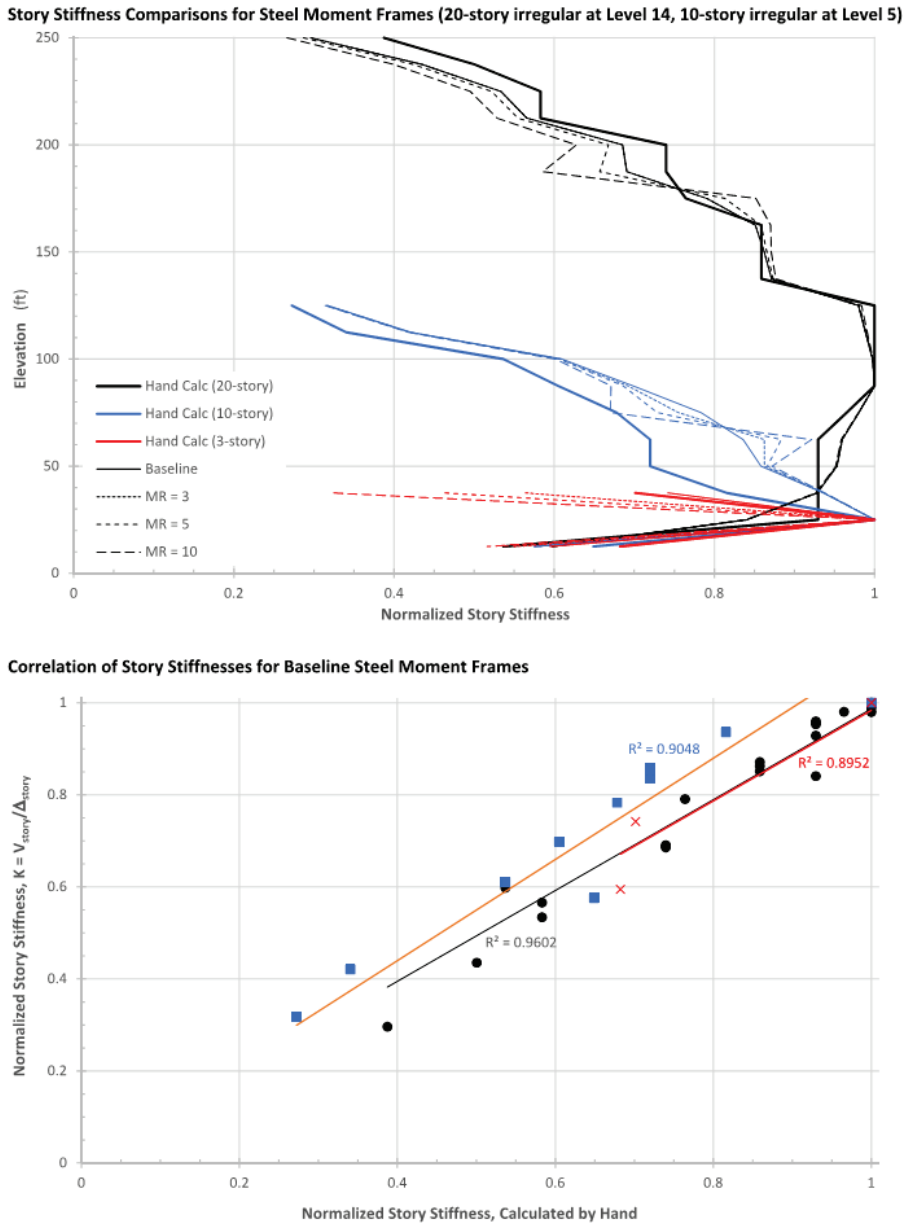

Figure G-2 Stiffness comparisons and correlations for steel moment frames.

Figure G-3 shows that trends for normalized story stiffnesses for regular (baseline) shear walls and their correlations to results from the finite element

method are reasonable for the 3-story archetype, but are unreliable for the taller archetypes.

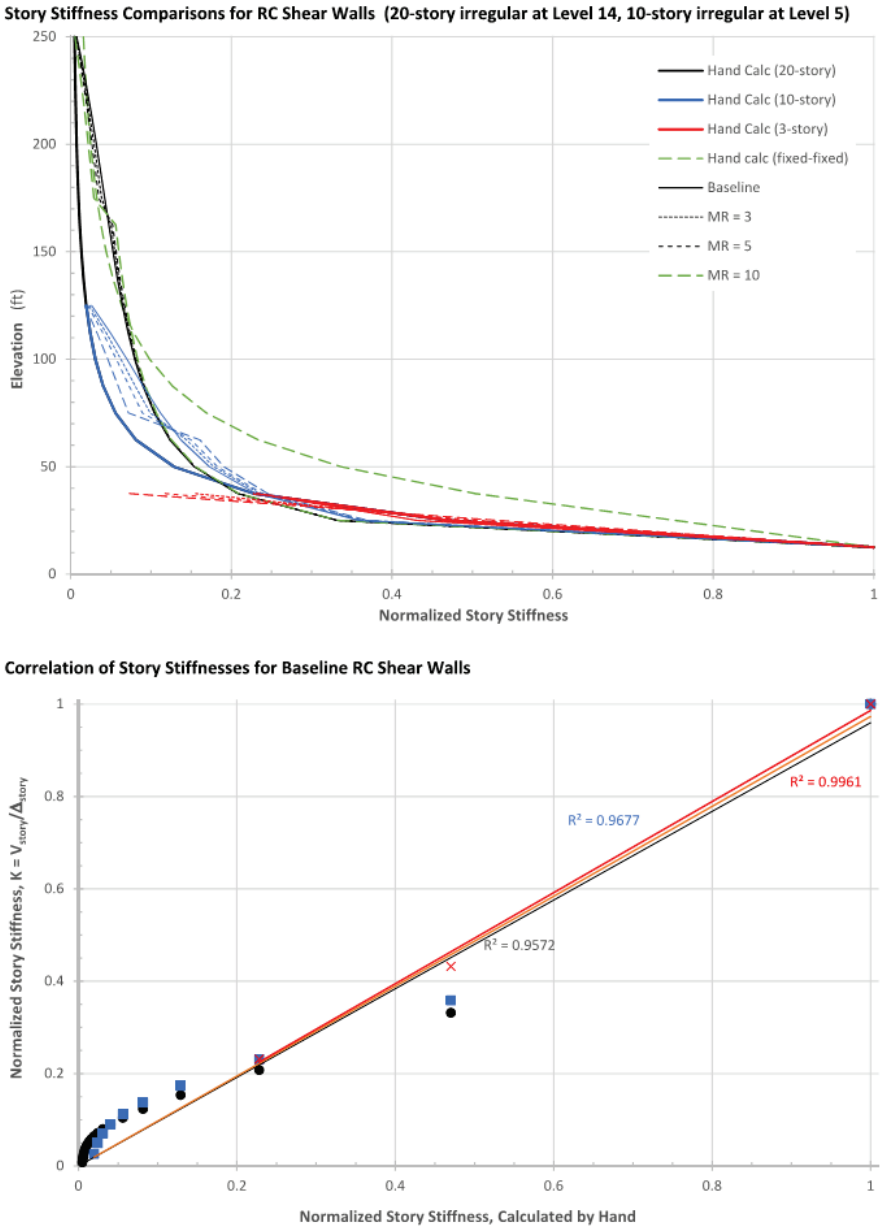

Figure G-3 Stiffness comparisons and correlations for concrete shear walls.

G.2.2 SEAOC Story Drift Ratio Method

According to SEAOC (2013), "recognizing that the basic intent of this irregularity check is to determine if the lateral-force distribution will differ significantly from the pattern prescribed by Section 12.8.3, which assumes a prescribed shape for the first dynamic mode of response, this type of irregularity can also be determined by comparing values of drift ratios due to the prescribed lateral forces. To compare displacements rather than stiffness,

it is necessary to use the reciprocal of the limiting percentage ratios of 70 and 80 percent as they apply to story stiffness, or reverse their applicability to the story or stories above." To use this method, story drifts and story drift ratios are determined, where the story drift ratio is the story drift divided by story height. Comparison of these ratios identifies changes in the slope of the displaced shape.

While this method has some merit, it suffers from at least two weaknesses:

1. "Using the story-drift ratios (drift based) to determine whether a soft story exists may result in the discovery of soft stories in the upper stories of multistory buildings that may not be correct" (SEAOC, 2013). For the design space analyzed as part of this project, the story drift ratio method produces a false soft-story positive at Level 17 of the 20-story baseline SMF even though that story has greater stiffness than the stories above based on either simple hand calculations or the apparent story stiffness method; the natural displaced shape of structures with shear-type response produces decreasing story drift ratios up the height, even where story stiffness is constant.
2. Since differences in story mass affect story drift, the story drift ratio method can produce false positives for soft story irregularity, as compared to explicit stiffness calculations. For the design space analyzed as part of this project, the story drift ratio method produces false soft-story positives at stories with mass irregularities in the top half of the SMF archetypes.

G.2.3 Apparent Story Stiffness Method

"The lateral stiffness of a story is generally defined as the ratio of story shear to story drift" (Shultz, 1992). Since story drift is affected by vertical distribution of lateral loads, the lateral stiffness of a story is not a stationary property, but an apparent one that depends on lateral load distribution. The ELF procedure uses "regular" loads—acting in the same direction on all floors, and varying from floor to floor in a controlled manner.

Shultz (1992) reports on analyses using three distributions of lateral load designated as constant, linear, and parabolic. These lateral load distributions have lateral loads on each floor that are of equal magnitude, are proportional to the height, or are proportional to the square of the height of each floor from the base of the frame, respectively. Shultz finds that the apparent story stiffnesses are not affected much by the type of lateral load distribution, and that the concept of a single-valued story stiffness is quite accurate if the distribution is regular.

For the design space analyzed as part of this project, significant mass irregularities were considered at various levels (with mass ratios of 3.0, 5.0, and 10.0). As may be seen in the top frames of Figures G-2 and G-3, even such substantial variations in story force have only minor impact on the apparent story stiffness, so the use of a single-value apparent story stiffness based on the ELF load distribution is judged to be sufficiently accurate.

G.3 Calculation of Story Strength

Assessment of strength regularity requires computation of lateral strength for each story in each direction. The intent "is to use a simple measure (elastic or plastic) to determine" the "total strength of all seismic-force-resisting elements sharing the story shear for the direction under consideration" (ASCE, 2017a; SEAOC, 2013). Where compliance with Table 12.3-3 of ASCE/SEI 7-16 is being assessed for determination of the redundancy factor, the summation excludes the strength of the element whose removal is being considered. This calculation does not require a rigorous 3-dimensional plastic analysis; instead, it is acceptable simply to sum the shear contributions of seismic-force-resisting elements in each of two orthogonal directions as follows:

- **Brace members:** The shear contribution is the horizontal component of the lower of the brace capacity (in tension or compression, depending on the direction of load application), or the connection capacity. Where uplift of a shallow foundation, column capacity, or the capacity of an element supporting a discontinuous frame controls the response, the computed strength should reflect that limit state.
- **Moment frame columns:** The shear contribution is that corresponding to the least lateral capacity. For frame columns with weak-column/strong-beam conditions, the shear contribution is the lower of that developed when the top and bottom of the column are at flexural capacity, or the column shear capacity. For frame columns with a strong-column/weak-beam condition, the shear contribution is the lower of the shear corresponding to development of flexural yielding at each end of the column (from adjoining beam yield hinges or column base connection capacity), or the column shear capacity.
- **Shear wall piers:** The shear contribution is the lower of either the shear at development of the flexural strength, or the shear strength. Where wall flexure controls the response, both the 1.2*D* and 0.9*D* axial load cases should be considered. Where the capacity of an element supporting a discontinuous wall controls the response, the computed strength should reflect that limit state.

G.4 Recommendations

G.4.1 Calculation of Story Stiffness

Section 12.7.3 of ASCE/SEI 7-16 requires use of a mathematical model of the structure for "determining member forces and structure displacements resulting from applied loads," which must "include the stiffness and strength of elements that are significant to the distribution of forces and deformations in the structure and represent the spatial distribution of mass and stiffness throughout the structure." Not only is such a model, which is suitable for application of the apparent story stiffness method described in Section G.2.3, consistent with the state of the practice and standard of care, it is required for code compliance. There is no reason to use "simple" hand calculations for story stiffness determinations; as described in Section G.2.1 those methods have serious flaws and actually require greater effort on the part of the designer than simply assessing the results from the more rigorous analytical model that is required for code compliance. Since the results of the analysis include both story shears and story drifts, there is no reason to use the story drift ratio method, which can produce erroneous results.

For assessment of soft story vertical configuration irregularities [V1], lateral forces from the ELF procedure should be applied to the mathematical model and the apparent story stiffness of each story should be determined in each direction. The apparent story stiffness should be computed as:

$$K_x = V_x / (\delta_x - \delta_{x-1})$$

where:

V_x = the story shear at level x determined by an elastic analysis using the forces defined in Section 12.8.3; and

δ_x = the deflection at level x determined by an elastic analysis using the forces defined in Section 12.8.3.

G.4.2 Calculation of Story Strength

Unlike the determination of story stiffness, calculation of story strength does not require use of a single, rigorous mathematical model. Instead, for assessment of weak story vertical configuration irregularities [V5], a simple summation of the shear contributions of seismic-force-resisting elements as recommended in Section G.3 is most meaningful and effective.

Appendix H

Steel Systems Not Specifically Detailed for Seismic Resistance

ASCE/SEI 7 identifies a class of seismic-force-resisting systems entitled, "Steel Systems Not Specifically Detailed for Seismic Resistance, Excluding Cantilever Column Systems." These systems have no height limit in Seismic Design Categories (SDC) B and C, but are not permitted in SDC D, E, and F. Seismic forces are obtained using Response Modification Factor (R) of 3 and the members are designed and detailed following the requirements of AISC 360, *Specification for Structural Steel Buildings*. In other words, because the design is based on smaller R-factors and the resulting seismic design forces are larger, the requirements found in AISC 341, *Seismic Provisions for Structural Steel Buildings*, need not be followed.

R = 3 systems were not specifically studied for this report; nevertheless, it may be possible to draw some general conclusions regarding the sensitivity of R = 3 systems to irregularities by examining the behavior of the steel buildings designed for SDC B. While wind drift limits governed the design of all the SDC B buildings, the difference between wind and seismic forces was not large for the 3-story building. On the other hand, the wind force on the 9-story and 20-story buildings was approximately three times larger. Thus, for SDC C it is likely that the 9-story and 20-story buildings also would be governed by wind while the 3-story building might or might not be depending on many design factors (e.g., building proportion, mass, total height).

H.1 Background

The premise behind the so-called "R = 3 systems" is that use of a low R-factor makes nearly elastic response more likely while still recognizing the inherent seismic resistance of these structures. The assumed lack of required inelastic deformation capability renders the ductile detailing and member proportioning requirements in AISC 341 unnecessary. Often, member sizes for these systems are governed by wind rather than seismic loads. It is assumed that choosing such a system in areas of low- to moderate-seismicity may be more cost-effective due to fabrication, erection and inspection savings compared to systems designed following AISC 341.

The following sections highlight key differences in design requirements between $R = 3$ designs and AISC 341 designs.

H.2 Configuration

AISC 360 places no significant configurational constraints on $R = 3$ seismic systems. AISC 341, on the other hand, addresses a number of configuration issues. For example, AISC 341 does not permit K-braced frames, where the brace delivers load to beam and column away from the column and beam centerline work point. The general concern is that column demands in K-braced frames may exceed column strength, particularly where the column is designed for code-based forces rather than the force the brace can deliver to the column. Given the importance of columns in carrying both gravity and seismic demands, increased column vulnerability is likely to increase the probability of collapse. The presence of irregularities found to be of significance likely exacerbates $R = 3$ system vulnerability.

H.3 Proportioning

H.3.1 Strong-Column/Weak-Beam Requirement

In $R = 3$ designs, beams would be sized to be as stiff as possible to satisfy drift demands consistent with any depth restrictions, as this is usually the most cost-effective approach. Columns would typically be designed for the moments caused by wind or seismic forces and associated axial loads due to gravity and lateral demands. It is likely that beams would be stronger in flexure than the columns, possibly by a significant margin.

The consequences of failing to meet strong-column/weak-beam requirements include the potential for collapse due to column-driven story mechanisms occurring prior to mobilization of beam plastic hinging on multiple floors. Based on comparisons of collapse probabilities between the ELF and MRSA methods used to design similar buildings described in this report, assuming that the appropriate limit states have been identified and correctly modeled, the consistently lower probabilities of collapse for the ELF-based designs suggest using higher base shears can minimize the consequences of certain design deficiencies.

H.3.2 Panel Zone Proportioning

AISC 360 requires that panel zones be designed to resist the panel zone shear developed by the governing force demands, most likely wind. AISC 341, on the other hand, requires that the panel zones be designed to resist the shear developed by the yielding of the frame beams. Thus, the $R = 3$ designs are likely to have weaker panel zones, particularly in the designs governed by

wind. The concern would be that excessive panel zone deformation delays beam hinging to the point that only the panel zone yields and the resulting local column flange deformation would lead to column flange fracture or beam flange-to-column flange weld fracture.

While the influence of weak panel zones was not an area of systematic study for this report, designs of taller buildings that had strong panel zones did not perform as well as those with panel zones more closely matched to the demand generated by the frame beams. This suggests that sharing energy dissipation and inelastic deformation between beam hinging and column panel zone yielding is desirable and concentrating deformation in either the beams or the column panel zones may negatively impact overall performance.

H.3.3 Connection Design Philosophy

Connection designs in $R = 3$ systems use the calculated demand from the governing lateral demand (i.e., wind or seismic) based on building code forces. On the other hand, most connections in seismic systems designed using ASIC 341 are proportioned using the expected strength produced by the member delivering forces to the connection. The difference in connection strength between $R = 3$ systems and those designed using AISC 341 can be significant, particularly for braced frames. Generally, AISC 341 requires brace connections to be designed to develop the expected strength of the brace in tension or using the code-derived forces multiplied by the overstrength factor. Given the potentially large difference in connection strength, it is suspected that $R = 3$ systems governed by seismic demands, and, perhaps even those governed by wind, may be unacceptably more prone to collapse than those designed using AISC 341. It is expected that irregularities found to be of significance for systems designed using AISC 341 would also prove to increase the probability of collapse in $R = 3$ systems.

H.4 Member Local Buckling and Lateral Bracing Requirements

As wind drift would govern in most cases for $R = 3$ designs, stiffness, not strength, would drive the selection of frame beams. For $F_y = 50$ ksi, effectively all wide flanges are considered compact sections and can develop the plastic flexural strength, M_p, of the beam before local buckling occurs. Local buckling, when it occurs after multiple cycles of yield-level displacements, effectively limits the demand placed on beam-to-column connections. The primary concern due to local buckling is strength degradation and low-cycle fatigue fracture.

Lateral torsional bracing for the frame beams designed to satisfy drift demands most likely could be spaced further apart than would be needed to develop M_p because the demand is not expected to be that high. Columns, on the other hand, being sized essentially for strength, would need to develop something on the order of M_p, adjusted for the axial load demand. The consequence of lateral torsional buckling of the frame beams is reduced frame strength and stiffness coupled with less effective local bracing of the columns in the area of high moment demand.

For braced frames, the more stringent local bucking requirements found in AISC 341 would not apply to members in the $R = 3$ frames. Experimental testing and post-earthquake damage assessments suggest that relatively thin member proportions, especially in HSS sections, can lead to premature brace fracture when local buckling occurs. This behavior may render an $R = 3$ braced frame significantly more vulnerable to collapse than a braced frame designed using the requirements of AISC 341 because load redistribution cannot occur. It is not known whether the higher seismic force used to design $R = 3$ braced frames provide a sufficient margin of safety against collapse. Given the relatively small difference in seismic force obtained for $R = 3$ designs and $R = 3.5$ ordinary braced frames, it is suspected that $R = 3$ braced frames governed by seismic demands, rather than by wind, would be relatively more prone to collapse. It is expected that irregularities found to be of significance for systems designed using AISC 341 would also prove to increase the probability of collapse in $R = 3$ braced frames.

H.5 Less Stringent Material Specifications and Inspection Requirements

AISC 360 does not limit the yield strength as does AISC 341, nor does it require that welding filler metals achieve a minimum Charpy V-notch toughness. In addition, many of the design provisions in AISC 341 are based on a mechanism approach that requires use of the expected member strength rather than its nominal strength. Although inspection requirements in AISC 360 have been more explicitly detailed in the relatively new Chapter N, AISC 341 requires significantly more stringent inspection requirements, with an emphasis on visual inspection rather than nondestructive testing (NDT). As the 1994 Northridge earthquake pointed out, over-reliance on NDT can produce a false sense of competency and reliability.

Symbols

The following is a list of key symbols referenced in the document, but it is not a comprehensive list. Many symbols in the list are defined in other standards and reports referenced in this document, including FEMA P695 and ASCE/SEI 7-16.

$ACMR$ = adjusted collapse margin ratio

C_d = deflection amplification factor per Table 12.2-1 of ASCE/SEI 7-16

C_s = seismic response coefficient per Section 12.8.1.1 of ASCE/SEI 7-16

C_u = upper-limit period coefficient per Table 12.8-1 of ASCE/SEI 7-16

CMR = collapse margin ratio

D = effect of dead load for use in load combinations per Section 2.3.6 of ASCE/SEI 7-16

EI_g = gross cross-sectional moment of inertia

F_a = short-period site coefficient (at 0.2-second period) per Section 11.4.4 of ASCE/SEI 7-16

F_v = long-period site coefficient (at 1.0-second period) per Section 11.4.4 of ASCE/SEI 7-16

F_y = yield strength of material

f'_c = compressive strength of unconfined concrete, based on standard cylinder test

f_y = yield stress of longitudinal reinforcement

g = constant acceleration due to gravity

h_n = vertical distance from the base to the highest level of the seismic force-resisting system of the structure, per Section 11.3 of ASCE/SEI 7-16

k = exponent used in the vertical distribution of seismic forces for the ELF procedure, which is intended to approximate the effect of higher modes per Section 12.8.3 of ASCE/SEI 7-16

L = effect of live load for use in load combinations of Section 2.3.6 of ASCE/SEI 7-16

P = axial load

R = response modification coefficient per Table 12.2-1 of ASCE/SEI 7-16

RC = reinforced concrete

S = snow load per Chapter 2 of ASCE/SEI 7-16

S_{DS} = design, 5% damped, spectral response acceleration parameter at short periods per Section 11.4.5 of ASCE/SEI 7-16

S_{D1} = design, 5% damped, spectral response acceleration parameter at a period of 1 second per Section 11.4.5 of ASCE/SEI 7-16

S_{MS} = the MCE_R, 5% damped, spectral response acceleration parameter at short periods adjusted for site class effects per Section 11.4.4 of ASCE/SEI 7-16

S_{M1} = the MCE_R, 5% damped, spectral response acceleration parameter at a period of 1 second adjusted for site class effects per Section 11.4.4 of ASCE/SEI 7-16

S_S = mapped MCE_R, 5% damped, spectral response acceleration parameter at short periods per Section 11.4.2 and Section 11.4.4 of ASCE/SEI 7-16

S_a = spectra acceleration, g

$S_a(T)$ = the spectral acceleration at the period, T

SMF = special moment frame

SSF = spectral shape factor

T = the fundamental period of the building, in seconds, based on the limits per Section 12.8.2 of ASCE/SEI 7-16 and the approximate fundamental period, T_a

T_1 = the fundamental period of the building, as determined by eigenvalue analysis of the structural model (seconds)

T_a = the approximate fundamental period of the building, in seconds, as determined in Section 12.8.2.1 of ASCE/SEI 7-16

TIR = torsional irregularity ratio, defined as the ratio of the maximum drift at a building's edge to the average drift given a lateral force with 5% eccentricity, as shown in Figure 4-1 in this report

T_s = short-period transition period of the building, in seconds, equal to S_{D1}/S_{DS} per Section 11.3 of ASCE/SEI 7-16

V = total design lateral force or shear at the base per ASCE/SEI 7-16

V_c = nominal shear strength provided by concrete per ACI 318-14

V_n = nominal shear strength including contributions from concrete and steel per ACI 318-14

V_s = nominal shear strength provided by shear reinforcement per ACI 318-14

V_u = shear demand

W = effective seismic weight of the building as defined in Section 12.7.2 of ASCE/SEI 7-16

w_x = portion of W that is located at or assigned to Level x

x = parameter of Equation 12.8-7 given in Table 12.8-2 of ASCE/SEI 7-16

δ_u = roof displacement used to approximate the ultimate displacement capacity of the seismic force-resisting system, as derived from pushover analysis

ϕ = strength reduction factor

μ_T = period-based ductility of an index archetype model

θ_p = plastic hinge rotation (radians)

ρ = redundancy factor based on the extent of structural redundancy present in a building as defined in Section 12.3.4 of ASCE/SEI 7-16

ρ (or ρ_{tot}) = ratio of total area of longitudinal reinforcement (for columns) or ratio of tensile longitudinal reinforcement (for beams)

ρ' = ratio of compressive longitudinal reinforcement (for beams)

ρ_{sh} = area ratio of transverse reinforcement in column hinge region

Ω = calculated overstrength of an index archetype analysis model

Ω_0 = overstrength factor appropriate for use in the load combinations of Section 12.4 of ASCE/SEI 7-16 (current values of Ω_0 are given in Table 12.2-1 of ASCE/SEI 7-16)

Glossary

Definitions

Archetype: A prototypical representation of a seismic-force-resisting system.

Base Shear: Total design lateral force or shear at the base (ASCE/SEI 7-16).

Building: Any structure whose intended use includes shelter of human occupants (ASCE/SEI 7-16).

Collapse Level Earthquake Ground Motions: The level of earthquake ground motions that cause collapse of the seismic force-resisting system of interest.

DBE: Displacement-based beam-column element used in OpenSees.

Design Earthquake Ground Motions: The earthquake ground motions that are two-thirds of the corresponding MCE_R ground motions (ASCE/SEI 7-16).

ELF: Equivalent lateral force procedure for seismic design per Section 12.8 of ASCE/SEI 7-16.

FBE: Force-based beam-column element used in OpenSees.

GILD: Gravity induced lateral demand.

Incremental Dynamic Analysis: Series of nonlinear response history analyses using an input ground motion that is incrementally scaled to increasing intensities until collapse is detected in the analysis.

Maximum Considered Earthquake (MCE) Ground Motions: The most severe earthquake effects considered, as defined by Section 11.4 of ASCE/SEI 7-16.

Modeling Uncertainty: Collapse uncertainty associated with the quality of the index archetype models.

MRSA: Modal response spectrum analysis procedure for seismic design per Section 12.9.1 of ASCE/SEI 7-16.

Nonbuilding Structure: A structure, other than a building, constructed of a type included in Chapter 15 of ASCE/SEI 7-16.

Non-Simulated Collapse: Structural collapse caused by collapse modes that are not represented in the analytical model. Non-simulated collapse occurs when a component limit state is exceeded, as defined by component fragility functions.

OMF: Ordinary moment frame.

Seismic Design Category: A classification assigned to a structure based on its Risk Category and the severity of design earthquake ground motions at the site per Section 11.4 of ASCE/SEI 7-16.

Seismic-Force-Resisting System (SFRS): That part of the structural system that is considered to provide the required resistance to seismic forces prescribed in ASCE/SEI 7-16.

SFI-MVLEM: Shear-flexure-interaction multi-vertical line-element model used in OpenSees.

Simulated Collapse: Structural collapse caused by collapse modes that are directly represented in the analytical model.

Site Class: A classification assigned to a site based on the types of soils present and their engineering properties, as defined in Chapter 20 of ASCE/SEI 7-16.

SMF: Special moment frame.

Structure: That which is built or constructed and limited to buildings and nonbuilding structures per ASCE/SEI 7-16.

References

ACI, 2014, *Building Code Requirements for Structural Concrete (ACI 318-14) and Commentary (ACI 318R-14)*, ACI Committee 318, American Concrete Institute, Farmington Hills, Michigan.

AIJ, 1995, *Preliminary Reconnaissance Report of the 1995 Hyogoken-Nanbu Earthquake*, English Edition, Architectural Institute of Japan, Tokyo, Japan.

AISC, 2010a, *Prequalified Connections for Special and Intermediate Steel Moment Frames for Seismic Applications*, ANSI/AISC 358-10, American Institute of Steel Construction, Chicago, Illinois.

AISC, 2010b, *Seismic Provisions for Structural Steel Buildings*, ANSI/AISC 341-10, American Institute of Steel Construction, Chicago, Illinois.

AISC, 2010c, *Specification for Structural Steel Buildings*, ANSI/AISC 360-10, American Institute of Steel Construction, Chicago, Illinois.

AISC, 2016, *Seismic Provisions for Structural Steel Buildings*, ANSI/AISC 341-16, American Institute of Steel Construction, Chicago, Illinois.

Ali, A., and Wight, J.K., 1991, "RC structural walls with staggered door openings," *Journal of Structural Engineering*, Vol. 117, No. 5, pp. 1514-1531.

Altoontash, A., 2004, *Simulation and Damage Models for Performance Assessment of Reinforced Concrete Beam-Column Joints*, Doctoral Dissertation, Stanford University, Stanford, California.

Anagnostopoulos, S.A., Alexopoulou, C., and Stathopoulos, K.G., 2010, "An answer to an important controversy and the need for caution when using simple models to predict inelastic earthquake response of buildings with torsion," *Earthquake Engineering & Structural Dynamics*, Vol. 39, No. 5, pp. 521–540.

Anagnostopoulos, S., Kyrkos, M., Papalymperi, A., and Plevri, E., 2015, "Should accidental eccentricity be eliminated from Eurocode 8?," *Earthquakes and Structures*, Vol. 8, No. 2, pp. 463-484.

Anagnostopoulos, S.A., Kyrkos, M.T., and Stathopoulos, K.G., 2015, "Earthquake induced torsion in buildings: Critical review and state of the art," *Earthquakes and Structures*, Vol. 8, No. 2, pp. 305-377.

Aoyama, H., 1981, "Outline of the earthquake provisions in recently revised Japanese Building Code," *Bulletin of the New Zealand National Society for Earthquake Engineering*, Vol. 14, No. 2.

ASCE, 2003, *Seismic Evaluation of Existing Buildings*, ASCE/SEI 31-03, American Society of Civil Engineers, Reston, Virginia.

ASCE, 2013, *Seismic Evaluation and Retrofit of Existing Buildings*, American Society of Civil Engineers, ASCE/SEI 41-13, Reston, Virginia.

ASCE, 2017a, *Minimum Design Loads and Associated Criteria for Buildings and Other Structures*, American Society of Civil Engineers, ASCE/SEI 7-16, Reston, Virginia.

ASCE, 2017b, *Seismic Evaluation and Retrofit of Existing Buildings*, American Society of Civil Engineers, ASCE/SEI 41-17, Reston, Virginia.

ATC, 1978, *Tentative Provisions for the Development of Seismic Regulations for Buildings*, ATC-3-06, Applied Technology Council, Redwood City, California.

Birely, A., 2012, *Seismic Performance of Slender Reinforced Concrete Structural Walls*, Dissertation, University of Washington, Seattle, Washington.

BOCA, 1993, *The BOCA National Building Code*, Building Officials and Code Administrators International, Inc.

Carrillo, J., and Alcocer, S., 2011, "Degredation properties of reinforced concrete walls with openings," *DYNA*, Vol. 78, No. 170, pp. 106-115, available at: http://www.revistas.unal.edu.co/index.php/dyna/article/view/29393/48781.

CFIA, 1986, *Código Sísmico de Costa Rica*, Colegio Federado de Ingenieros y Arquitectos (CFIA), Costa Rica.

Charney, F.A., 2008, "Unintended consequences of modeling damping in structures," *Journal of Structural Engineering*, Vol. 134, No. 4, pp. 581-592.

De la Llera, J.C., and Chopra, A.K., 1994, "Using accidental eccentricity in code-specified static and dynamic analyses of buildings," *Earthquake Engineering & Structural Dynamics*, Vol. 23, No. 9, pp. 947-967.

De Stefano, M., and Pintucchi, B., 2008, "A review of research on seismic behaviour of irregular building structures since 2002," *Bulletin of Earthquake Engineering*, Vol. 6, No. 2, pp. 285-308.

DeBock, D.J., Liel, A.B., Haselton, C.B., Hooper, J.D., and Henige, R.A., 2014, "Importance of seismic design accidental torsion requirements for building collapse capacity," *Earthquake Engineering & Structural Dynamics*, Vol. 43, No. 6, pp. 831-850.

DeBock, D.J., Wade, K.F., Cook, D.T., and Haselton, C.B., 2016, "New developments in FEMA P-58 Seismic Risk Assessment of Wood Light-Frame Buildings," *Proceedings*, 2016 SEAOC Convention, Maui, Hawaii.

Dhakal, R.P., and Maekawa K., 2002a, "Path-dependent cyclic stress–strain relationship of reinforcing bar including buckling," *Engineering Structures*, Vol. 24, No. 11, pp. 1383-1396.

Dhakal, R.P., and Maekawa, K., 2002b, "Modeling for postyield buckling of reinforcement," *Journal of Structural Engineering*, Vol. 128, No. 9, pp. 1139-1147.

Dupuis, M., Best, T., Elwood, K., and Anderson, D., 2014, "Seismic performance of shear wall buildings with gravity-induced lateral demands," *Canadian Journal of Civil Engineering*, Vol. 41, No. 4, pp. 323-332.

Elkady, A., 2016, *Collapse Risk Assessment of Steel Moment Resisting Frames Designed with Deep Wide-Flange Columns in Seismic Regions*, Doctoral Dissertation, McGill University, Montreal, Canada.

Eroglu, T., and Akkar, S., 2010, "Lateral stiffness estimation in frames and its implementation to continuum models for linear and nonlinear static analysis," *Bulletin of Earthquake Engineering*, Vol. 9, No. 4, pp. 1097-1114.

European Committee for Standardization, 2004, *Design of Structures for Earthquake Resistance – Part 1: General Rules, Seismic Actions and Rules for Buildings*, Eurocode 8, EN 1998-1, Brussels, Belgium.

FEMA, 1986, *NEHRP Recommended Seismic Provisions for the Development of Seismic Regulations for New Buildings*, FEMA 95, 1985 Edition, prepared by the Building Seismic Safety Council for the Federal Emergency Management Agency, Washington, D.C.

FEMA, 1988, *NEHRP Recommended Seismic Provisions for the Development of Seismic Regulations for New Buildings*, FEMA 95, 1988 Edition, prepared by the Building Seismic Safety Council for the Federal Emergency Management Agency, Washington, D.C.

FEMA, 2000a, *State of the Art Report on Connection Performance*, FEMA 355D, prepared by the SAC Joint Venture, a partnership of the Structural Engineers Association of California, Applied Technology Council, and California Universities for Research in Earthquake Engineering, for the Federal Emergency Management Agency, Washington, D.C.

FEMA, 2000b, *State of the Art Report on System Performance of Steel Moment Frames Subject to Earthquake Ground Shaking*, FEMA 355C, prepared by the SAC Joint Venture, a partnership of the Structural Engineers Association of California, Applied Technology Council, and California Universities for Research in Earthquake Engineering, for the Federal Emergency Management Agency, Washington, D.C.

FEMA, 2009, *Quantification of Building Seismic Performance Factors*, FEMA P695, prepared by the Applied Technology Council for the Federal Emergency Management Agency, Washington, D.C.

FEMA, 2011, *Quantification of Building Seismic Performance Factors: Component Equivalency Methodology*, FEMA P-795, prepared by the Applied Technology Council for the Federal Emergency Management Agency, Washington, D.C.

FEMA, 2012a, *Seismic Evaluation and Retrofit of Multi-Unit Wood-Frame Buildings With Weak First Stories*, FEMA P-807, prepared by the Applied Technology Council for the Federal Emergency Management Agency, Washington, D.C.

FEMA, 2012b, *Seismic Performance Assessment of Buildings*, FEMA P-58, prepared by the Applied Technology Council for the Federal Emergency Management Agency, Washington, D.C.

FEMA, 2015, *NEHRP Recommended Seismic Provisions for New Buildings and Other Structures*, FEMA P-1050-1, Volume I, prepared by the Building Seismic Safety Council for the Federal Emergency Management Agency, Washington, D.C.

Filippou, F.C., Popov, E.P., and Bertero, V., 1983, *Effects of Bond Deterioration on Hysteretic Behavior of Reinforced Concrete Joints*, Technical Report UCB/EERC-83/19, Earthquake Engineering Research Center, University of California, Berkeley, California.

FUNVISIS, 2001, *Edificaciones Sismorresistentes, Parte 1: Articulado*, Norma Venezolana Covenin 1756-1:2001, Fundación Venezolana de Investigaciones Sismológicas (FUNVISIS), Ministry of Science and Technology, Caracas, Venezuela.

Goel, S.C., and Chao, S.-H., 2008, *Performance-Based Plastic Design*, International Code Council.

Gupta, A., and Krawinkler, H., 1999, *Seismic Demands for the Performance Evaluation of Steel Moment Resisting Frame Structures*, Doctoral Dissertation, Stanford University, Stanford, California.

Haselton, C.B., Liel, A.B., Lange, S.T., and Deierlein, G.G., 2008, *Beam-Column Element Model Calibrated for Predicting Flexural Response Leading to Global Collapse of RC Frame Buildings*, PEER Report No. 2007/03, Pacific Earthquake Engineering Research Center, University of California, Berkeley, California.

Haselton, C.B., Liel, A.B., Deierlein, G.G., Dean, B.S., and Chou, J.H., 2011, "Seismic collapse safety of reinforced concrete buildings. I: Assessment of ductile moment frames," *Journal of Structural Engineering*, Vol. 137, No. 4, pp. 481-491.

Hueste, M.B.D., Kang, T.H.-K., and Robertson, I.N., 2009, "Lateral drift limits for structural concrete slab-column connections, including shear reinforcement effects," *Proceedings,* Structures Congress 2009, Austin, Texas.

Ibarra, L., 2003, *Global Collapse of Frame Structures Under Seismic Excitations*, Ph.D. Dissertation, Department of Civil and Environmental Engineering, Stanford University, Stanford, California.

Ibarra, L.F., Medina, R.A., and Krawinkler, H., 2005, "Hysteretic models that incorporate strength and stiffness deterioration," *Earthquake Engineering & Structural Dynamics*, Vol. 34, No. 12, pp. 1489-1511.

IDIEM, 2010, *Peritaje Estructural Edificio Alto Río, Ciudad de Concepción, Informe Final, Descripción de Caida y Factores Asociados al Colapso*, Informe No. 644.424-00, Centro de Investigación, Desarrollo e Innovación de Estructuras y Materiales (IDIEM), University of Chile, Santiago, Chile.

International Conference of Building Officials, 1976, *Uniform Building Code*, Whittier, California.

International Conference of Building Officials, 1985, *Uniform Building Code*, Whittier, California.

International Conference of Building Officials, 1988, *Uniform Building Code*, Whittier, California.

International Conference of Building Officials, 1994, *Uniform Building Code*, Whittier, California.

ISCDF, 2004, *Normas Técnicas Complementarias para Diseño por Sismo*, Instituto para la Seguridad de las Construcciones en el Distrito Federal (ISCDF), Mexico City, Mexico.

Junta Técnica de Ingeniería y Arquitectura, 2004, *Reglamento para el Diseño Estructural en La República de Panamá*, Ministry of Public Works, Panama City, Panama.

Kashani, M.M., Lowes, L.N., Crewe, A.J., and Alexander, N.A., 2016, "Nonlinear fibre element modelling of RC bridge piers considering inelastic buckling of reinforcement," *Engineering Structures*, Vol. 116, pp. 163-177.

Kato, D., Noda, H., and Sugishita, Y., 1999, *Strength and Deformation Capacity of Cantilever Structural Walls with Openings*, PEER Report, Pacific Earthquake Engineering Research Center, Berkeley, California.

Kolozvari, K., Orakcal, K., and Wallace, J.W., 2015a, "Modeling of cyclic shear-flexure interaction in reinforced concrete structural walls. Part I: Theory," *Journal of Structural Engineering*, Vol. 141, No. 5.

Kolozvari, K., Tran, T.A., Orakcal, K., and Wallace, J.W., 2015b, "Modeling of cyclic shear-flexure interaction in reinforced concrete structural walls. Part II: Experimental validation," *Journal of Structural Engineering*, Vol. 141, No. 5.

Kolozvari, K., Orakcal, K., and Wallace, J.W., 2018, "New OpenSees models for simulation of nonlinear flexural and shear-flexural interaction behavior of reinforced concrete walls and columns," *Computers and Structures Journal*, Vol. 196, pp. 246-262.

Korolyk, M.J., and Wagner, A.M., 2016, "Improving design for plan torsion," *Proceedings*, 2016 SEAOC Convention, Maui, Hawaii.

Liel, A.B., 2008, *Assessing the Collapse Risk of California's Existing Reinforced Concrete Frame Structures: Metrics for Seismic Safety Decisions*, Stanford University, Stanford, California.

Lignos, D.G., and Krawinkler, H., 2009, *Sidesway Collapse of Deteriorating Structural Systems Under Seismic Excitations*, Rep. No. TB 172, John A. Blume Earthquake Engineering Center, Stanford University, Stanford, California.

Lignos, D.G., and Krawinkler, H., 2011, "Deterioration modeling of steel components in support of collapse prediction of steel moment frames under earthquake loading," *Journal of Structural Engineering*, Vol. 137, No. 11, pp. 1291-1302.

Lignos, D.G., Krawinkler, H., and Whittaker, A.S., 2011, "Prediction and validation of sidesway collapse of two scale models of a 4-story steel moment frame," *Earthquake Engineering & Structural Dynamics*, Vol. 40, No. 7, pp. 807-825.

Lowes, L.N., Mitra, N., and Altoontash, A., 2004, *A Beam-Column Joint Model for Simulating the Earthquake Response of Reinforced Concrete Frames*, PEER Report No. 2003/10, Pacific Earthquake Engineering Research Center, University of California, Berkeley, California.

MacRae, G., and Deam, B., 2009, *Building Regularity for Simplified Modeling*, EQC Project No. 06/514, University of Canterbury, Christchurch, New Zealand.

Magliulo, G., Ramasco, R., and Realfonzo, R., 2002, "A critical review of seismic code provisions for vertically irregular frames," *Proceedings*, Third European Workshop on the Seismic Behaviour of Irregular and Complex Structures, Florence, Italy.

Marafi, N.A., Ahmed, K., Lowes, L.N., and Lehman, D.E., 2018, "Variability in seismic collapse probabilities of solid and coupled-wall buildings," *Journal of Structural Engineering*, American Society of Civil Engineers (in press).

Marius, M., 2013, "Seismic behaviour of reinforced concrete shear walls with regular and staggered openings after the strong earthquakes between 2009 and 2011," *Engineering Failure Analysis*, Vol. 34, pp. 537-565.

McKenna, F., Fenves, G.L., Scott, M.H., and Jeremie, B., 2000, *Open System for Earthquake Engineering Simulation*, OpenSees, University of California, Berkeley, California.

Michalis, F., Dimitrios, V., and Manolis, P., 2006, "Evaluation of influence of vertical irregularities on the seismic performance of a nine-storey steel frame," *Earthquake Engineering & Structural Dynamics*, Vol. 35, No. 12, pp. 1489-1509.

Ministry of Construction of the People's Republic of China and the State Quality Supervision and Quarantine Bureau, 2001, *Code for Seismic Design of Buildings*, GB 50011-2001, China Architecture & Building Press, Beijing, China.

Moehle, J., Lehman, D., and Lowes, L., 2006, "Beam-column connections," *New Information on the Seismic Performance of Existing Buildings*, Earthquake Engineering Research Institute (EERI) Technical Seminar.

Moehle, J.P., 2015, *Seismic Design of Reinforced Concrete Buildings*, McGraw-Hill, New York, New York.

Naeim, F., Schindler, B., Martin, J.A., and Lynch, S., 1990, "Hidden zones of high stress in seismic response of structural walls," *Proceedings*, 1990 SEAOC Convention, pp. 402-422.

National Research Council of Canada, 2015, *National Building Code of Canada*, Issued by the Canadian Commission on Building and Fire Codes.

Neuenhofer, A., 2006, "Lateral stiffness of shear walls with openings," *Journal of Structural Engineering*, Vol. 132, No. 11, pp. 1846-1851.

NISEE, 1971a, *Karl V. Steinbrugge Collection*, NISEE/PEER/UCB, National Information Service for Earthquake Engineering/Pacific Earthquake Engineering Research Center/University of California, Berkeley, California, Available at: https://nisee.berkeley.edu/elibrary/Image/S4060.

NISEE, 1971b, *Karl V. Steinbrugge Collection*, NISEE/PEER/UCB, National Information Service for Earthquake Engineering/Pacific Earthquake Engineering Research Center/University of California, Berkeley, California, Available at: https://nisee.berkeley.edu/elibrary/Image/S4003.

NISEE, 1971c, *Karl V. Steinbrugge Collection*, NISEE/PEER/UCB, National Information Service for Earthquake Engineering/Pacific Earthquake Engineering Research Center/University of California, Berkeley, California, Available at: https://nisee.berkeley.edu/elibrary/Image/S4043.

NISEE, 1971d, *William G.Godden (Vol 4) Collection*, NISEE/PEER/UCB, National Information Service for Earthquake Engineering/Pacific Earthquake Engineering Research Center/University of California, Berkeley, California, Available at: https://nisee.berkeley.edu/elibrary/Image/GoddenJ74.

NISEE, 1983, *William G.Godden (Vol 4) Collection*, NISEE/PEER/UCB, National Information Service for Earthquake Engineering/Pacific Earthquake Engineering Research Center/University of California, Berkeley, California, Available at: https://nisee.berkeley.edu/elibrary/Image/GoddenJ29.

NISEE, 1987, *Karl V. Steinbrugge Collection*, NISEE/PEER/UCB, National Information Service for Earthquake Engineering/Pacific Earthquake Engineering Research Center/University of California, Berkeley, California, Available at: https://nisee.berkeley.edu/elibrary/Image/S6008.

NISEE, 1989, *Loma Prieta Collection*, NISEE/PEER/UCB, National Information Service for Earthquake Engineering/Pacific Earthquake Engineering Research Center/University of California, Berkeley, California, Available at: https://nisee.berkeley.edu/elibrary/Image/LP0374.

NISEE, 1994, *Northridge Collection*, NISEE/PEER/UCB, National Information Service for Earthquake Engineering/Pacific Earthquake Engineering Research Center/University of California, Berkeley, California, Available at: https://nisee.berkeley.edu/elibrary/Image/NR338.

NIST, 2010, *Evaluation of the FEMA P-695 Methodology for Quantification of Building Seismic Performance Factors*, NIST GCR 10-917-8, prepared by NEHRP consultants Joint Venture, a partnership of the Applied Technology Council and the Consortium of the Universities for Research in Earthquake Engineering, for the National Institute of Standards and Technology, Gaithersburg, Maryland.

NIST, 2011, *Seismic Design of Cast-in-Place Concrete Special Structural Walls and Coupling Beams: A Guide for Practicing Engineers*, NIST GCR 11-917-11REV-1, prepared by NEHRP consultants Joint Venture, a partnership of the Applied Technology Council and the Consortium of the Universities for Research in Earthquake Engineering, for the National Institute of Standards and Technology, Gaithersburg, Maryland. Revised 2012.

NIST, 2012, *Tentative Framework for Development of Advanced Seismic Design Criteria for New Buildings*, NIST GCR 12-917-20, prepared by NEHRP consultants Joint Venture, a partnership of the Applied Technology Council and the Consortium of the Universities for Research in Earthquake Engineering, for the National Institute of Standards and Technology, Gaithersburg, Maryland.

NIST, 2013, *Development of NIST Measurement Science R&D Roadmap: Earthquake Risk Reduction in Buildings*, NIST GCR 13-917-23, prepared by the National Institute of Building Sciences for the National Institute of Standards and Technology, Gaithersburg, Maryland.

NIST, 2014, *Recommendations for Seismic Design of Reinforced Concrete Wall Buildings Based on Studies of the 2010 Maule, Chile Earthquake*, NIST GCR 14-917-25, prepared by NEHRP consultants Joint Venture, a partnership of the Applied Technology Council and the Consortium of the Universities for Research in Earthquake Engineering, for the National Institute of Standards and Technology, Gaithersburg, Maryland.

NIST, 2017, *Guidelines for Nonlinear Structural Analysis for Design of Buildings, Part IIa – Steel Moment Frames*, NIST GCR 17-917-46v2, prepared by the Applied Technology Council for the National Institute of Standards and Technology, Gaithersburg, Maryland.

Noda, N., Sugishita, Y., and Kato, D., 1997, "Tests of reinforced concrete cantilever walls with openings," *Transactions of the Japan Concrete Institute*, Vol. 19, pp. 311-316.

Obayashi, 1995, *Preliminary Report on the 1995 Southern Hyogo Prefecture Earthquake*, Obayashi Corporation, Technical Research Institute, Tokyo, Japan.

Orakcal, K., Conte, J.P., and Wallace, J.W., 2004, "Flexural modeling of reinforced concrete structural walls - model attributes," *ACI Structural Journal*, Vol. 101, No. 5, pp. 688-698.

Orakcal, K., and Wallace, J.W., 2006, "Flexural modeling of reinforced concrete walls - experimental verification," *ACI Structural Journal*, Vol. 103, No. 2, pp. 196-206.

Orakcal, K., Ulugtekin, D., and Massone, L.M., 2012, "Constitutive modeling of reinforced concrete panel behavior under cyclic loading," *Proceedings*, 15th World Conference on Earthquake Engineering, Lisbon, Portugal.

Pan, A.D., and Moehle, J.P., 1992, "An experimental study of slab-column connections," *ACI Structural Journal*, Vol. 89, No. 6, pp. 626-638.

PEER, 2006, *PEER NGA Database*, Pacific Earthquake Engineering Research Center, University of California, Berkeley, California.

PEER, 2010, *Guidelines for Performance-Based Seismic Design of Tall Buildings*, prepared by the Tall Building Initiative (TBI) Working Group, Pacific Earthquake Engineering Research Center, University of California, Berkeley, California.

Pugh, J.S., 2012, *Numerical Simulation of Walls and Seismic Design Recommendations for Walled Buildings*, Ph.D. Thesis, University of Washington, Seattle, Washington.

Pugh, J.S., Lowes, L.N., and Lehman, D.E., 2015, "Nonlinear line-element modeling of flexural reinforced concrete walls," *Engineering Structures*, Vol. 104, pp. 174-192.

Pujol, S., Galeotti, F., Lehman, D., and Sumearll, J., 2017, "RAPID/Collaborative Research: Investigation of Reinforced Concrete Buildings Damaged in the Magnitude 6.4 Southern Taiwan Earthquake of February 2016," *DesignSafe-CI*, Dataset, doi:10.17603/DS2CP4W.

Saatcioglu, M., and Razvi, S., 1992, "Strength and ductility of confined concrete," *Journal of Structural Engineering*, Vol. 118, No. 6, pp. 1590-1607.

Scott, B.D., Park, R., and Priestley, M.J.N., 1982, "Stress-strain behavior of concrete confined by overlapping hoops at low and high strain rates," *ACI Journal Proceedings*, Vol. 79, No. 1, pp. 13-27.

SEAOC, 1975, *Recommended Lateral Force Requirements and Commentary*, Seismology Committee of the Structural Engineers Association of California, Sacramento, California.

SEAOC, 1988, *Recommended Lateral Force Requirements and Tentative Commentary*, Seismology Committee, Structural Engineers Association of California, San Francisco, California.

SEAOC, 1990, *Recommended Lateral Force Requirements and Commentary*, Structural Engineers Association of California, Sacramento, California.

SEAOC, 1996, *Recommended Lateral Force Requirements and Commentary*, Structural Engineers Association of California, Sacramento, California.

SEAOC, 1999, *Recommended Lateral Force Requirements and Commentary*, Structural Engineers Association of California, Sacramento, California.

SEAOC, 2013, *Structural/Seismic Design Manual for the 2012 IBC*, Volume 1 Code Application Examples, Structural Engineers Association of California, Sacramento, California.

SEAOC, 2015, *IBC SEAOC Structural/Seismic Design Manual*, Structural Engineers Association of California, Sacramento, California.

Shiu, K.N., Daniel, J.I., Aristizabal-Ochoa, J.D., Fiorato, A.E., and Corley, W.G., 1981, *Earthquake Resistant Structural Walls: Test of Walls with and without Openings*, NASA STI/Recon Technical Report No. 82.

Shoraka, M., Dupuis, M., Macauley, J., Elwood, K., Anderson, D., and Simpson, R., 2014, "Seismic performance of shear wall buildings with gravity-induced lateral demands," *Proceedings*, Tenth U.S. National Conference on Earthquake Engineering, Anchorage, Alaska.

Shultz, A.E., 1992, "Approximating lateral stiffness of stories in elastic frames," *Journal of Structural Engineering*, Vol. 118, No. 1, pp. 243-263.

Taylor, C.P., 1995, *Design of Slender Reinforced Concrete Structural Walls with Openings*, Thesis, Clarkson University.

Thomsen, J., and Wallace, J., 1995, *Displacement-Based Design of RC Structural Walls: An Experimental Investigation of Walls with Rectangular and T-Shaped Cross Sections*, Technical Report No. CU/CEE-95/06, Department of Civil Engineering, Clarkson University, Potsdam, New York.

Tremblay, R., and Poncet, L., 2005, "Seismic performance of concentrically braced steel frames in multistory buildings with mass irregularity," *Journal of Structural Engineering*, Vol. 131, No. 9, pp. 1363-1375.

Vamvatsikos, D., and Cornell, C.A., 2002, "Incremental dynamic analysis," *Earthquake Engineering & Structural Dynamics*, Vol. 31, No. 3, pp. 491-514.

Wey, E.H., and Durrani, A.J., 1992, "Seismic response of interior slab-column connections with shear capitals," *ACI Structural Journal*, Vol. 89, No. 6, pp. 682-691.

Whitman, Z., 2015, *Investigation of Seismic Failure Modes in Flexural Concrete Walls Using Finite Element Analysis*, Master's Thesis, University of Washington, Seattle.

Wu, H., 2005, *Design of Reinforced Concrete Walls with Openings for Strength and Ductility*, Thesis, Nanyang Technological University, Singapore, available at: http://hdl.handle.net/10356/12115.

Yanez, F.V., Park, R., and Paulay, T., 1992, "Seismic behaviour of walls with irregular openings," *Proceedings*, Tenth World Conference on Earthquake Engineering, Vol. 6, pp. 3303-3308, Balkema, Rotterdam.

Yassin, M., 1994, *Nonlinear Analysis of Prestressed Concrete Structures Under Monotonic and Cyclic Loads*, Ph.D. Dissertation, University of California, Berkeley.

Project Participants

FEMA Oversight

Michael (Mai) Tong (Project Officer)
Federal Emergency Management Agency
400 C Street, SW, Suite 313
Washington, D.C. 20472

Farzad Naeim (Subject Matter Expert)
Farzad Naeim, Inc.
100 Spectrum Center Drive, Suite 900
Irvine, California 92618

ATC Management and Oversight

Jon A. Heintz (Program Executive, Program Manager)
Applied Technology Council
201 Redwood Shores Parkway, Suite 240
Redwood City, California 94065

Ayse Hortacsu (Project Manager)
Applied Technology Council
201 Redwood Shores Parkway, Suite 240
Redwood City, California 94065

Veronica Cedillos (Project Manager)
Applied Technology Council
201 Redwood Shores Parkway, Suite 240
Redwood City, California 94065

Project Technical Committee

Michael Valley (Project Technical Director)
Magnusson Klemencic Associates
1301 Fifth Avenue, Suite 3200
Seattle, Washington 98101

Laura N. Lowes
University of Washington
233C More Hall, 352700
Seattle, Washington 98195

Curt Haselton
Haselton Baker Risk Group, LLC
728 Cherry Street, Suite C
Chico, California 95928

Rafael Sabelli
Walter P Moore
595 Market Street, Suite 2130
San Francisco, California 94105

Charles A. Kircher
Kircher & Associates
1121 San Antonio Road, Suite D-202
Palo Alto, California 94303

Thomas A. Sabol
Englekirk Structural Engineers
888 South Figueroa Street, Eighteenth Floor
Los Angeles, California 90017

Project Review Panel

Gregory G. Deierlein
Stanford University
318 Parkside Drive
Palo Alto, California 94306

Larry A. Fahnestock
University of Illinois
620 Pittsfield Drive
Champaign, Illinois 61822

James R. Harris
J. R. Harris & Company
1175 Sherman Street, Suite 2000
Denver, Colorado 80203

Conrad Hohener
Degenkolb Engineers
300 South Grand Avenue, Suite 3850
Los Angeles, California 90071

John Hooper
Magnusson Klemencic Associates
1301 Fifth Avenue, Suite 3200
Seattle, Washington 98101

Ryan A. Kersting
Buehler & Buehler Structural Engineers
600 Q Street, Suite 200
Sacramento, California 95814

Roberto Leon*
Virginia Tech
102D Patton Hall (0105)
Blacksburg, Virginia 24061

*ATC Board Contact

Working Group

Kamal Ahmed
University of Washington
Box 352700
Seattle, Washington 98195

Dustin Cook
Haselton Baker Risk Group, LLC
728 Cherry Street, Suite C
Chico, California 95928

D. Jared DeBock
California State University, Chico
400 West 1st Street
Chico, California 95929

Sara Essila
Haselton Baker Risk Group, LLC
728 Cherry Street, Suite C
Chico, California 95928

Katie Fitzgerald
Haselton Baker Risk Group, LLC
728 Cherry Street, Suite C
Chico, California 95928

Heavenz Kaur
Englekirk Structural Engineers
888 South Figueroa Street, Eighteenth Floor
Los Angeles, California 90017

Kristijan Kolozvari
California State University, Fullerton
800 N. State College Boulevard
Fullerton, California 92834

Dawn Lehman
University of Washington
214B Moore Hall, Box 352700
Seattle, Washington 98195

Nasser Marafi
University of Washington
2209 North 38th Street
Seattle, Washington 98103

Diane Nishi
Englekirk Structural Engineers
888 South Figueroa Street, Eighteenth Floor
Los Angeles, California 90017

Josh Pugh
Department of Civil and Environmental Engineering
Seattle University
901 12th Avenue, ENGR 525
Seattle, Washington 98122

Ricardo Roldan
Englekirk Structural Engineers
888 South Figueroa Street, Eighteenth Floor
Los Angeles, California 90017

Negin A. Tauberg
University of California, Los Angeles
405 Hilgard Avenue
Los Angeles, California 90024

Tsenguun Tsoqbadrakh
University of Washington
2209 North 38th Street
Seattle, Washington 98103

Workshop Participants

David Bonneville
Degenkolb
1300 Clay Street, 9th Floor
Oakland, California 94612

Dan Dolan
Washington State University
405 Spokane Street, Sloan 101
Pullman, Washington 99164

Anindya Dutta
Simpson Gumpertz & Heger, Inc.
100 Pine Street, Suite 1600
San Francisco, California 94111

Ken Elwood
The University of Auckland
Dept. of Civil and Environmental Engineering
3 Grafton Road
Auckland, New Zealand

Michael Gannon
American Institute of Steel Construction
1 E Upper Wacker Drive
Chicago, Illinois 60601

S. K. Ghosh
S. K. Ghosh Associates Inc.
334 East Colfax Street, Unit E
Palatine, Illinois 60067

Ronald O. Hamburger
Simpson Gumpertz & Heger, Inc.
100 Pine Street, Suite 1600
San Francisco, California 94111

Robert D. Hanson
Federal Emergency Management Agency
500 C Street, SW
Washington, DC 20472

Bret Lizundia
Rutherford + Chekene
375 Beale Street, Suite 310
San Francisco, California 94105

James O. Malley
Degenkolb Engineers
375 Beale Street, Suite 500
San Francisco, California 94105

Justin Moresco
Applied Technology Council
201 Redwood Shores Parkway, Suite 240
Redwood City, California 94065

Kevin Wong
National Institute of Standards and Technology
Engineering Laboratory
100 Bureau Drive
Gaithersburg, Maryland 20899

Noelle Yuen
Maffei Structural Engineering
98 Battery Street, Suite 300
San Francisco, California 94111

Farzin Zareian
University of California, Irvine
The Henry Samueli School of Engineering
Irvine, California 92697

FEMA

FEMA P-2012
Catalog No. 18166-1